STRUCTURE AND KINEMATICS OF LARGE SUBMARINE MASS WASTING DEPOSITS

SUZANNE BULL

Submitted in partial fulfilment of the requirements for the degree of Ph.D

Cardiff University

July 2009

ProQuest LLC
789 East Eisenhower Parkway
P.O. Box 1346
Ann Arbor, MI 48106-1346

DECLARATION

This work has not previously been accepted in substance for any degree and is not being concurrently submitted in candidate for any degree

Signed.....(candidate)

Date.....

STATEMENT 1

This thesis is the result of my own investigations, except where otherwise stated. Other sources are acknowledged by footnotes giving explicit references. A bibliography is appended.

Signed.....(candidate)

Date.....

STATEMENT 2

I hereby give consent for my thesis, if accepted, to be available for photocopying and for inter-library loan, and for the title and summary to be made available to outside organisations.

Signed.....(candidate)

Date.....

SUMMARY

This thesis uses a combination of industrially acquired seismic reflection data, along with supplementary bathymetry and geotechnical borehole data, to investigate the architecture, structural elements and evolution of submarine mass wasting deposits. The primary study area is the mid-continental margin of Norway and the Levant margin, east-Mediterranean Sea serves as a secondary study area. The principal aim is to gain an improved understanding of the evolution of submarine mass wasting deposits and the processes involved. To this end this thesis consists of three core research chapters which present the results of investigations into the mechanism responsible for the formation of a non-typical example of a submarine mass wasting deposit, the spectrum of geological features that can be found associated with submarine mass wasting deposits, and an example of a frontally confined submarine mass wasting deposit.

In the first core chapter, an example of a non-typical submarine mass wasting deposit from the Norwegian continental margin was investigated using three-dimensional (3D) seismic data. The mass wasting deposit, informally named the 'South Vøring Slide' (SVS) was found to differ from previously documented examples in that it showed significant thinning and volume loss which could not be accounted for by the transfer of material downslope over a basal shear surface. Analysis of the deformation and geometry of the SVS suggests that it developed due to the mobilisation of an approximately 40 m thick interval at the lower part of the SVS, and its removal from beneath a thin overburden which subsequently underwent extensional fragmentation.

Submarine mass wasting deposits exhibit many different types of kinematic indicators from which information relating to the dynamic emplacement of the event can be deduced. The second core research chapter presents a classification scheme and comprehensive compilation of all of the various kinematic indicator types, fully illustrated using best examples taken from the 3D seismic database available from the Norwegian and Levant margins. For each kinematic indicator, a definition and seismic recognition criteria are presented along with discussion and worked examples of the kinematic information which they provide. It was shown that the application of 3D seismic data to the study of submarine mass wasting deposits can yield much information pertaining to the direction and magnitude of transport, mode of emplacement, dominant mass wasting process and rheology. In particular, it was shown that 3D seismic data allows swift and confident evaluation of the direction of translation, and in many cases also allows the degree of translation of the displaced material to be constrained.

The final core research chapter documents and describes an example of a large frontally confined submarine mass wasting deposit from the Norwegian margin. The mass wasting deposit, informally named the 'Confined Storegga Slide (CSS)', is unique in that it detaches along a deep-seated basal horizon at a depth of 640 m below the seabed and exhibits spectacular contractional deformation in its distal region. Using a combination of 2D and 3D seismic data and bathymetry data, it has been possible to fully delimit the extent of the CSS, which has a section length of 135 km and involves some 1,227 km^3 of material. The results of this study show that the CSS developed as part of the large, multi-phase Holocene Storegga Slide, and demonstrates how subsequent phases Storegga Slide development induced later deformation and volumetric changes which have not previously been recognised.

A NOTE ON THESIS STRUCTURE

Two of the principal research chapters of this thesis (chapters two and three) have been prepared as scientific papers for publication in two different international journals. The present status of each publication is summarized as follows:

- **Chapter two** is in press for Basin Research as: *A subsurface evacuation model for submarine slope failure.* Suzanne Bull, Joe Cartwright and Mads Huuse.

- **Chapter three** has been published as: *A review of kinematic indicators from mass transport complexes using 3D seismic data.* Suzanne Bull, Joe Cartwright and Mads Huuse. Marine and Petroleum Geology 26 (2009), pp. 1132-1157.

Although each article is jointly authored with the project supervisors they are the work of the lead author, Suzanne Bull. Project supervisors provided editorial support in accordance with a normal thesis chapter.

ACKNOWLEDGEMENTS

There are so many more people than I could possibly thank here, who have helped or influenced me in some way towards the completion of this project. First and foremost, sincere thanks are due to my inspirational supervisor Joe Cartwright, for his guidance, encouragement and enthusiasm from day one. I feel I have learned and developed so much as a result of his input. I am also grateful to my second supervisor Mads Huuse, for yet more enthusiasm and advice on all things geophysical.

Statoil are thanked, and Andreas Helsem in particular, for providing the data for this project and permission to use in it presentations and publications. The AAPG are acknowledged for provision of a grant–in-aid award. I owe a debt of gratitude to the various reviewers of my papers including Marc De Batist, Carls Fredrik Forsberg, Tore Kvalstad, Leslie Wood, and those who chose to remain anonymous. David James is thanked for several technical discussions at various stages throughout the project. Gwen Pettigrew, Andrew Wiltshire and Derek John are all gratefully thanked for help with IT and software issues, which are well beyond my capabilities.

Various members of the 3D Lab deserve special thanks: Jose, for laying the foundations for this project with his previous work on submarine landslides; Aggie, the Geoframe guru; Jenny, for a crash course in ArcGIS, and Tom for help in the field during a trip to New Zealand. These, along with other members of the 3D Lab past and present, are thanked warmly for both friendship and technical help, including Claudia, Paivi, Cat, Sepribo, Simon, William, Mostyn, Gordon, Ian, Davide and Cristina. I take away fond, fond memories of my time in Cardiff with this group and our regular meetings and various attempts at cake-making!

I have been blessed with wonderful friends from my school days who have thankfully been nearby, and so I must acknowledge the Risca crew: Emma, Natalie, Sarah, Sian and Stacey, and their various children, for always being so kind and encouraging. It has certainly helped to provide balance and perspective throughout the past few years.

The people to whom I owe my most personnel and heartfelt thanks are those closest to me. I cannot express my gratitude to my parents June and David, for working so hard to give us the very best in life and opportunities. I could certainly not have completed or even embarked on this project without them and the continuing support that they provide, and as such, I dedicate this thesis to them. I am grateful for my grandmother, who sadly passed away last year, who was such a wicked spirit despite her years, and for my inspirational big sib Ang and niece Emma, who have always rooted for me. I am grateful to my twin sister Leigh and my nephew James, who possesses such heartbreaking innocence and mischief, for providing a true ray of sunshine whatever the circumstances. She probably doesn't know it, but Leigh has been my greatest source of inspiration with her unwavering love and resilience, and she is nothing short of my hero. Finally, thank you to Rob, for being so accepting and always encouraging me to have some belief in myself! His love, support and confidence have been a blessing throughout this difficult task. Like all things in life worth doing, it had its peaks and troughs (no seismic pun intended!)

TABLE OF CONTENTS

CHAPTER FOUR

CHAPTER FIVE

CHAPTER SIX

LIST OF FIGURES

	disruption which is interpreted as early development of a basal detachment surface and limited slip of material. The fact that a toe region has not developed (e.g. contractional deformation or accumulation of material) in the downslope position is taken as evidence for the immature stage of slope failure development. Location shown in (A).	

LIST OF TABLES

CHAPTER ONE

CHAPTER FOUR

LIST OF ENCLOSURES

Published papers:

Bull, S., Cartwright, J. A. and Huuse, M. *A subsurface evacuation model for submarine slope failure.* Basin Research (in press).

Bull, S., Cartwright, J. A. and Huuse, M. *A review of kinematic indicators from mass transport complexes using 3D seismic data.* Marine and Petroleum Geology 26 (2009), pp. 1132-1157.

Bull, S. and Cartwright, J.A. *Small scale insights into seismic-scale slumps: a comparison of slump features from the Waitemata Basin, New Zealand, and the Møre Basin, offshore Norway.* Submarine mass movements and their consequences, proceedings of the 4th International conference (in press).

GLOSSARY OF KEY TERMS

Classical retrogression – a type of slope failure whereby downslope translation takes place above a discrete slip plane, with material above deforming as a coherent slab undergoing extension (Kvalstad *et al.* 2005). Failed blocks accelerate downslope, created an unsupported scarp which then itself fails, creating a further failed block which moves downslope. Failure thus progresses in a sequentially backwards, upslope-stepping sequence. This model has been used to explain the majority of mass wasting events from the primary study area.

Confined Storegga Slide – the name given herein to the confined element of the Storegga Slide whose toe zone is comprised by the previously recognised 'compression zone' of Haflidason et al., (2004).

Frontally confined – a type of submarine mass wasting deposit which can be defined by a toe zone which is buttressed against its distal margin, and detaches along a deep-seated basal detachment horizon (Frey-Martinez et al. 2006)

Frontally emergent – a type of submarine mass wasting deposit which can be defined by a toe zone comprised of a relatively thin, laterally extensive compressive zone which has ramped up from the original basal detachment horizon and translated freely across the sea floor (Frey-Martinez et al. 2006).

Horst – (chapter four) a fault bound block from within the Confined Storegga Slide which has undergone relatively little deformation but may have experienced some displacement across the basal detachment surface.

Kinematic indicator - a geological structure or feature associated with a submarine mass wasting deposit, which records information related to the type and direction of motion at the time of emplacement, and as such they are of great use to our understanding of the initiation, dynamic evolution and cessation of slope failures.

Liquefaction – a type of sediment mobilisation involving the total loss of strength of a sediment in which pore fluid pressures reach lithostatic values.

Mobilisation – a term used to describe both the rendering of a sediment capable of motion, and the bulk movement that can occur as a result (Maltman and Bolton 2003).

MWD – mass wasting deposit. This term has been chosen for use throughout this project to refer to the complex geological units which result from the failure of submarine slopes, without implying a dominant type of mass wasting process. Processes are discussed for individual examples within this project once analysis allowing identification of dominant types of mass wasting has been performed.

Pressure ridge – a feature resulting from compressive stress, commonly observed from the toe zones of frontally emergent-type submarine mass wasting deposits. In this project, pressure ridges are distinguished from other compressive features observed from toe zones owing to their size, and are interpreted as the top-surface expression of thrusts and folds which are below the scale of seismic resolution.

Quick clay - a highly sensitive, high water content clay found in glaciated and uplifted regions such as Canada and Scandinavia, which can readily liquefy following mechanical disturbance (Bjerrum 1955).

South Vøring Slide (SVS) – the name given to the MWD identified and studies in chapter two of this project.

Spread – a type of mass movement involving extension and downslope displacement of a sediment unit above a deforming mass of softer material (Varnes, 1978).

Storegga Slide Complex (SSC) – the term used to refer to the area affected by the mass wasting which occurred during the Holocene Storegga Slide, along with those mass wasting episodes which preceded it throughout the Late Pliocene (Evans et al. 2005).

CHAPTER ONE

1.0 Introduction

1.1 Rationale

Submarine mass wasting commonly occurs on the world's continental margins, comprising one of the major processes through which sediments are transferred from the continental slope to the deep ocean (Masson et al. 2006), and play a major role in the morphology and stratigraphy of the margin (Pratson et al. 2001). In the submarine realm, mass wasting can involve large volumes of material, affect vast areas of the seafloor and transport material over huge distances: sediment volumes of c. 3500 km^3 are reported to have been involved in the Holocene Storegga Slide on the Norwegian continental margin, where a total area of 95,000 km^2 is affected and a maximum run-out distance of some 800 km is recorded (Bryn et al. 2005a). Submarine mass wasting is also of relevance in a social and economic sense as seafloor instability can threaten offshore installations, and in several instances submarine mass wasting events have been associated with the generation of tsunamis (Hampton et al. 1996).

Once a submarine slope failure initiates, the event may progress by means of a number of the mass wasting processes (see Martinsen 1994). The various processes exist as part of a continuum, whereby one may evolve into or trigger another, and include translational sliding, rotational slumping, fluidal and plastic flows (Fig. 1.1; Martinsen 1994). Mass wasting deposits are therefore likely to be highly complex and may have involved a number of processes, possibly active at different stages of failure. Common to all of these processes however, is the translation of material

downslope. Classical models suggest the formation of slope failure events depends critically on the necessary failure conditions being exceeded on a discrete basal shear surface (Bjerrum 1967; Martel 2004; Petley et al. 2005). This basal surface evolves morphologically during failure to become the base of the slope failure, over which the material is translated. The distribution and volume of the translated material overlying the basal shear surface is largely a function of its location within the slope failure, as it is generally expected that net depletion in the upslope realm of the slope failure occurs due to mobilisation and translation of the failed mass downslope. This is balanced at some point downslope in a zone of general accumulation due to arrest and deposition of the mass (*sensu* Varnes 1978; Frey Martinez et al. 2006). These volumetric changes from the pre-failure slope template, based on the original thickness and morphology of the slope prior to failure, are reflected in the style of deformational features present within submarine mass wasting deposits (MWDs), with extension typically dominating the upslope region, and compression more prevalent downslope (Lewis 1971; Varnes 1978; Farrell 1984; Martinsen 1994; Frey Martinez et al. 2006). However, it has been increasingly noted that the complexity of some examples cannot be accounted for by the classical model (Strachan 2002a).

Due to the complex nature of the MWDs, several important aspects of submarine slope failure development and occurrence remain poorly understood. For example: (1) the physical processes involved in the transition from failure to post-failure stages of development (Locat and Lee 2002); (2) the mechanisms responsible for generating exceptional mobility and long run out distances (Locat and Lee 2002); and (3) how to better predict the timing and location of future submarine slope failure events (Pratson et al. 2001).

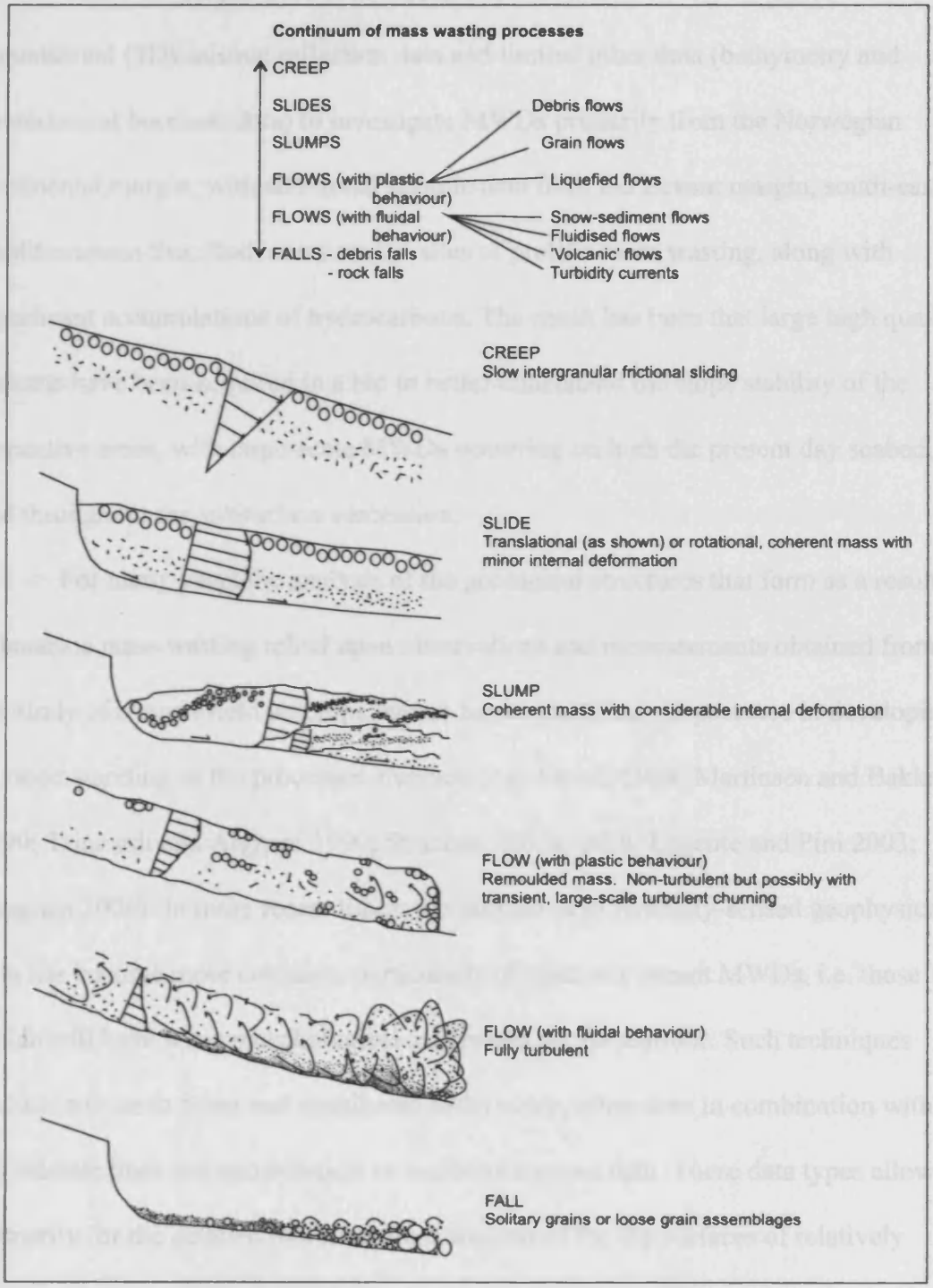

Figure 1.1. Continuum of mass movement processes and classification of process types based on rheology. Modified after Nemec 1990.

This PhD project uses commercial two-dimensional (2D) and three-dimensional (3D) seismic reflection data and limited other data (bathymetry and geotechnical borehole data) to investigate MWDs primarily from the Norwegian continental margin, with additional seismic data from the Levant margin, south-east Mediterranean Sea. Both areas are the sites of prolific mass wasting, along with significant accumulations of hydrocarbons. The result has been that large high quality datasets have been acquired in a bid to better understand the slope stability of the respective areas, with large-scale MWDs occurring on both the present day seabed, and throughout the subsurface succession.

For many years the analysis of the geological structures that form as a result of submarine mass wasting relied upon observations and measurements obtained from the study of ancient field outcrops, which have been of key importance in developing an understanding of the processes involved (e.g. Farrell 1984; Martinsen and Bakken 1990; Trincardi and Argnani 1990; Strachan 2002a and b; Lucente and Pini 2003; Strachan 2006). In more recent times, the utilization of remotely-sensed geophysical data has become more common, particularly of relatively recent MWDs, i.e. those which still have some morphological expression on the seafloor. Such techniques include side-scan sonar and multibeam bathymetry, often used in combination with 2D seismic lines and geotechnical or sedimentary core data. These data types allow primarily for the detailed morphological analysis of the top surfaces of relatively recent mass wasting deposits (i.e. those which affect the modern seafloor) and can be used to interpret the processes that control formation and morphology (e.g. Prior et al. 1984; Masson et al. 1993; Urgeles et al. 2006).

The three-dimensional nature of modern seismic surveys enables the structure of MWDs to be assessed beyond what is apparent at the surface, with detailed

mapping and imaging of the basal surface and internal areas made possible. Importantly, 3D seismic data affords complete analysis of the geometries of internal architectural units, which may not be inferred from the study of bounding surfaces alone. The geometry and internal deformation of MWDs are consequences of the mechanism of failure and the morphology of the slope over which translation occurs (Strachan 2002a; Lucente and Pini 2003). In addition, the mode of deformation will be influenced by the rheology of the rock; itself dependant on several factors including lithology and strain rate (Cosgrove 2007). It is therefore possible, through the characterisation and analysis of the external geometry and internal distribution of deformational structures, to unravel the strain history of individual mass wasting deposits and formulate a kinematic model of emplacement. The continued identification, mapping and characterisation of MWDs is therefore vital in order to yield further pertinent observations to help to resolve the existing complexities and unknowns, and ultimately, build an improved understanding of the evolution of submarine mass wasting events and their future prediction. The present chapter now introduces the aims of the project, the geographical and geological setting of the study areas, the project database and methodology of the investigation.

1.2 Aims of the project

The major aim of this project is concerned with improving the current understanding of the evolution of submarine mass wasting events and the processes involved. The large number and scale of the MWDs present in the study areas and the high quality of the data available presents the opportunity to carry out the detailed description of

the external and internal architecture of the various deposits, and the related structural elements. As such, the specific objectives of this project are:

1) Describe and document the architecture and structural elements of submarine mass wasting deposits using 3D seismic data

1a. Identify and map the mass wasting deposits imaged by the dataset.

1b. Identify suitable examples for more focussed characterisation and analysis of internal architectures and structural elements.

1c. Document previously un-described examples.

2) Utilise the described internal deformational characteristics to reconstruct the deformational history and evolution of selected examples.

2a. Compare selected examples to existing models for mass wasting.

2b. Suggest appropriate models for the formation of the selected examples based on the observed geometry and deformation.

3) Catalogue structural elements identified from the mass wasting deposits

3a. Compile the various types of features and devise a suitable classification scheme for their presentation.

3b. For each type of feature, establish a definition, recognition criteria and mode of formation.

3c. Analyse and discuss process understanding and kinematic information yielded by each feature and illustrate using representative examples taken from the study areas.

1.3 Geographical and Geological Setting

1.3.1 The Norwegian continental margin

This is the primary study area for this project, where the investigation focuses on the sediments of the adjacent Vøring and Møre Basins (Fig. 1.2). The basins dominate the study area and are flanked by palaeo-highs and platforms (Fig. 1.2). The platforms to the west are termed the Møre and Vøring Marginal highs and the boundary between the marginal high and basinal area is formed by the Faeroe-Shetland escarpment in the south of the area and the Vøring Escarpment in the north of the study area (Fig. 1.2). The dominant NE-SW structural grain is comprised by faults which probably originated in the Late Palaeozoic and remained active throughout the subsequent tectonic phases (Brekke 2000). An older structural grain, trending NW-SE, represented by the Jan-Mayen fracture zone (JMFZ) and the Bivrost Lineament (Fig. 1.2) is likely to reflect the Precambrian grain of the crystalline basement, and controlled the tectonic activity throughout the Cretaceous and Tertiary time (Brekke 2000). The JMFZ separates the Møre Basin to the south from the Vøring Basin to the north (Fig. 1.2), and also delimits the Trøndelag Platform to the south. Initiation of basin development can be traced back to Devonian – Early Carboniferous lithospheric stretching following the Caledonian Orogeny (Bukovics and Ziegler 1985). Intermittent rifting then began, starting in the Carboniferous and culminating in the Early Eocene with seafloor spreading in the Norway-Greenland Sea, and related thermal subsidence and volcanism (Brekke 2000). In-plate rifting in the Carboniferous was followed by a further phase in the late Mid-Jurassic to Early Cretaceous which saw the beginning of the evolution of the basins and their bounding features, with the base of the Cretaceous successions in both the Møre and Vøring

Basins strongly affected by block faulting (Bukovics and Zieger 1985). A final phase in the Late Cretaceous to Early Eocene is linked to relative motion along plate boundaries (Brekke 2000). Subsidence during the Cretaceous saw the basin flanks evolve by flexure as opposed to faulting, leading to the exceptionally thick basin fills of some 10 km (Bukovics and Ziegler 1985). Throughout this time in the Vøring Basin, early thermal subsidence was followed by tectonically driven subsidence and intermittent normal faulting, compression and folding (Brekke 2000). Tectonic activity during the Tertiary in the Vøring Basin was comprised of strike-slip compression coincident with the Alpine Orogeny in Late Eocene and Mid-Miocene times, leading to N-S trending dome structures (Fig. 1.2; Brekke 2000), which are known to be the sites of hydrocarbon accumulation (Bünz et al. 2005). There is evidence of the formation of a fossil Opal A-opal CT transition and extensive marine erosion in the Mid-Miocene and Late Pliocene times (Brekke 2000). The Møre Basin was generally tectonically quiet throughout the Cretaceous and Tertiary periods, experiencing mainly continuous subsidence (Brekke 2000).

The post-Cretaceous fill of the basins is made up of fine-grained hemipelagic oozes of the Palaeogene age Brygge Fm and Miocene – Early Pliocene Kai Fm, and contourites, hemipelagites and glacigenic sediments of the Plio-Pleistocene Naust Formation (Evans et al. 2002). The Naust Formation is divided into subunits to reflect glacial episodes which affected the margin from the Late Pliocene onwards, with ice-sheets first reaching the shelf break at c. 1.2 Ma (Berg et al. 2005). In the Vøring Basin in the north of the study area, the Naust Formation is subdivided into 8 units (A – H; Evans et al. 2002), and the succession is largely intact (Fig. 1.3A). In the Møre Basin in the south of the study area, the Naust Formation is subdivided into five main

sequences (W, U, S, R and O) and is heavily dissected by mass wasting events (Bryn et al. 2005a; Fig. 1.3A & B).

Mass wasting

The Holocene age Storegga Slide is one of the largest known submarine mass wasting events (Bryn et al. 2005a), and perhaps the most intensely studied. The Ormen Lange gas discovery, located beneath the steep headscarp region of the Storegga Slide, is the second-largest gas field in Norway (Bryn et al. 2005a). Following its discovery in 1997, an intensive phase of data acquisition and analysis began, to establish the reasons for the large scale mass wasting and assess the current conditions in order to safely develop the field. The Storegga Slide marked the end of repetitive large-scale mass wasting in the area beginning in Late Pliocene times (Evans et al. 2005), and occupies a large seabed depression, hereinafter referred to as the 'Storegga Slide Complex' (SSC) whose architecture reflects the historic instability of the area (Fig. 1.4).

Large-scale sliding in the region has been related to climatic variability following onset of regular shelf glaciations at 0.5 Ma (Bryn et al. 2005a). During peak glacial conditions, glacially-derived debris flows were deposited on the continental slope (Berg et al. 2005). Throughout comparatively longer periods of reduced ice cover, normal marine to distal glaciomarine sedimentation prevailed with contourites developing on the slope (Berg et al. 2005). Laterally extensive, sheet-like contourites form deposits up to 150 m thick throughout the Naust succession (Bryn et al. 2005b), and consist of clays with silty and sandy laminae (Berg et al. 2005). Contourite sediments are characterised by high water contents and the tendency to develop excess pore pressures when rapidly loaded by glacial debris flow deposits (Bryn et al. 2005b). Laterally continuous layers of increased sensitivity within contourite drifts

are thought to have served as the main glide planes for slope failures in the area, including the Storegga Slide (Bryn et al. 2005a). The Storegga Slide, dated at 8150 B.P. (Berg et al. 2005) removed some 3500 km^3 of material, affecting an area of c. 95,000 km^2 (Bryn et al. 2005a). A number of older mass wasting events have been identified within the SSC, with the greatest concentration occurring in the Mid-Pleistocene (Naust S and R; Evans et al. 2002).

The southern margin of the SSC juxtaposes deformed and dissected sediments with relatively undeformed strata preserved in the thick prograding sediment wedge overlying the Møre Basin, known as North Sea Fan (King et al. 1996). The North Sea Fan consists of massive glacigenic debris lobes, gravity flows and hemipelagic sediments (King et al. 1996; Nygård et al. 2005). The large volume of sediment is the result of deposition during the glacial cycles and input from the Norwegian channel, a deep trough skirting the whole of the south and west Norwegian coast, during the late Cenozoic (Evans et al. 1996; King et al. 1996; Nygård et al. 2005). Although predominantly depositional, the North Sea Fan succession records its own mass wasting which includes the well documented Møre and Tampen slides (Fig. 1.4), all of which pre-date the first Storegga Slide event (Evans et al. 1996; King et al. 1996; Evans et al. 2005). The Møre and Tampen slides cover significant areas (>15,000km^2) and displaced sediment volumes of greater than 3000 km^3 (Evans et al. 1996). The mid-Pleistocene Tampen Slide is disrupted and truncated to the east by Storegga Slide events (Fig. 1.4; Evans et al. 1996). A number of other pre-Holocene large-scale mass wasting events have been identified in and around the study area (Fig. 1.4; Evans et al. 1996; King et al. 1996; Evans et al. 2002).

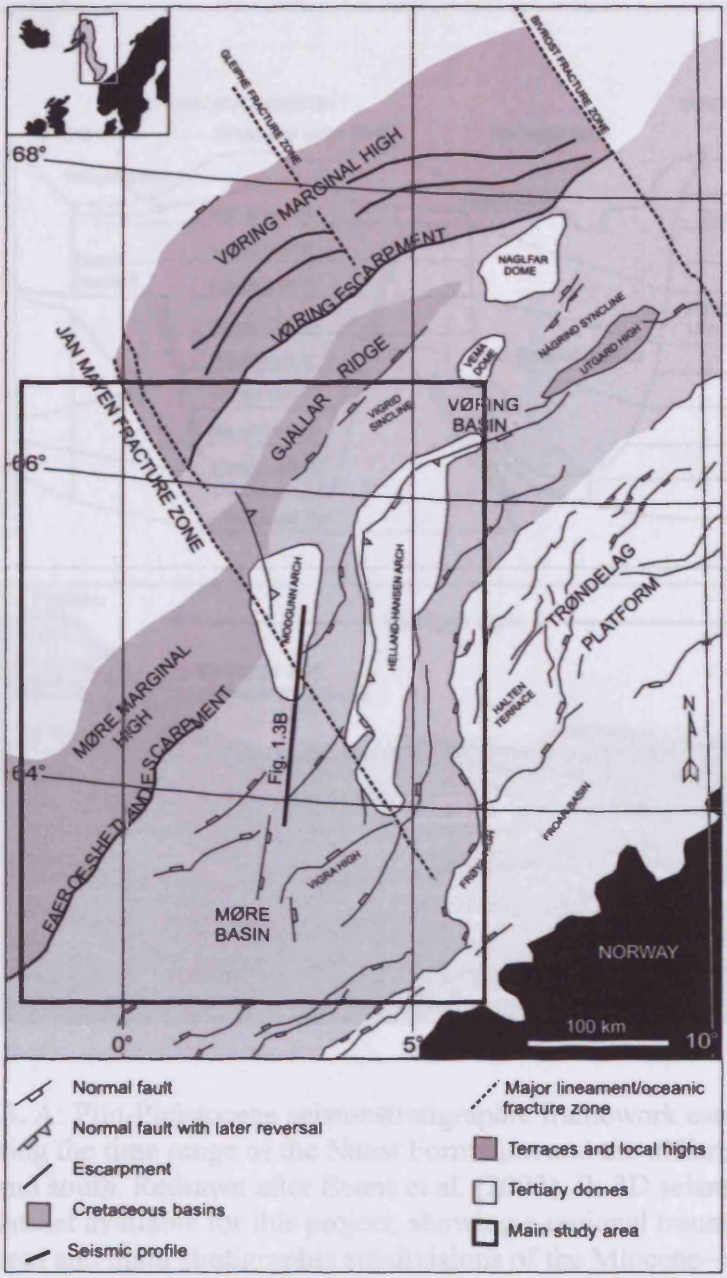

Figure. 1.2. Simplified structural map of the mid-Norwegian continental margin showing location of primary study area. Modified from Brekke 2000.

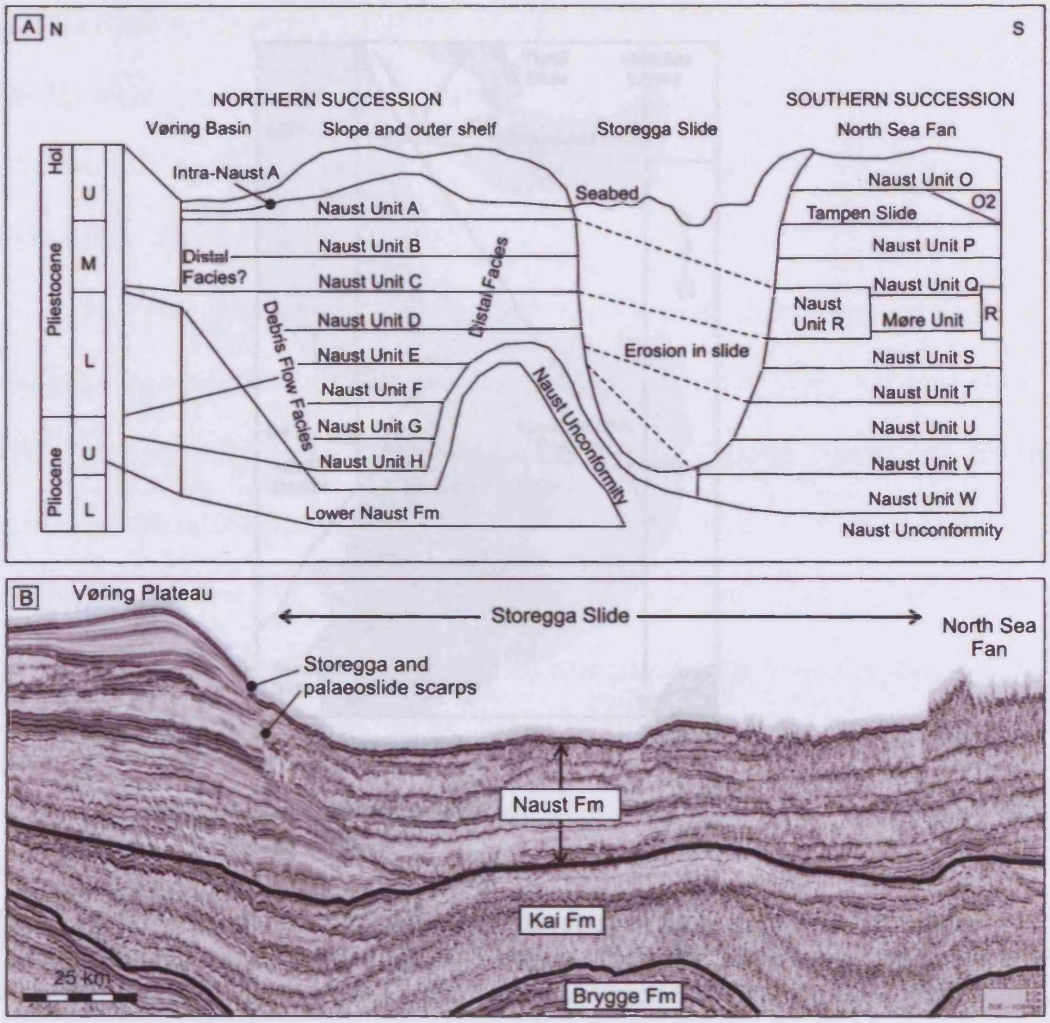

Figure. 1.3. A: Plio-Pleistocene seismostratigraphic framework established for the area, showing the time range of the Naust Formation and the differing subdivisions in the north and south. Redrawn after Evans et al. (2002). B: 2D seismic profile taken from the dataset available for this project, showing a regional transect across the Storegga area and main stratigraphic subdivisions of the Miocene–Pleistocene succession. Location shown in Fig. 1.2.

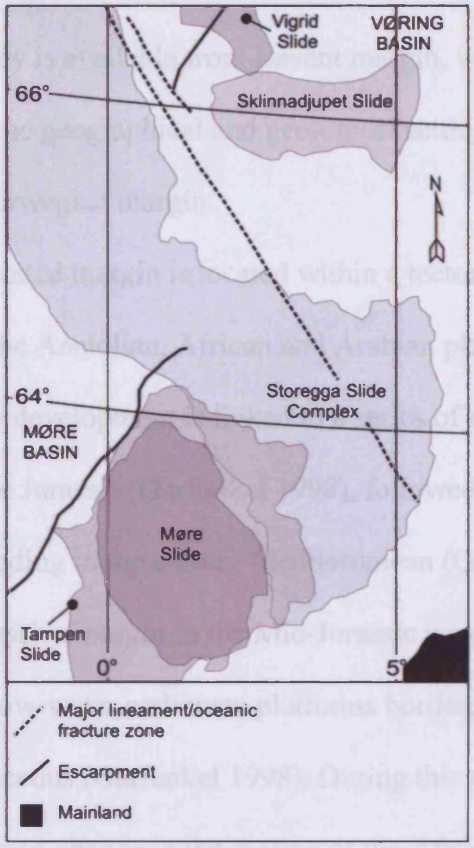

Figure. 1.4. Location and outlines of the Storegga Slide Complex, Møre Slide, Tampen Slide, Sklinnadjupet Slide, and Vigrid Slide. For further information on the Sklinnadjupet and Vigrid Slides, the reader is referred to Hjelstuen et al. 2007.

1.3.2 The Levant margin

One 3D seismic survey is available from Levant margin, which forms a secondary study area. As such, the geographical and geological setting is not discussed in as much detail as the Norwegian margin.

This non-glaciated margin is located within a tectonically active zone of interaction between the Anatolian, African and Arabian plates (Frey Martinez et al. 2005; Fig. 1.5). Early development is linked to a series of rifting events from the early Permian to the middle Jurassic (Garfunkel 1998), followed by continental break-up and initiation of spreading in the eastern Mediterranean (Garfunkel and Derin 1984). Establishment of a passive margin in the Mid-Jurassic was followed by the development of shallow-water carbonate platforms bordered by deepwater basins during the Late Cretaceous (Garfunkel 1998). During this time, a compressional stress regime was induced by a change in the motion of the African plate relative to the Eurasian plate, leading to the formation of the Syrian Arc system (Ben-Avraham 1989; Tibor and Ben-Avraham 1992; Eyal 1996). Opening of the Red Sea and initiation of the Dead Sea Transform began in the Miocene resulting in localised tectonic uplift and intermittent emergence of the shelf. The onset of the Messinian Salinity Crisis in the mid-Miocene interrupted normal marine sedimentation leading to the deposition of thick evaporates in deep basinal areas (Bertoni and Cartwright 2006). Major Pliocene transgression followed, leading to increased clastic input into rapidly increasing accommodation space (Buchbinder and Zilberman 1997), resulting in a strongly aggradational configuration with sigmoidal clinoforms linking shelf to slope (Frey Martinez et al. 2006). Beginning in the late Pliocene, large-scale slope instability and gravitational tectonics, detaching above or within the evaporites (Bertoni and Cartwright 2006) alternated with hemipelagic deposition, and has led to

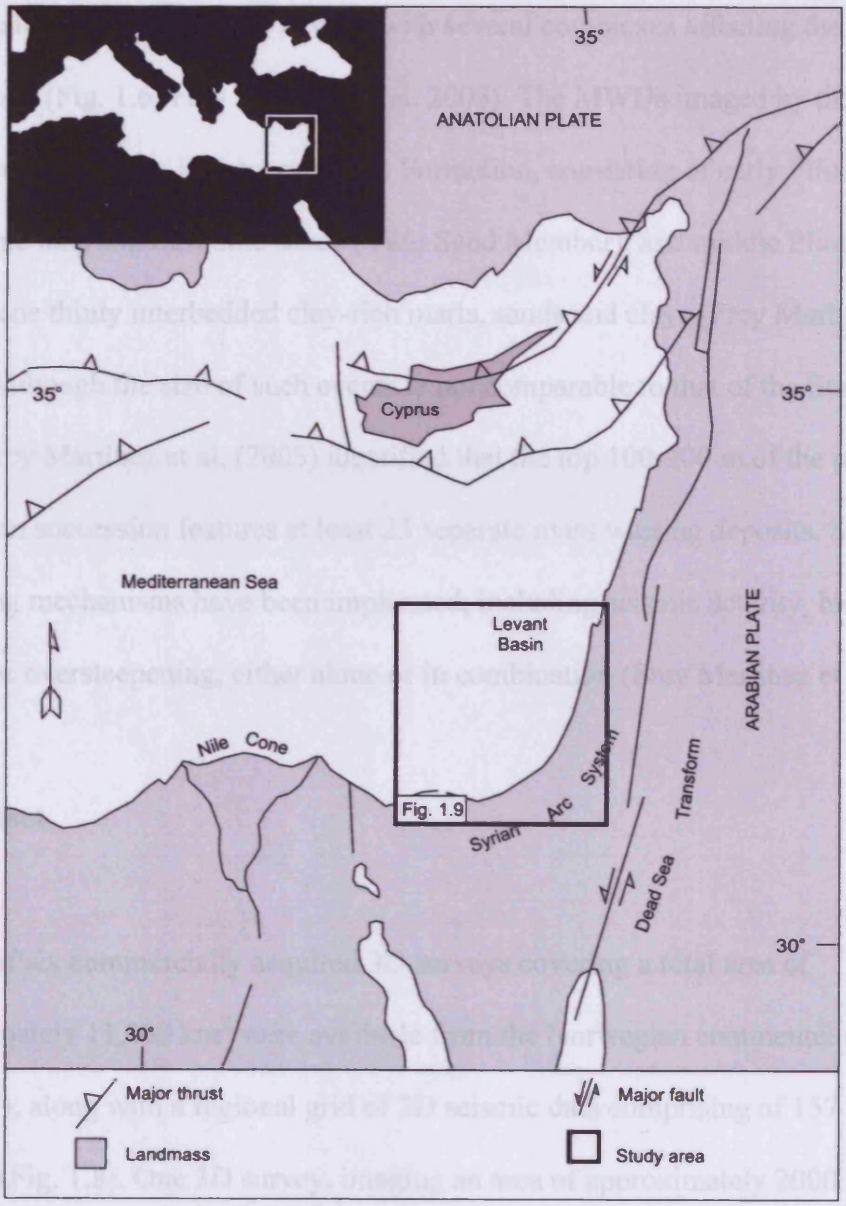

Figure. 1.5. Geological sketch of the Eastern Mediterranean area showing major structural elements. The box shows the location of the Levant margin study area and Figure. 1.9. Redrawn from Frey Martinez et al. 2005.

a succession featuring tens of MWDs with several complexes affecting the present day seabed (Fig. 1.6; Frey Martinez et al. 2005). The MWDs imaged by the available data occur in the Plio-Pleistocene Yafo Formation, consisting of early Pliocene submarine fans and turbiditic sands (Yafo Sand Member), and middle Pliocene-Pleistocene thinly interbedded clay-rich marls, sands and clays (Frey Martinez et al. 2006). Although the size of such events is not comparable to that of the Storegga Slide, Frey Martinez et al. (2005) identified that the top 100-200 m of the post-Messinian succession features at least 25 separate mass wasting deposits. Several triggering mechanisms have been implicated, including seismic activity, biogenic gas and slope oversteepening, either alone or in combination (Frey Martinez et al. 2005).

1.4 Dataset

A total of six commercially acquired 3D surveys covering a total area of approximately 11,000 km^2 were available from the Norwegian continental margin (Fig. 1.7), along with a regional grid of 2D seismic data comprising of 157 separate profiles (Fig. 1.8). One 3D survey, imaging an area of approximately 2000 km^2 was available from the Levant margin (Fig. 1.9). All of the 3D surveys are time-migrated and have been processed to near zero phase characteristics, meaning that the geophysical interface that has produced the reflection is located at the positive amplitude peak or negative amplitude trough of the wavelet (Fig. 1.10; Simm and White 2002). The zero phase nature of these data was determined by studying the geophysical response of the seabed in the various surveys (Fig. 1.10). The principal attributes of the data are shown in Table 1.1. The dominant frequency of the seismic data varies from survey to survey and with depth as P and S wave velocity tends to

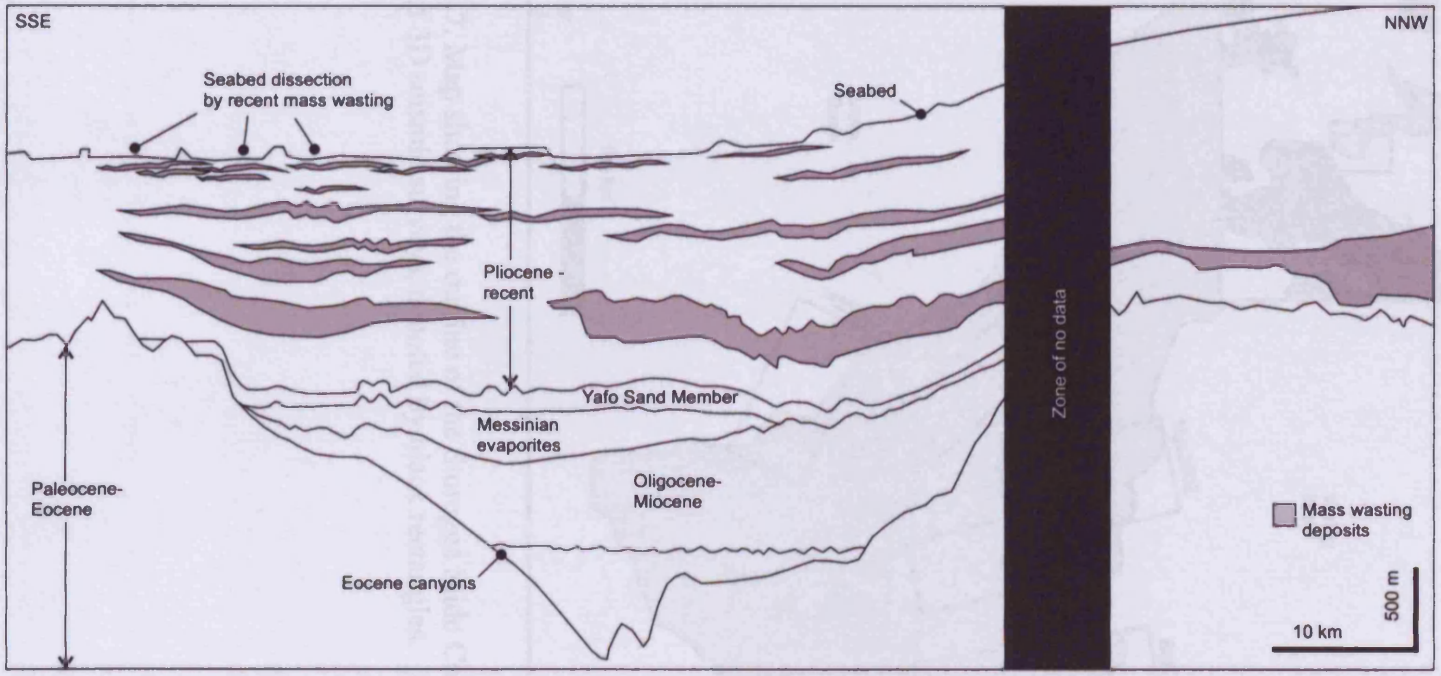

Figure 1.6. Interpreted cross section from the Levant 3D survey area. Location shown in Figure 1.9. Redrawn from Frey Martinez et al. 2005.

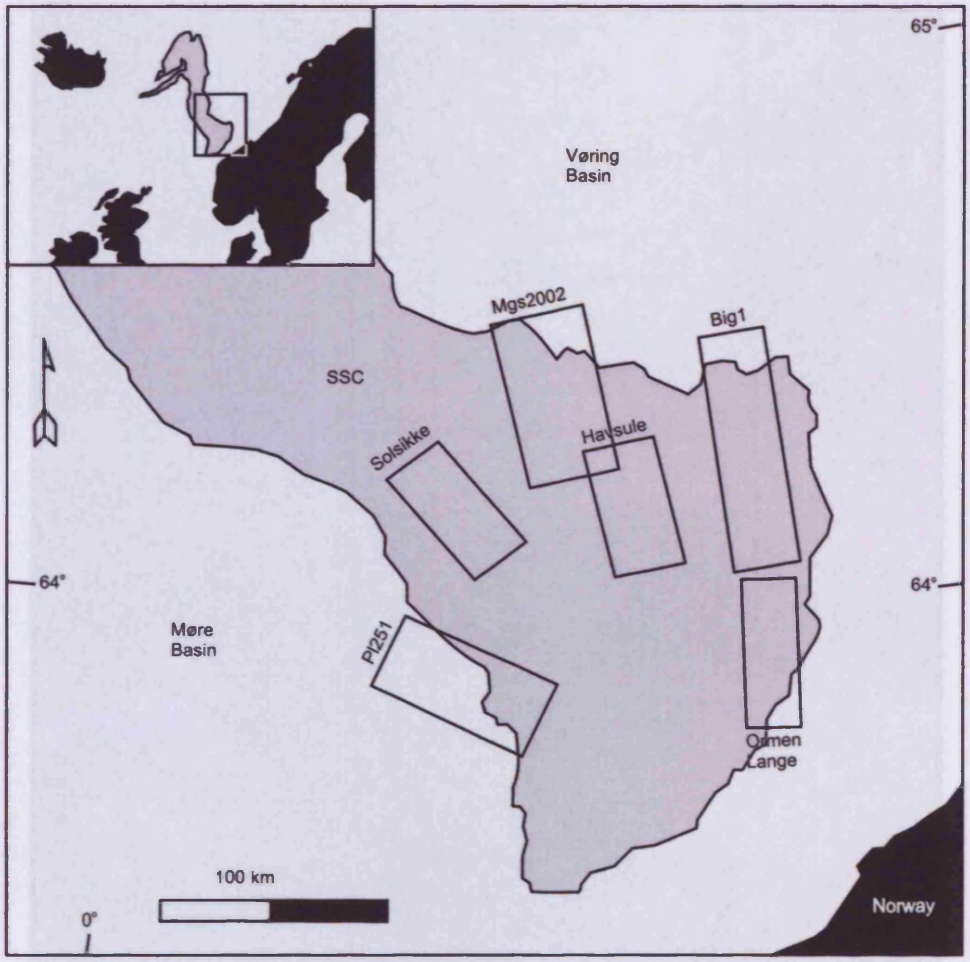

Figure. 1.7. Map showing the outline of the Storegga Slide Complex (SSC) and location of 3D seismic surveys, denoted by black rectangles.

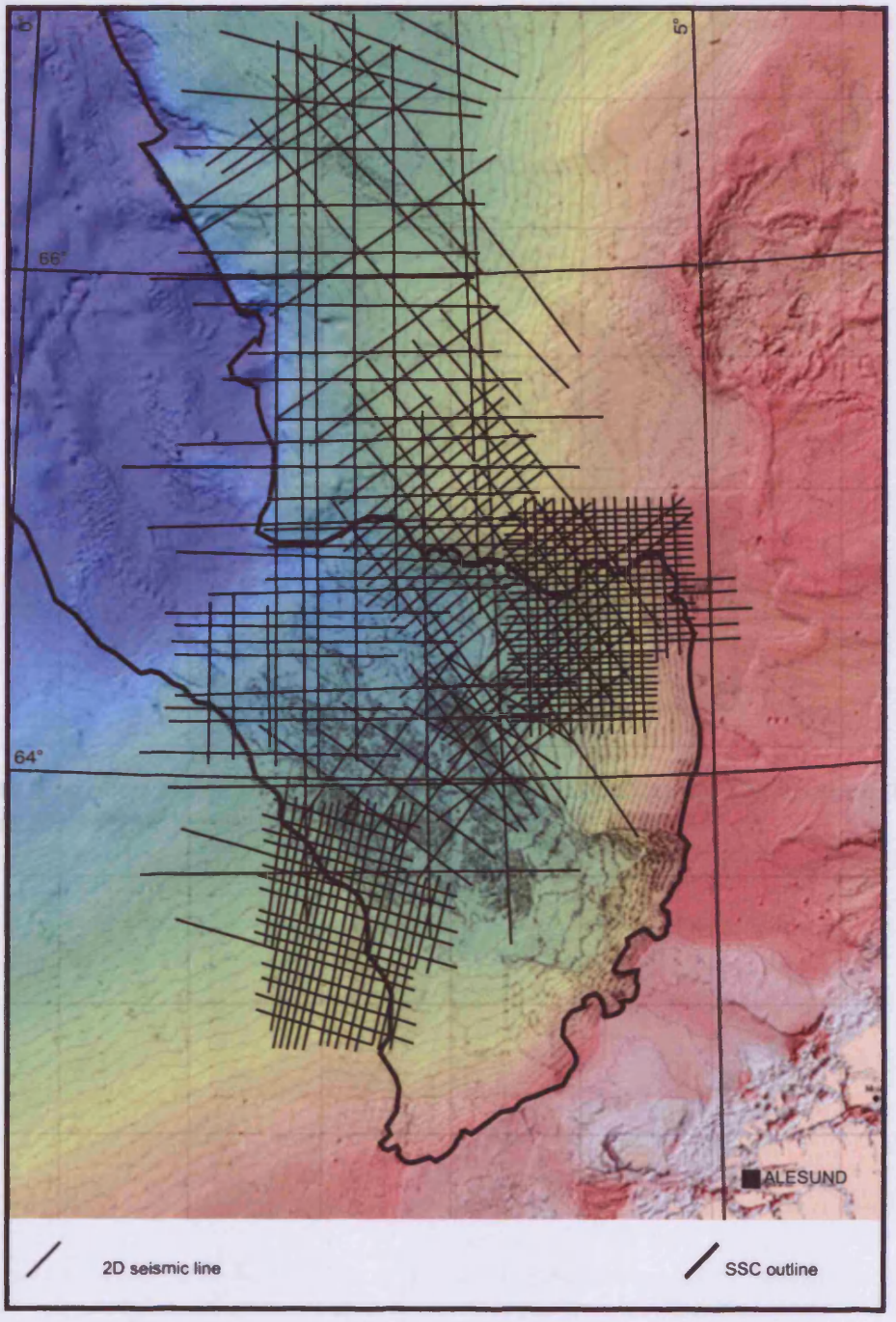

Figure. 1.8. Bathymetry data over the primary study area, showing outline of the Storegga Slide Complex and location of 2D seismic profiles.

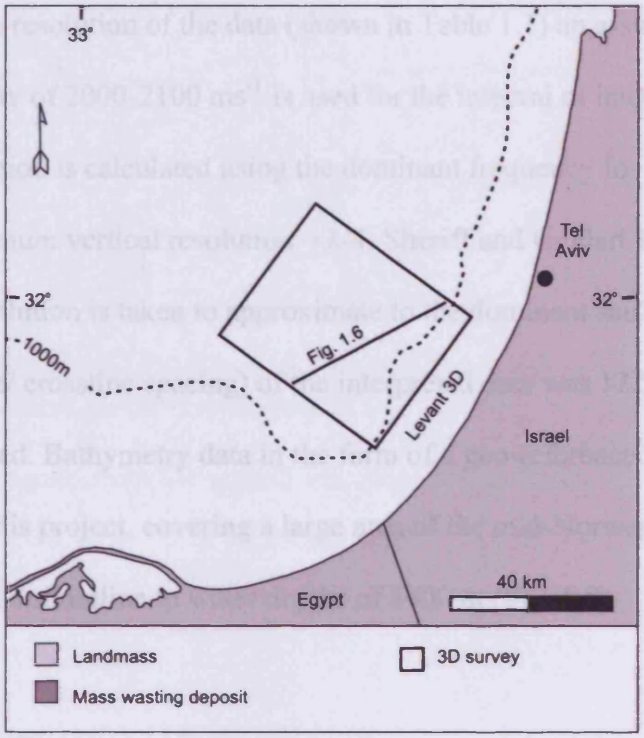

Figure 1.9. Location map for the Levant margin study area showing location of the Levant 3D seismic survey and Figure 1.6.

increase with depth due to compaction and diagenesis (Brown 2003). When calculating the resolution of the data (shown in Table 1.1) an assumed average seismic velocity of 2000-2100 ms^{-1} is used for the interval of interest. Maximum vertical resolution is calculated using the dominant frequency for the interval of interest (maximum vertical resolution = $\lambda/4$; Sheriff and Geldart 1983), and the horizontal resolution is taken to approximate to the dominant seismic wavelength. The bin size (inline/ crossline spacing) of the interpreted data was 12.5 x 12.5 for all of the 3D surveys used. Bathymetry data in the form of a geo-referenced TIFF file was available for this project, covering a large area of the mid-Norwegian continental margin from the shoreline to water depths of 3400 m (Fig. 1.8).

1.5 Methodology

Central to the recognition of MWDs in seismic data is the identification of a disrupted or chaotic seismic facies unit representing the failed mass, underlain by a basal shear surface and overlain by a surface at the upper limit of the disrupted facies (Fig. 1.11; Embley and Jacobi 1977; Moore et al. 1976; Woodcock 1979; Trincardi and Normark 1989; O'Leary 1993; Martinsen 1994; Hampton et al. 1996; Frey-Martinez et al. 2005). Failed material is translated over the basal shear surface, which is usually conspicuous in seismic data, forming a laterally continuous, often bed-parallel undeformed reflection occurring beneath the deformed translated material (Frey-Martinez et al. 2005). The limit of the upslope occurrence of the MWD is marked by a headwall scarp, which occurs where the basal shear surface steepens and cuts through increasingly shallower stratigraphy to intersect the surface (Williams and Chapman 1983; Farrell 1984; Trincardi and Argnani 1990; Martinsen 1994). This occurs due to

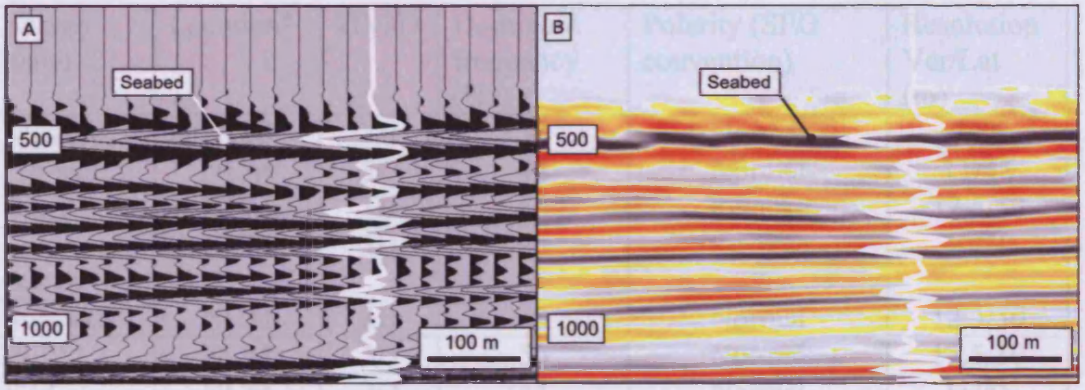

Figure 1.10. 3D seismic data phase. A: Variable area; and B: variable intensity seismic section through the seabed from PL251 survey showing the near zero-phase character of the seabed reflection. An individual trace is shown in white on both parts to emphasize waveform of the seabed and deeper reflections.

Survey name	Location*	2D/3D	Dominant frequency (Hz)	Polarity (SEG convention)	Resolution Ver/Lat (m)
Mgs2002	NCM	3D	55	Normal	9/36
Havsule	NCM	3D	44	Normal	11/45
Big 1	NCM	3D	50	Reverse	12.5/50
Ormen Lange	NCM	3D	46	Reverse	10/40
Solsikke	NCM	3D	50	Normal	12.5/50
PL251	NCM	3D	50	Normal	12.5/50
E2d	NCM	2D	44	Normal	11/45
Levant 3D	LM	3D	50	Normal	10/40

*NCM: Norwegian continental margin; LM: Levant margin

Table 1.1. Summary table showing some principal attributes of seismic reflection data used in this project.

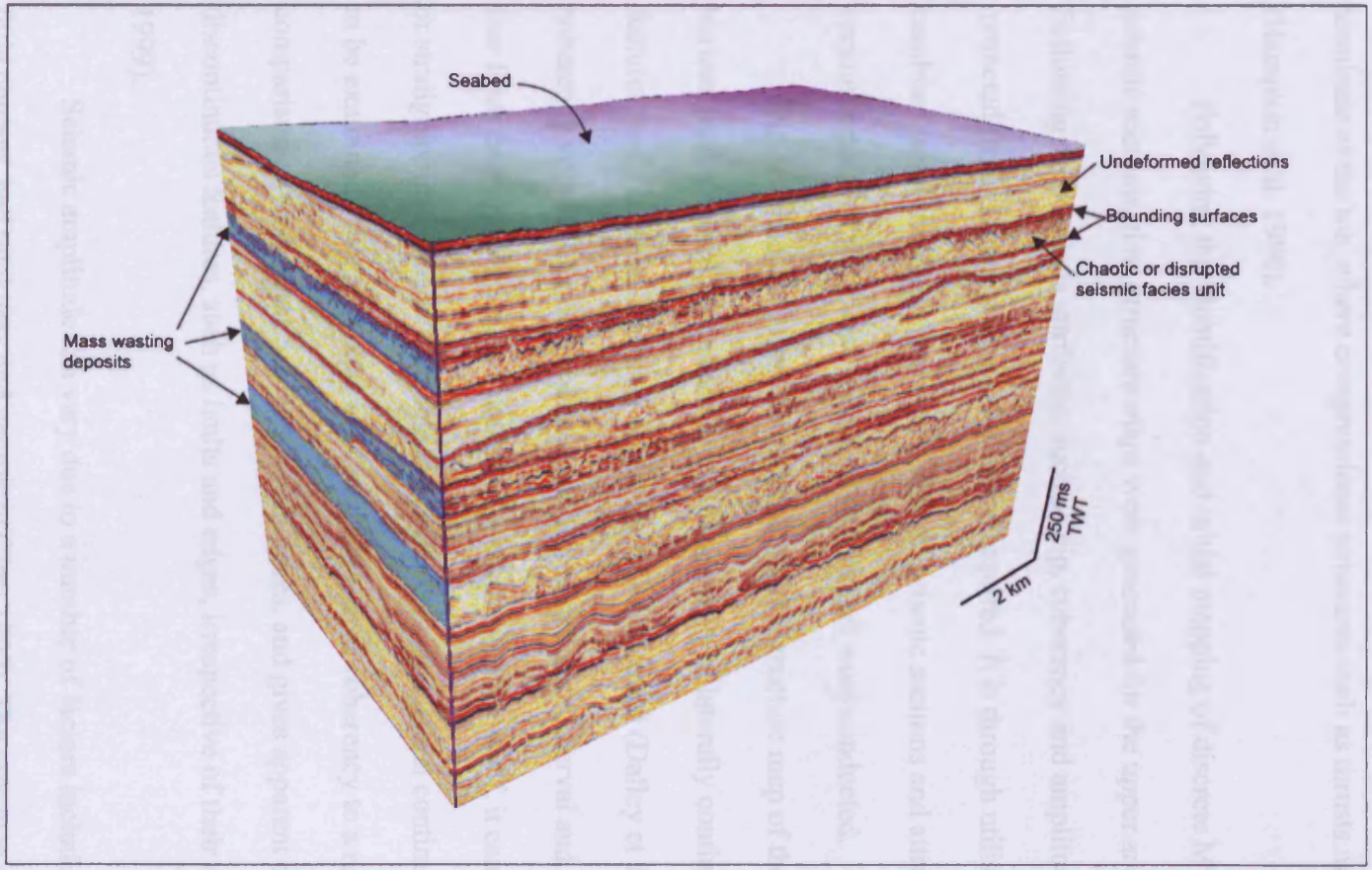

Figure. 1.11. 3D seismic visualization of example seismic sections and seabed horizon from the PL251 survey to illustrate the character of mass wasting deposits as seen from seismic data. The mass wasting deposits present within the succession are highlighted in blue on the left of the Figure.

lithological, strength or pore pressure contrasts (Martinsen 1994), and often at roughly the point of maximum slope inclination (Lastras et al. 2006). Downslope, MWDs terminate at the toe, where compressional structures such as thrusts may occur (Hampton et al. 1996).

Following the identification and initial mapping of discrete MWDs in vertical seismic sections, time structure maps were generated for the upper and lower surfaces. Following this, various attributes, such as dip, coherency and amplitude, were extracted from representative areas where required. It is through utilising a combination of time structure maps, vertical seismic sections and attributes, that the various aspects of the investigations of this project were conducted.

Dip is calculated from the interpreted time structure map of the chosen horizon, and is useful for enhancing the appearance of laterally continuous geological features, such as faults, that may otherwise be overlooked (Dalley et al. 1989). A coherency volume may be generated for a specified time interval and area, and so is free from interpretation bias. Like the 3D seismic volume itself, it can be horizontally or stratigraphically sliced to enable the areal extent and lateral continuity of features to be examined. This technique allocates a degree of coherency to a region based on comparison of waveforms across adjacent traces, and gives apparent continuity to discontinuous features, such as faults and edges, irrespective of their orientation (Hart 1999).

Seismic amplitude can vary due to a number of factors including porosity, fluid content, bed thickness and geometry (Hart 1999). The presence of structures, sedimentological features and lithological changes may therefore cause organised amplitude patterns, such as linear or areal trends or polarity changes (Enachescu 1993). Following the mapping of a particular horizon, amplitude can be extracted

along it and displayed as a continuous horizon map. Amplitude can also be extracted from a specified time interval or window above, below or around a particular horizon. Amplitudes are added, regardless of their polarity, and a cumulative amplitude for the whole window is arrived at (Brown 1999), providing more information for the specified interval which can be interpreted in a morphological sense. To illustrate the use of each attribute, examples of each are shown along with a time structure map over the same area in Figure 1.12.

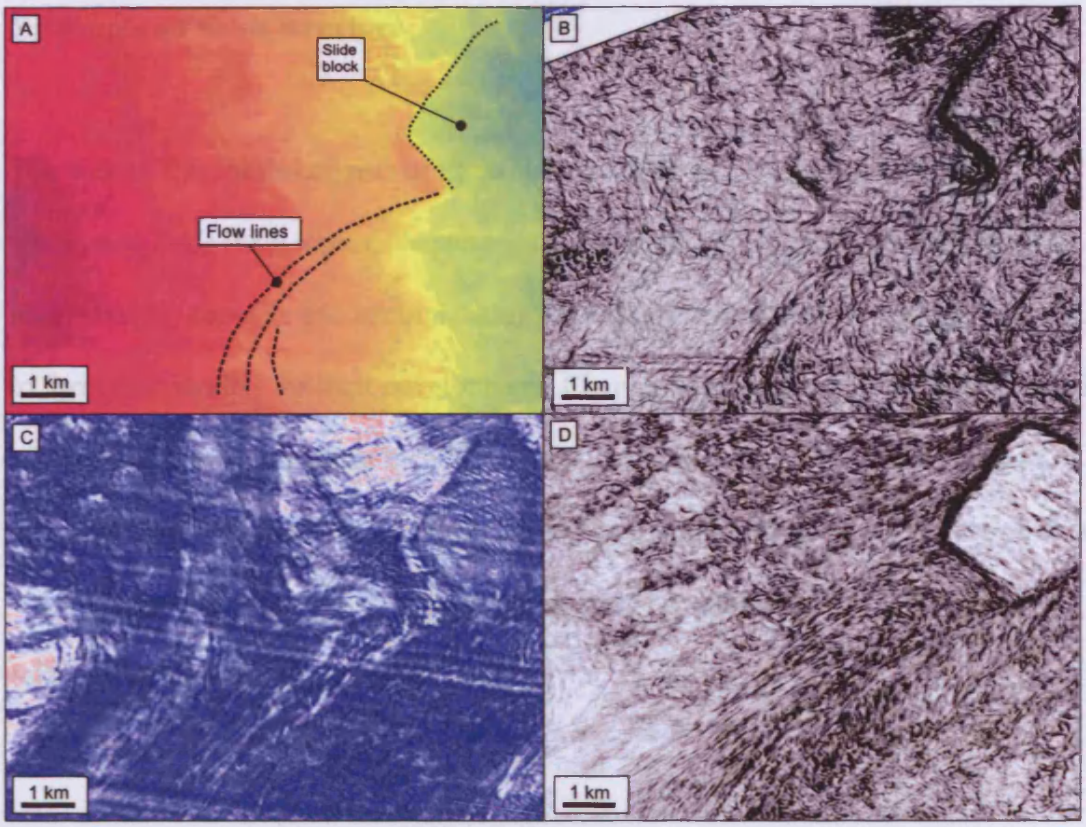

Figure. 1.12. Comparison of examples of 3D seismic interpretation techniques. Each figure part shows the same sub area of the top surface of a buried MWD from the PL251 survey area which reveals an intact slide block and apparent flow lines: A: Time structure map; B: Dip attribute map; C: Seismic amplitude map; and D: Slice through a coherency volume generated for the same area.

1.6 A note on thesis structure

The core of this thesis consists of three chapters (chapters two, three and four) addressing three main topics: chapters two and four describe specific examples of mass wasting deposits and attempt, using the observed architectures and deformation, to formulate models for their development. Chapter three presents a compilation of all of the deformational features identified throughout the duration of the study, and describes how they may be identified, defined and utilised in the study of further mass wasting deposits. Chapters five and six discuss and conclude, respectively, the main scientific results of this project.

CHAPTER TWO

2.0 A subsurface evacuation model for submarine mass wasting

2.1 Summary

Analysis of three-dimensional (3D) seismic data from the Norwegian continental margin provides an insight into an unusual, buried submarine mass wasting deposit (MWD) which occurred adjacent to the later Holocene-age Storegga slide. The identified MWD, informally named the 'South Vøring Slide', occurs in fine-grained hemipelagic and contourite sediments on a slope of 0.5°, and is characterised by a deformed seismic facies unit consisting of closely spaced pyramidal blocks and ridges bound by small normal faults striking perpendicular to the slope. The South Vøring Slide contrasts with other previously described submarine MWDs in that it cannot be explained by a retrogressive model. The defining characteristic is the high relative volume loss, with the area affected by sliding having thinned by some 40%, seen in combination with very modest extension in the translation direction, with line length balancing yielding an extension value of only 4.5%. The volume loss is explained by the mobilisation of an approximately 40 m thick interval at the lower part of the unit and its removal from beneath a thin overburden, which subsequently underwent extensional fragmentation. Evidence for the mobilisation of a thick fine-grained interval in the development of a submarine MWD from a continental margin setting may have implications for the origins of other large-scale MWDs on the Norwegian margin and other glacially influenced margins worldwide.

2.1 Rationale

One of the points highlighted in chapter one, section 1.1, was the need to better understand the processes involved in the early evolution of submarine mass wasting events. Since further characterisation studies have been identified as a way to progress our understanding, one of the initial stages of this project was to undertake regional mapping in the primary study area, the Norwegian continental margin. Many submarine MWDs were identified and mapped as a result (a list of seismic horizons and a compilation of maps generated for the bounding surfaces of the various MWDs are presented in Appendix I and II). Of particular use in the continued investigation of MWDs is the examination of examples which deviate from typical models, as they may provide potential end-member models to fully define the spectrum of deformation possible in such deposits. Initial reconnaissance mapping identified such a non-typical example from the Norwegian continental margin, which on first inspection did not appear to conform to the typical model previously invoked to explain many of the MWDs in the area. Further investigation was therefore deemed appropriate as it may help to establish the more uncommon aspects of submarine mass wasting formation and evolution.

The aim of this chapter therefore, is to use 3D seismic reflection data to describe a submarine MWD from the Norwegian continental slope that contrasts markedly with previously described examples in both gross morphology and process of origin. The MWD described in this chapter differs from the classical models in a number of critical features. Firstly, it is characterised by extension throughout the body with no evidence of compressional strain towards the downslope limits. Secondly, a significant fraction of the initial pre-failure slope sediments have been

almost completely removed from the succession, resulting in significant volume loss that is not balanced by a zone of accumulation that can be correlated with the main body of the MWD. Finally, the base of the MWD is not defined by a discrete surface that developed due to progressive shear failure. Further sections within this chapter will firstly characterise and describe the MWD, and propose a mechanism for its development.

2.3 Specific study area and dataset

This study focuses on a deformed unit situated on the northern flank of the Storegga Slide (Fig. 2.1). The primary source of data for this study is the 3D survey Mgs2002 (Fig. 2.2), which images an area measuring 2670 km^2. The main focus of the chapter is the detailed mapping and analysis of a sub-area of a deformed unit where it is imaged by the 3D survey, with supplementary data taken from the regional 2D grid (Fig. 1.8) and a geotechnical borehole (6404/5-GB1; Fig. 2.1). Further information regarding the characteristics of the seismic data can be found in chapter one, section 1.4.

2.4 3D seismic interpretation

The deformed unit on which this study focuses (labelled in Fig. 2.2) occurs within Naust subdivision B on the southern outer slope of the Vøring Plateau (Figs. 2.1 and 2.2). Naust B, deposited between 330-200 ka, is composed of thin, well stratified interglacial hemipelagites and contourites on the outer slope (Fig. 2.2; Berg et al. 2005). The sediments are characterised by low amplitude, continuous seismic facies

developed in parallel reflection configurations (Fig. 2.2), which define downslope-thinning packages when mapped in 3D. Upslope on the plateau itself, Naust B is comprised of seismically massive, lens-shaped bodies interpreted as glacial debris flow deposits (GDFs of Hjelstuen et al. 2004), which interfinger with the hemipelagites and contourites on the outer slope (Fig. 2.2). The predominant lithology of Naust B is silt-rich clay, with a high water content, and decreasing silt content towards the top of the unit (Berg et al. 2005; Hjelstuen et al. 2005).

The deformed unit is buried at a depth of approx 200 m below the seabed (based on an assumed seismic velocity of 2000 ms^{-1} for the shallow succession) by Naust subdivision A, which represents the last 250 ka of sedimentation (Hjelstuen et al. 2004). A laterally continuous bottom simulating reflector (BSR; labelled in Fig. 2.2, 2.3A and 3.3C) underlies a large portion of the northern margin of the Storegga Slide (Bünz et al. 2005), and is present below the upslope region of the deformed unit (Fig. 2.2). It has been shown by previous studies that the BSR is due to the presence of gas hydrates (Berndt et al. 2004), which may have played a minor role in the more recent large-scale sliding on the margin (Bryn et al. 2005a).

The top and base of the deformed unit are both defined by high amplitude positive reflections (coloured red and labelled 'Horizon X' and 'Horizon Y' respectively on Fig. 2.3B). Horizon X is distinctive in that it exhibits a highly disrupted, 'crinkled' character (Fig. 2.3B). Detailed study of this horizon reveals that its appearance is due to the presence of numerous, laterally equivalent inclined segments, separated by abrupt terminations. The inclined segments dip at up to 30°, and form positive relief of up to 12 m. Inclined segments often share a common sense and magnitude of dip as individual 'rafts' of reflections within the interior of the Unit

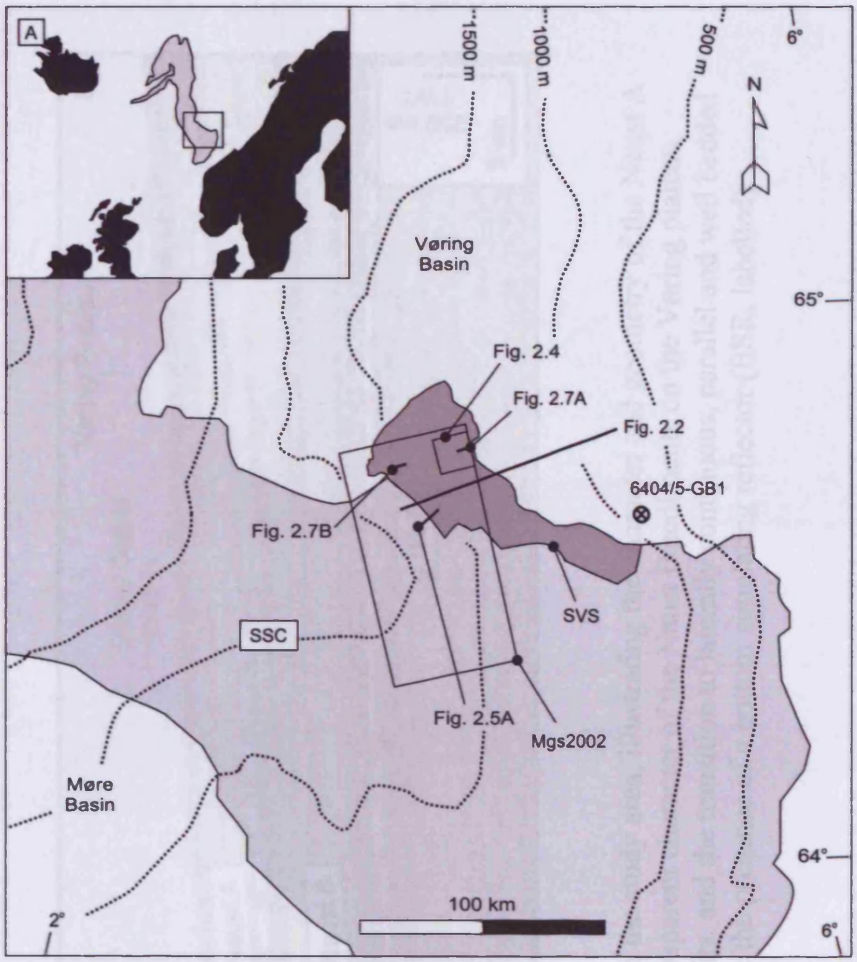

Figure 2.1. Location map showing the specific study area, extent of the South Vøring Slide (SVS), and locations of the 3D survey Mgs2002, geotechnical borehole 6404/5-GB1, and figures. SSC: Storegga Slide complex.

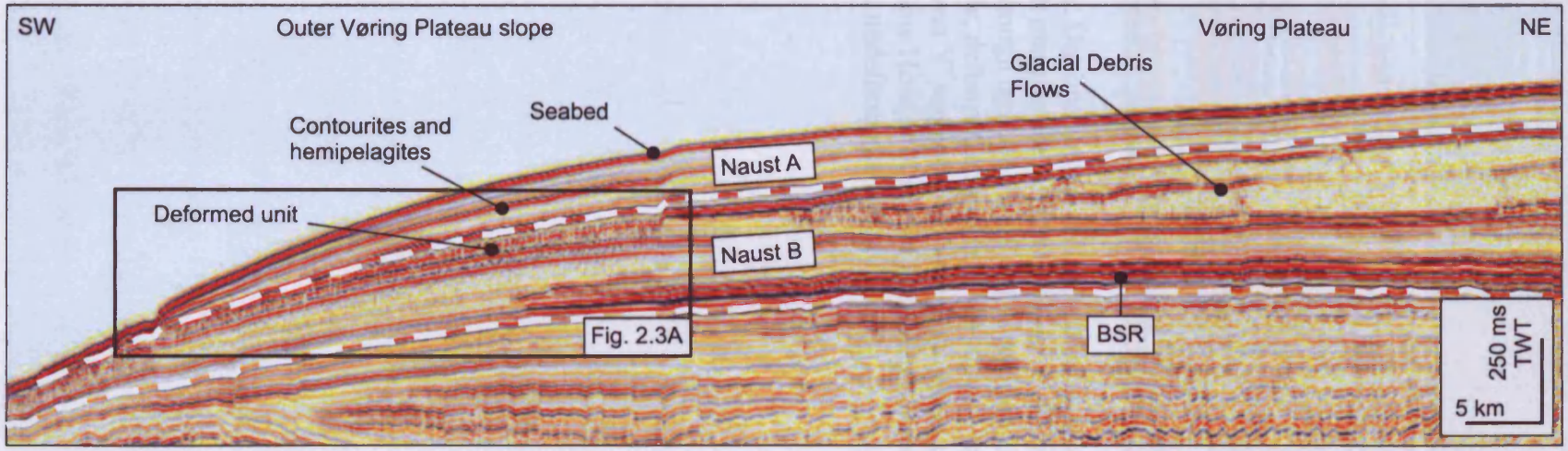

Figure 2.2. 2D seismic line showing a SW-NE transect across the study area, illustrating the character and geometry of the Naust A and Naust B sediments. Note the seismically massive and transparent character of the Naust B sediments on the Vøring plateau, where they are comprised of glacial debris flow (GDF) deposits, and the transition to laterally continuous, parallel and well bedded contourite sheet deposits on the outer plateau slope. Also note the presence of a bottom simulating reflector (BSR, labelled) underlying Naust B. Location shown in Fig. 2.1.

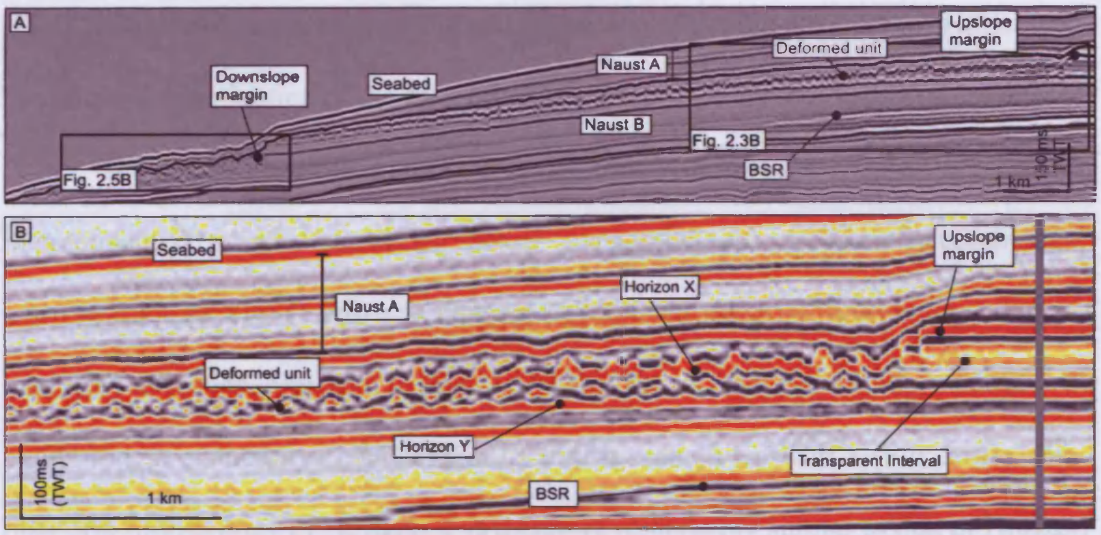

Figure 2.3. A: Dip line showing the up- and downslope margins of the deformed unit. Note that both margins are infilled by Naust A sediments. Location shown in Fig. 2.2. B: Dip line through upslope region of the deformed unit showing upslope margin and high amplitude, deformed character of the top and basal reflections, labelled 'Horizon X' and 'Horizon Y' respectively. Note the thickness change across the upslope margin, and how Horizon X is readily correlated from the upslope deformed region updip into the undeformed slope sediments.

(Fig. 2.3B). Time structure mapping and extraction of the dip attribute for Horizon X has allowed examination of the top Unit surface morphology in detail (Fig. 2.4A).

The inclined segments and intervening terminations form an unusual pattern of interconnected 'troughs' separating 'peaks' and sometimes more laterally continuous, narrow structural highs to give an unusual ribbed or 'fingerprint' morphology. The base Unit reflection, Horizon Y, (Fig. 2.3B) also shows evidence of deformation, exhibiting an undulatory character similar to that seen on Horizon X (Fig. 2.4B). The planform morphology of Horizon Y is therefore remarkably similar to that of Horizon X, although Horizon Y is not affected by faults and the deformation it exhibits appears closer to ductile folding than brittle fracture (Fig. 2.4B).

Correlation of Horizon X and Y reveals that the Unit forms a downslope tapering wedge across a slope of 0.5° inclination, characterised internally by inclined, discontinuous 'rafts' of reflections (Fig. 2.3A). Regional 2D seismic lines were used to establish the position of the edges of the Unit and show it to exhibit an almost elliptical planform geometry covering an area measuring approximately 850 km^2 (Fig. 2.1). The Unit has a maximum thickness in its upslope region of 65 m, and thins to approximately 35 m downslope (Fig. 2.3A). At its upslope margin, deformed slope sediments are juxtaposed against updip undeformed slope sediments (Fig. 2.3A and 3B), and a key observation is that it is possible to correlate Horizon X updip into the undeformed slope section (Fig. 2.3B). At this point a marked thickness change occurs, with Horizon X being observed to ramp up through the interval at an angle of c. 18° in the landward direction, by c. 40 m. Landward of this feature, Horizon X is continuous and parallel to the dip of the slope (Fig. 2.3B). A sharp topographic break with onlap is observed directly above this position in Naust A (right hand margin of Fig. 2.3B).

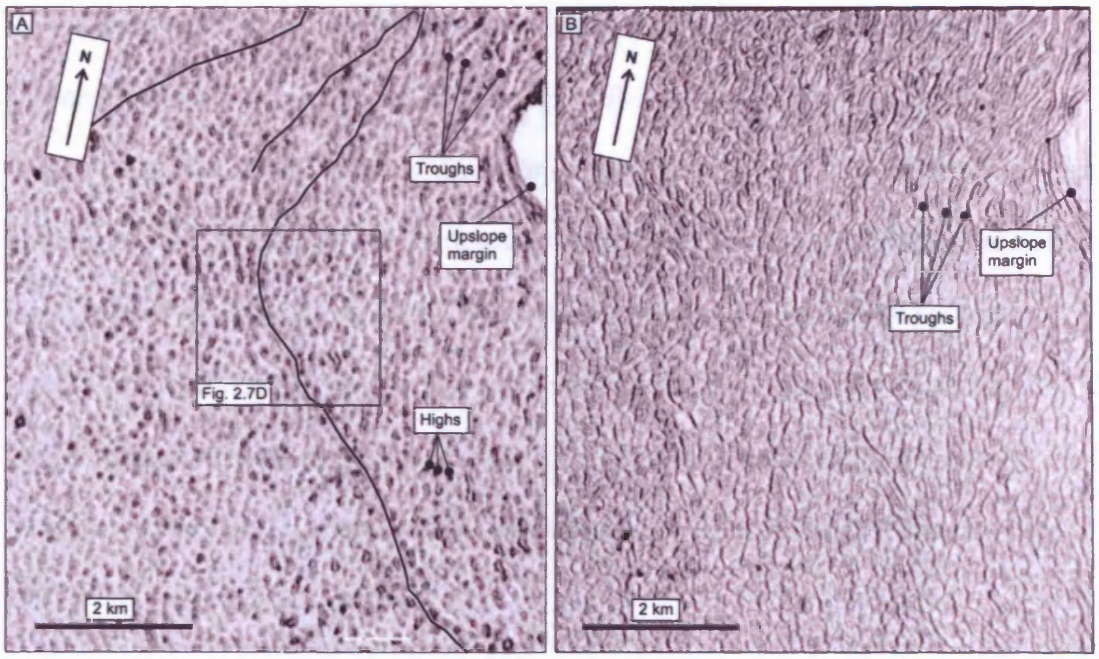

Figure 2.4. Dip-attribute map of Horizon X showing the morphology which characterises the top of the deformed unit. The pattern is comprised by laterally continuous 'troughs' (continuous troughs linked by black continuous lines), shown on the dip-map by areas of lighter shading, which separated less continuous 'highs', shown on the dip-map by the darker areas (both labelled). Similar features are described by Micallef et al. (2007) from the north-eastern headwall area of the Storegga Slide. B: Dip-attribute map of Horizon Y showing similar ribbed morphology. Location shown in Fig. 2.1.

Downslope, the Unit terminates above the updip margin of a further seismic facies unit characterized by contorted and disrupted reflections, with discrete blocks of intact and rotated, but laterally discontinuous reflections (Fig. 2.5). The base of this downslope unit (Fig. 2.5A) occurs at a stratigraphically lower level than the base of the deformed Unit, by some 200 m. The Unit is overlain and infilled by younger Naust B sediments, which are in turn succeeded by those of Naust A (Fig. 2.3A). Downslope correlation of these packages shows that the downslope unit is also overlain and infilled by lateral and therefore age-equivalent Naust B sediments (Fig. 2.3A).

2.5 Interpretation

Using established recognition criteria (Embley and Jacobi 1977; Moore et al. 1976; Woodcock 1979; Trincardi and Normark 1989; O'Leary 1993; Martinsen 1994; Hampton et al. 1996; Frey Martinez et al. 2005), the deformed unit is interpreted as a submarine MWD which we name the 'South Vøring Slide' (SVS) from its location on the outer slope of the Vøring Plateau (Fig. 2.1). It should be noted however, that use of the term 'slide' is for ease of reference and should not be taken to imply a dominant mass wasting process. This interpretation is based on: (1) the correlation of distinctive top and basal surfaces (Horizons X and Y) bounding a chaotic seismic facies unit which contrasts significantly with the more continuous, undisrupted reflections characteristic of the sedimentary units above and below; (2) the abrupt transition from undeformed sediments updip, to downdip deformed sediments; (3) the abrupt thickness change at the steep ramp which forms the upslope margin is interpreted as a headscarp, and upslope of which is preserved the intact, pre-failure stratigraphy

(undeformed slope template, labelled on Fig. 2.6A); (4) the alignment of rotated faults blocks orthogonal to the direction of slope; (5) its planform geometry, and (6) its context and location in close vicinity to other slope failures (see chapter one, section 1.3.1 of this thesis for information on the mass wasting in the study area). This interpretation is summarised in Figure 2.6A.

Within the SVS, the abrupt reflection terminations and offsets bounding each of the inclined segments which make up the remarkable 'crenulate' character of Horizon X are interpreted as normal faults (Fig. 2.3A, 2.7A & 2.7B). These tip out at the base of the SVS, and delimit inclined horizon segments that define individual fault blocks (Fig. 2.5A). Examination of seismic sections from both the upslope and downslope limits of the SVS (Fig. 2.7A & B) reveal that the entire SVS is affected by these extensional faults, with fault density only slightly decreasing towards the downslope termination. Strain analysis of the faults was based on line balancing of 4 representative dip-lines taken across the SVS (summation of heaves assuming no volume change or ductile deformation of the fault blocks), along with over 40 measurements of strike, dip and throw. The predominant strike of the faults is NW – SE, normal to the local slope direction (Fig. 2.7D). Maximum fault throws and dips were used to calculate an extension value of 4.5 %, and a net extension of 1.25 km in the downdip cumulative slip direction measured from average heave vectors (assuming dip slip on individual fault planes).

To quantify the degree of thinning observed in the extended region of the SVS, comparisons were made between the SVS and the c. 90 m thick undeformed slope sediments preserved updip of the headscarp (Fig. 2.6A). From measurements made on isopach maps of the deformed interval, and by comparing the thickness change observed across the headscarp into the undeformed upslope template with

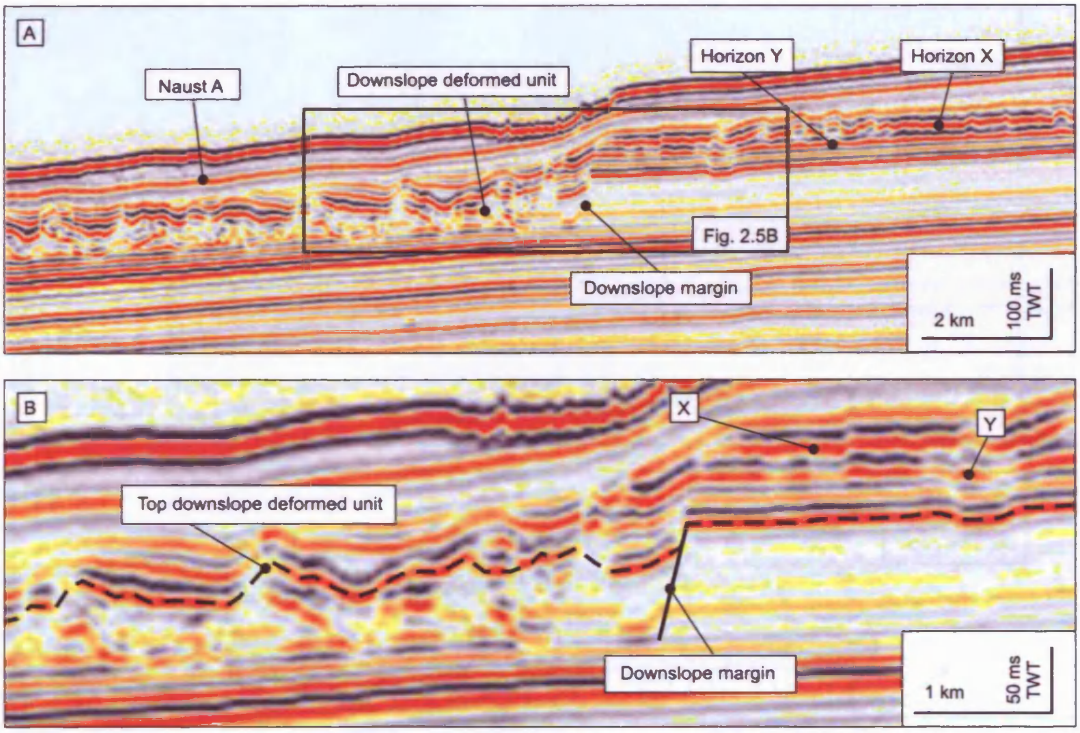

Figure 2.5. A: Seismic section showing the downslope margin of the deformed unit, where it terminates above an abrupt change from undeformed slope sediments to a further, downslope deformed seismic facies unit (labelled), characterised by contorted and disrupted reflections with discrete blocks of intact and rotated, but laterally discontinuous reflections. Note the positions of Horizons X and Y. Location shown in Fig. 2.1. B: Zoomed in section showing in more detail the relationship between the deformed unit and the downslope deformed unit. It is possible to correlate Horizons Y (coloured purple) into the downslope deformed unit. Location shown in (A), and Fig. 2.3A for context.

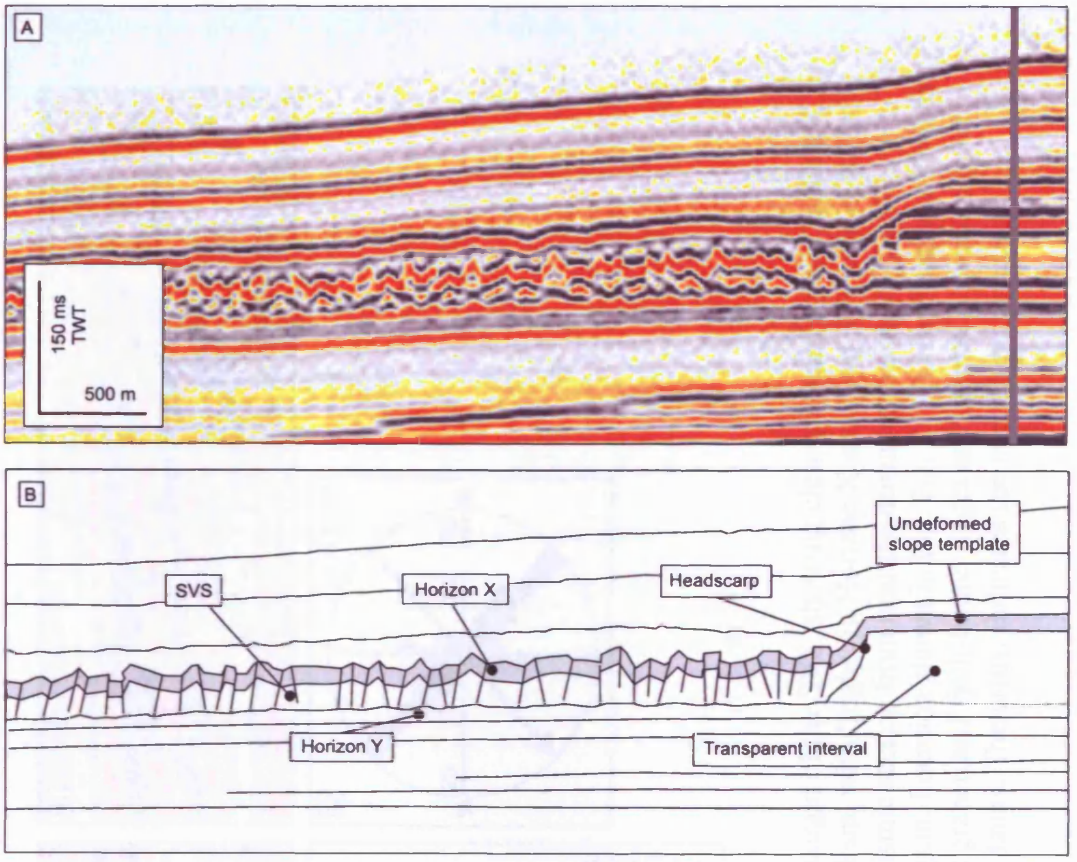

Figure 2.6. A: Unintepreted seismic section showing the upslope region and headscarp of the SVS. B: Summary interpretation diagram for the SVS. Note the undeformed slope template landward of the headscarp, the degree of thinning observable in the deformed region, and the transparent interval removed during development of the SVS.

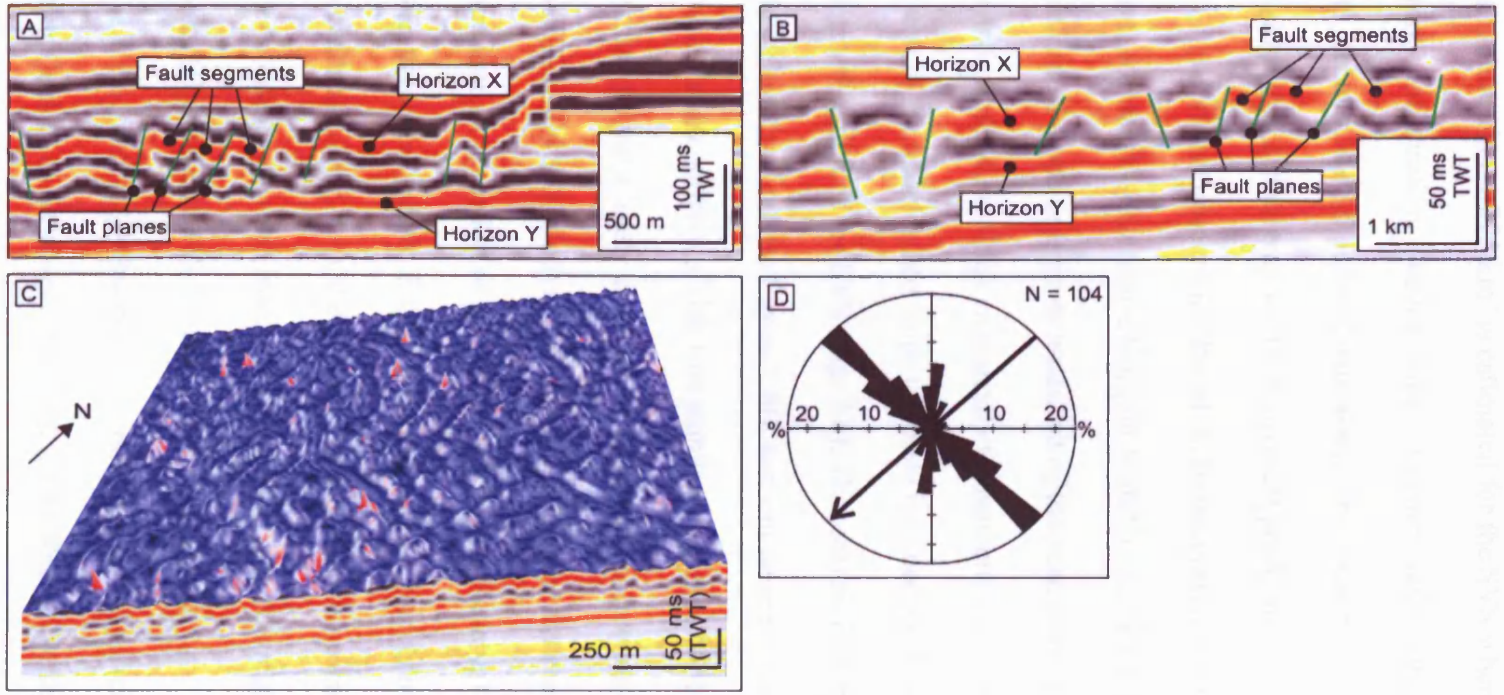

Figure 2.7. A: Zoomed in seismic section from near the updip margin of the SVS, showing closely spaced normal faults and fault-bound blocks. Note how Horizons X and Y exhibit parallelism, with 'highs' in Horizon X underlain by a high in Horizon Y, and vice versa. Location shown on Fig. 2.1. B: Zoomed in seismic section from near the downdip margin of the SVS, showing that normal faults are also present in the downslope region. Location shown in Fig. 2.1. C: 3D visualisation illustrating the ribbed and extended morphology of the slide due to the fault graben and fault-bound ridges and blocks. Location shown in Fig. 2.4A. D: Rose plot showing the dominant orientation of the faults. The arrow indicates the local slope direction.

the thickness of the SVS, it is estimated that a mean thinning of 40 % has occurred. A total volume loss of 25 km^3 is estimated for the SVS when compared to the likely pre-failure configuration. Uncertainties in the pre-failure configuration are estimated as < 10%, because the 3D seismic data allows for excellent correlation along the strike of the slope into a stratigraphically equivalent position.

A critical observation based on stratal correlation updip into the undeformed slope sediments is that while Horizon X and Y can be tracked directly updip into the undeformed slope sediments landward of the headscarp (Fig. 2.3B and 2.6A), an approximately 40 m thick seismically transparent and laterally homogeneous unit present in the undeformed slope template is almost completely missing within the deformed region of the SVS (Fig. 2.6). This critical missing interval is labelled 'transparent interval' on Figure 2.6B, and can be seen from the 3D seismic data to consist almost entirely of this low amplitude seismic facies unit. Importantly, we consider the most likely cause of the apparent volume loss to be due to its remobilisation and removal during failure. This interpretation of the wholesale evacuation or depletion of a specific stratigraphic interval is central to the genetic model presented below. From correlation with a geotechnical borehole 2 km north of the headscarp (Fig. 2.1), the transparent unit is most probably composed of a high water content, clay-rich interval deposited as part of a regionally extensive contourite system (Berg et al. 2005, Forsberg and Locat 2005).

An interesting observation concerning the basal reflection, Horizon Y, is the distinct lack of shear observable (Fig. 2.4B). Recent studies using 3D seismic data have facilitated the imaging of large tracts of the basal surfaces of submarine landslides and led to the identification of various associated features (Frey Martinez et al. 2005; Gee et al. 2005; Moscardelli et al. 2006). Basal surfaces are dominated by

shear deformation, often recordng information related to the dynamic emplacement of MWDs (Gee et al. 2005), such as the passage of intact blocks which disintegrate and erode the substrate (i.e. the basal surface), forming erosive features such as striations or grooves which are typically orientated downslope and record directly the movement of slide material downslope (Posamentier and Kolla 2003; Gee et al. 2005). Horizon Y does not show evidence of the translation of material downslope, and is instead dominated by ductile fold-type features (Fig. 2.3A and 2.4B) which when mapped in 3D, appear elongate perpendicular to the slope direction, forming a system of ridges which closely resembles the pattern of ridges and troughs exhibited by Horizon X.

The SVS is associated with a further downslope failure unit (Fig. 2.5), above which it terminates abruptly (Fig. 2.3A & B), which is also interpreted as a MWD, hereinafter referred to as 'Slide D'. Slide D exhibits features typical of those associated with large-scale, retrogressive sliding in the region (e.g. Evans et al. 1996; King et al. 1996), such as a well defined, steep headscarp with rotated and translated blocks of failed material separated by normal faults in the close vicinity, and progressive disaggregation of material with increasing distance downslope from the headscarp (Evans et al. 1996).

The close proximity of Slide D to the SVS offers the opportunity to compare the morphological characteristics of the SVS with those more commonly observed in submarine MWDs on the Norwegian margin. In some places at the downslope margin of the SVS, it is possible to correlate reflections from the SVS across the headscarp of Slide D, suggesting that SVS material infills Slide D (Fig. 2.5B). This interpretation is taken as evidence for Slide D occurring first, before being partially infilled by the SVS material. This relationship is not visible everywhere however, due to the

resolution limitations of the 3D data. Both the SVS and Slide D are overlain and infilled by the same seismic facies unit, interpreted as Naust A sediments (Fig. 2.3A). Therefore, it is likely that the two MWDs occurred in close temporal succession, with Slide D occurring in a downslope position before the subsequent development of the SVS. Deposition of Naust A sediments, which infill the SVD and Slide D scarps began at 250 ka (Hjelstuen *et al.* 2004), providing a minimum age constraint.

2.6 Discussion: A subsurface evacuation mechanism for submarine mass wasting

The defining characteristic of the SVS which sets it apart from other previously described MWDs, is the anomalous volumetric depletion of the lower part of the SVS with respect to the modest concomitant extension of the deformed body in the downslope direction. The c. 40% thinning of the SVS combined with the observation of the missing transparent interval is consistent with a failure mechanism that involves the wholesale depletion of a substantial volume of the lower part of the original slope template, combined with only mild extension and limited downslope translation of material (maximum of 1.25 km). The top SVS reflection, Horizon X, can be correlated directly across the SVS headscarp (Fig. 2.3B and 2.6A) where it shows a distinct downward shift in stratigraphic level in the downslope direction consistent with the degree of thinning caused by the removal of the transparent interval. Based on these main characteristics, it is clear that the SVS is strikingly different from the classical models of MWDs described from continental margin settings (c.f. Varnes 1978; Frey Martinez et al. 2006).

Historically, a retrogressive slide model has been invoked to explain observed zones of failure in the Storegga Slide complex, including areas near to the SVS in the

Storegga Slide headwall region which display a similar morphology (Gauer et al. 2005; Kvalstad et al. 2005). In classical retrogressive models, downslope translation takes place above a discrete slip plane, with material above deforming as a coherent slab undergoing extension (Kvalstad *et al.* 2005). The resulting morphology typically consists of ridge and graben structures, with ridges resulting from the deposition of intact triangular ridges of slab material, and grabens formed by acceleration of material downslope. Actual extension is typically limited to around 10% (Micallef et al. 2007), and lowering of the seabed topography is achieved through the gravity or lateral spreading of the slide material, with no actual loss of material. In the case of the SVS however, a number of key features differ significantly from the classical retrogressive slide model

(1) it is not possible to observe the entire sequence preserved in the undeformed slope template in the area affected by the SVS. Stratal correlation indicates that a significantly thick transparent interval is missing in the SVS area (Fig. 2.6A), suggesting that the material above the basal surface of the SVS did not behave as a coherent slab;

(2) lowering of the (palaeo)seabed topography in the SVS area (with resultant later onlap of the headscarp) is more likely to have occurred due to the loss of the transparent interval material (Fig. 2.6A), rather than through gravitational spreading. The top SVS reflection, Horizon X, can be correlated directly across the SVS headscarp (Fig. 2.3B & 2.6A) where it shows a distinct downward shift in stratigraphic level in the downslope direction consistent with the degree of thinning caused by the removal of the transparent interval,

(3) the lack of downslope accumulation to balance the upslope depletion, as it does not thicken downslope from a depletion zone to an accumulation zone (Varnes,

1978). Rather, it thins uniformly in a downslope direction and terminates above a deeper-cutting scarp (Fig. 2.3A). It is quite possible that the evacuated material, behaving in a highly mobile manner, travelled for a significant distance downslope and was eventually deposited some distance away from the study area and therefore outside of the area covered by our data.

Based on these critical differences, the classical retrogressive model is not considered a viable mechanism for the development of the SVS. What process then, can account for the detailed morphology, internal structure, and critically, the loss of volume from the lower part of the original undeformed slope template? In answer to this question, we suggest that an analogy can be drawn with a process which is well known to occur onshore in Norway, and in other glaciated regions. Landslides onshore in these glaciated regions can occur as a result of liquefaction-remobilisation of deposits of quick clay.

Quick clay is a highly sensitive, high water content clay found in glaciated and uplifted regions such as Canada and Scandinavia. Such 'quick clay' slides are known for their rapid and destructive nature and occur when quick clay deposits, which commonly occur shallowly buried beneath a relatively thin overburden, readily liquefy following mechanical disturbance (Bjerrum 1955; Rosenqvist 1966; Carson 1977). Critically, the liquefied layer then flows out from beneath the immobile overburden, with enlargement by retrogression through expansion of the liquefaction front (Carson 1977; Fig. 2.8). Evacuation of the mobilised clay layer results in subsidence, collapse, and break-up of the immobile crust, often leaving ridges and rafts stranded on the residuum (Odenstad 1951; Mollard and Hughes 1973). The base of this landslide is not a discrete shear plane, but rather a contact between the residuum of the mobilised layer and the substrate.

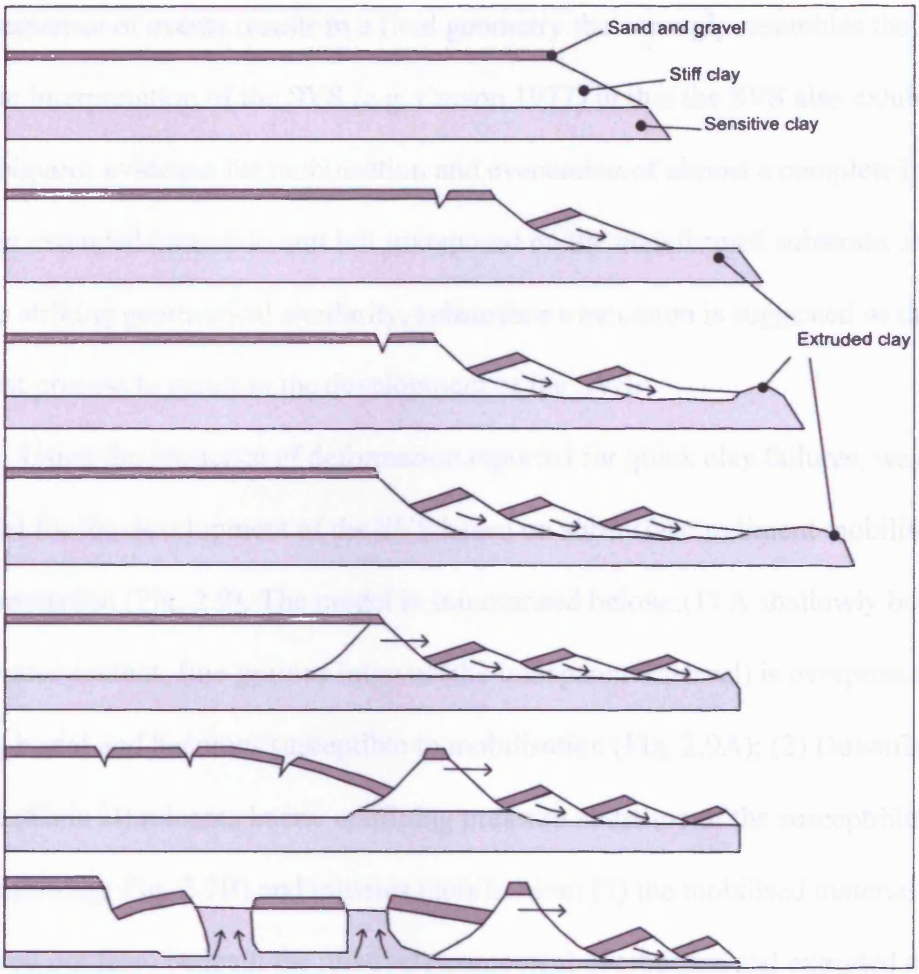

Figure 2.8. Diagram to illustrate the progression of a quick clay landslide. Note the remobilisation of the sensitive (quick) clay and its extrusion from beneath the more competent overburden, which then breaks up, with individual blocks undergoing subsidence or even being rafted by the mobile clay. Modified from Abbott 1996.

This sequence of events results in a final geometry that strongly resembles the 3D seismic interpretation of the SVS (e.g. Carson 1977) in that the SVS also exhibits unambiguous evidence for mobilisation and evacuation of almost a complete layer, with an extended immobile unit left juxtaposed on the undeformed substrate. Based on this striking geometrical similarity, subsurface evacuation is suggested as the likeliest process to result in the development of the SVS.

Using the sequence of deformation reported for quick clay failures, we suggest a model for the development of the SVS based on subsurface sediment mobilisation and evacuation (Fig. 2.9). The model is summarised below: (1) A shallowly buried high water content, fine-grained interval (the transparent interval) is overpressured during burial and becomes susceptible to mobilisation (Fig. 2.9A); (2) Downflank failure (Slide D) releases lateral confining pressure at the toe of the susceptible unit (Undermining; Fig. 2.9B) and initiates mobilisation; (3) the mobilised material is squeezed out from beneath the relatively competent overburden and extruded onto the seabed, and may have moved downslope for a considerable distance. The rigid overburden begins to extend, fracture, and subside due to the volumetric depletion of the underlying unit (Fig. 2.9C), which continues until all of the mobilised material is extruded, forming the collapsed, extended crust observed today (Fig. 2.9D).

This model assumes highly fluid-like behaviour of the mobilised material, such that extrusion continued as the first fragments of the extended crust (in a downslope position) began to subside. Aomplete subsidence or grounding of downslope fragments is not considered to have occurred prior to subsidence of sequential upslope fragments. Mechanical modelling studies based on onshore occurrences of quick clay slides, such as Carson (1977), discuss the concept of 'backward propagating liquefaction fronts', such that liquefaction progresses in a

sequentially backward, upslope-stepping manor, fuelled by juxtaposition of solid, mechanically stable portions of sediment with identical sediments which have suddenly liquefied. It is quite possible that the evacuated material, behaving in a highly mobile manner, travelled for a significant distance downslope and was eventually deposited some distance away from the study area and therefore outside of the area covered by the data. The depletion of the transparent interval from beneath a more competent, deformed overburden is the key diagnostic evidence arguing for the near complete subterranean evacuation of the remobilized sediments.

Such a model requires a plausible mechanism for the remobilisation of the material within the transparent interval (Fig. 2.6B). From correlation with a nearby borehole (Fig. 2.1), the transparent interval is interpreted to constitute part of the widespread sheet-like contourite drift system widely present on the southern Vøring Plateau (Berg et al. 2005; Bryn et al. 2005b; Hjelstuen et al. 2005), which is known to have a high clay content and water content. Contourites are known to form substantially thick, high water content sediment bodies which readily develop overpressure and sensitivity due to their fine-grained lithology and rapid accumulation, and are thought to have hosted glide planes of MWDs which occurred in the adjacent Storegga Slide area (Haflidason et al. 2004; Bryn et al. 2005b).

Micallef et al. (2007) presented a detailed analysis of an area from within the Storegga Slide main headwall, to the SE of the SVS, which is characterised by a ridge and trough morphology similar to that observed from the SVS. The morphology was attributed to the process of spreading, a type of mass movement involving extension and downslope displacement of a sediment unit above a deforming mass of softer material (Varnes, 1978). Micallef et al. (2007) showed how the movements of displaced blocks increased exponentially with distance downslope, and had to assume

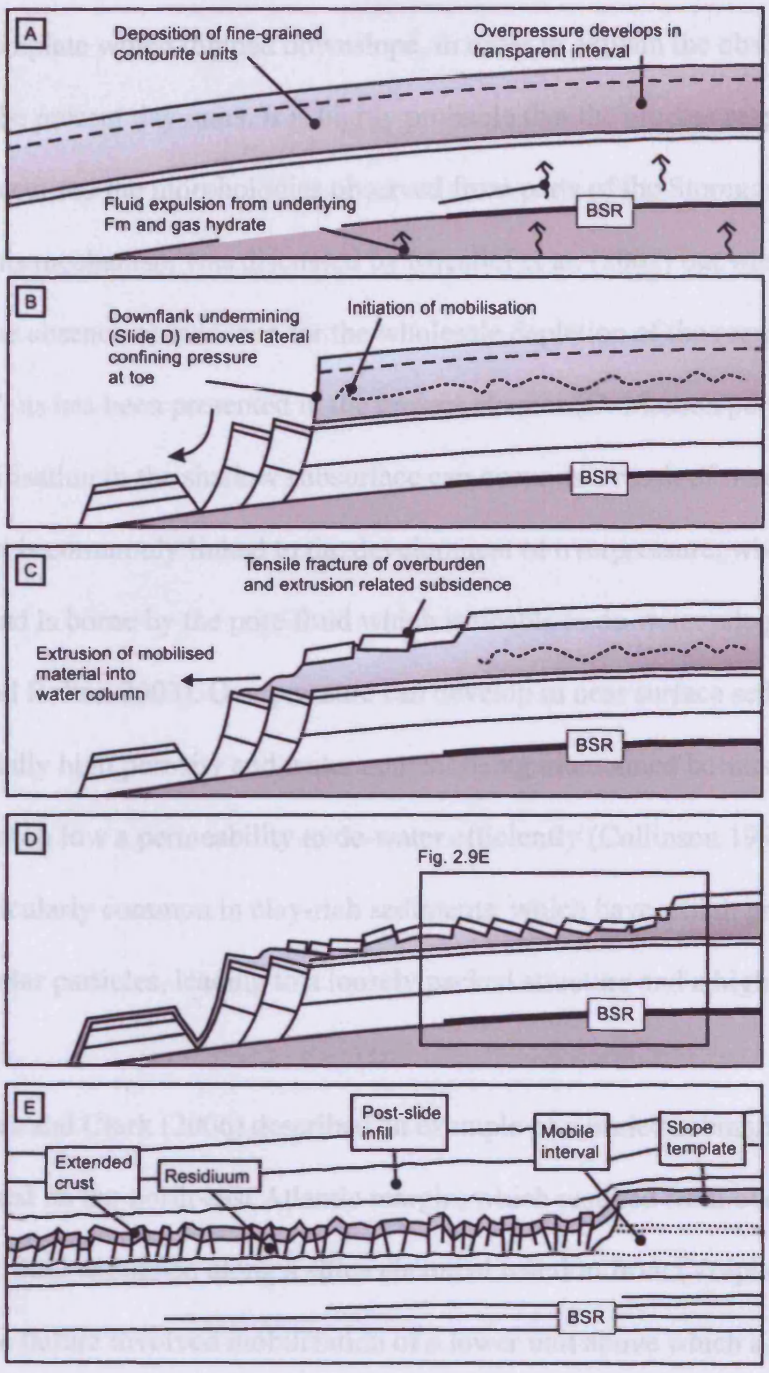

Figure 2.9: Schematic diagram showing the development of the SVS. A: Deposition of fine-grained, high water content transparent interval part of regionally extensive sheet-drift contourite system, and rapid burial beneath a thin cover of more competent sediment. B: Downflank undermining by Slide D removes the downslope confining pressure suffice to initiate mobilisation of the transparent interval. C: Mobilised material is extruded from beneath the more competent overburden, which undergoes extension, fracture and subsidence. D: Process continues until mobilised material is almost completely evacuated. E: Renewed interpretation, showing the 'transparent interval' present within the undeformed 'slope template'. In the deformed region, an 'extended crust' forms the top surface of the SVS following the mobilisation and evacuation of the transparent interval.

a pre-slide template which thinned downslope, in order to explain the observed thinning of the present day units. It is highly probable that the process responsible for the SVS also caused the morphologies observed from parts of the Storegga Slide headwall. This mechanism was discussed by Micallef et al. (2007) but was not pursued in the absence of evidence for the wholesale depletion of the required 'soft spread layer', as has been presented in the present chapter (D. Masson pers comm.).

Mobilisation in the shallow subsurface can occur as a result of many different processes but is commonly linked to the development of overpressure, where additional load is borne by the pore fluid which is unable to de-water adequately (Maltman and Bolton 2003). Overpressure can develop in near surface sediments as a result of initially high porosity and water content being maintained because the sediment has too low a permeability to de-water efficiently (Collinson 1994). This effect is particularly common in clay-rich sediments, which have a high proportion of platy or acicular particles, leading to a loosely packed structure and a high water content.

Davies and Clark (2006) described an example of a buried submarine MWD which occurred on the north-east Atlantic margin, which resulted from overpressure generated by fluid expulsion along a silica chemical reaction front (Volpi et al., 2003). Similarly, the failure involved mobilization of a lower unit above which a rigid, coherent unit was translated and broken up. The failure described by Davies and Clark (2006) differs from the SVS in that no significant volume loss occurred, with the exception of localised venting of material which escaped upwards along faults in the overburden. The failure developed in a confined manner (sensu Frey Martinez et al. 2006), with both the lower mobilized unit and overlying coherent material buttressed against downslope undeformed sediments.

To account for the almost complete depletion of the lower part of the SVS, we suggest that mobilisation must have involved a substantial degree of liquefaction of all or part of the material. Liquefaction involves the total loss of strength of a sediment in which pore fluid pressures reached lithostatic values. Although clay rich sediments are generally thought of as being less prone to liquefaction than coarser-grade sediments due to their cohesive nature, the liquefaction of clayey deposits has been observed in number of instances (Gratchev et al. 2006), including in the case of quick clay failures, and has been implicated in the submarine environment by Bugge (1981).

The susceptibility to liquefaction depends on the content and mineralogy of clays within the sediment (Gratchev et al. 2006). Given the large proportional volume of material removed from the South Vøring Slide and the efficiency with which is has been evacuated, we favour the involvement of a true liquefaction mechanism as opposed to failure due to overpressure build-up and resulting hydroplastic deformation of the failed interval. The lack of evidence for shear along the base of the South Vøring Slide (Fig. 2.3B) supports this, as MWDs which occur due to overpressure build up often result in shear failure along a discrete layer (the basal shear surface).

Invoking a liquefaction-remobilisation process to account for the depletion evident in the SVS is considered here the most likely explanation of the observed geometry, but can we infer anything about the specifics of the liquefaction process from what we know of the depositional context? Liquefaction is the mechanism responsible for mobilisation of clays in geometrically similar onshore quick clay slides, where it is attributed to a number of possible processes linked to pore fluids. These include groundwater invasion, where the saline pore fluid of the clay is partially replaced by fresher water. Changes in the pore water chemistry result in

catastrophic loss of strength, and liquefaction (Rosenqvist 1966). Although groundwater invasion is unlikely as a mechanism in the slope setting of the Norwegian margin, there are several mechanisms that could be viable in a marine setting. For example, low salinity fluids may have interacted with shallowly buried sediments through diagenetic processes.

The contourite drifts of the Naust Fm in this area are underlain by the polygonally faulted Kai Fm (Fig. 2.1), where fluid flow indicators suggest fluid expulsion has been occurring since Miocene times (Berndt et al. 2004). It is thought that such fluid flow may contribute to increased pore pressure (and therefore overpressure) in the overlying sediments and contribute to instability in the Naust Fm sediments (Bryn et al. 2005b). Another possible fluid interaction could occur as a result of hydrate dissociation. Gas hydrates are known to be present in the study area (Berndt et al. 2004; Brown et al. 2006), as seen from the base hydrate reflection (BSR; Fig. 2.2, 2.3A & 2.3C). Dissociation of hydrates in the past would have released significant quantities of fresh water (Tréhu et al. 2003), and dilution of salinity might have initiated liquefaction.

In addition to the pore fluid chemical mechanisms for liquefaction, are a group of mechanisms that can be regarded as purely mechanical. Triggering of mass wasting events in the Storegga area has been linked to seismicity due to isostatic rebound (Evans et al. 2002). In particular, cyclic loading due to the oscillatory transmission of seismic waves has been heavily implicated in submarine MWDs due its ability to induce elevated pore fluid pressures which often fail to be completely dissipated before the next pore fluid response (Maltman 1994). The rapidity of such loading can therefore have the affect of reducing the effective stress to zero, and liquefaction can occur (Maltman 1994). Notwithstanding the likely occurrence of small magnitude

earthquakes in the study area at the time of the SVS, we suggest a mechanical trigger for liquefaction that develops during undermining of a layer (Carson 1977).

Undermining by failure of lateral support is a common precursor to onshore quick clay slides, with the removal of lateral confining pressure at the toe of the susceptible unit often proving sufficient to initiate remobilisation (Carson 1977). In the SVS area, the development of Slide D downflank from what would become the SVS would have created a steep, unsupported scarp of c. 120 m which extends along a significant proportion of the SVS distal margin. Correlation of key horizons from within the SVS into the Slide D area suggests that Slide D preceded the SVS. Unloading at such a substantial and laterally extensive headwall may well have removed sufficient lateral support such that liquefaction initiated, and so we favour a triggering mechanism due to undermining as the most likely cause for the SVS.

2.7 Conclusions

1. A submarine MWD, the South Vøring Slide, which underlies the northern margin of the Storegga slide on the Norwegian margin, has been identified and mapped using 3D seismic data.
2. In contrast to the many other submarine MWDs in the area, the SVS exhibits a departure from typical retrogressive models of MWD development, and is instead better explained by a subsurface sediment mobilisation and extrusion mechanism.
3. A fine-grained unit of approximately 40 m thickness which makes up part of a regionally extensive contourite system has undergone mobilisation and been extruded onto the seabed, forming a heavily depleted, 850 km^2 unit.

4. Based on infilling by Naust subdivision A, the South Vøring Slide occurred before 250 ka, coincident with the initiation of sliding in the adjacent Storegga slide complex (Evans et al. 2002).

5. The recognition of a MWD which developed due to the mobilisation of a significantly thick subsurface unit in a region of such prolific large-scale mass wasting raises implications for its role in the development of other mass wasting events, both on the Norwegian margin and other glaciated margins worldwide. If the conditions for remobilisation are met, it maybe that such units are widespread, but are yet to be identified.

CHAPTER THREE

3.0 Kinematic indicators from submarine mass wasted deposits using 3D seismic data

3.1 Summary

Kinematic indicators are geological structures or features which may be analysed to allow the direction, magnitude and mode of transport of submarine mass wasting deposits (MWDs) to be constrained. This chapter presents a compilation of all of the various indicator types, which have been classified according to where they may typically be found within the MWD body – the headwall domain, translational domain and toe domain. Aspects of their formation, identification using seismic data and their kinematic value are discussed, and illustrated using worked examples taken from 3D seismic data from the continental margin of Norway and the Levant margin, east Mediterranean Sea both of which have been influenced by repetitive large-scale slope failure in the recent past. 3D seismic data are proven to be an excellent tool for the imaging of kinematic indicators, as they provide large areal coverage which allows swift and confident evaluation of the direction of translation, and in many cases also allow the degree of translation of the displaced slide material to be constrained. Imaging of the basal shear surface, analysis of internal architectures and determination of transport direction are areas which are of particular benefit from the analysis of 3D seismic. The descriptions and applications of the various kinematic indicators detailed in this study should find broad applicability for seismic interpreters working on MWDs in many different settings and locations.

3.2 Introduction

We define a kinematic indicator as a geological structure or feature which records information related to the type and direction of motion at the time of emplacement, and as such they are of great use to our understanding of the initiation, dynamic evolution and cessation of slope failures. To date, many studies of submarine slope failures have identified various kinematic indicators, using both geophysical methods (Prior et al. 1984; Masson et al. 1993; Bøe et al. 2000; Laberg et al. 2000; Laberg and Vorren 2000; Haflidason et al. 2004; Wilson et al. 2004; Frey Martinez et al. 2005; Gee et al. 2005; Schnellmann et al. 2005; Frey Martinez et al. 2006; Lastras et al. 2006) and the study of ancient outcrops (Farrell 1984; Martinsen and Bakken 1990; Trincardi and Argnani 1990; Strachan 2002a and b; Lucente and Pini 2003). However, it came to our attention that there is currently no catalogue or compilation of all of the various deformational features, no guide as to how to recognise them using seismic data, how they may be analysed, or what they may tell us about the mass wasting deposits. The aim of this chapter is therefore to identify all of the various types of deformation structures and features associated with mass wasting deposits and present them using a suitable classification scheme and with illustrated worked examples taken from the data available for this study. A further aim is to develop a recognition criteria for each feature using seismic data, and a workflow for their analysis in terms of kinematic information. The examples of kinematic indicators illustrated here are sourced primarily from the mid-Norwegian continental margin, with additional kinematic indicator examples taken from the Levant margin. Although the examples illustrated here are specific to the study areas, the ideas and results

should find broad applicability, and prove useful to seismic interpreters working on MWDs from other areas.

3.3 Data used

Four 3D seismic surveys (Fig. 3.1A) from the mid-Norwegian continental margin were used in this study along with one 3D survey from the Levant margin (Fig. 3.1B). In addition, relevant 2D seismic lines from a regional grid available from the Norwegian margin were utilised (Fig. 1.7). When calculating the resolution of the data, an assumed average seismic velocity of 2000-2100 ms^{-1} is used for the interval of interest. Characteristics of the data used can be found in chapter one, section 1.4.

3.4 Methodology

Extensive mapping of 3D seismic horizons was conducted across the Norwegian margin study area using the named 3D surveys in order to a) identify and delimit the various MWDs; and b) identify any kinematic indicators present within. Focussed mapping of the seabed horizon was carried out in the Levant 3D survey from the Levant margin. Initially, time structure maps were generated in order to examine the various surfaces, after which more focussed attribute analysis was performed, as explained in chapter 1, section 1.5, in order to define kinematic indicator examples. Once identified, kinematic indicators were catalogued using the classification scheme developed as part of this study and analysed to deduce any information pertaining to the direction and magnitude of transport, mode of emplacement, dominant mass wasting process or rheology. The best examples resulting from this process were then

chosen to illustrate each individual kinematic indicator type presented in this compilation, along with a brief discussion of the results of their analysis.

3.5 Kinematic indicators

Lewis (1971) proposed an idealised model for units resulting from slope failure, showing that typically a systematic distribution of strain is exhibited; with extensional structures characterising the upslope region, and compressional structures characterising the downslope region. Many described MWDs do not fit the upslope extension-downslope compression model however, as it does not account for the huge variety and association of structures observed (Woodcock 1979; Farrell 1984; Elliott and Williams 1998; Martinsen 1989; Martinsen and Bakken 1990; Trincardi and Argnani 1990; O'Leary 1991; Strachan 2002a and b; Lucente and Pini 2003; Canals et al. 2004; Frey Martinez et al. 2005). Such structures typically include folds, boudins and normal and reverse faults, with extensional deformation sometimes juxtaposed with, or even overprinted by, compression and vice-versa (Farrell 1984; Martinsen and Bakken 1990; Strachan 2002a). For the purposes of the present study we have grouped the various kinematic indicators according to the domain in which they are most likely to occur within a MWD exhibiting a typical 'tripartite' anatomy (Martinsen 1994; Lastras et al. 2002): the headwall domain, translational domain and the toe domain (Fig. 3.2). Although there may be some overlap, a clearly defined classification scheme is vital for the practical application of the presented work. All examples are illustrated with reference to a summary diagram (Fig. 3.2), and key geometrical and geological criteria are summarised in Fig. 3.3.

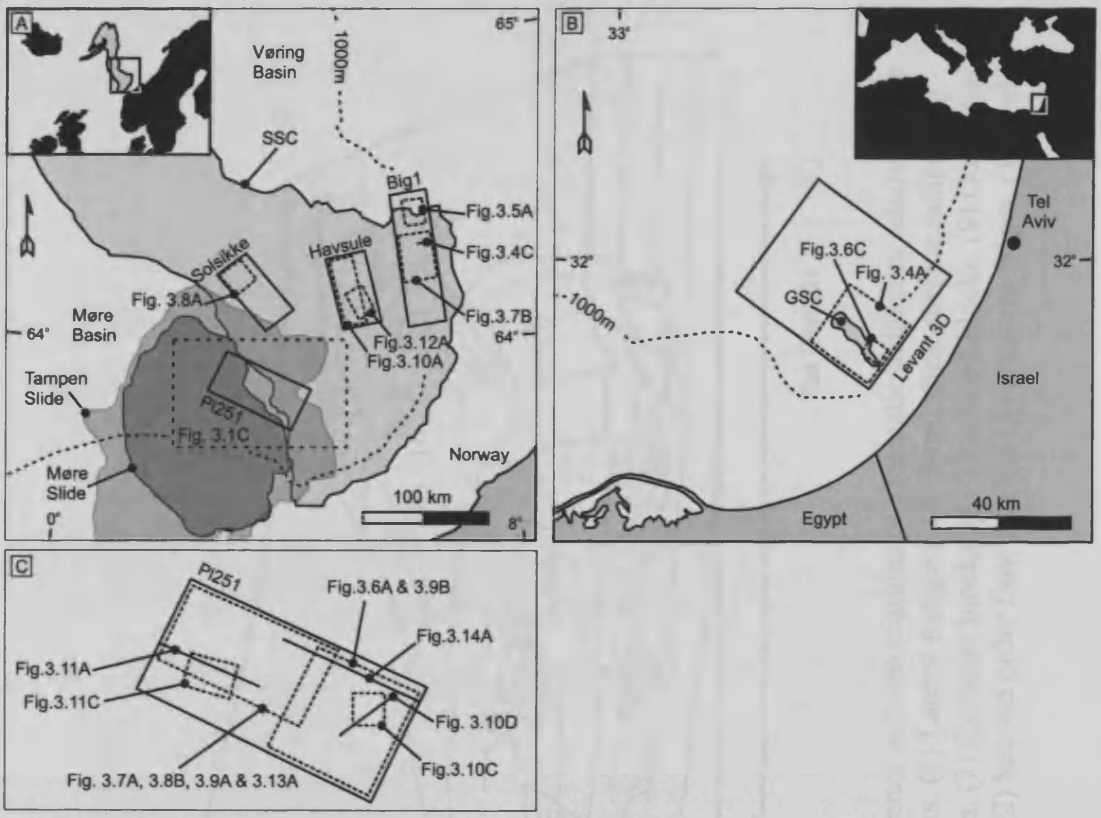

Figure 3.1. Location of figures. (A) Norwegian continental margin study area, showing outlines of major MWDs, 3D surveys and figure locations. 3D surveys (PL251, Solsikke, Havsule and Big 1) are outlined by solid black rectangles. The outlines of the Møre and Tampen Slides are after Solheim et al. (2005). SSC – Storegga Slide complex. (B) Levant margin study area and location of figures. Outline of the 3D survey (Levant 3D) is shown by a solid black rectangle. GSC: Gaza slump complex (after Frey Martinez et al. 2005); (C) Zoom in of 3D survey PL251 and location of various figures.

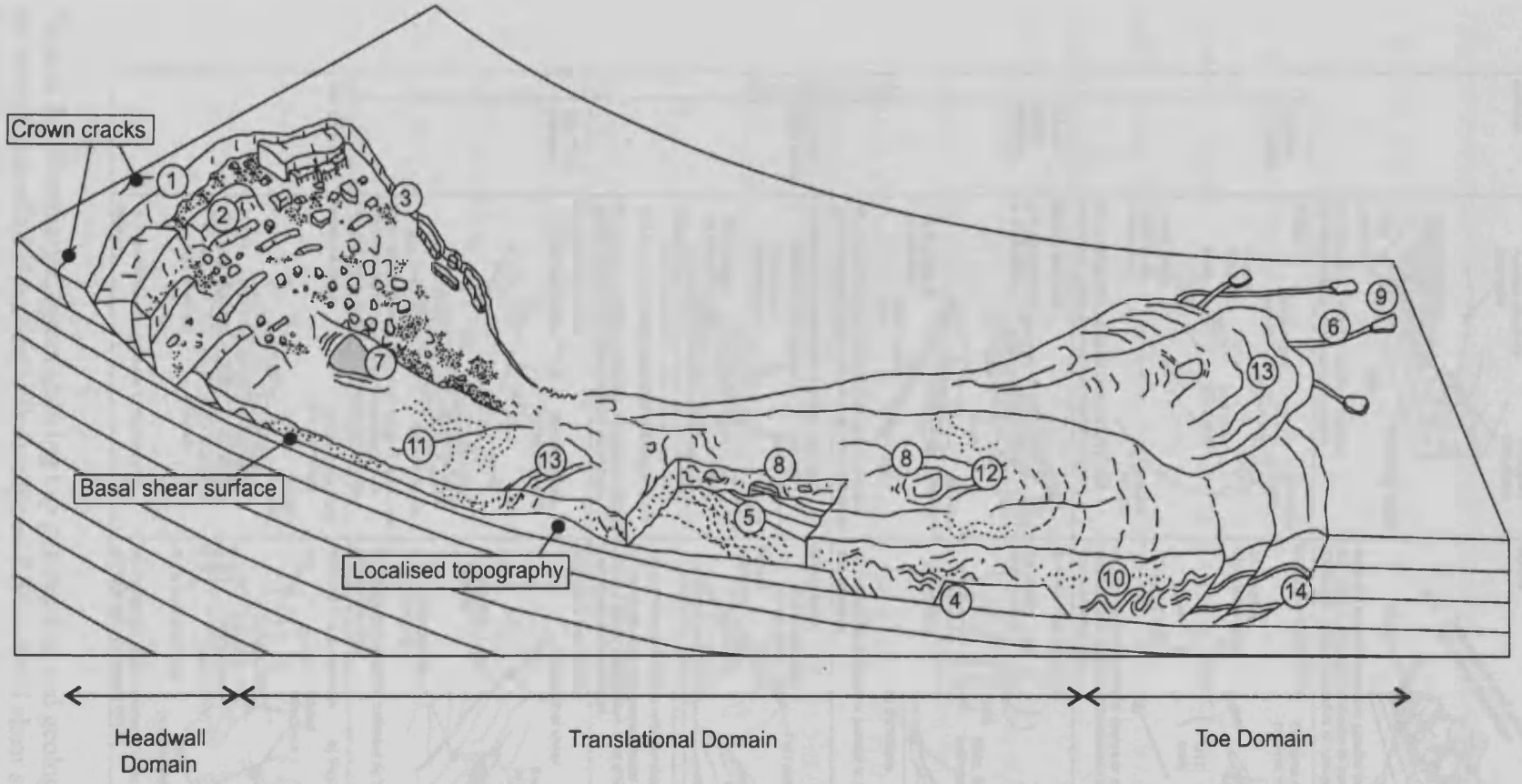

Figure 3.2. Schematic representation of a MWD and the likely occurrence and associations of kinematic indicators relative to the various domains. (1) Headwall scarp. (2) Extensional ridges and blocks. (3) Lateral margins. (4) Basal shear surface ramps and flats. (5) Basal shear surface grooves. (6) Basal shear surface striations. (7) Remnant blocks. (8) Translated blocks. (9) Outrunner blocks. (10) Folds. (11) Longitudinal shears/ first order flow fabric. (12) Second order flow fabric. (13) Pressure ridges. (14) Fold and thrust systems.

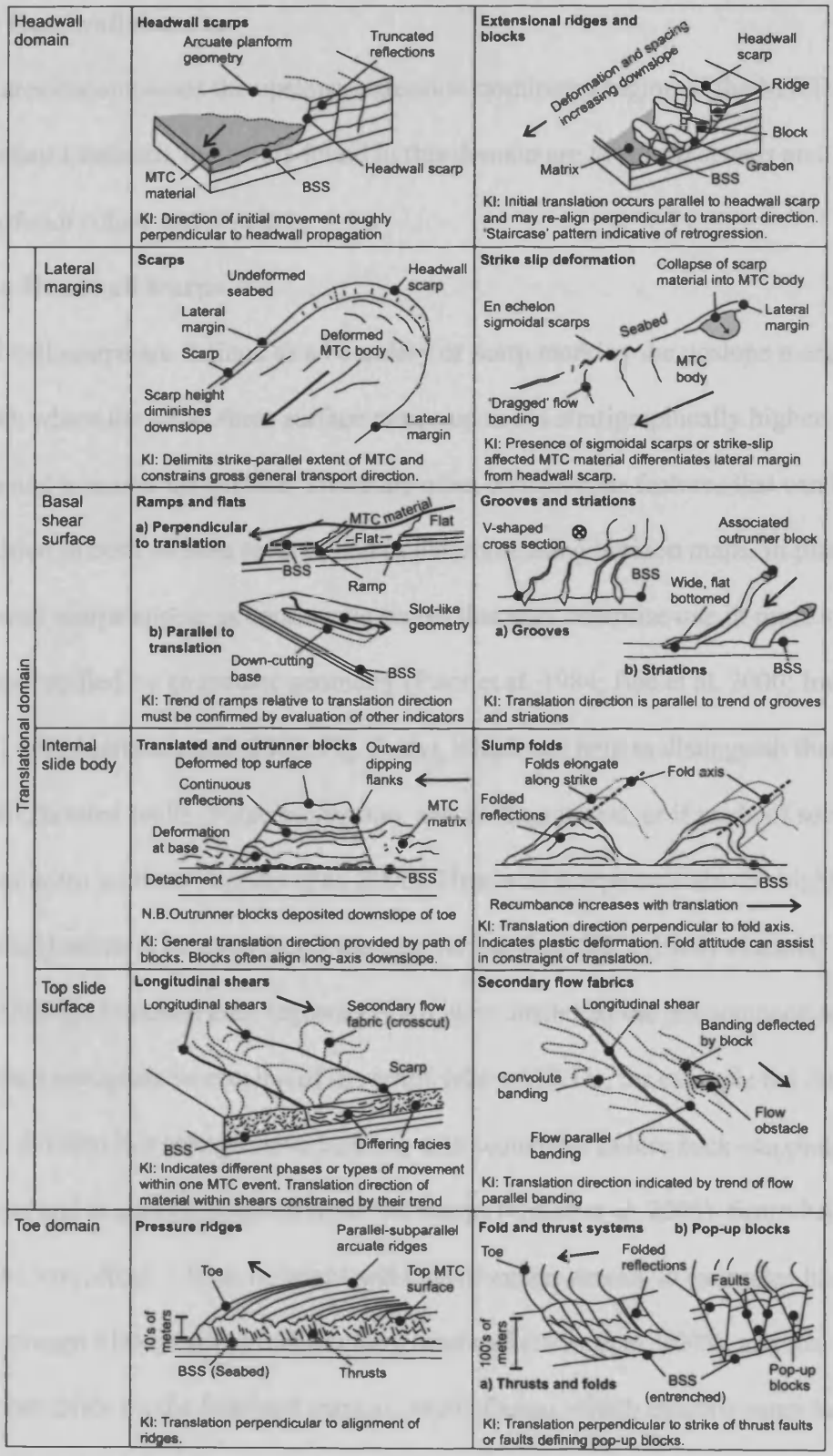

Figure. 3.3. Summary diagram showing key geometrical and geological criteria for the recognition of all kinematic indicator types. BSS – Basal shear surface. KI – Kinematic information. Bold arrows indicate direction of translation.

3.5.1 Headwall domain

This area encompasses the upslope, extension-dominated region of the MWD. Two important kinematic indicators found in this domain are *headwall scarps* and *extensional ridges and blocks.*

3.5.1a Headwall scarps

Headwall scarps are defined as a boundary or scarp marking the upslope margin of a MWD, where the basal shear surface ramps up to cut stratigraphically higher, younger strata and intersect the surface. These are often conspicuous features that can be easily identified in both seismic section, and in planform using horizon maps. In plan-view, headwall scarps appear as continuous scarps that may comprise one or more salients and are typified by an arcuate geometry (Prior et al. 1984; Bøe et al. 2000; Imbo et al. 2003; Frey Martinez et al. 2005; Fig. 3.4A), which can help to distinguish them from tectonic normal faults. Some scarps may appear fragmented, as if made of several shorter scarp sections (Lastras et al. 2006). Headwall scarps may also be highly sinuous (Lastras et al. 2004), as is the case for the Gela Slide (Sicily channel) described by Trincardi and Argnani (1990), who attributed the phenomenon to localised retrogressive erosion of the scarp. Many MWDs, for example the Storegga Slide, develop in a retrogressive fashion, with sequential failure back-stepping upslope and creating a series of headwall scarps (Gauer et al. 2005). Scarp heights and lengths vary, from < 10 m in height and tens of meters across, to examples like that of the Storegga Slide; with its 300 km long headwall (Bryn et al. 2005), and the Hinlopen Slide on the Svalbard margin, Arctic Ocean, which exhibits scarp heights of up to 1600 m (Vanneste et al. 2006; Winkelmann et al. 2008).

A headwall scarp essentially represents an extensional failure surface, and therefore forms in the same way as extensional faults. The headwall propagates along-

strike perpendicular to the direction of the minimum compressive stress (σ_3; Anderson 1936), which will generally be oriented parallel to the slope due to the effect of gravity acting on the sediment mass. In this sense, the orientation of the headwall scarp can yield kinematic information as it reveals the initial direction of bulk material movement. Figure 3.4A shows an example of several headwall scarps from the Levant margin, all of which trend roughly NE-SW. This suggests initial translation to the NW, consistent with the local slope direction. The planimetric morphology of the headwall scarp can also be used to gain insight into the initial slope failure mechanism. For example, O'Leary (1991) attributed the polygonal, stepped salients of so-called 'slab slide' headwalls to the successive removal of 'slabs' of material due to brittle failure at varying stratigraphic levels.

Headwall scarps are steeply dipping, with typical inclinations of $15 - 35^{\circ}$ (Imbo et al. 2003; Bryn et al. 2005; Frey Martinez et al. 2005; Vanneste et al. 2006; Winkelmann et al. 2008), and the sense of slip is predominantly dip-slip, with material being transported directly downslope and away from the scarp. With a defining feature of headwall scarps being the presence of some degree of curvature in planform however, it is likely that some obliquity of slip vector occurs towards the lateral extremes. The specific controlling factors in the angles and development of curvature in headwall scarps are not clearly understood. A further feature often associated with or found in the landward vicinity of headwall scarps are crown-cracks; subtle, elongate depressions or linear features in plan-form which in seismic section are shown to be small-scale faults or fractures (Fig. 3.2; Frey Martinez et al. 2005). Crown-cracks occur in otherwise undeformed and undisplaced strata in the vicinity of the headwall and form as a result of extensional stresses related to the upslope propagation of retrogressive failure (Varnes 1978; Frey Martinez et al. 2005).

In cases where examples of MWDs have occurred relatively recently, and so their morphological expression on the seafloor, including the headwall scarp, has not yet been infilled (Prior et al. 1984; Bøe et al. 2000; Laberg et al. 2000; Laberg and Vorren 2000; Canals et al. 2004; Haflidason et al. 2004; Wilson et al. 2004; Frey Martinez et al. 2005; Schnellmann et al. 2005; Lastras et al. 2004; 2006; Fig. 3.4A & B), identification of headwall scarps in seismic sections and map views can be relatively straightforward, with the headwall being defined by a seabed scarp which abruptly truncates the undeformed upslope stratigraphy (Fig. 3.4B & C). Where the MWD under study is older, infilling, burial and compaction can complicate recognition of the scarp (Fig. 3.4C). Thickness changes across identified scarps, indicative of missing strata (Gee et al. 2006), and the juxtaposition of undeformed strata upslope of the scarp with deformed material downslope aids the interpretation (Frey Martinez et al. 2005).

The identification of older headwall scarps in seismic section may be complicated by it being immediately overlain by a later MWD (Fig. 3.4C); and also by complete evacuation and later infilling of the headwall region. In the former, it may be possible to distinguish between individual events by the presence of a basal shear surface separating the two, or by differing seismic facies characters of individual MWDs. If total evacuation of the headwall and proximal area has occurred, the truncation of sediments in the headwall scarp may be difficult to identify if infilling by background sedimentation of similar dip and/ or seismic facies character has occurred. The best way to proceed if such uncertainty exists is to identify the basal shear surface at some point below the main body of the MWD and attempt to trace it upslope to the headwall region, or utilize coherence or amplitude slices flattened on the basal shear surface.

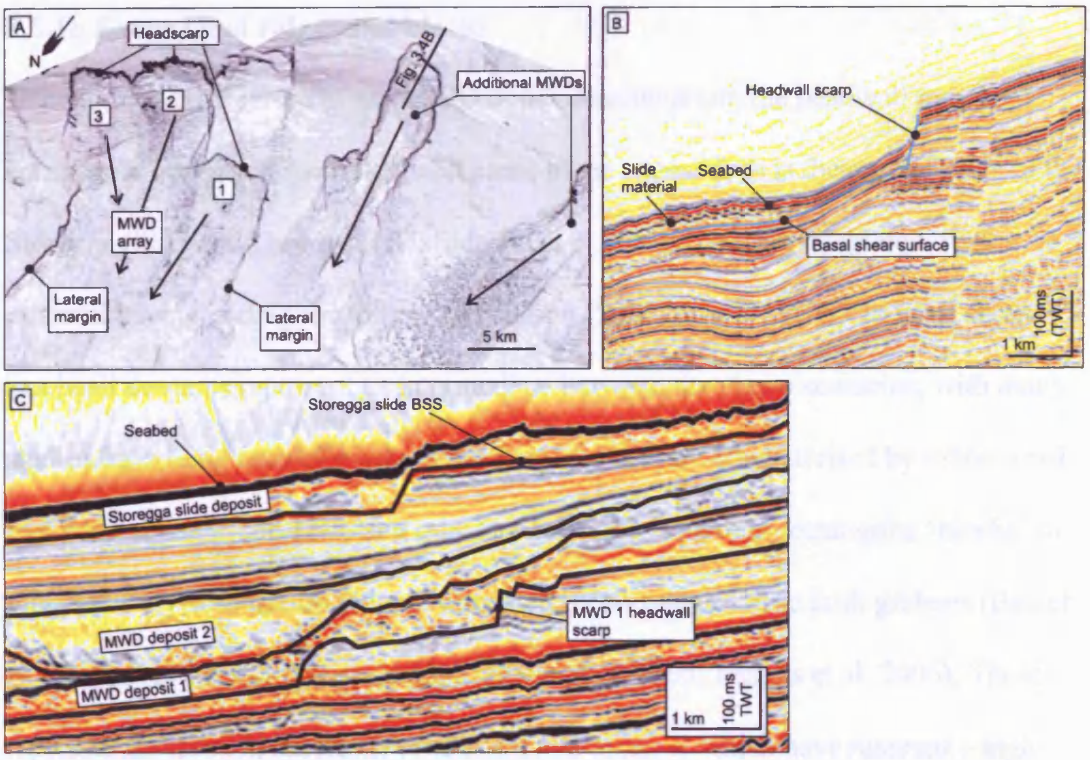

Figure 3.4. Examples of headwall scarps from the headwall domain. (A) Perspective view of an area of the seabed in the Levant margin study area (location shown in Fig. 3.1B) featuring a number of MWDs. Note arcuate geometry of the headscarps and presence of an array of MWDs (labelled) which can be separated into 3 separate events, labelled 1 - 3. (B) Seismic section through headwall scarp of a Levant margin MWD (location shown in A). (C) Seismic section from the headwall domain of the Storegga Slide showing Storegga Slide deposits and older MWDs (labelled 1 and 2, respectively) lower in the succession. Note infilling of the earlier headscarp (labelled 'MWD 1 headscarp') by the subsequent MWD 2. Location shown in Fig. 3.1A). BSS – Basal shear surface. The arrows represent the gross transport direction of MWD material.

3.5.1b Extensional ridges and blocks

Depending on the nature of the MWD under consideration, the headwall may be completely evacuated, with the basal shear plane exposed, as is the case in parts of the Storegga Slide main headwall (Haflidason et al. 2004); or barely depleted, with material having undergone limited translation (Solheim et al. 2005). In most cases, headwall domains represent an intermediate between the above scenarios, with many studies describing examples where headwall regions are characterised by extensional features, typically deformed and translated, roughly square to rectangular 'blocks' or more laterally continuous 'ridges' separated by normal or listric fault grabens (Bøe et al. 2000; Frey Martinez et al. 2005; Solheim et al. 2005; Lastras et al. 2006). These represent discrete, detached units of translated material which have retained a high degree of internal coherency (Homza 2004; Lastras et al. 2006). The blocks may occur on a variety of scales and may undergo varying degrees of translation, with spacing, deformation and disintegration tending to increase with distance away from the headwall scarp (Laberg and Vorren 2000; Gee et al. 2006). Such blocks can be identified in planform from top MWD surface or in the case of relatively recent events, seabed time-structure, amplitude or dip maps. Time, stratal or coherency slices flattened on the basal shear surface are also of use.

The blocks are typically elongate in the along-strike direction, due to their association with extensional faults which propagate along strike orthogonal to the direction of the minimum confining stress (σ_3), and oriented parallel-to-subparallel to the headwall scarp (Varnes 1978; Bøe et al. 2000; Laberg and Vorren 2000; Frey Martinez et al. 2005; Lastras et al. 2006). Examples of blocks that are continuous across the entire headwall region have been described (Lastras et al. 2006). In addition, a step-like, or 'stair-case' pattern may be observed in dip-section (e.g.

Kvalstad et al. 2005; Lastras et al. 2006), which is often taken to be indicative of a retrogressive or 'back-stepping' pattern of failure development (Kvalstad et al. 2005; Solheim et al. 2005; Lastras et al. 2006; Micallef et al. 2007).

Initially, blocks, ridges and intervening grabens share a common orientation with the section of the headwall scarp from which they originated (Fig. 3.5). This situation can be complicated where the headwall scarp is irregular or composed of more than one salient, and the orientation of the various segments can vary widely, to the point of being parallel downslope. Figure 3.5 shows an example of extensional ridges and blocks from the northern edge of the Storegga Slide headwall scarp. Many ridges and blocks are identified in planview (Fig. 3.5A), and those in close vicinity to the headwall scarp share with it a common orientation. Blocks and ridges show evidence for both disaggregation and reorientation with increasing distance downslope from the headwall scarp, with decreasing size and continuity and a change from original orientation parallel to the headwall scarp to become parallel to the general transport direction.

In seismic sections, detached blocks can be identified as localised packages of undisrupted, continuous reflections bounded by normal-listric faults, and which may be separated from the headwall scarp or other blocks by considerable gaps depending on the degree of translation (Fig. 3.5B). Intervening grabens may be filled with a contemporaneous matrix (Huvenne et al. 2002), or by subsequent sedimentation. The blocks imaged in the northern Storegga Slide headwall have a maximum height of 60 m and measure up to 120 m across (Fig. 3.5B).

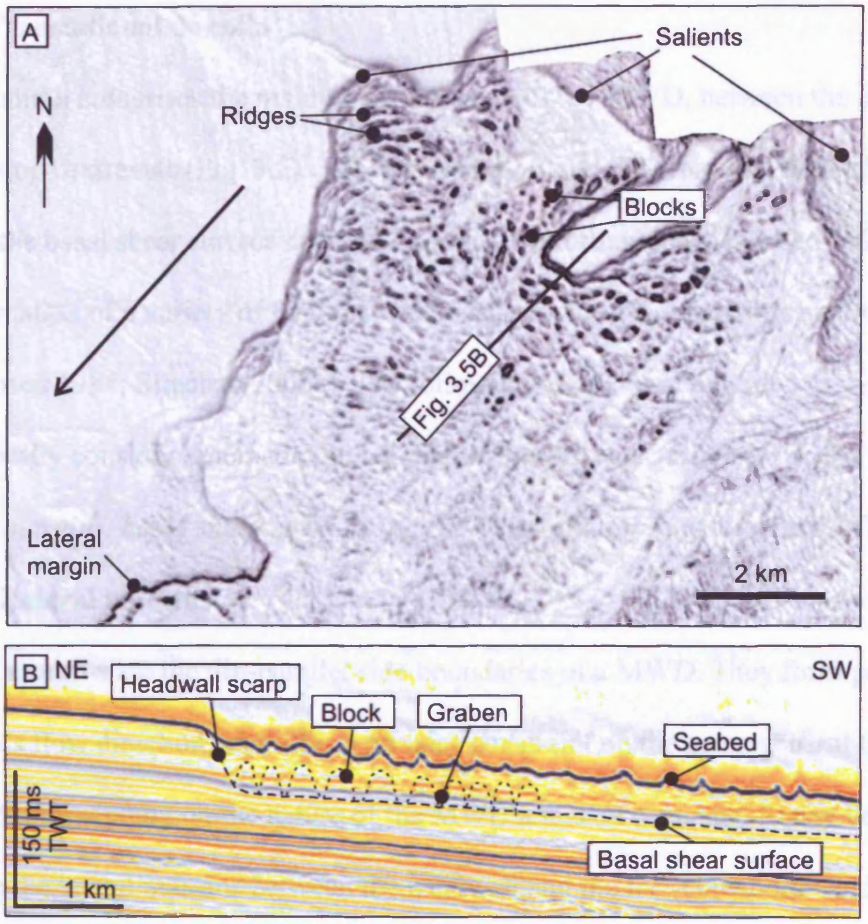

Figure 3.5. Example of extensional ridges and blocks. (A) Seabed dipmap from the northern Storegga Slide headwall scarp (see Fig. 3.1A for location). Note that blocks and ridges in close vicinity to the headwall scarp share its orientation, and with increasing translation downslope, they realign to become orientated perpendicular to the transport direction. Slope direction indicated by bold arrow. (B) Seismic section through part of headwall scarp showing a series of blocks and intervening grabens.

3.5.2 Translational domain

This domain comprises the main translated body of the MWD, between the up- and down-slope extremes (Fig. 3.2). The movement of the failed material downslope across the basal shear surface can lead to intense deformation (Martinsen 1994), and the formation of a variety of features which can provide kinematic information (Martinsen 1994; Strachan 2002a). The following section is subdivided to individually consider kinematic indicators that typically occur in association with the *lateral margins, basal shear surface, internal body* and *top surface* of a MWD.

3.5.2a Lateral margins

Lateral margins are the dip-parallel side boundaries of a MWD. They form parallel to the gross flow direction, and offer a primary constraint on the gross general transport direction. Depending on the nature of the MWD and data coverage, it may be possible to trace the lateral margins between the headwall and the toe (Gawthorpe and Clemmey 1985). Lateral margins are associated with strike-slip movement (Martinsen and Bakken 1990; Martinsen 1994; Frey Martinez et al. 2005), although transpressional or transtensional deformation may occur if the MWD scar widens or narrows (Martinsen 1994). Detection of such deformation may be important in distinguishing the lateral margins from the headwall or toe domains (Martinsen 1994), and the situation is further complicated by the possibility of localised dip-slip collapse of high, steep lateral scarps inwards, towards the centre of the MWD body (Varnes 1978). The actual formation and propagation of lateral margins is a complex topic and is further discussed in section 3.6.1 of this chapter.

Lateral scarps may be difficult to trace downslope due to the tendency for scarp relief to diminish rapidly away from the headwall scarp, and the possibility of the deformed mass ramping up from the initial basal shear surface and cutting up-

section to translate across the seafloor at the toe domain (O'Leary 1991; Frey Martinez et al. 2006). In planform, a lateral margin may appear as a scarp or linear feature roughly parallel to the slope direction which separates a smooth, undeformed region of the seabed or top MWD age-equivalent horizon from the adjacent region that has been affected by failure (Fig. 3.6A & B).

Conversely, they can also be expressed as raised, positive features due to localised or net accumulation of material in the translational or toe domain of the MWD (Prior et al. 1984; Trincardi and Normark 1989). A seismic section across a lateral margin may show a scarp of positive or negative relief, or in the case of a lateral margin with no discernable relief, a change in seismic facies from undeformed strata outside of the area affected by slope failure processes, to that of the disrupted facies symptomatic of MWDs (Fig. 3.6A & B). In this respect, the identification of lateral margins becomes difficult where the translational domain does not exhibit a high degree of disruption. The example shown in Fig. 3.6 is taken from the southern margin of the Storegga Slide where material affected by instability in the Storegga zone is juxtaposed with undeformed strata to the south.

The identification of lateral margins can be of great value to the kinematic study of MWDs, as they offer a primary constraint on the flow direction of the MWD. Where entire MWDs are imaged, the geometry and local slope direction can be used to determine the overall translation direction (Masson et al. 1993). Figure 3.4A shows an image of the Levant margin, which features a number of MWDs at the seabed (Frey Martinez et al. 2006). A MWD array (labelled on Fig. 3.4A) features lateral margins that are conspicuous features in planform; generally dip-parallel, continuous and linear, but they do exhibit discontinuities and localised changes in trend. The lateral margins trend N-S, indicating that gross general transport also took place in

this direction. Closer examination of the array reveals that it comprises three separate MWDs (labelled 1 to 3 on Fig. 3.4A), each delimited by separate headwall scarps and lateral margins. Analysis of the cross-cutting relationships of the lateral margins is very potent in revealing the relative chronology of the MWDs, and in this case it is apparent that MWD 1 (Fig. 3.4A) occurred first, and is cross-cut and partially obliterated by MWD 2, which in turn is cross cut by MWD 3. These relationships are confirmed by examination of a seismic cross section through the seabed. Part of the eastern lateral margin of a further MWD from the Levant margin (Fig. 3.6C) shows a number of small, closely spaced en echelon scarps where the lateral margin is segmented (Fig. 3.6C). Some of the segments are sigmoidal due to rotation of the central portion of the fracture (Twiss and Moores 1992), and are evidence of strike-slip deformation.

3.5.2b Basal shear surface

Recognition of a detachment surface – a requirement of all sliding (Varnes 1978; Martinsen 1994) invariably yields important kinematic information about the dynamic emplacement of such events (Gee et al. 2005). The basal shear surface is often continuous and concordant to bedding, but may be affected by faults, bedding plane or material variations (Varnes 1978). In addition, variations in the basal shear surface may be caused by the movement and nature of the material overlying it, and so may reveal several features which provide important kinematic information.

Ramps and flats

Several studies have described 'ramps' – whereby the basal shear surface cuts up or down to a new stratigraphic level, and intervening 'flats', both from offshore, geophysically imaged examples (Trincardi and Argnani 1990; Lucente and Pini, 2003; Frey Martinez et al. 2005), and from ancient field outcrops (Gawthorpe and

Clemmey 1985; Strachan 2002a). A ramp is defined as a segment of the basal shear surface that cuts discordantly across bedding, whereas the 'flat' sections are bedding-parallel segments of the basal shear surface. The ramps therefore connect 'flat' segments of the basal shear surface at differing stratigraphic levels (Trincardi and Argnani 1990). Lucente and Pini (2003) likened the ramp and flat geometry to shallow level deformation in accretionary wedges, and Gawthorpe and Clemmey (1985) assigned the terms 'contractional' if the basal shear surface cuts up section, and 'extensional' if it cuts down.

In seismic section, ramps are easily identifiable in a similar way to faults or the headwall scarp (Frey Martinez et al. 2005), by first tracking the basal shear surface and identifying where it ramps up or down to truncate bed-parallel strata below. In planform, the ramps can be seen as scarps or linear features that mark sharp topographical variations of the basal shear horizon (Fig. 3.7A). Trincardi and Argnani (1990) and Gawthorpe and Clemmey (1985) report that most ramps trend perpendicular to the main flow or movement direction.

Good examples of basal shear surface ramps from the Møre Slide (Evans et al. 1996), which deforms mid-Pleistocene age sediments south of the Storegga Slide, (Evans et al. 2002; Fig. 3.1) are shown in Figure 3.7. A number of previous studies have established that the head and side walls trend WSW-ENE and SSE-NNW respectively (Evans et al. 1996; Nygård et al. 2005; Hjelstuen et al. 2007; see Møre Slide outline on Fig. 1.3), from which it can be inferred that the gross transport direction was downslope to the NW and perpendicular to the basal shear surface ramps.

Figure 3.7A illustrates the planimetric morphology of two of these ramps. Within the limits of the 3D survey used to map the slide (Fig. 3.1), two main ramps

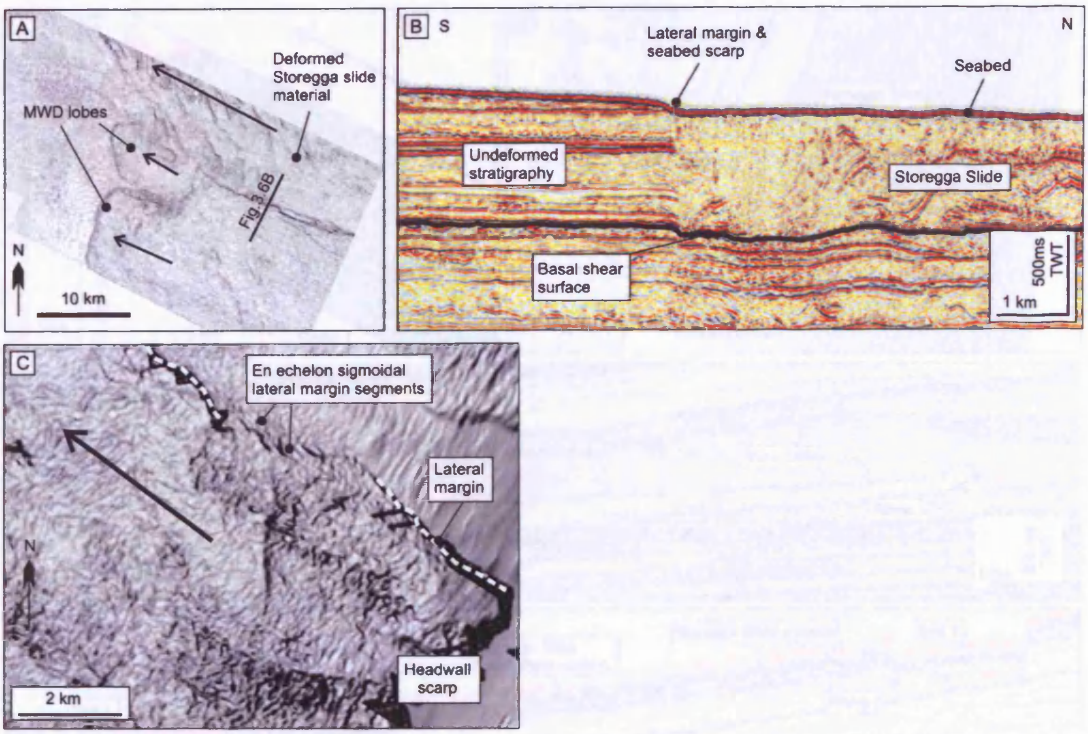

Figure 3.6. Examples of lateral margins. (A) Seabed dip map from the PL251 3D survey (location shown in Fig. 3.1C), showing the seabed expression of deformed material from the Storegga Slide. (B) Seismic section through lateral margin of Storegga Slide material and adjacent undeformed strata (location shown in A). Note dramatic change in seismic character from undisrupted strata in the south, to highly disaggregated immediately to the north. (C) Zoom in of a section of a lateral margin from a MWD affecting the Levant margin seabed (location shown in Fig. 3.1B), showing evidence for strike-slip deformation. Arrows indicate translation direction.

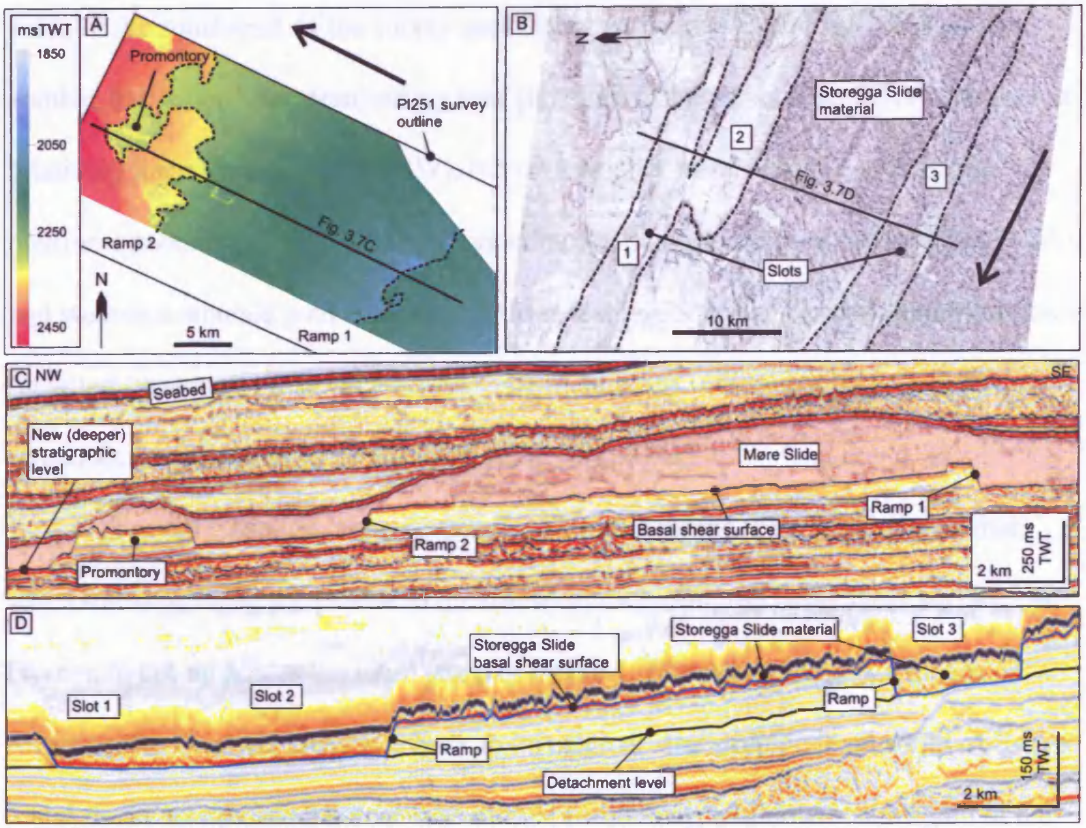

Figure 3.7. Examples of basal shear surface ramps. (A) Time structure map of the basal shear surface of the Møre slide taken from the PL251 3D survey (location shown in Fig. 3.1C). Arrow indicates translation direction. (B) Seabed dip map from the Storegga Slide headwall domain showing 'slots'. Location shown in 3.1A. (C) Seismic section through Møre slide basal shear surface (location shown in A), note steep, discordant nature of ramps. Arrow indicates translation direction. (D) Seismic section through slots (location shown in B), note common detachment level.

exist, in the south-east of the survey area (labelled 'Ramp 1' on Fig. 3.7A), and another in the north-western survey area (labelled 'Ramp 2' on Fig. 3.7A). Ramp 1 is relatively linear in trend (NE – SW), but on a smaller scale exhibits an irregular planform geometry. Ramp 2 has a more complex planimetric morphology (Fig. 3.7A), and weaves a sinuous path comprising of several inlets and a peninsula-like protrusion (labelled 'promontory' on Fig. 3.7A). The main scarp is elongate in a NE-SW direction, roughly parallel to the main ramp (Fig. 3.7A).

A seismic section taken perpendicular to the ramps (Fig. 3.7C) shows that when tracking along the profile in the transport direction, the basal shear surface can be seen to cut up across the main scarp of Ramp 1. Ramp 2 represents a means of lowering the basal shear surface back to its original stratigraphic level south of Ramp 1 and then cuts up onto the near-side of the promontory, and down once again at the north-western ramp forming the other side of the promontory. The basal shear surface returns to its original stratigraphic level at Ramp 2, but cuts down to a deeper stratigraphic level, by some 40 m on the north-western side of the promontory. These types of relationships are relatively common in major slides, where switching between two or more preferred stratigraphic levels for the flat segments of the basal shear surface possibly reflects the availability of more than a single surface of low shear strength. In this case of the Møre Slide, the cyclic stratigraphy of low strength contourite sediments alternating with higher strength glacial deposits (Bryn et al. 2005) could be the main factor predisposing the failure surface to adopt the ramp and flat morphology.

Ramps have been directly linked to deformational features within the main body of some MWDs, with previous studies reporting the presence of slump folds above upward stepping ramps, to accommodate the change in gradient (Trincardi and

Argnani 1990; Frey Martinez et al. 2005). It has not been established why such ramp and flat geometries develop, although Rupke (1967) reported that basal incision may be due to localised zones of high intensity shear, while Frey Martinez et al. (2005) postulated that changes in the mechanical properties of the basal shear surface, or the failed mass, or possible a combination of the two are responsible. This topic is given further consideration in section 3.6.2 of this chapter.

Although most previous descriptions of ramps have focused on features that are orthogonal to the transport direction, ramps may also occur trending parallel to the main transport direction. When they do, they frequently form in closely spaced pairs, and thereby delimit narrow, 'slot'-like zones (Fig. 3.7B & D), elongated parallel to the transport direction, which we refer to simply as 'slots'. These are readily identifiable on seismic profiles and on maps of the basal shear surface, and are excellent kinematic indicators.

Slots have not been widely recognised or described. Perhaps the first description of these extraordinary features can be ascribed to O'Leary (1986, 1993) who described the development of a narrow, steep-sided 'axial trough' at the base the Munson-Nygren Slide from the Georges Bank, and who showed it to cut down below the level of the initial basal shear surface. One of the clearest examples of a slot that we have mapped using 3D seismic data is from the Storegga Slide (Fig. 3.7B & D). A dip map of the seabed from the area (Fig. 3.7B) taken from the Big1 3D survey (Fig. 3.1) shows three downslope-elongate, narrow features delimited by steep ramps which cut discordantly down section to some 80 m below the level of the original basal shear surface (Fig. 3.7D). In this case, intervening 'flat' sections form the floor of the slots, which are approximately 3-4 km wide, and from correlation with overlapping 2D lines are up to 30 km long trending NW (Fig. 3.7). All of the slots detach at the same level.

Slot 3 appears to be infilled with the same material that is found at the seabed in the area, and is presumably highly disaggregated material from the Storegga Slide. Slots 1 and 2 differ somewhat in that the material contained within is thinner at the up-dip extreme, and thicker downslope, where the termination of the slots coincide with a compressive bulge of material. They occur in an area where the seabed MWD material cover is thinner (or absent) than in the vicinity of slot 3, and appear to overlap slightly (labelled on Fig. 3.7D). Based on the infilling of slot 3 by MWD material, it is likely it developed during the progression of Storegga Slide by down-cutting of the basal shear surface. Further examination of the infill material of slots 2 and 3 would be required to reach a conclusion on the possible timing of their formation.

Whilst slots clearly provide a direct indicator of transport direction, at present there is no obvious mechanism explaining their genesis, or why they develop in particular positions within larger MWDs. We have only identified them positively on the basal shear surfaces of a few large slides, but this does not mean they do not occur on smaller slides, and might simply reflect resolution limits. Further research is certainly needed to strengthen their use as kinematic indicators and to set them in a process framework.

Grooves and striations

The term '*grooves*' here defines long, linear or sinuous features that are 'v' shaped in cross section (Posamentier and Kolla 2003), and are equivalent to the 'furrows' described by Gee et al. (2006). Such features may be continuous over many kilometres and are generally orientated downslope, and may diverge seawards (Posamentier and Kolla 2003; Gee et al. 2006; Gee et al. 2008). These features are interpreted to be the result of the erosional action of coherent blocks of translated

material being transported at the base of a debris-like flow (Posamentier and Kolla 2003; Gee et al. 2008). Grooves are most obvious from attribute maps of the basal shear surface of a MWD, such as dip or amplitude. Figure 3.8A shows an amplitude map of a small area of the base of the Storegga Slide from the Norwegian margin, imaged by the 3D seismic survey Solsikke (Fig. 3.1). Several linear grooves, spaced an average of 700 m apart are seen, trending SE-NW to SSE-NNW. Grooves maybe difficult to identify in seismic section without reference to a base MWD map as they are typically narrow (Fig. 3.8C). The grooves shown here, with their distinctive 'v'-shaped cross sections, have typically eroded to a depth of c.7 m.

In a separate example, Figure 3.8B shows sinuous grooves which affect the basal shear surface of a MWD imaged from the area south of the Storegga Slide (Fig. 3.1). These grooves are 'v' shaped in cross section (Fig. 3.8D), and can be traced for 30 km across the 3D seismic survey, and probably extend further. The identification of grooves is useful as they directly record the translation of the MWD body across the basal shear surface, revealing both the transport direction, and given their association with debris flows, an indication of the dominant process active at that point in the development of the MWD. In addition, continuous grooves can provide some direct constraint on the minimum distance travelled by individual fragments of material within a MWD. The trend of the examples shown in Figures 3.8A & B, when combined with a local slope direction to the NW, suggest a transport direction to the NW for both MWDs. Moscardelli et al. (2006) interpreted similar erosive scouring affecting the base of a MWD from the eastern Trinidad margin as being indicative of transport direction and domination of debris flow processes, and further used them to infer flow transformation from frictionally attached (erosive) to hydroplaning (non-erosive).

'*Striations*' are defined as continuous, linear features affecting the basal shear surface of MWDs, but can be differentiated from grooves due to their wider, flat-bottomed cross section and the absence of downslope divergence (Gee et al. 2005; Gee et al. 2006). Although covered in the same section here, striations are different from grooves both in their character and the way in which they are formed. In kinematic terms however, they provide similar information.

Like grooves, striations are also associated with the translation of intact blocks of coherent material that 'plough' the basal shear surface (Gee et al. 2005), but in this case the striations represent 'glide-tracks' left behind by intact blocks which detach from the leading edge of the MWD and move downslope ahead of it and beyond it. Nissen et al. (1999) described flat-based, linear 'glide-tracks' with downslope terminations associated with intact 'outrunner' blocks which came to rest downslope of the toe of a MWD from the Nigerian continental margin. Striations up to 9km long, 200 m across and 15 m deep have been described (Nissen et al. 1999; Gee et al. 2005).

As with grooves, identification and recognition of these features is easiest when viewing attribute maps of base MWD horizons (Nissen et al. 1999; Gee et al. 2005). In the same way as grooves, striations provide directional information related to the translation of intact rafts of material, either within or in front of the main body of the MWD , and therefore indicate a general translation direction. Striations have not been identified from the dataset available for this study, and the reader is referred to Nissen et al. (1999), Gee et al. (2005; 2006) and Moscardelli et al. (2006) for excellent examples.

Other basal shear surface features

Attribute maps of basal shear surfaces often reveal many remarkable features not obvious from seismic section or time-structure maps. Examples of amplitude maps are shown in Figure 3.9, taken from the basal shear surfaces of two MWDs imaged by 3D seismic survey PL251 (see Fig. 3.1 for location). Figure 3.9A shows an acoustic amplitude map taken from the same horizon used to illustrate sinuous grooves in Fig. 3.8B.

In addition to the sinuous grooves identified from the dip-attribute map, a series of sinuous streaks and bands are revealed, mirroring the paths taken by the grooves discussed in the previous section. Streaks and bands that show up on basal shear surface amplitude maps are taken to be indicative of basal erosion (Gee et al. 2005), which in this case is confirmed by the presence of resolvable grooves (Fig. 3.8C & D). The exact mechanism of erosion or reason for the amplitude expression is unclear, but the broad extent indicates erosion by a body that is broader and smoother than that involved in the formation of the grooves and striations. The streaks and bands provide the same kinematic information as grooves and striations, and so amplitude maps can provide important kinematic and process information in the absence of conspicuous or resolvable erosional features.

A further example of an amplitude map from the base of a MWD is shown in Figure 3.9B. The amplitude map, from the base of the Tampen Slide (Fig. 3.1; Evans et al. 1996; Solheim et al. 2005), shows a remarkable pattern of deformation as delimited by the distribution of high and low amplitudes. A remarkable 'blocky' amplitude signature that can be related in seismic section to the discontinuous nature of the disaggregated remnants of blocks of material within the MWD body (Fig. 3.9C) is revealed. In planform, the blocky pattern is similar to that shown by Huvenne et al.

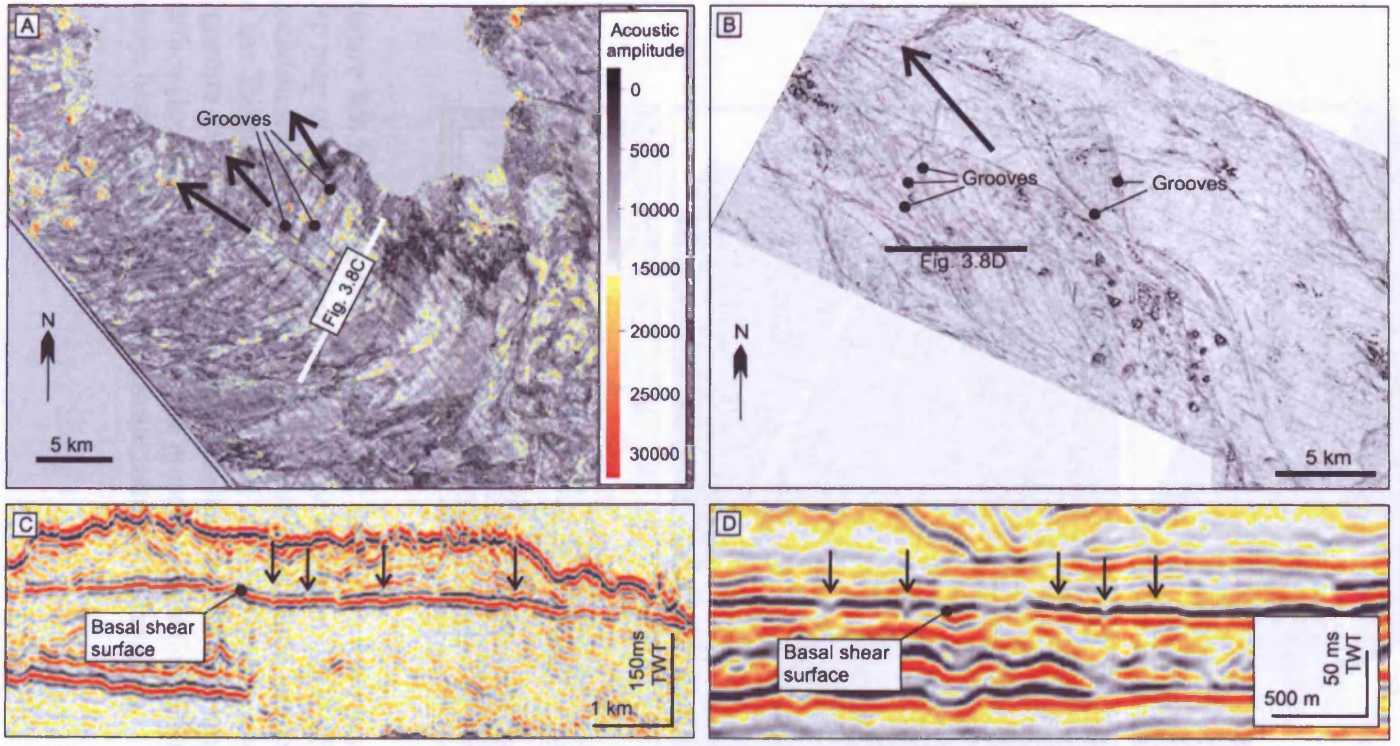

Figure 3.8. Examples of grooves in the basal shear surface. (A) Acoustic amplitude map of the basal shear surface of the Storegga Slide from within the Solsikke 3D survey area (location shown in Fig. 3.1A). NW-SE orientated banding is an acquisition artefact. (B) Dip map of a basal shear surface from the PL251 3D survey area (location shown in Fig. 3.1C). (C) Seismic section showing the grooves from the Storegga Slide basal shear surface in profile (location shown in A). Downward-pointing arrows indicate location of grooves. (D) Seismic section through horizon shown in C. Downward-pointing arrows indicate location of grooves. Note narrow, 'v'-shaped cross sectional character (location shown in B). Bold arrows in (A) and (C) indicate translation direction.

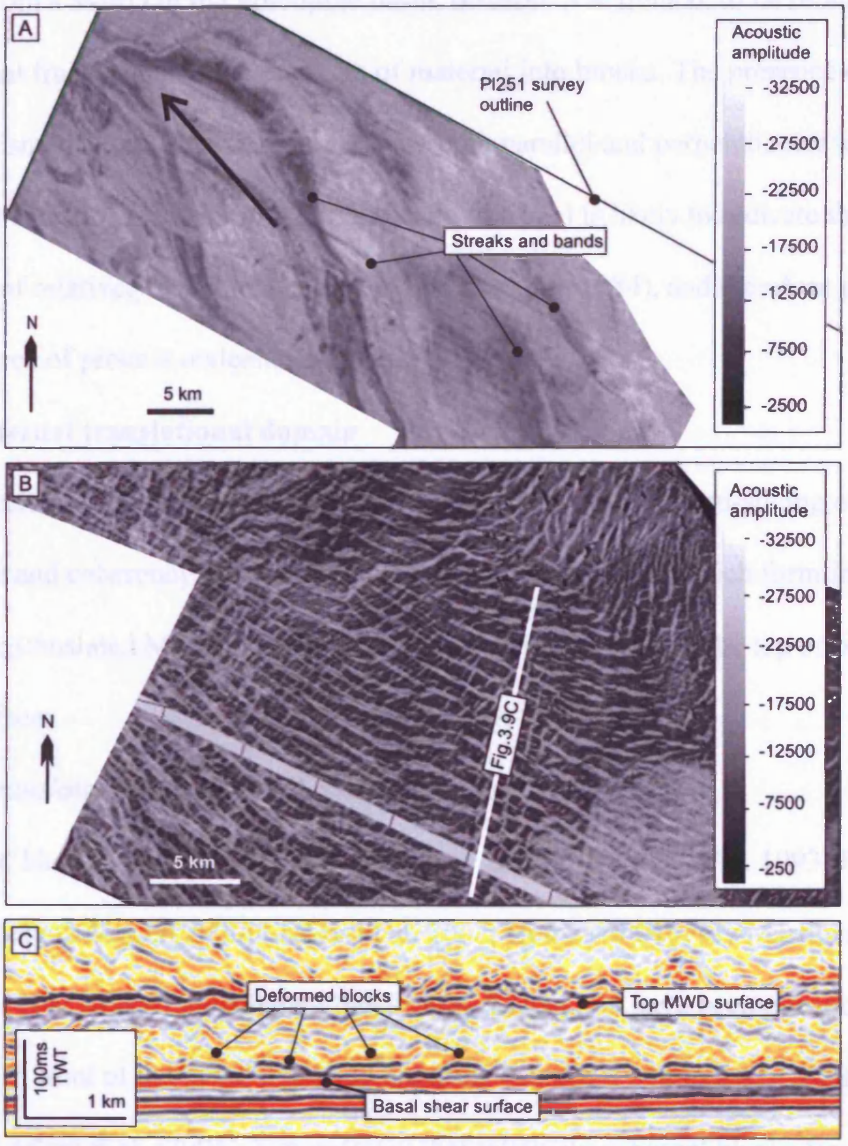

Figure 3.9. Examples of other kinematic indicators from basal shear surfaces. (A). Dip map of the basal shear surface of a MWD from the PL251 3D survey area (location shown in Fig. 3.1C). (B) Acoustic amplitude map of the basal shear surface of the Tampen slide (location shown in Fig. 3.1C), note remarkable 'blocky' signature. (C) Seismic section through small area of the Tampen slide basal shear surface (location shown in B). Note presence of partially coherent blocks of material above basal surface. Arrows indicate translation direction.

(2002), from a MWD in the Porcupine basin, offshore SW Ireland, to be related to extensional fracturing and the break up of material into blocks. The presence of relatively small extensional faults which are both parallel and perpendicular to presumed direction of maximum stress (i.e. downslope) is likely to indicate the presence of relatively consolidated material (Prior et al. 1984), and therefore provides some degree of process understanding.

3.5.2c Internal translational domain

Several techniques including time slicing, coherency slicing, and iso-slicing on amplitude and coherency volumes allow us to examine features which form internally within the translated MWD body, and may have no expression on the top or bounding basal surfaces.

Translated, outrunner and remnant blocks

Translated blocks, also called 'rafted' or 'intact' blocks (Masson et al. 1993; Bøe et al. 2000; Laberg & Vorren 2000; Lastras et al. 2002; Homza 2004; Frey Martinez et al. 2005; Gee et al. 2008), are coherent blocks of sediment that have been transported within or in front of the failed mass and are often deposited within the translational domain. Lastras et al. (2005) demonstrated that relatively coherent blocks from the BIG'95 debris flow on the Ebro margin, Mediterranean Sea, were pushed, sheared and accelerated by the more mobile coarse-grained matrix, resulting in the translation of the block over some 15 km. Translated blocks are recognised through the identification of areas of laterally concordant and continuous seismic facies, often in significant contrast to the chaotic facies of the MWD body, from which they may be separated by steeply outward dipping flanks (Frey Martinez et al. 2005; Gee et al. 2005). Although the blocks represent relatively competent pieces of MWD material, they may exhibit increasing deformation with increasing translation or duration of

sliding (Laberg and Vorren 2000, Huvenne et al. 2002; Gee et al. 2005; Lastras et al. 2005). The blocks shown in Figure 3.10A & B exhibit deformation in the form of upward-tapering cross sectional geometries, rotation and subtle disruption of internal reflections. In contrast, 'out-runner' blocks are those which detach from the leading edge of the deforming MWD body and move downslope beyond it (Nissen et al. 1999; section 3.2.2). These are often associated with 'glide tracks' or 'striations' (Gee et al. 2005; section 3.5.2b) which can be used to reconstruct the pathway of the blocks (Nissen et al. 1999). Moscardelli et al. (2006) reported similar glide tracks (referred to as 'secondary scours'), linked to outrunner blocks, from the base of a buried MWD from the deep marine margin of eastern Trinidad.

The size of translated blocks can vary, from those which may be below the resolution of the data (<8 m high), to examples such as those from the Hinlopen Slide on the Svalbard margin, Arctic Ocean, from which blocks of up to 5 km across and 450 m high have been observed (Vanneste et al. 2006; Winkelmann et al. 2008). Translated and outrunner blocks, irrespective of their location in relation to the main body of the MWD, can be used as directional indicators. Blocks which have been transported in the main body for a sufficient distance tend to become aligned with their long axis parallel to the direction of flow, and the same is generally true for out-runner blocks (Nissen et al. 1999). Where translated blocks are subject to localised compression or deposited in the toe domains of MWDs, they may become orientated with long axes perpendicular to the transport direction (Huvenne et al. 2002).

Blocks of undisturbed and continuous reflections may remain as undeformed 'islands' surrounded by the deformed translated mass (Frey Martinez et al. 2005). Like translated blocks, they exhibit laterally concordant and continuous seismic facies but are clearly coupled to the undeformed sedimentary succession below with no

visible detachment surface (Frey Martinez et al. 2005; Fig. 3.10D). These 'remnant blocks' are interpreted to represent isolated blocks of material that have not experienced failure. Frey Martinez et al. (2005) used these remnant blocks to place significant constraints on the kinematics of the surrounding MWD body by excluding the possibility that large scale translation could have occurred in the vicinity of the remnant block. Both translated and remnant blocks may be associated with flow lines recorded within, and on the top surface of the deformed mass (Masson et al. 1993; Fig. 3.10C). These may represent faster flow of the main deformed mass around slower moving translated blocks (Masson et al. 1993; Lastras et al. 2005) or the passage of material around stationary remnant blocks.

An example of a remnant block is shown in Figures 3.10C and D. The remnant block measures 3 km across its long axis and c. 75 m high. A seismic section across the block (Fig. 3.10D), shows no basal detachment or shear induced deformation visible beneath the block, although the top surface and edges appear to have been deformed and denuded. The block is clearly visible in a coherency slice as an area of smoother texture and higher coherence compared to the surrounding area (Fig. 3.10C). NE-SW trending lineations are defined in the coherency volume in the downslope wake of the remnant block (Fig. 3.10C), and are seen to converge slightly before diverging to the SW. The trend of the lineations suggests a localised transport of material to the SW. The lineations are discussed further in section 3.2.4.

Folds

A variety of fold styles have been observed from MWDs, and have been previously described from field outcrops, where they are traditionally used in the determination of palaeoslope direction (Farrell 1984; Farrell and Eaton 1988; Webb and Cooper 1988; Eva and Maltman 1994; Bradley and Hanson 1998; Strachan 2002a and b;

Strachan 2006). Farrell and Eaton (1987, 1988) proposed that MWDs which have undergone relatively little translation will feature upright folds developed by buckling, and progressively more deformed (i.e. more translated) MWDs will be characterised by tight to isoclinal, and recumbent folds. Such features develop due to simple shear (Escher and Waterson 1974), which through time will rotate fold axial surfaces towards parallelism with the upper and lower MWD surfaces, and fold hinges towards the downslope direction (Farrell and Eaton, 1988). Folds in the translated body of a MWD can therefore be useful in identifying the transport and palaeoslope direction, and possibly in determining the degree of translation.

An example of upright folding is shown in Figure 3.11, taken from a large, buried MWD south of the Storegga Slide (Fig. 3.1). Two large mounded structures have been observed from this interval, occurring within the MWD body, delimited by a convex upward and discontinuous upper boundary, correlated with a continuous, undeformed lower reflection which also forms the basal shear surface (Fig. 3.11A & B). Internally, continuous seismic reflections have been deformed into a series of convex upward, disharmonic folds which also appear to be affected by brittle discontinuities. The structures (labelled 1 and 2 respectively in Fig. 3.11) are elongate in planform, with the fold hinges corresponding to the long axis, and measure up to 1.75 km in length, 1 km across and c. 250 m thick. Structure 1 is orientated NE-SW whilst structure 2 is orientated N-S (Fig. 3.11C). The axis of folds in MWDs originate parallel to sub-parallel to the strike of the slope (Bradley and Hanson 1998), thus indicating both the palaeoslope direction and gross transport direction (Farrell and Eaton 1987). On this basis, the folds shown here indicate a transport direction roughly to the W - NW (Fig. 3.11C). The presence of these features provides a small degree of

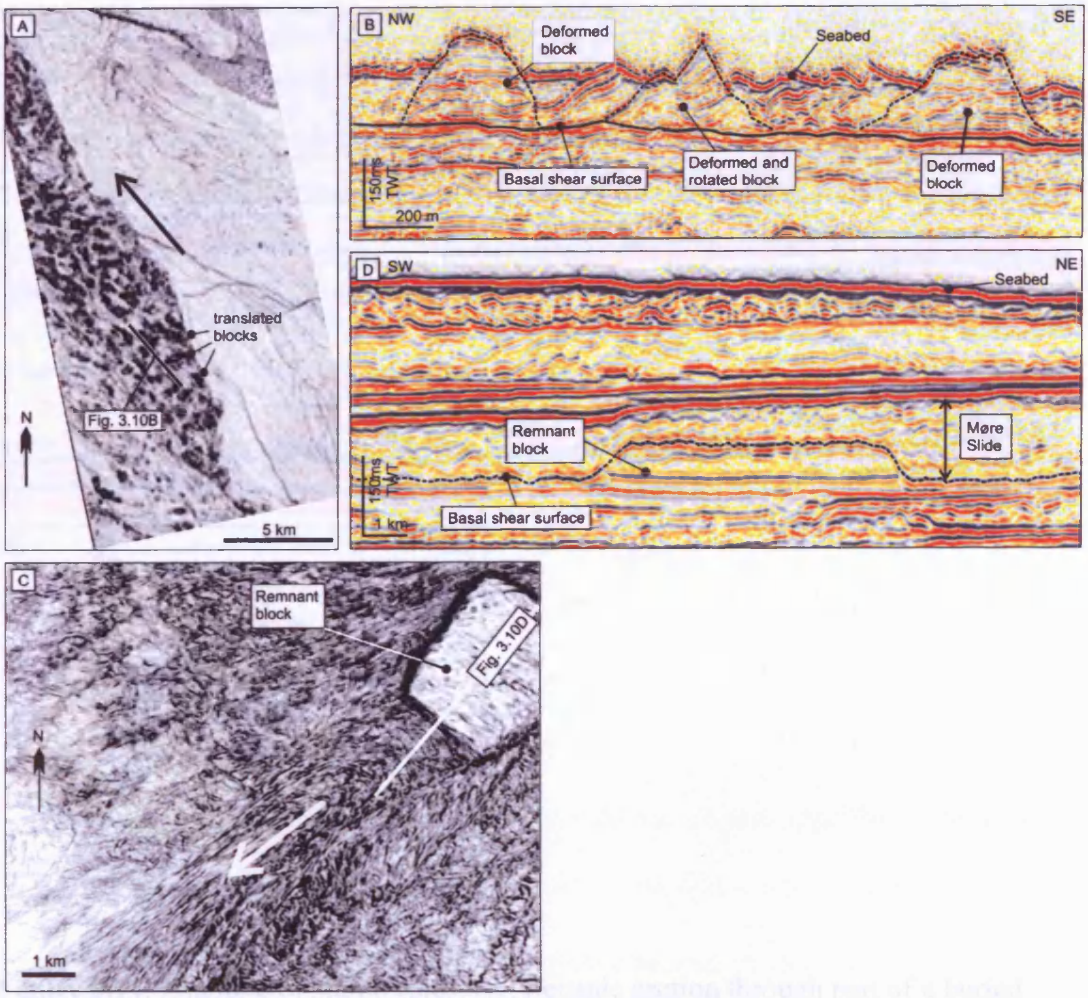

Figure 3.10. Examples of translated and remnant blocks. (A) Seabed dip map of an area within the Havsule 3D survey (location shown on Fig. 3.1A), showing a number of closely spaced translational blocks. Arrow indicates translation direction of MWD. (B) Seismic section through area of translated blocks. Note upward tapering cross sectional block geometries, rotation and disruption of internal reflectors (location shown in A). (C) Slice taken from a coherency volume generated for a small area within the PL251 3D survey area (location shown in Fig. 3.1C), showing remnant block in the Møre slide (D) Seismic section though remnant block (location shown in Fig. 3.1C). Note degraded top surface of block. Bold white arrow indicates direction of movement of MWD matrix.

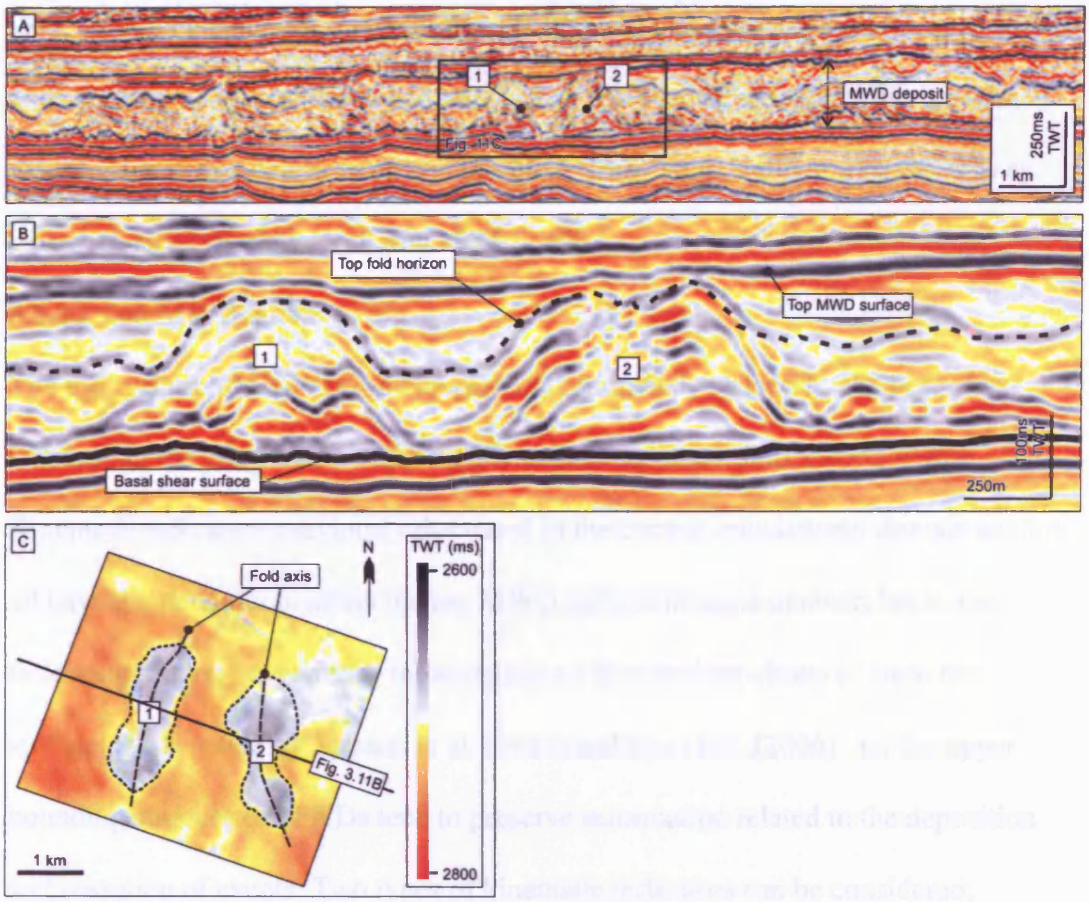

Figure 3.11. Example of slump folds. (A) Seismic section through part of a buried MWD from within the PL251 3D survey (location shown in Fig. 3.1C). (B) Zoomed in area of seismic section (location shown in A). (C) Top fold horizon structure map showing planform geometry of the slump folds (location shown in Fig. 3.1C).

process understanding of the deforming MWD body, with material deforming ductily and retaining a high degree of continuity. The fact that these features are upright, would suggest that deformation and therefore, translation had not progressed to an advanced stage (Farrell and Eaton 1987; 1988).

3.5.2d Top MWD surface

The top surface of a MWD is a complex one, intimately shaped by the processes involved in the progression of the MWD and the resultant deformation within. Kinematic indicators previously discussed in the current translational domain section all have the potential to affect the top MWD surface in some manner, but in the following section we consider those indicators that are best observed from this surface. It was noted by Masson et al. (1993) and Gee et al. (2006) that the upper bounding surfaces of MWDs tend to preserve information related to the deposition and cessation of events. Two types of kinematic indicators can be considered; *longitudinal shear lines (primary flow fabric);* and *secondary flow fabrics.*

Longitudinal shear zones

Continuous, distinct downslope trending lineaments, often marked by a low scarp are commonly observed from the top surface of MWDs (Prior et al. 1984; Masson et al. 1993). The lineaments are likely to occur in pairs and crosscut finer-scale or more superficial banding or lineations ('secondary flow fabrics', this study; Masson et al. 1993). These are interpreted as longitudinal shear zones, which separate zones of material moving at different speeds or at different times (Masson et al. 1993; Gee et al. 2005). Although the shear zones extend through the thickness of the MWD body, their subtle nature means that their presence is often only detected from examination of attribute maps of the top-MWD surface. Longitudinal shears indicate a complex system in which material within the bands is being transported at a different speed to

material outside of them, or that material within the bands was in motion at a different time than that outside. This attests to more than one process being active at once, or different phases of MWD activity being temporally separated. Prior et al. (1984) described longitudinal shears arranged in pairs, forming the edges of chute-like sediment movement zones. In seismic sections, longitudinal shear zones are visible as small scarps affecting the top MWD horizon, which may correspond to zones of visibly different facies within, and outside of the shear zones.

The kinematic information afforded here is primarily directional. Longitudinal shears are attributed to the differential downslope movement of MWD material, and reveal the direction of motion. In many cases the subtle scarps are below the vertical resolution of the seismic data, and may not be observable. Figure 3.12 shows an example of longitudinal shears taken from an area of the seabed within the Storegga Slide. A pair of longitudinal shears is seen trending NNW-SSE across the seafloor, crosscutting smaller scale fabrics. Combined with local slope direction from stratigraphic interpretation of the underlying sedimentary units, the trend indicates that the material within the pair of shears was being transported to the NNW. A seismic section taken across the features (Fig. 3.12B) shows that subtle seabed scarps, of only a few meters in height correspond with the striking lineations on the seafloor, but does not show any significant difference in the seismic character of the material inside of the bands, versus that outside. This could be due to the highly disaggregated and homogenised nature of the MWD material, or reflect the fact that only limited translation of the material inside the bands has occurred relative to the material outside of them.

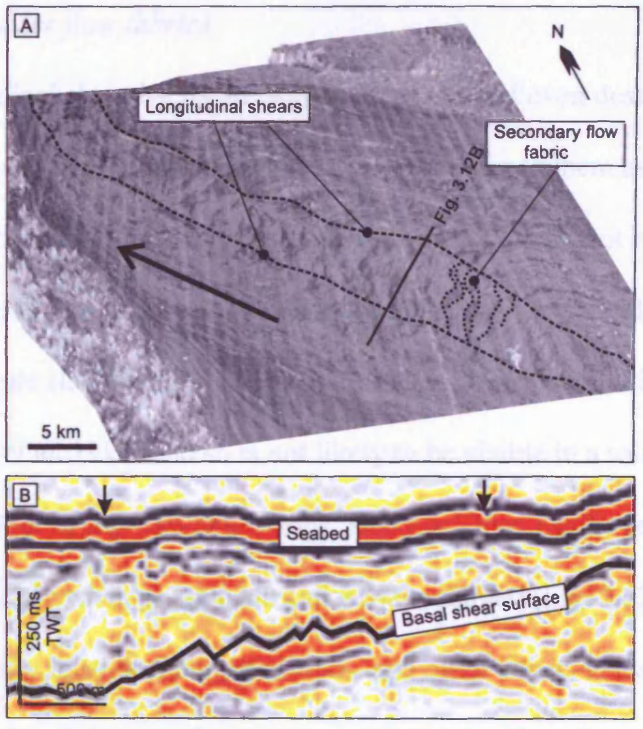

Figure 3.12. Example of primary (longitudinal shear) and secondary flow fabrics. (A) Seabed dip map taken from the area within the Havsule 3D survey (location shown in Fig. 3.1A), showing primary and secondary flow fabrics from the top surface of the Storegga Slide. Bold arrow indicates transport direction. Striped effect is an acquisition artefact (B) Seismic section through seabed (location shown in A). Downward-pointing arrows indicate location of longitudinal shear lines.

Second order flow fabrics

Because longitudinal shear bands are able to cross cut and even destroy preceding or smaller scale flow banding (Masson et al. 1993), we refer to them as a 'primary flow fabric'. This section discusses lineations or banding which are not primary, i.e. that which is not laterally continuous or cross-cutting, and occurs at a relatively finer-scale. Smaller scale flow banding has very limited topographical relief (estimated at <1m by Masson et al. 1993) and so is not likely to be visible in a seismic cross-section through the seafloor or top-MWD horizons. However, they can be seen in horizon map view, especially when seismic attributes are exploited (Fig. 3.12). Second order banding is typically localised, highly sinuous, and often occurs in association with topographical or basal shear surface texture variation, or obstacles to flow (Masson et al. 1993). Such obstacles include translated and remnant blocks (see section 3.2.3; Masson et al. 1993). An example of this association is shown in Figure 3.10D, where flow banding, revealed by horizontal slicing of a coherency volume, appears in the lee of a remnant block. The lineations converge slightly before diverging seaward in the direction of transport.

3.5.3 Toe domain

The toe domain represents the downslope region of the MWD unit, including the downslope termination point, or 'toe' (Fig. 3.2). MWD toes often have an overall convex-downslope morphology (Prior et al. 1984; Frey Martinez et al. 2005), and the main kinematic indicators contained within them are *pressure ridges* and *thrust and fold systems.* Frey Martinez et al. (2006) subdivided the toe domain into those which are 'frontally confined', whereby the translated mass is buttressed downslope against stratigraphically equivalent undisturbed strata; and 'frontally emergent' occurring

when the translated mass is able to ramp up from the original level of the basal shear surface and move freely across the seafloor. The present study has found that this classification holds true for all of the MWDs described in the examples taken from the available datasets from Norway and the Levant, and also for those described by previous studies. Frontally confined MWDs are characterised by the development of large-scale thrust and fold systems (Huvenne et al. 2002; Frey Martinez et al. 2006; Gafeira et al. 2007), whilst those which are frontally emergent typically exhibit pressure ridges (e.g. Prior at al. 1984).

There is overlap between the two extremes, with some frontally emergent MWDs developing impressive fold and thrust systems when the translating material becomes buttressed against a seabed obstacle of positive topography (Lewis 1971; Moscardelli et al. 2006). Pressure ridges and fold and thrust systems are discussed separately in the following section. Both features form due to compression at the toe of MWDs, but there is often a marked difference in scale, and because of resolution limitations, only larger structures such as thrusts and folds on a scale of >10's m in height and spacing are likely to be well imaged on our data. Pressure ridges are interpreted as the surface expression of thrusts that are below the resolving power of the data, and so in the following section, we consider examples that occur on a scale of 10's of meters, and which are not fully resolved by the data in seismic section.

3.5.3a Pressure ridges

These features are defined here as positive, parallel to sub-parallel, linear to arcuate ridges orientated perpendicular to flow direction, (Prior et al. 1984; Masson et al. 1993; Martinsen 1994; Bøe et al. 2000; Laberg and Vorren 2000; Posamentier and Kolla 2003; Frey Martinez et al. 2006; Lastras et al. 2006; Moscardelli et al. 2006). Pressure ridges are commonly observed in both submarine and subaerial MWDs, and

are usually confined to the toe domain. They can however, occur elsewhere due to localised topographical variations in the basal shear surface, or obstacles to flow (Masson et al. 1993). Pressure ridges are best viewed on top MWD surface maps. The use of seismic attribute maps, such as dip and amplitude, and further 3D seismic techniques such as the generation of coherency volumes are often useful in the identification and characterisation of these features. Due to their scale relative to the seismic resolution, they may not be obvious in attribute slices whilst not being detectable in seismic cross sections.

An excellent example of pressure ridges can be seen from a MWD from offshore Norway (Fig. 3.13). Pressure ridges are present in the form of continuous arcuate ridges which are convex in the downslope direction (Fig. 3.13A). In seismic profile (Fig. 3.13B) it is possible to identify localised areas where there is sufficient continuity of reflections to define packages of parallel, steeply landward (upslope) dipping reflections which are separated by offsets and which appear to affect the top-MWD surface, showing relief of up to 15 m. These packages of reflections are interpreted as thrusts which are slightly below the resolving power of the data.

Pressure ridges have been associated with debris flow deposits (Posamentier and Kolla 2003), and occur where MWDs are free to spread-out in an unconfined manner to form convex downslope, lobe like morphologies ('frontally emergent', after Frey Martinez et al. 2006; Prior et al. 1984; Lucente and Pini 2003). Kinematically, pressure ridges are important because of the directional information they provide. Assuming a simple gravitationally induced compressional regime, they develop perpendicular to the main flow direction to which the maximum compressive stress will become orientated (Frey Martinez et al. 2006; Lastras et al. 2006). Towards the lateral flanks of MWD toe however, the situation may be complicated by a change

in orientation of the pressure ridges, presumable due to a realignment of the maximum compressive stress, causing different rates of displacement across the width of the MWD toe (Frey Martinez et al. 2006). Prior et al. (1984) suggested that the development of pressure ridges may progress through a combination of 'stopping' forces and resistance of the undeformed sediments underlying the MWD unit. Episodic flow has also been implicated in their development (Prior et al. 1984; Lucente and Pini 2003). In this sense, it is prudent to measure only the orientation of pressure ridges along the line in which the downslope-most points of successive ridges align, as this will be the only point at which the maximum compressive stress is due to the downslope translation of material alone, and not interference from drag or 'stopping' forces. When performed for the example shown in Fig. 3.13A, the local direction of transport of the MWD material took place to the NW.

3.5.3b Thrust and fold systems

Impressive thrust and fold systems are commonly described from the toe domains of MWDs (e.g. Lewis 1971; Trincardi and Argnani 1990; Martinsen 1989, Frey Martinez et al. 2006), where they may affect sections as thick as 500 m (Gafeira et al. 2007), placing them on a similar scale to some tectonic thrusting. The distal limit of a frontally confined MWD is typically demarcated by an abrupt frontal ramp (Frey Martinez et al. 2006). Thrusts typically affect the entire thickness of the MWD body in the vicinity of the ramp above the basal shear surface, into which they detach. In seismic sections, the presence of thrusts may be identified by the presence of sufficiently continuous reflections, offset along potentially steep, landward dipping surfaces (Fig. 3.14A). Measurements of thrust dimensions from the type example of a frontally confined MWD from the Levant margin yielded heights of 167 - 236 m, lengths (perpendicular to strike) of 550 - 1200 m, thrust plane angles of 9 – 22°, and

displacements of up to 60 m (Frey Martinez et al. 2006). Huvenne et al. (2002) describes a frontally confined submarine MWD from the Porcupine Basin, offshore SW Ireland that similarly failed to overthrust the undeformed downslope strata. The MWD is up to 85 m thick and comprised of large blocks of coherent material, up to 500 m across in a chaotic 'matrix'. Blocks in the toe are folded and thrusted, and lack the internal stratification that defines them within the translated domain of the MWD (Huvenne et al. 2002).

A remarkable example of a MWD fold and thrust system is taken from the compressional zone of the Storegga Slide (Bryn et al. 2005), shown in Figure 3.14. The complex has developed along the mid-southern margin of the Storegga Slide (Fig. 3.1), a considerable distance from the true toe zone. However, the deformation has occurred above a basal detachment layer which can be traced directly into a section of the headwall which is associated with a distinct phase of failure in the multi-phase Storegga event, with material from other phases being deposited in the distal toe area (Bryn et al. 2005). This complex is interpreted to be the result of a compressional regime induced by the downslope displacement of a material from the Storegga Slide headwall region (Haflidason et al. 2004; Gafeira et al. 2007), and is therefore considered to be equivalent to a frontally confined MWD. The frontal thrust fault (Fig. 3.14A) dips at 22° and ramps up through c.500 m of sediments, separating completely deformed strata landward of the thrust and undeformed strata downslope. Landward of the thrust, are a series of regularly spaced thrust-bounded blocks. The thrust faults occur in pairs of opposite verging dip up to 40°, and define regularly spaced (average 1.43 km) pop-up structures with maximum displacements of up to

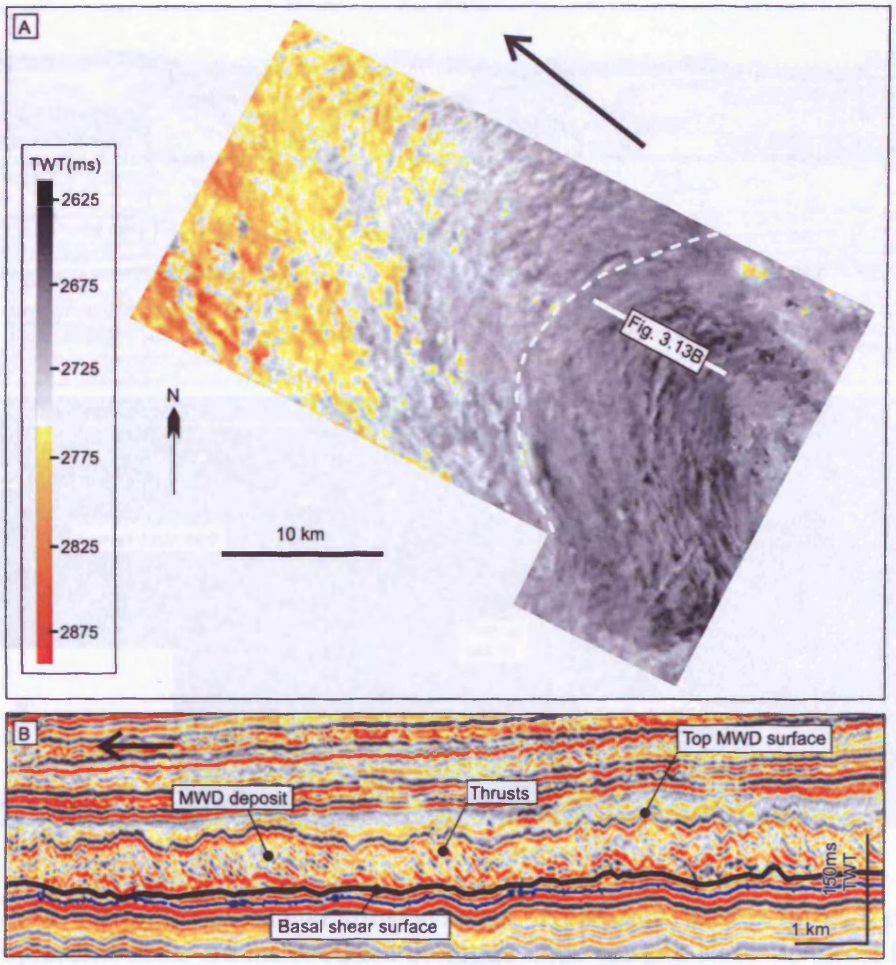

Figure 3.13. Example of pressure ridges. (A) Time structure map of the top surface of a buried MWD from within the PL251 3D survey area (location shown in Fig. 3.1C). Note steeply dipping parallel reflection separated by offsets within the MWD body. These are interpreted as small-scale thrusts which form the ridges seen in planform. Arrow indicates transport direction. (B) Seismic section through pressure ridges (location shown in A). Arrow indicates general transport direction (NW).

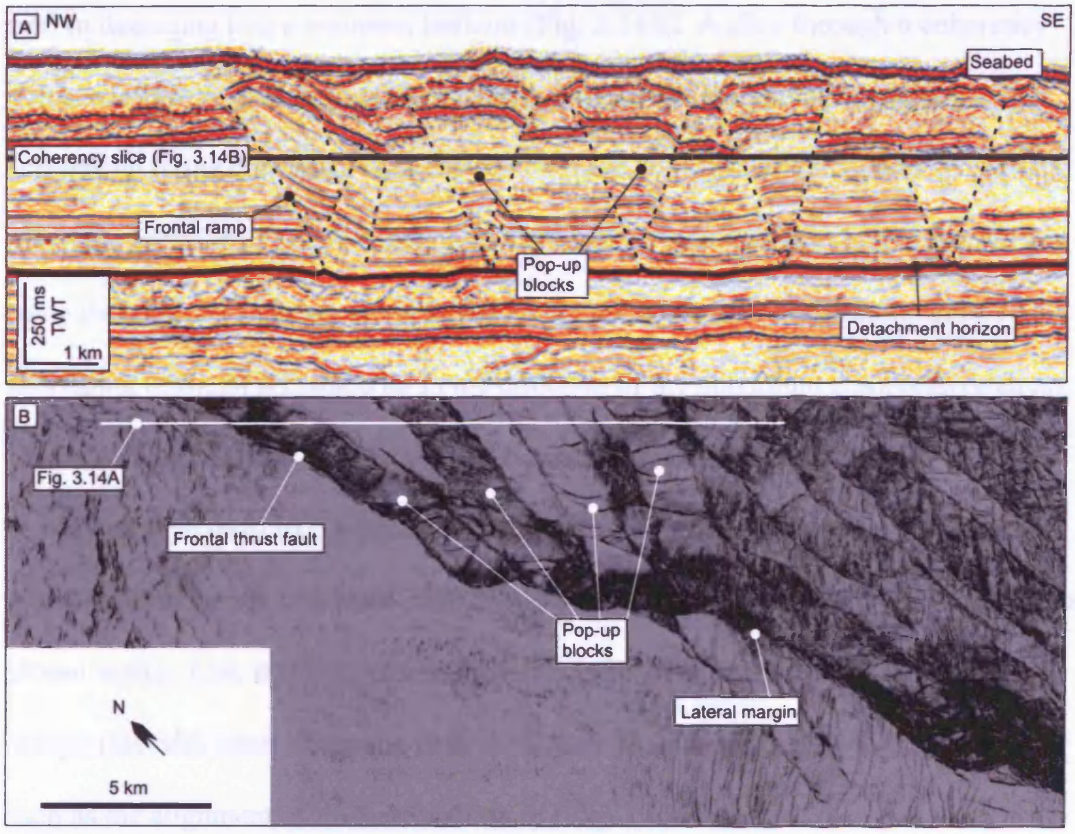

Figure 3.14. Example of fold and thrust systems. (A) Seismic section through part of the 'compression zone' on the southern Storegga Slide margin. Note the thrust faults which occur in pairs of opposite verging dip up to 40°, and define regularly spaced (average 1.43 km) pop-up structures with maximum displacements of up to c.65 m detaching into a common horizon. Location shown in B. (B) Slice through a coherency volume (Position of slice shown in A). Note the N-trending lineaments which define fault detachments.

c.65 m detaching into a common horizon (Fig. 3.14A). A slice through a coherency volume reveals a remarkable pattern of sub-parallel NNE-trending lineations which correspond to the detachments of the frontal ramp and successive faults (Fig. 3.14B). The maximum thrust height is c.650 m. Correlation on 2D seismic lines suggests that some thrust faults continue along strike for some 28 km. The thrust faults define a shortening of the MWD material in the direction of the maximum compressive stress, which, as with pressure ridges, will be orientated in the direction of primary MWD movement. The most likely transport direction is perpendicular to the strike of the thrust faults (Ramsey and Lisle 2000). Therefore, from the central area of the complex shown in Fig. 3.14, it is likely that translation took place to the NW, which is compatible with other kinematic indicators taken from further upslope in the MWD, such as the alignment of the headwall scarp (Fig. 3.4).

3.6 Discussion

The broad applicability of 3D seismic reflection data to the study of many aspects of structural geology and basin analysis has been highlighted in a number of recent reviews (Cartwright and Huuse 2005; Cartwright 2007; Posamentier et al. 2007). Commercial interest in deep water settings and the resultant increasing availability of industrially acquired 3D seismic surveys has been a major factor in our increased understanding of deep-water geological processes (Posamentier and Kolla 2003; Cartwright and Huuse 2005). In recent years the interpretation of sidescan sonar and multibeam bathymetry data, often used in combination with 2D seismic lines and geotechnical or sedimentary data have yielded much new information on the geomorphology, internal architecture and causative processes associated with MWDs

(e.g. Prior et al. 1984; Urgeles et al. 2006). These data types allow for the detailed morphological analysis of the top surfaces of relatively recent MWDs (i.e. those which affect the modern seafloor) and can be used to interpret the processes that control the formation and morphology of MWDs (e.g. Masson et al. 1993).

Whilst significant advances have been made using a 'top surface' morphological approach, 3D seismic data now affords an opportunity to adopt a truly volumetric approach to the interpretation and analysis of MWDs. The three-dimensional nature of modern seismic surveys enables the structure of MWDs to be assessed beyond what is apparent at the surface, with detailed mapping and imaging of the basal surface and internal structure made possible. Importantly, 3D seismic data affords complete analysis of the geometries of internal architectural units within the MWD body, which may not be inferred from the study of bounding surfaces alone. Furthermore as demonstrated in this study, attribute maps such as dip, amplitude and coherency enable the detection and analysis of subsurface geological details that are too small or subtle to be described using other data types (Cartwright and Huuse, 2005), and can yield information related to transport direction, process and the rheology of the displaced MWD material.

Attribute analysis of the internal elements also potentially opens the way to recognising the lateral variability of the strain characteristics, and then relating these to physical properties through acoustic inversion. Correlation and mapping of the bounding horizons of buried MWDs can be used to identify discrete MWD events in the subsurface, facilitating morphological interpretations in a similar fashion to those MWDs present on the modern seafloor, and allowing the role played by slope instability in the development of a particular basin or margin to be more thoroughly

evaluated. The seismic approach thus opens a route to investigation of repeated slope failures in specific basins, and to studies of the spatial distribution of MWDs.

The focus of this study has been to draw attention to the variety of kinematic indicators that can be gleaned from MWDs when studied using 3D seismic data. One of the major strengths of 3D seismic data that is evident from the examples presented above is the relative ease and confidence with which both gross and localised transport directional regimes can be identified from MWDs. Most of the kinematic indicators considered in the present study provide some degree of transport direction information, which can be taken from the top MWD surface, internal characteristics of the MWD and its basal shear surface, and these indicators are to be found in all three MWD domains. Transport direction can in turn be used to give the orientation of the slope over which the MWD translated, an interpretation that from traditional outcrop studies requires great care in both the initial recognition of the MWD, and accurate measurement of the axes and vergence of many individual folds (Bradley and Hanson 1998). An ultimate goal of compiling kinematic indicators from 3D seismic data must surely be to gain greater insights into failure propagation mechanisms (e.g. Martel 2004; Petley et al. 2005), and to provide better constraints on the volumetric strains involved in the different end members of the spectrum of MWDs.

It is therefore clear that there is much to gain from the exploitation of 3D seismic data in the wider study of MWDs, and continued research in this field will undoubtedly lead to further advances in our understanding of mechanisms and process. It is also apparent however, that the study of kinematics based on 3D seismic data is at an early stage, and major questions regarding the formation and significance of various MWD features remain to be answered. In the following section, we highlight the potential for further research in this field by discussing selected

examples of kinematic indicators from MWDs whose genetic mechanisms are amongst the most poorly understood, and suggest how 3D seismic data could potentially be used to resolve the open questions.

3.6.1 Lateral margins

The propagation of headscarps and the toe have been considered in some recent studies (e.g. Gauer et al. 2005; Frey Martinez et al. 2006), but almost no consideration has been given to the development of the lateral margins of submarine MWDs. The lateral margin has been considered to essentially represent a strike-slip fault (Martinsen 1994) as it is associated with horizontal shear, and by analogy with tectonic strike-slip faults, could be expected to develop as steep, planar surfaces perpendicular or subparallel to the direction of gross displacement (Twiss and Moores 1992). Owing to gross depletion in the headwall domain (Varnes 1978), the nature of the lateral margin will be transtensional in this area, and transpressional in the vicinity of the toe, where bulk accumulation occurs (Varnes 1978). By comparison with onshore analogues, it is likely that lateral margins bounding slope failures propagate from the basal detachment at depth upwards to the surface, and will develop only after displacement of material downslope has begun (Fleming and Johnson 1989).

Furthermore, Fleming and Johnson (1989) highlighted the potential of structures found on lateral margins for indicating material rheology, displacement magnitude and the stage of lateral margin development. Lateral margins develop by way of an evolving sequence of structures, and in examples formed in relatively brittle material, en echelon tension cracks, orientated 45° to the trend of the propagating strike slip fault, were observed as the first formed structures (Fleming and Johnson 1989). En echelon cracks are ephemeral and as downslope displacement

continues they may link to form a through going fracture (Fleming and Johnson 1989). In more ductile material, the first-formed structure was a simple through-going strike-slip fault (Fleming and Johnson 1989).

This study has documented the presence of both en echelon tensile failures and simple through-going strike slip faults on the lateral margins of MWDs from the Levant margin. By comparing these features to those documented onshore, it is possible to gain insights into the material rheology and stage of development of the MWD in the submarine realm in the absence of core or geotechnical data. For example, the lateral margin of a MWD from the Levant margin shown in Fig. 3.6A is characterised by both en echelon tensile failures and through-going strike slip faults. Considering the influence of rheology on structural development, this division of structural style could be used to differentiate areas of contrasting rheology. Alternatively, the differing structural styles may be a consequence of varying displacement along the lateral margin, with en echelon tensile failures indicating areas of relatively low displacement.

3.6.2 Basal ramps and flats

The enigmatic stratigraphic 'jumping' of the basal shear surface by way of ramps and intervening flat sections has been recognised from several studies (Trincardi and Argnani 1990; Strachan 2002a; Frey Martinez et al. 2005). Down-cutting or up-stepping ramps represent shear surfaces that depart from the bedding-parallel configuration of the larger part of the basal shear surface, and must therefore reflect localised variations in the stress conditions for shear failure. However, no studies have been undertaken to specifically analyse the position of ramps in a broader context, nor to quantify their dimensions and dip. These quantitative descriptions would be easy to

obtain using good quality 3D seismic data, and could yield useful constraints to input into a mechanical model.

One key question is what factors control the development of ramps. One factor could be related to the mechanical properties of the basal shear plane (e.g. lateral variations in friction). Another may relate to stresses generated as the failed material moves over the basal shear surface, or indeed, a combination of these two factors may be critical (Strachan 2002a; Frey Martinez et al. 2005). Strachan (2002a) postulated that pre-existing weaknesses in the basal shear surface, caused by original deposition of the sediments, may be exploited by localised erosion by the translating failed mass, and that localised down-cutting may indicate a change from easy-slip along the basal shear surface to reduced slip.

The formation of upward cutting ramps can be compared to the development of thrust faults, which typically propagate up through the stratigraphy in steps, alternating between following flat bedding planes or easily deformed layers, then cutting up section in the direction of displacement (Twiss and Moores 1992). The steepening of the basal shear surface to form up-stepping ramps possibly indicates the influence of mechanical asperity due to localised variation in the mechanical properties of the material overlying the basal shear surface (Frey Martinez et al. 2005), i.e. relatively higher strength, such that it did not undergo failure, and the basal shear surface was forced to deflect its path to a higher stratigraphic level.

There are two different ways in which down-cutting ramps may occur. Steeply dipping ramps which truncate significant thicknesses of strata underlying the original basal shear surface and give rise to a step-wise geometry are often observed from near the headwall regions of MWDs (Solheim et al. 2005; Fig. 3.7A & C), or where translation of material across the basal shear surface is limited (Frey Martinez et al.

2005). In this context, the basal shear surface propagates downwards to link with a deeper weak layer. The basal shear surface will often ramp up and down to a particular horizon more than once and return to its original stratigraphic level by way of an up-stepping ramp (Fig. 3.7A & C; Frey Martinez et al. 2005; Solheim et al. 2005). The specific and selective nature of the localisation of the basal shear surface ramps strongly suggests that some degree of control is exerted by the horizons exploited by flat sections. In the case of the Møre Slide example discussed earlier, the availability of more than one weak surface predisposed the basal shear surface to ramp downwards to a number of different flats. Since the basal shear surface represents a weak layer capable of allowing slip across its surface, it can be assumed that when ramps cut down to a new stratigraphic level, they do so to a similarly weak layer which will also accommodate slip and translation. Seismic based evidence for this concept was provided by Solheim et al. (2005), who noted that the jumps in basal shear surfaces from the Norwegian MWDs all did so in sedimentary units characterised by similar stratified seismic signatures.

It is interesting to note that down-cutting ramps share several characteristics with headwall scarps: they truncate strata underlying the original basal shear surface, and often develop striking perpendicular to the translation direction and dipping steeply downslope (Gawthorpe and Clemmey 1985; Trincardi and Argnani 1990; Frey Martinez et al. 2005). This similarity means it may be appropriate to consider their formation using the mechanical framework that is widely applied to headscarp development. Solheim et al. (2005) implicated failed retrogressive phases in the formation of such ramps from Norwegian margin MWDs.

Down-cutting of the basal shear surface also occurs where the failed mass actively erodes into the substrate to cut down to a deeper stratigraphic level by way of

a more shallow ramp (Strachan 2002a). Such ramps are likely to develop where the failed mass initially steps upward beyond the datum of the basal shear surface and translates freely across the seafloor. The development of down-cutting ramps in this context is linked to the erosion by the failed translating mass of pre-existing weakness or perturbations in the surface over which translation is occurring (i.e. the seafloor), such as zones of relatively weak or mobile sediment generated during deposition (Strachan 2002a), faults or fractures, or variations in slope. The presence of erosive features such as grooves and striations at the base of MWDs is evidence that MWDs are capable of cutting down into the substrate. Moscardelli et al (2006) was able to determine areas where a buried MWD from offshore Trinidad was eroding the basal shear surface from areas where there was a high degree of frictional shear resulting in large scale erosional scouring. Ramps formed in this manner therefore reflect the ability of a MWD to locally cut down and entrain material from below the basal shear surface (Strachan 2002a), and represent the maximum depth to which the MWD can erode.

In conclusion, much further research is required to clarify the exact origins and mechanical significance of some of the kinematic indicators discussed in this paper. However, the full potential of 3D seismic data to capture the subtleties of geometry and acoustic variation evident in all MWDs is only now starting to be realised, and there is considerable scope for much more quantitative analyses in the future.

3.7 Conclusions

This study has shown that 3D seismic analysis is an excellent tool for the study of MWDs and its application yields many pertinent observations that allow for insights

into mechanisms and processes. One of the major advantages of the use of 3D seismic data in this capacity is the speed and confidence with which the general transport direction can be constrained. Furthermore, exploration of key aspects of MWD analysis which have been poorly understood, such as the development of large-scale toe zones and ramp and flat basal shear surface geometries has been facilitated. With the continued acquisition of, and improvements in the technology used to acquire, process and manipulate such data, it will be possible to continue to study new and previously undescribed examples of MWDs which will contribute further to our understanding.

CHAPTER FOUR

4.0 A 'frontally confined' submarine mass wasting deposit recognised from the Holocene Storegga Slide

4.1 Summary

The area of the Storegga Slide historically referred to as the 'compression zone' has been mapped and characterised using a combination of 2D and 3D seismic data and bathymetry data. The compression zone has previously been interpreted as a zone of contractional deformation resulting from the downslope and west-wards movement of a large intact slide block as part of one of the intermediate phases of Storegga Slide development. The present study shows that the compressional features can be linked laterally and up-dip with a number of other features diagnostic of submarine mass wasting deposits, across an extensive basal detachment horizon. The identification of a headwall, lateral margins, zone of extensional deformation, translated and remnant slide blocks which can be linked genetically with the compression zone shows that the latter represents the distal region of a frontally confined-type submarine mass wasting deposit, first identified by Frey Martinez et al. (2006). Furthermore, it can be demonstrated that extensional deformation in the up-dip region represents a later, separate stage of deformation which involved the removal of a significant volume of material as part of the final stages of Storegga Slide development, instead of the minor volumes reported in previous studies.

4.2 Introduction

The compressional structures formed within the toe zones of large-scale submarine MWDs can yield valuable kinematic information relating to the magnitude and direction of translation, and for ancient examples, can be used to determine palaeoslope direction (Frey Martinez et al. 2006). Recently, a detailed study based on 3D seismic data has resulted in the identification of two end members of submarine MWDs based on their mode of frontal emplacement (Frey-Martinez et al. 2006). *Frontally emergent* types occur where the translated mass is able to ramp up from the original level of the basal shear surface and move freely across the seafloor (Frey Martinez et al. 2006; Fig. 4.1A). This typically leads to a relatively thin deposit which has spread-out in an unconfined manor, and which typically exhibits pressure ridges (e.g. Prior et al. 1984; Frey Martinez et al. 2006). Pressure ridges are interpreted as the surface expression of relatively small-scale thrusts (i.e. fault heights in the range of 10's of meters) which are not fully resolved by modern seismic data in cross-section (chapter three, section 3.5.3a). *Frontally confined* types occur when the translated mass is buttressed downslope against stratigraphically equivalent undisturbed strata, involving a deep-seated detachment surface and typically developing a toe zone characterised by large-scale thrust and fold systems (e.g. Huvenne et al. 2002; Frey Martinez et al. 2006; Fig. 4.1B).

The mechanisms governing the development of toe zones from large-scale submarine MWDs are still the topic of debate however, with several studies proposing various models: Farrell (1984) likened the development of a MWD to that of a theoretical dislocation loop. In this model, the fault tip line spreads out radially from a

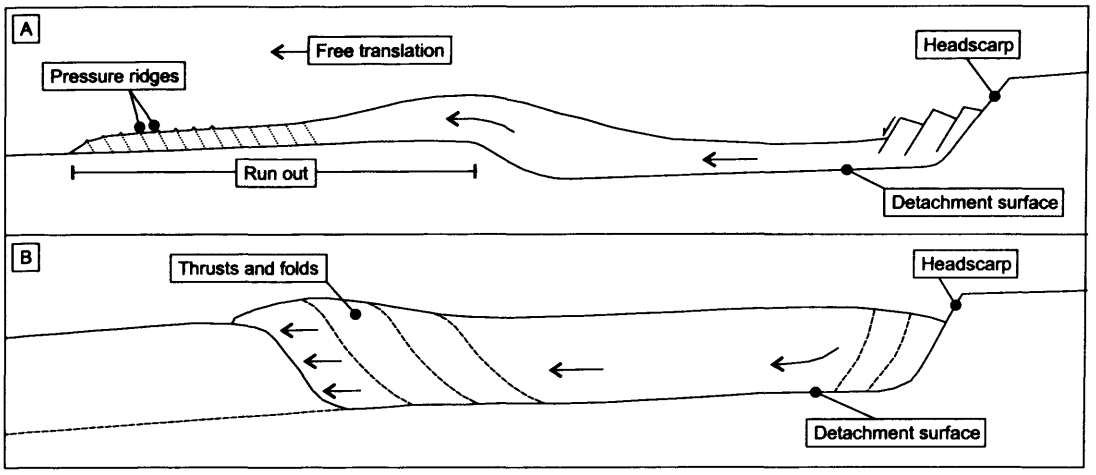

Figure 4.1. Schematic representation of the two main types of submarine mass wasting deposits according to their style of frontal emplacement. A: Frontally emergent; the basal shear plane ramps up to the seabed to allow the free translation of failed material to move in an unrestrained fashion across the seafloor. Typical characteristics of such examples include broad, relatively thin lobes with convex downslope terminal margins and pressure ridges (chapter two, section 3.5.3a). B: Frontally confined. The failed mass is buttressed against the frontal ramp which is formed by the deeply-seated basal shear surface ramping up steeply to intersect the seabed. The failed mass does not abandon the original basal shear surface and typically large-scale slump and fold systems develop landward of the distal margin (chapter two, section 3.5.3b). Modified after Frey Martinez et al. 2006.

point of initial failure, within which material has slipped and outside of which material is unslipped. Extensional strain in the MWD would therefore develop where the dislocation propagates in the opposite direction to the slip direction, and contractional strain would be evident where the dislocation propagates in the same direction as the slip direction (Farrell 1984). It follows therefore, that the contractional strain will develop downslope of the initial failure (Farrell 1984). It was further suggested that cessation of the slope failure event occurs due to the failed mass regaining cohesion with the underlying failure surface, with the failed mass halting at its distal edge first, followed by propagation of a compressional strain wave towards the proximal region (Farrell 1984).

Martel (2004) carried out a study based on a 3D elastic model for the development of a basal shear surface of an onshore slope failure, in which the basal surface was considered to be a shear fracture. The study found that the observed surficial deformation would initiate at the upslope head of the MWD and propagate downslope in an 'unzipping' fashion, as deformation propagated across and upward from the underlying failure surface. Frey Martinez et al. (2006) postulated that the large-scale contractional deformation which develops in frontally-confined type submarine MWD's does so due to the deep-seated nature of the basal failure surface which causes the translating mass to become 'locked' within the original (pre-failure) stratigraphic template. Progressive displacement of the failed mass is accommodated in the development of the large-scale structures, with downslope propagation of the MWD most likely occurring through bulldozing of the foreland, based on the geometrical similarity between the distal region of the type example of a frontally confined MWD, and that of imbricate thrust fans (Frey Martinez et al. 2006).

The following chapter focuses on the 'compression zone' of the Storegga Slide (Haflidason et al. 2004; Bryn et al. 2005a), which defines an area along its mid-southern margin characterised by spectacular, large-scale compressional deformation linked to failure in the main headwall area (Fig. 4.2). The true 'toe zone' of the Storegga Slide, which developed by way of several major phases of failure (Bugge 1983; Haflidason et al. 2004), is located in the deep waters of the Norway Basin some 800 km from the main Storegga Slide headwall scarp (Fig. 4.2; Haflidason et al. 2004). Some 250 km^3 of material is estimated to have been deposited in this region in the form of turbiditic flows (Haflidason et al. 2004), superficially giving the Storegga Slide the requisites of a classical 'frontally emergent' mass wasting deposit.

In contrast with this, the deformation in the 'compression zone' has occurred above a basal detachment surface which can be traced directly into a section of the headwall associated with a distinct phase of failure in the multi-phase Storegga event (Haflidason et al., 2004; Bryn et al., 2005a; Bünz et al. 2005), with material from other slide phases being deposited in the 'true' distal toe area (Fig. 4.2; Bryn et al. 2005a). The 'compression zone' is interpreted to be the result of a compressional regime induced by the downslope displacement of material from the Storegga Slide headwall region (Haflidason et al. 2004; Bryn et al. 2005a; Gafeira et al. 2007; Færseth and Sætersmoen 2008). For the purposes of this study, the compression zone is inferred to be the buttressed toe zone representing a discrete, frontally confined type submarine MWD that occurred as part of the multi-phase Storegga Slide.

This chapter aims to fully define, document and characterize the compression zone using the broad data coverage afforded by 2D seismic data and bathymetry data (Fig. 1.8), and test the Frey Martinez model by attempting to identify and correlate a detachment surface updip to determine the full extent of the slope failure event of

which the compression zone represents a part. Further considerations of this study involve an evaluation of the strain history and volumetric changes which have occurred, and the effect of subsequent phases of failure during the Storegga Slide. Further detailed insight is provided by two 3D surveys located on the southern lateral margin, and in the central headwall region of the Storegga Slide, respectively (Fig. 4.2). Previous work on the compression zone (Haflidason et al. 2004: Bryn et al. 2005; Gafeira et al. 2007; Færseth and Sætersmoen 2008) have provided some description of the structures and made estimates of shortening and displacements, but have not shown explicitly how the compression zone is genetically linked to the main headwall area, nor considered volumetric balancing.

4.3 Specific study area

This chapter focuses on the deformed Plio-Pleistocene sediments of the Møre Basin (Fig. 4.2). The distal margin of the compression zone event is located almost 140 km downslope of the main headwall of the Storegga Slide, where sediments deformed and dissected by Storegga area events are juxtaposed with relatively undeformed strata preserved in the thick progradational sediment wedge known as North Sea Fan (Fig. 4.2; King et al. 1996). The North Sea Fan succession is comprised of massive glacigenic debris lobes, gravity flows and hemipelagic sediments (Fig. 1.3; King et al. 1996; Nygård et al. 2005). The large volume of sediment is the result of deposition during the glacial cycles (see chapter 1, section 1.3.1) and input from the Norwegian channel, a deep trough skirting the whole of the south and west Norwegian coast, during the late Cenozoic (Evans et al. 1996; King et al. 1996; Nygård et al. 2005).

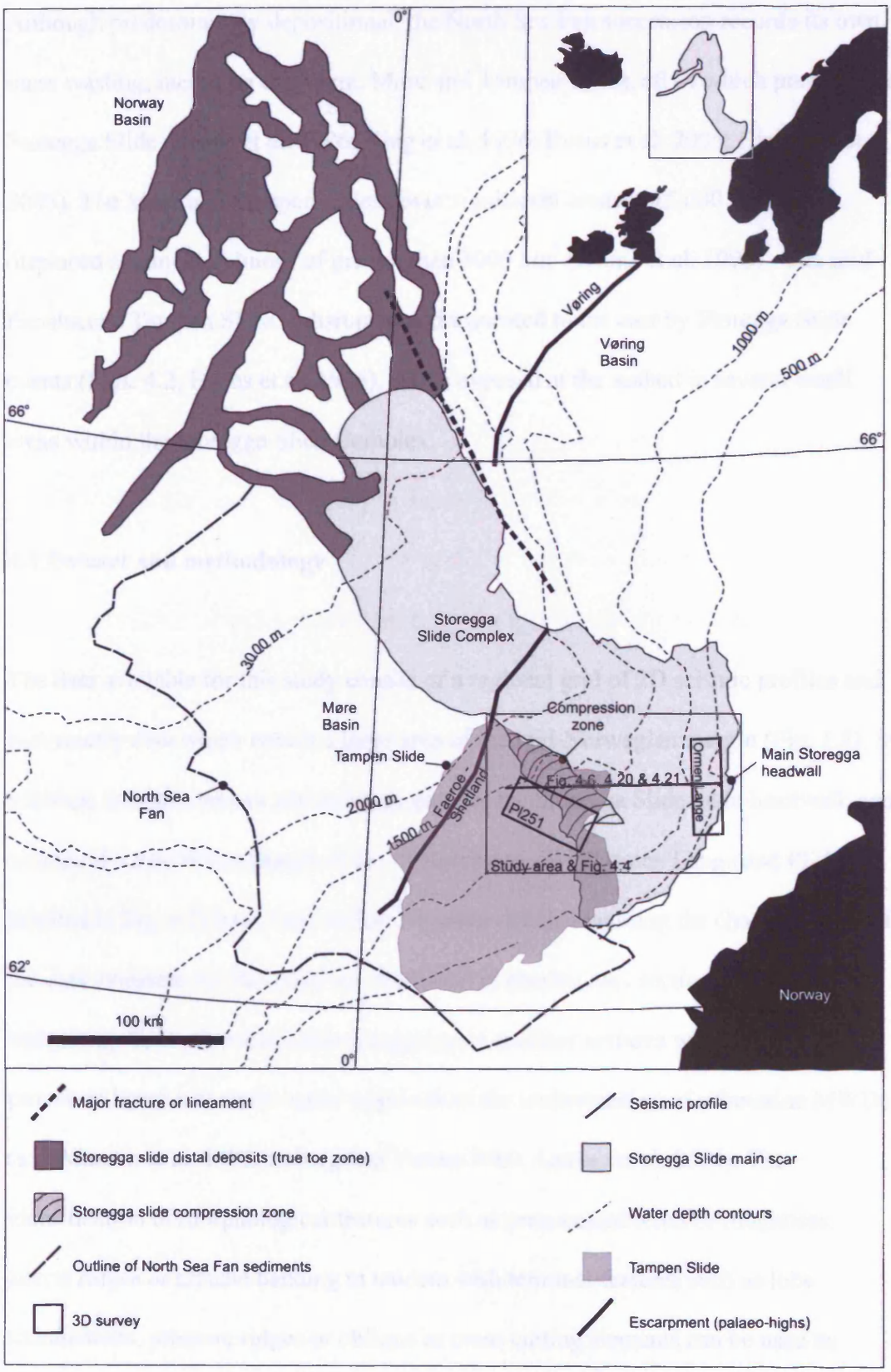

Figure 4.2. Map showing the study area, seabed contours, outlines of the Tampen Slide, the Holocene Storegga Slide and compression zone, location of the distal turbidite deposits resulting from the Storegga Slide, and the data used.

Although predominantly depositional, the North Sea Fan succession records its own mass wasting, including the Vigra, Møre and Tampen slides, all of which pre-date the Storegga Slide (Evans et al. 1996; King et al. 1996; Evans et al. 2005; Hjelstuen et al. 2005). The Møre and Tampen slides cover significant areas (>15,000 km^2) and displaced sediment volumes of greater than 3000 km^3 (Evans et al. 1996). The mid-Pleistocene Tampen Slide is disrupted and truncated to the east by Storegga Slide events (Figs. 4.2; Evans et al. 1996), and is exposed at the seabed in several small areas within the Storegga Slide Complex.

4.4 Dataset and methodology

The data available for this study consist of a regional grid of 2D seismic profiles and bathymetry data which covers a large area of the mid-Norwegian margin (Fig. 1.8). In addition, two 3D surveys which image parts of the Storegga Slide main headwall, and an area of the southern margin of the compression zone (Ormen Lange and Pl251, labelled in Fig. 4.2) have been utilised. Further details regarding the characteristics of the data available for this study are presented in chapter one, section 1.4. The bathymetry data allow the detailed mapping of seafloor textures which have been proven to be an extremely useful approach to the understanding of submarine MWDs (e.g. Masson et al. 1993; Laberg and Vorren 2000; Lastras et al. 2004). The identification of morphological features such as pronounced relief or roughness, lateral ridges or arcuate banding in tandem with terminal features such as lobe terminations, pressure ridges or oblique or cross cutting elements can be used to characterise the mass wasting deposits and draw attention to deformational structures associated with its dynamic emplacement (Masson et al. 1993; chapter three, this

study). The Storegga Slide is a good candidate for such an approach as it is a relatively recent event (c. 8200 yr B.P.; Bryn et al. 2005a) which has subsequently experienced low rates of sedimentation (Haflidason et al. 2004). Hence, the seabed expression is well preserved (Haflidason et al. 2004). The 2D and 3D seismic data available for this study facilitates imaging of subsurface elements which in combination with bathymetry data allow for a holistic characterisation of the compression zone and associated deformation.

4.5 Characterising and constraining the compression zone

The large volume of sediments mobilised and displaced during the Storegga Slide has resulted in variety of morphological signatures at the seabed, which have been used as primary factors in determining the provenance and sequence of the various slide phases (Haflidason et al. 2004). The compression zone is best defined by the geomorphological signature of the seabed, which is characterised by laterally continuous, downslope-convex, subparallel lineations which are orientated between NW – SE and N – S (Fig. 4.3). The lineations define a downslope tapering area of the seabed, and are continuous along-slope for distances of between 7 and 28 km.

A representative 2D seismic dip-profile taken through the distal region of the compression zone is shown in Figure 4.4. Sediments in close proximity to the distal margin appear substantially thickened (maximum thickness of 640 m above the detachment horizon) and it is found that seabed lineations correspond to broad ridges exhibiting positive topography of up to 30 m (Fig. 4.4A). The ridges are the seabed expression of upwardly displaced, laterally continuous blocks bound by pairs of thrust faults exhibiting opposing dip, and detaching into a common basal detachment

horizon. The basal detachment is defined as a continuous horizon which clearly separates the deformed sediments above from undeformed sediments of differing seismic facies characteristics below (Fig. 4.4A). The upwardly displaced blocks are therefore interpreted as 'pop-up' blocks, and measurements of key parameters taken from the thrust faults are summarised in Table 4.1.

A package of deformed slope sediments that are generally assigned to the Tampen Slide are contained within the slope units that were subsequently to be remobilised during the latest slide succession. These comprise a chaotic seismic facies unit bound by high amplitude top and basal surfaces (Fig. 4.4). As such, this earlier slide unit provides an excellent marker interval within the compression zone, along with the Base Møre Slide horizon to a lesser degree, and both can be traced well into the Storegga Slide complex (Fig. 4.2 & 4.4).

Within the pop-up blocks, evidence of folding is observed in the form of upward-convex deflections of individual reflections (Fig. 4.4B). The thrust faults pairs are spaced an average of 0.6 km apart and fault angles range from 33° to 65°. A total of 32 thrust fault pairs and associated pop-up blocks have been identified within the compression zone from key 2D seismic dip-profiles. Correlation with the linear features observed from the bathymetry data show that they are laterally continuous across the breadth of the compression zone (Fig. 4.3).

Throw values were measured for all of the thrust faults which are sufficiently well imaged, and show a wide range of values from 14 m to 100 m. Heave measurements taken from sufficiently well imaged faults (based on high-confidence correlation of the Base Tampen Slide horizon) were used to estimate the amount of shortening undergone by the sediments in the compression zone. From 30 well imaged offsets, a total thrust-related shortening of 2.05 km was calculated assuming

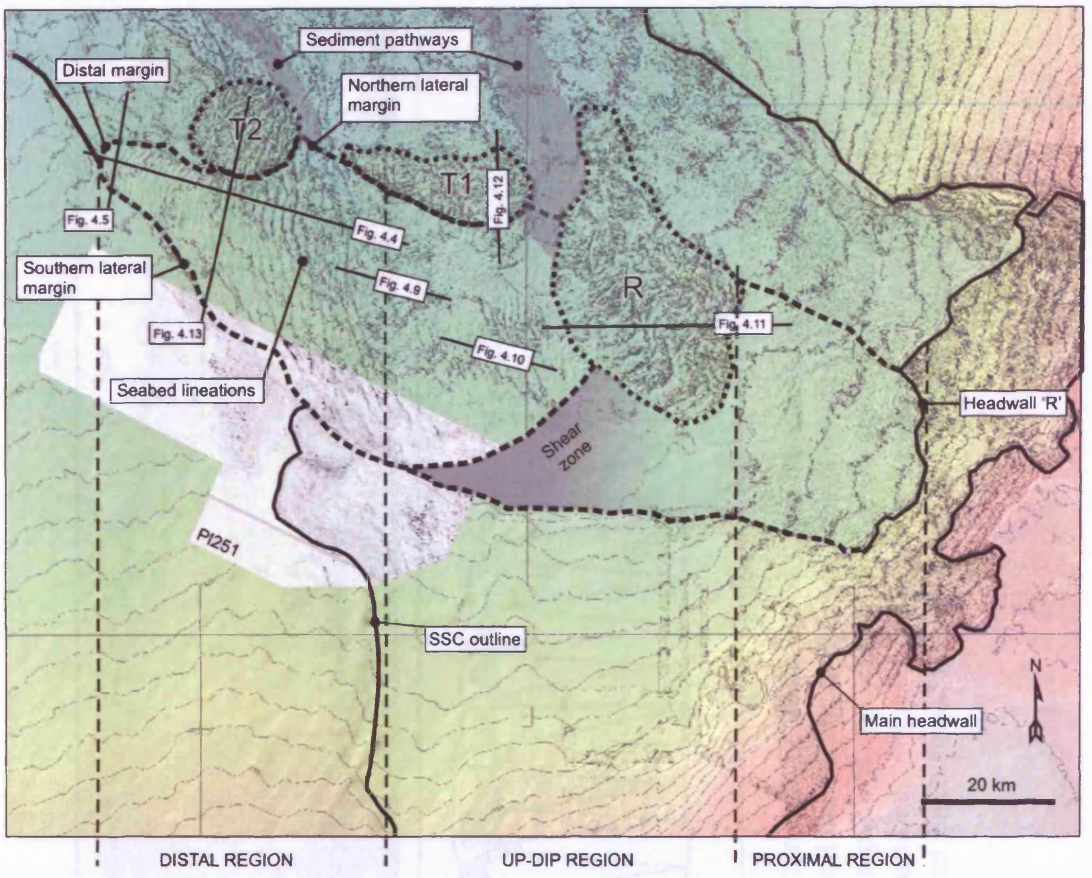

Figure 4.3. Bathymetry map of the Storegga Slide 'compression zone' and surrounding area showing seabed character and location of various figures. The compression zone is characterised by NW-SE and N-S trending seabed lineations (labelled). Notice that the seabed lineations change in character to become less pronounced in the region up-dip of the distal region (labelled). Note the positions of the distal and lateral margins of the compression zone which delineate the unusual downslope-narrowing planform geometry. Sediment 'pathways' and the planform extent of a sheared zone are shaded in grey. Note the position and planform geometry of 'Headwall R' of the Storegga Slide which is linked to the compression by a detachment horizon, and by lateral margins delimiting the northern and southern extent of the compression zone and related up-dip features. The low-relief character of the seabed in the proximal region is inferred to represent a thin-cover (i.e. 40 – 60 m) of highly disaggregated mass wasted material. Three large slide bodies are identified from a combination of their seabed expression and seismic character in profile. 'Slide Block R' is interpreted as an intact and partially translated slide block, and T1 and T2 are interpreted as rooted, untranslated remnant blocks of pre-Storegga Slide stratigraphy which have preserved outliers of Tampen Slide deposits. Within the PL251 3D survey area, a seabed dip-map has been overlaid to fully illustrate the seabed features associated with the southern lateral margin. SSC: Storegga Slide Complex. Location shown in Fig. 4.2.

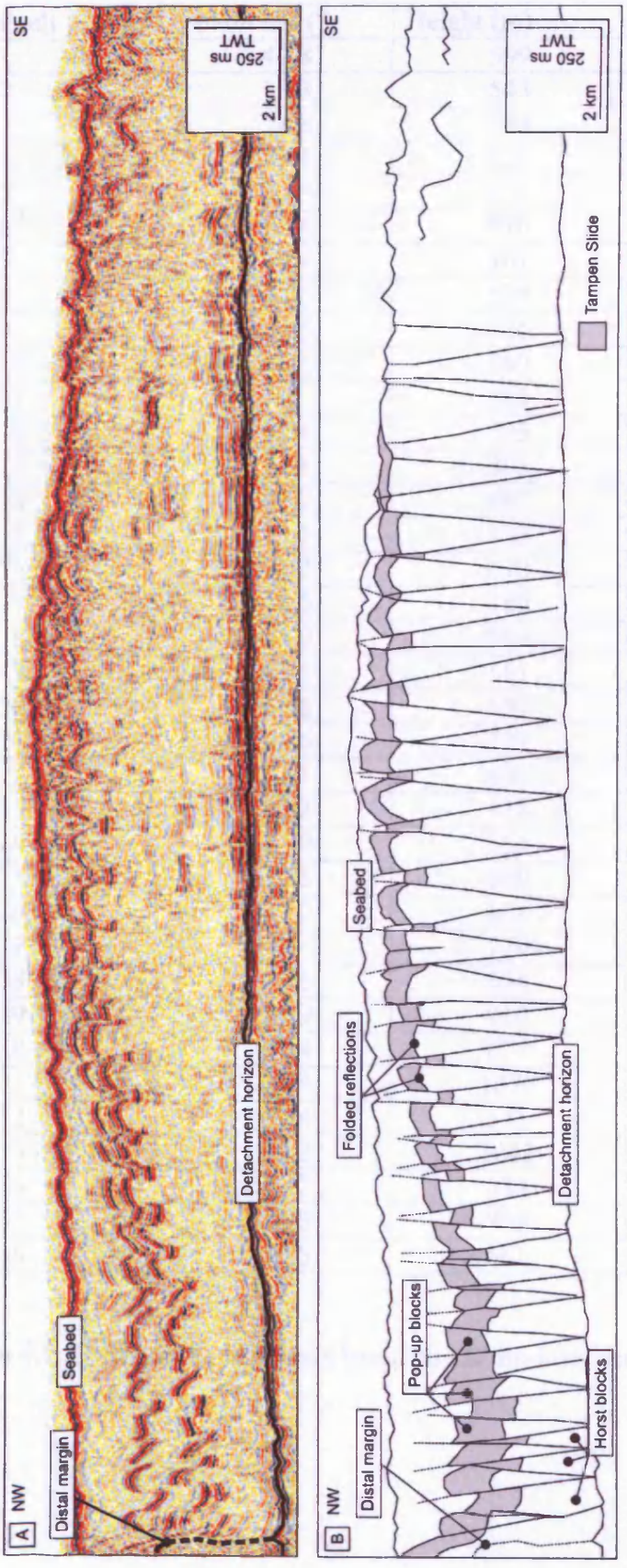

Figure 4.4. 2D seismic dip-profile showing a central profile taken through the distal region of the compression zone. A: Uninterpreted profile. B: Interpreted profile. Note the basal detachment horizon and the thickness of the sediments which overlie it (maximum thickness of 640 m). Note the numerous thrust faults which occur in pairs of opposing dip and define upwardly displaced 'pop-up blocks', detaching into the detachment horizon. Also note the depositional unit resulting from the Tampen Slide (labelled), which form a chaotic interval bound by continuous, high amplitude top and basal surfaces and provide a sequence of stratigraphic markers. Location shown in Fig. 4.3.

Fault	Fault dip (°)	Height (m)	Maximum throw (m)
1	42.8	599	84
2	73.3	543	59
3	78.8	363	68
4	83.1	523	67
5	39.5	876	59
6	65.4	570	76
7	46.4	701	76
8	86.6	524	48
9	87.5	336	14
10	64.3	560	24
11	50	604	62
12	60.4	505	26
13	34.1	808	69
14	82.7	487	43
15	33.1	833	40
16	78.2	470	48
17	38.5	780	75
18	55.9	594	73
19	45.5	561	34
20	66.8	557	40
21	41.6	729	65
22	71.1	608	50
23	39.2	918	57
24	71.9	551	65
25	37.5	850	100
26	87.9	634	63
27	45	779	62
28	62.3	634	56
29	38.9	910	61
30	61.4	674	64
31	35.4	1076	58
32	67.4	643	52
33	37.2	1043	30
34	77.2	588	24
35	50.3	709	32
36	56.5	661	41

Table 4.1. Thrust fault parameters based on 2D dip-lines across the distal region.

purely dip-slip kinematics. If this shortening is representative for the total number of thrust faults which have been identified (62), the total shortening for the central area of the compression zone is estimated as 4.24 km. It is noted that minor additional shortening is accommodated in the fold component of the many contractional structures as for example is evident from the buckled geometry of the Top and Base Tampen Slide horizons within some of the pop-up blocks (Fig. 4.4B). Measurement of bed length in the folded zones shows that this is responsible for an additional 400 – 600 m of shortening in the distal region, yielding a total shortening (line length change due to folding plus heave of thrusts) of the order of 5 km.

The planform geometry of the compression zone exhibits a pronounced narrowing in the downslope direction, terminating in a distal margin which is just 7 km across (Fig. 4.3). This downslope-narrowing shape is in marked contrast to classical examples of toe zones from submarine MWDs, which typically exhibit a broad, downslope-convex morphology (Prior et al. 1984; Frey Martinez et al. 2005; chapter three, section 3.5.3). A strike-section through the distal region illustrates its laterally confined nature (Fig. 4.5). In the vicinity of the distal margin, the lateral margins are represented by broad (up to 1 km across) inward-dipping zones of deformation across which reflections are disrupted and offset, and define an area of raised seabed topography that equates to the thickened succession (Fig. 4.5A). Horizons are offset by up to 200 m in a reverse sense across the disrupted zones, which are interpreted as lateral margins and feature thrust faults with associated folding that is indicative of an element of compression orientated parallel to the lateral margins (Fig. 4.5B).

Within the compression zone, there is some repetition of the succession across individual thrusts, with the Tampen Slide appearing substantially thickened (Fig.

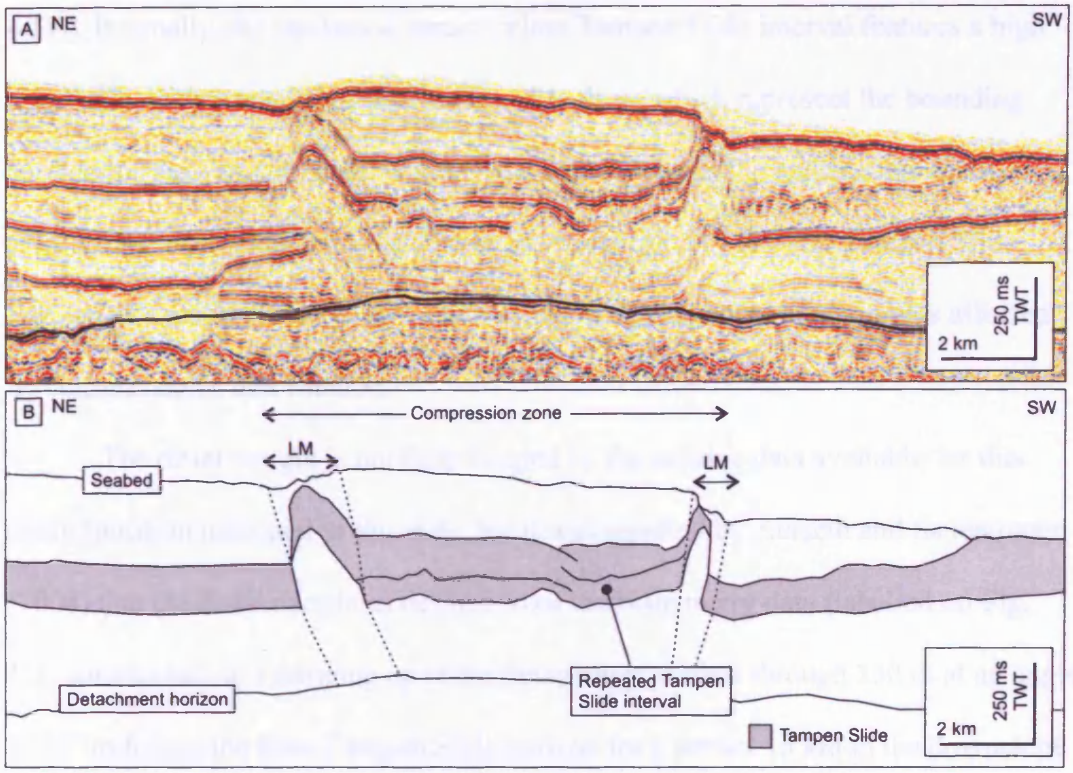

Figure 4.5. 2D seismic strike-profile through the distal region of the compression zone, close to the distal margin. A: Uninterpreted profile. B: Interpreted profile. Note the steeply dipping, offset reflections which form the lateral margins of the compression zone, and repetition of the Tampen Slide deposit. LM: Lateral margin. Location shown in Fig. 4.3.

4.5B). Internally, the thickened, structureless Tampen Slide interval features a high amplitude, undeformed reflection identical to those which represent the bounding surfaces of the Tampen Slide, which is continuous across the entire strike section (Fig. 4.5B). This reflection is interpreted as a repetition of the Top Tampen Slide horizon as a result of the upward and basinward displacement of sediments affected by compressional deformation.

The distal margin is not fully imaged by the seismic data available for this study (position indicated in Fig. 4.4), but it was reported by Færseth and Sætersmoen (2008) that the distal margin as defined from the bathymetry data (labelled on Fig. 4.3) corresponds to a ramping up of the detachment surface through 250 m at an angle of 30° to follow the Base Tampen Slide horizon for a further 15 km in the downslope direction. The ramp is associated with fault-bend folding affecting the seabed which has subsequently been partially eroded (Færseth and Sætersmoen 2008).

4.5.1 Up-dip correlation

Having delimited and characterised the compression zone, is it possible to correlate the observed deformation up-dip and link it genetically with further, more proximal slope failure features in order to fully define a discrete mass wasting unit? All of the previously described deformational features detach into a common horizon, clearly identified from the various 2D profiles (e.g. Fig. 4.4). From correlation across the 2D grid this detachment horizon is continuous across the study area (Figures 4.6 & 4.7). This horizon is identified as INS2, a reflection that occurs in Naust subunit S, deposited between 420 – 380 ka (Haflidason et al. 2004; Berg et al. 2005; Bryn et al. 2005a). INS2 is reportedly a regional reflection which can be confidently tracked into

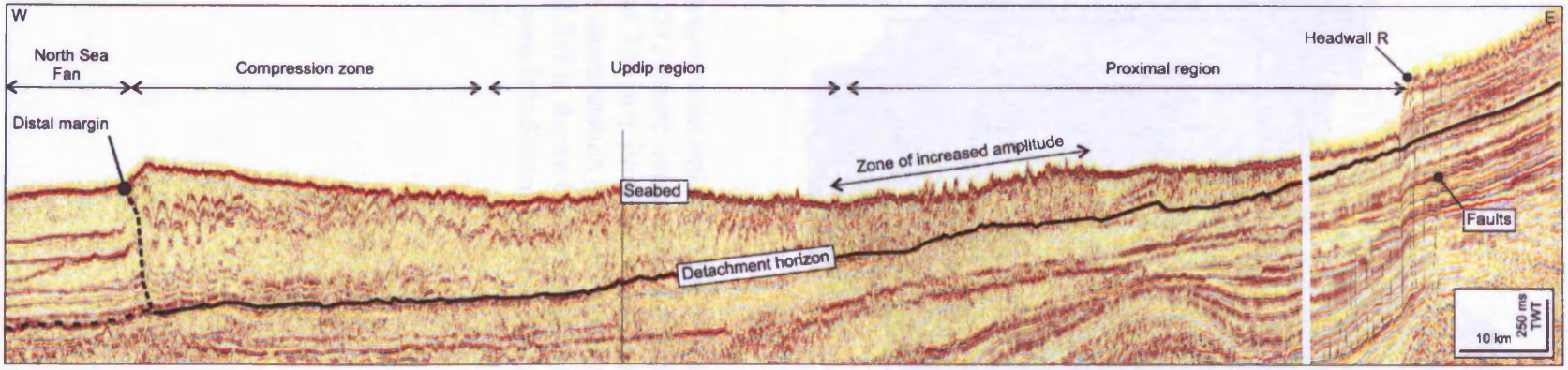

Figure 4.6. Composite seismic dip-profile taken through the study area showing the position and continuity of the basal detachment horizon which links the headwall area of the Storegga Slide to the distal margin of the compression zone. The basal detachment horizon is recognised as the regional reflector INS2 (indicated by continuous black line; Haflidason et al. 2004; Berg et al. 2005; Bryn et al. 2005a). Location shown in Fig. 4.2.

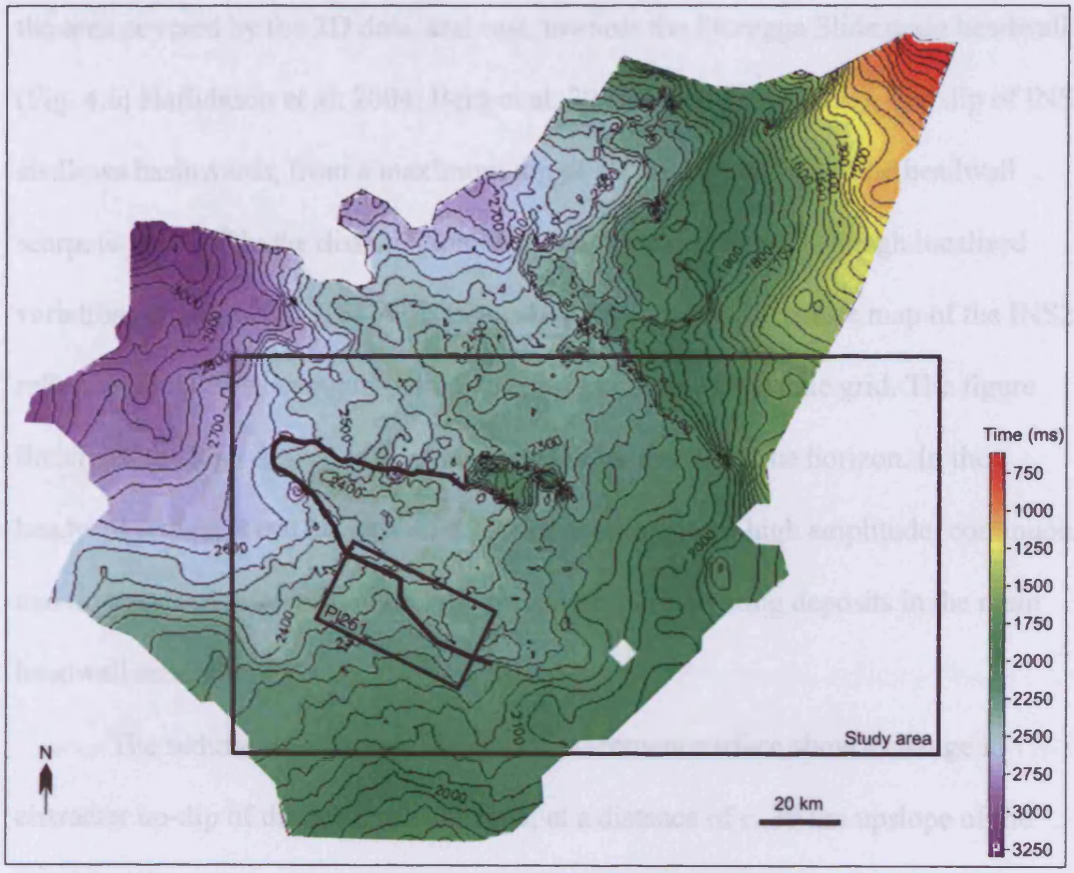

Figure 4.7. Contoured time structure map of the horizon INS2, based on the interpretation of 2D seismic lines, which forms the basal detachment horizon of the compression zone. The map illustrates the extensive nature and high level of confidence in the interpretation of the reflector. Contours are every 50 ms. The 3D seismic survey PL251 is shown by the black rectangle and the approximate outline of the compression zone is indicated by the continuous black line.

the area covered by the 2D data, and east, towards the Storegga Slide main headwall (Fig. 4.6; Haflidason et al. 2004; Berg et al. 2005; Bryn et al. 2005a). The dip of INS2 shallows basinwards, from a maximum dip of 13° in the vicinity of the headwall scarp, to just 0.3° in the distal region of the compression zone, although localised variations are observed (Fig. 4.6). Figure 4.7 shows a time structure map of the INS2 reflector which has been interpreted across part of the 2D seismic grid. The figure illustrates the high degree of continuity and broad extent of the horizon. In the headwall region, it can be seen on a 3D dip-profile to be a high amplitude, continuous and undeformed reflection underlying proximal mass wasting deposits in the main headwall area (Fig. 4.8A).

The sediments overlying the basal detachment surface show a change in character up-dip of the compression zone, at a distance of c. 30 km upslope of the distal margin. This transition is defined by a marked change in the character of the seabed lineations which characterise the compression zone. Up-dip, they exhibit relatively lower relief, as can be seen from the bathymetry data (Fig. 4.3) and representative 2D seismic dip-profiles shown in Figures 4.9 and 4.10. The cross-sectional character of the seabed in this region along with the change in character of the underlying sediments show a progressive increase in the degree of deformation, and decreasing thickness above the basal detachment horizon in the landward direction (Fig. 4.3, 4.9 and 4.10).

Deformational features in the subsurface are identified from offsets and geometries of sufficiently well-imaged horizons, along with the characteristics of the seabed. The deformational feature to be identified from the 2D profile shown in Figure 4.9 is a thrust fault pair and pop-up block, which corresponds to a broad, upward convex (positive) seabed feature (Fig. 4.9A). The next deformational feature

along in the proximal direction is interpreted as a pair of normal faults and associated graben block, with horizons exhibiting normal offsets within a zone which corresponds to a locally depressed, relatively flat area of the seabed (Fig. 4.9A & B). Increasingly in the proximal direction, further graben blocks are identified, most tellingly from a sequence of strong, continuous reflections close to the detachment surface, which show several sharply defined structureless zones (labelled on Fig. 4.9B). Correlation of the boundaries of such zones to corresponding sections of the seabed reflection which are depressed and flat-lying define inward-dipping geometries within which some reflections can be seen to be displaced downwards (Fig. 4.9B). With increasing distance in the proximal direction, the interpreted graben blocks show increasing distance between the individual detachment points of the faults within each pair (Fig. 4.9B). The average spacing of the fault pair detachments in this region is 2.3 km. Horst blocks are interpreted from the presence of intervening zones of relatively undeformed, bed-parallel reflections bound by outward dipping flanks (Fig. 4.9B).

Continuing in the landward direction, a further change in the character of deformation is noted (Fig. 4.10A). The sediments here show a similar degree of deformation as seen in the previous profile (Fig. 4.9). Where horizons are imaged with a sufficient degree of coherence and continuity, a series of ridges and occasional offsets are observed, associated with inclined segments of the seabed, the majority of which dip landward (labelled in Fig. 4.10B). In planview, this configuration corresponds to the broad, low relief seabed lineations which characterise the area up-dip of the distal region (Fig. 4.3). Laterally discontinuous, inclined and deformed reflections define systematic inclinations and offsets of reflections throughout the succession above the detachment horizon (Fig. 4.10B), which in combination with

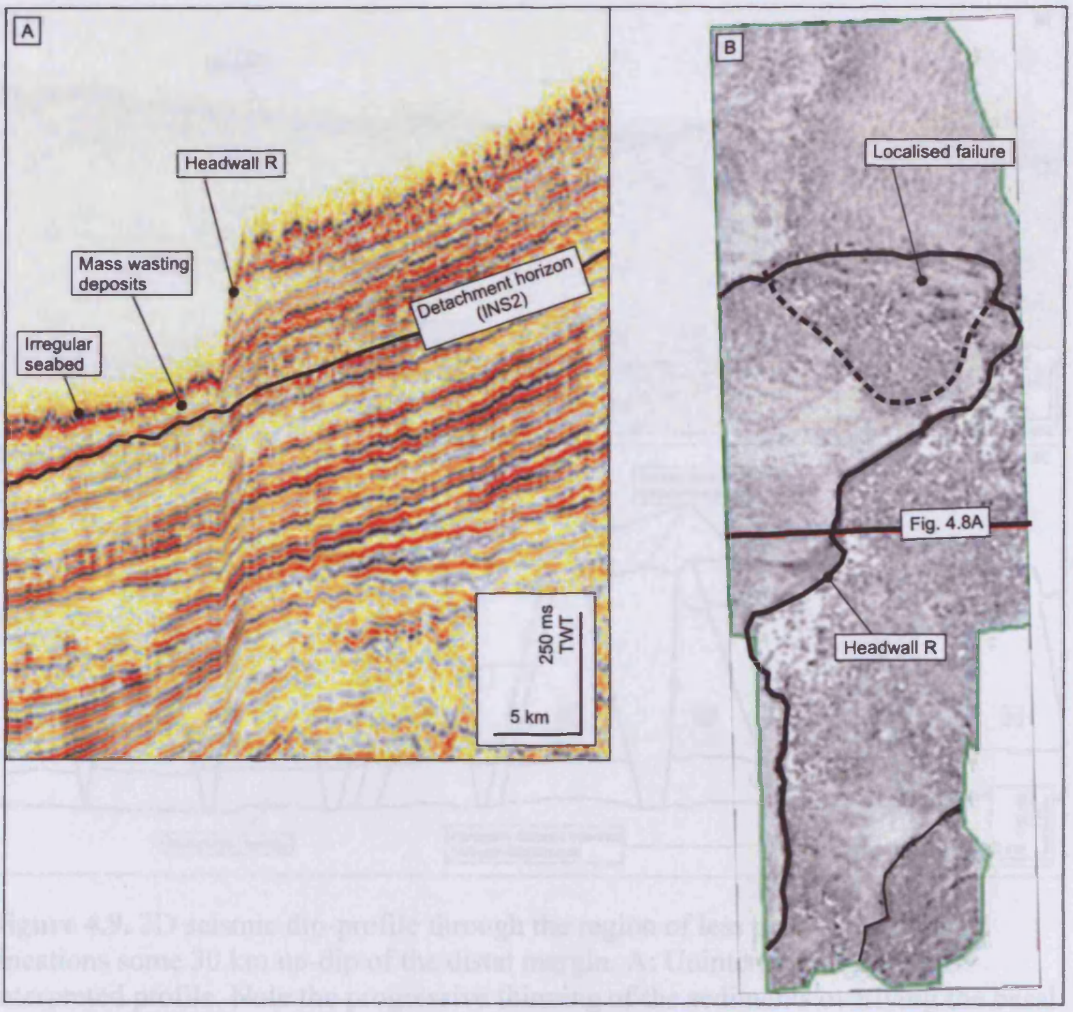

Figure 4.8. A: 3D seismic dip-profile through Storegga Slide headwall R which is linked to the compression zone by the detachment horizon INS2 (location shown in B). B: Seabed dipmap from within the 3D survey Ormen Lange (location shown in Fig. 4.2). Note the position and dip of INS2, and the relatively thin, chaotic mass wasting deposits which overlie it basinward of the headwall. The planform trend of the headwall, distribution and highly disaggregated nature of the mass wasting deposits is evident from the seabed dipmap.

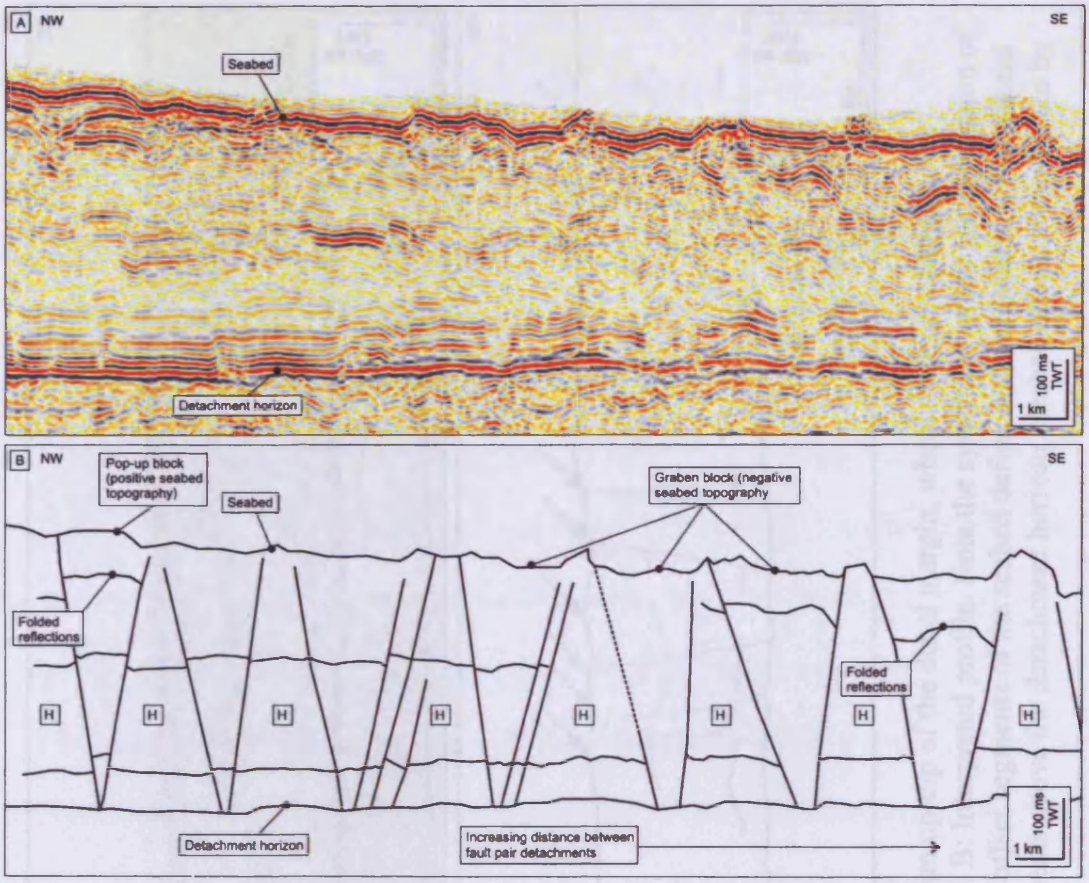

Figure 4.9. 2D seismic dip-profile through the region of less pronounced seabed lineations some 30 km up-dip of the distal margin. A: Uninterpreted profile. B: Interpreted profile. Note the progressive thinning of the sediments overlying the basal detachment horizon in the landward direction, and succession of deformational features which shows upwardly displaced pop-up blocks imaged in the NW extreme of the profile being succeeded by increasingly deformed fault blocks which have been displaced downwards by fault pairs which show normal offsets. The downward-displaced blocks are interpreted as graben blocks. H: Horst block. Location shown in Fig. 4.3.

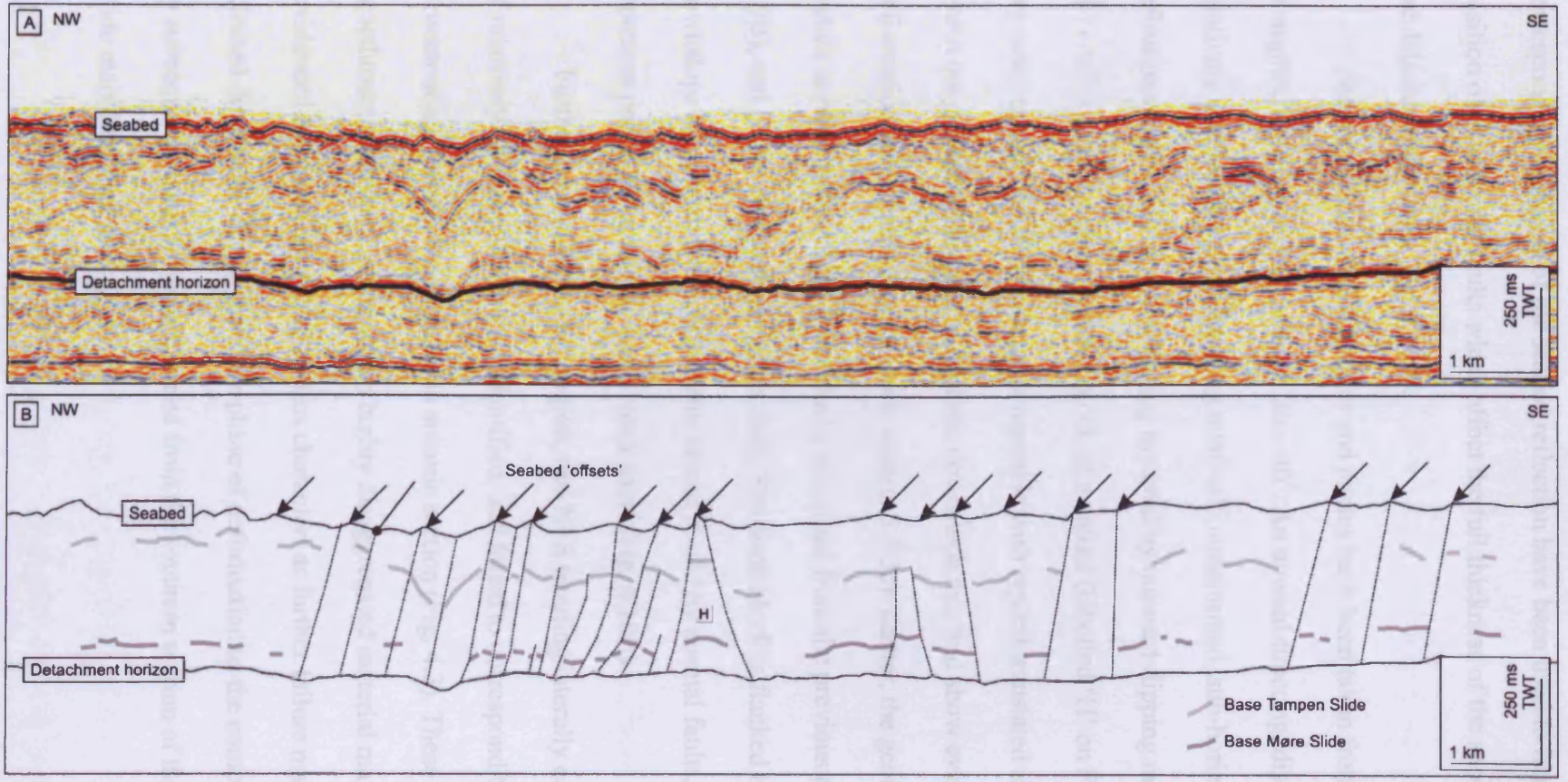

Figure 4.10. 2D seismic dip-profile taken through the region 40 km up-dip of the distal margin, where a further change in the character of the deformation is observed. A: Uninterpreted profile. B: Interpreted profile. Note the systematic offset and inclination of marker horizons which in conjunction with similarly inclined and offset segments of the seabed define landward-dipping extensional faults which in many cases affect the entire thickness of the sediments above the detachment horizon. Seabed offsets are indicated by arrows. H: Horst block. Location shown in Fig. 4.3.

corresponding segments of the seabed reflection have been used to interpret the position of extensional faults which affect the full thickness of the succession above the detachment horizon (Fig.4.10B).

Measurements of fault heights and angles have been taken from selected examples, which recorded values of 30 – 40°. An upward-tapering, discrete zone of relatively coherent material featuring relatively undeformed, sub-horizontal reflections separated from surrounding material by outward-dipping margins at angles 39° - 41° is interpreted as an intact block of material (labelled 'H' on Fig 4.10B). The geometry of this feature appears incompatible with typical translated slide blocks which are generally elongate along their downslope axis and show evidence of shear deformation at the base (chapter three, section 3.5.3c). Rather, the geometry of this feature is reminiscent of the horst blocks described from the previous profile (Fig. 4.9B), and is therefore interpreted as such. The horst block is flanked both up- and downslope by oppositely-inclined fault blocks bound by normal faults, which may represent partial failure of the horst block itself (Fig. 4.10B).

Furthermore in the up-dip region, two N- S trending laterally confined zones of relatively low relief seabed are identified, and found to correspond to zones of structureless, low amplitude facies in seismic section (Fig. 4.3). These are interpreted as sediment 'pathways' along which highly disaggregated material may have passed (evidenced by seismically structureless character) as further failure material was released downslope during the same phase of deformation as the compression zone, or by subsequent phases which originated from the southern section of the Storegga Slide main headwall area.

4.5.2 Headwall region

The basal detachment horizon can be correlated up-dip from the compression zone into the headwall area of the Storegga Slide (Fig. 4.6). It can be seen that the detachment horizon is associated with a seabed scarp of c. 200 m height (Fig. 4.6, 4.4 & 4.8B). The scarp is a laterally continuous feature previously named 'headwall R' of the Storegga Slide (Fig. 4.3; Bryn et al., 2005a). In planview, the headwall exhibits a general trend from NNE – SSW and comprises two arcuate salients (Fig. 4.3). In the immediate vicinity of the headscarp, the mass wasting deposits above the detachment horizon are thin and highly disaggregated in character (Fig. 4.8A). These deposits are partially imaged by the 3D survey Ormen Lange (Fig. 4.2), from which a dip-profile is shown in Figure 4.8A. On the dip-line, the proximal deposits are characterised by a 40 - 60 m thick, low amplitude, structureless seismic facies unit underlain by the basal detachment horizon. A seabed dip-attribute map taken from the 3D survey area illustrates the corresponding small-scale irregularity of the seabed (Fig. 4.8B). The broader scale presence of similar mass wasting deposits in the headwall region is inferred from the bathymetry data which exhibits a low relief signature in the 3D survey area, and out-with to the south (Fig. 4.3).

4.5.3 Slide blocks

4.5.3a Translated slide block

Thirty kilometers downslope from headwall R, a large elliptical body defined by a distinctly rough seabed character from the bathymetry data (Fig. 4.3) corresponds in seismic section to a conspicuous high amplitude zone (Fig. 4.6 & 4.11). Areas of relatively higher amplitude and reflectivity in seismic profile may be used to indicate a higher degree of intact material, and therefore are likely to represent areas which

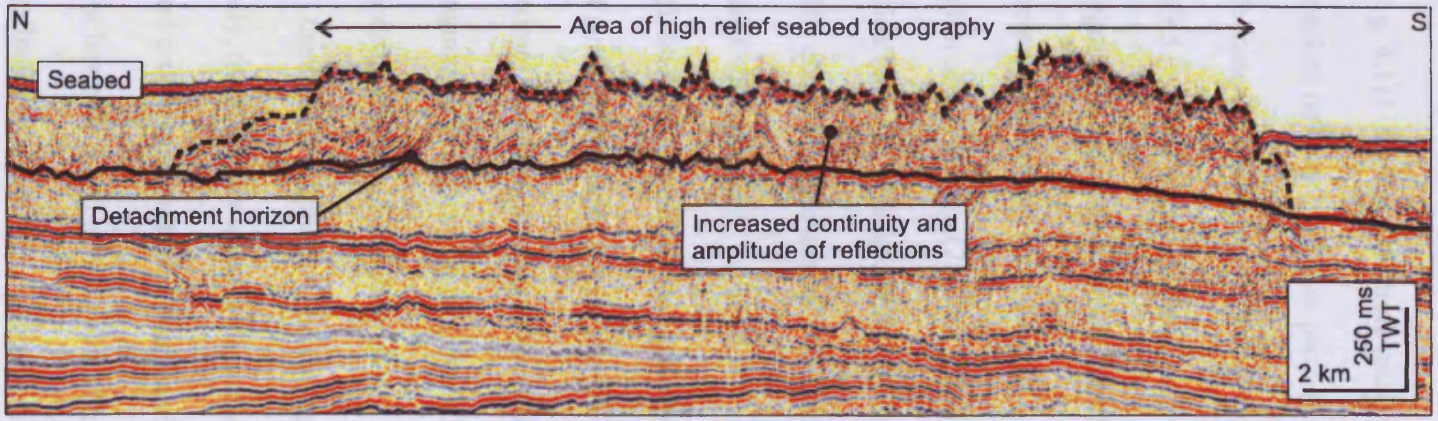

Figure 4.11. 2D seismic dip-profile taken through a conspicuous zone of high seabed relief some 30 km downslope of headwall R. Note the character of the seabed and the position of the detachment horizon. Internally, many laterally discontinuous segments of high amplitude reflections are observed, often forming discrete packages. The packages are interpreted as deformed blocks of material forming a larger translated and partially disaggregated block. Location shown in Fig. 4.3.

have experienced a lesser degree of deformation and disaggregation compared to relatively low amplitude, structureless areas (Brown 1999). Internally, the body features numerous coherent, continuous and inclined high amplitude segments of reflections (Fig. 4.11) including discrete packages of laterally continuous and concordant, stacked reflections. These packages are interpreted as relatively intact blocks of slide material which have not undergone extensive disaggregation (chapter three, section 3.5.3c). The high amplitude zone as a whole is interpreted as a large, partially disaggregated intact slide block, which has experienced locally varying degrees of internal deformation as a result of downslope translation. This agrees with the interpretation of Bryn et al., (2005a), who labelled it 'slide block R', which we adopt here. Slide block R measures some 50 km in breadth, and 28 km along its downslope axis, comprising an area of c. 795 km^2 (Fig. 4.3).

4.5.3b Remnant slide bodies

Two further distinctive seabed features occur in close proximity to the compression zone, situated along its northern lateral margin (labelled 'T1' and 'T2' on Figure 4.3). The most proximal feature is seen from the bathymetry data to be defined by an area of notably irregular seabed topography (Fig. 4.3), forming a down-slope elongate, downslope-tapering feature 31 km long and 11 km wide. In 2D seismic profiles the irregularity of the seabed is apparent, exhibiting up to 30 m of positive relief (Fig. 4.12). Internally, the succession above the detachment horizon is clearly divisible into two units based on the seismic facies characteristics (Fig. 4.12). Immediately above the detachment horizon, a 230 m thick low amplitude package of coherent, relatively undeformed reflections is observed. The unit is succeeded by a 180 m thick relatively high amplitude chaotic unit defined at its base by a continuous horizon (indicated on Fig. 4.12). The upper unit includes many discontinuous, high amplitude segments of

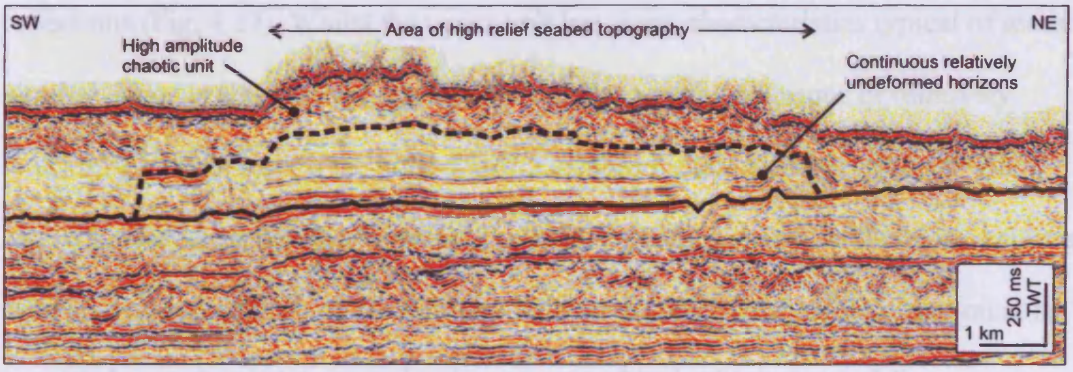

Figure 4.12. 2D seismic strike-profile through a zone of irregular seabed topography located c. 30 km up-dip of the distal margin of the compression zone. Notice the seabed character and basal detachment horizon. The intervening sediments are clearly divisible into two differing seismic facies, with low amplitude, continuous, layered reflections being succeeded by high amplitude, chaotic facies which are interpreted as Tampen Slide deposits. The feature as a whole is interpreted as an intact block of pre-slide stratigraphy which is rooted to the underlying strata and has not been translated. Location shown in Fig. 4.3.

reflections (Fig. 4.12). Whilst the upper unit has many characteristics typical of mass wasting deposits (chapter one, section 1.4), the underlying sequence of relatively intact reflections suggests the presence of a localised intact block of material which has been unaffected by mass-wasting. Further 2D profiles show that the block appears to be rooted into underlying stratigraphy with no evidence of shear deformation at its base, and as such it is interpreted to be a remnant block of intact, pre-failure stratigraphy as opposed to a block of translated mass wasted material. The mass wasted unit forming the upper part of this feature has been interpreted as a remnant outlier of Tampen Slide deposits by previous studies (Haflidason et al. 2004; Bryn et al. 2005a), and is hereinafter referred to as 'T1' (Fig. 4.3).

The second, more distal seabed feature occurs in close proximity to the downslope termination of the compression zone (Fig. 4.3). This feature is also defined by an area of raised, irregular seabed topography identified from the bathymetry data, and is circular in planform, measuring 17 km across in the downslope direction and 15 km along slope. 2D seismic lines taken through this feature illustrate the highly irregular character of the seabed which exhibits up to 50 m of relief (Fig. 4.13A). Like T1, the underlying sediments can be divided into two distinct units based on seismic facies characteristics, with a relatively low amplitude, 360 m thick lower unit which in dip-profile can be seen to be characterised by laterally continuous, relatively coherent reflections overlying the detachment horizon (Fig. 4.13A). In profiles of differing orientation however, the low amplitude nature of this unit renders its appearance structureless. The upper unit is 230 m thick and defined at its base by a high amplitude, continuous but deformed reflection (Fig. 4.13A). Internally, it is characterised by numerous high amplitude, deformed and discontinuous reflections, indicative of a high content of disaggregated material. Such characteristics are

diagnostic of a mass wasted deposit, and the continuous underlying horizon is interpreted as the basal detachment horizon (Fig. 4.13B). This feature is therefore similarly interpreted as an outlier of intact pre-failure stratigraphy overlain by Tampen Slide deposits, and is herein referred to as 'T2' (Fig. 4.3). T2 is closely juxtaposed with the northern margin of the compression zone, which is locally represented by a fault which dips at approximately 56° (Fig. 4.13A). The Tampen Slide shows a dramatic thickness change across the margin of the compression zone (Fig. 4.13B), within which it is notably thinner than in the T2 area. At the seabed, T2 is affected by along-slope continuations of the seabed lineations which characterise the distal region of the compression zone (Fig. 4.3). Whilst T2 is interpreted as a rooted, remnant slide block, the Tampen Slide deposit, which comprises its upper section, has clearly been affected by contractional deformation.

4.5.4 Lateral margins

The lateral margins delimit the slope-parallel boundaries of a MWD (chapter three, section 3.5.2a), extending between the headwall and distal margin. The southern lateral margin of the compression zone marks a change from the relatively smooth, undeformed seabed of the North Sea Fan to the south, to the area affected by deformation within the compression zone event to the north (Fig. 4.3). Further up-dip, where the seabed shows a change in character from pronounced to more subtle lineations, the southern lateral boundary of the deformed sediments updip of the compression zone can similarly be delimited by the juxtaposition of deformed seabed character to the north versus undeformed seabed character to the south (Fig. 4.3). In this area, the sediments above the detachment horizon become increasingly deformed

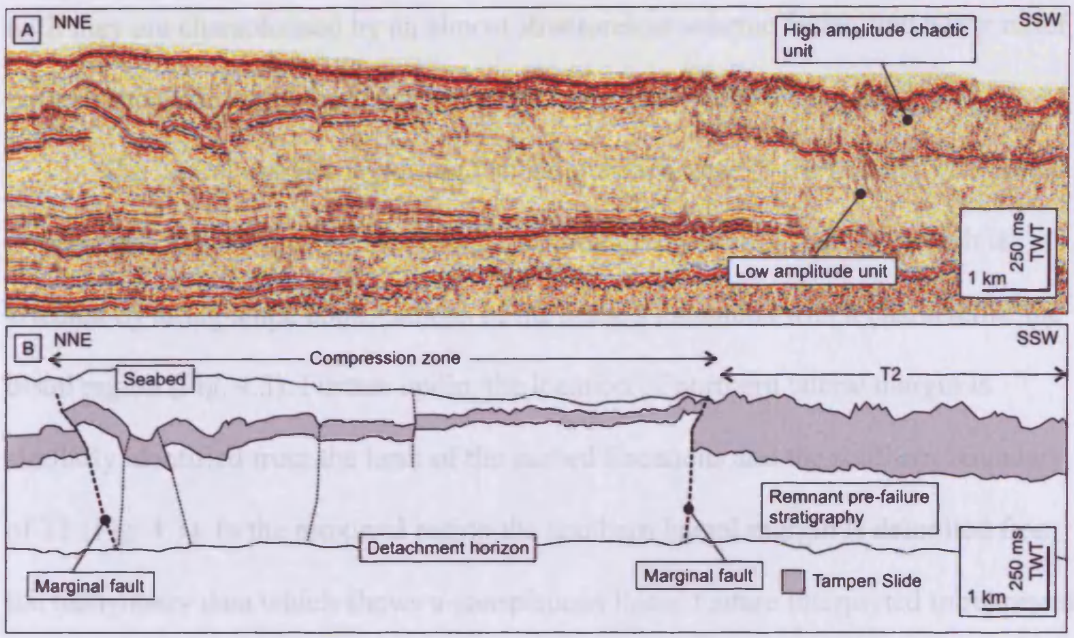

Figure 4.13. 2D seismic strike-profile through the lateral margin of the compression zone and area of irregular seabed topography located c. 10 km up-dip of the distal margin. Note that the sediments underlying the area of irregular seabed topography shows a clear division of seismic facies character, with the sediments immediately above the detachment horizon showing a low amplitude, continuous and layered character, and those closer to the seabed appearing high amplitude and chaotic. This feature is similarly interpreted as a remnant block which has preserved an outlier of Tampen Slide deposits. In this area, the northern lateral margin of the compression zone is represented by a steeply dipping fault across which the Tampen Slide deposit shows a marked change in thickness. Location shown in Fig. 4.3.

until they are characterised by an almost structureless seismic facies, and a low relief seabed signature, which has been interpreted as a shear zone (Fig. 4.3).

The lateral margin delimiting the compression zone to the north is interpreted to correspond to the limit of the seabed lineations and encompasses T2, which is affected by along-slope continuations of the seabed lineations which characterise the distal region (Fig. 4.3). Further updip, the location of northern lateral margin is similarly identified from the limit of the seabed lineations and the southern boundary of T1 (Fig. 4.3). In the proximal region the southern lateral margin is delimited from the bathymetry data which shows a conspicuous linear feature interpreted to represent a break in seabed topography (i.e. a scarp) and can be linked between the southern lateral margin in the distal region of the compression zone and the headwall (Fig. 4.3). The northern lateral margin is less distinct in the proximal region and in the present study has been interpreted to encompass the large translated slide block R (Fig. 4.3), and is tentatively correlated across a broad region of low relief seabed to the southern salient of the headwall (Fig. 4.3).

4.6 3D seismic interpretation

Detailed insight into the deformational structures within the compression zone event can be gained from the 3D survey PL251 which images an area along the southern lateral margin (Fig. 4.2). The lateral margin is represented by the boundary of a seabed depression characterised by irregular seabed lineations which trend NW – SE, interpreted as along-slope continuations of the diagnostic seabed lineations associated with the compression zone (Fig. 4.14A). The section of the lateral margin imaged by the 3D data exhibits a general NW-SE trend which is convex to the SW (Fig. 4.14A).

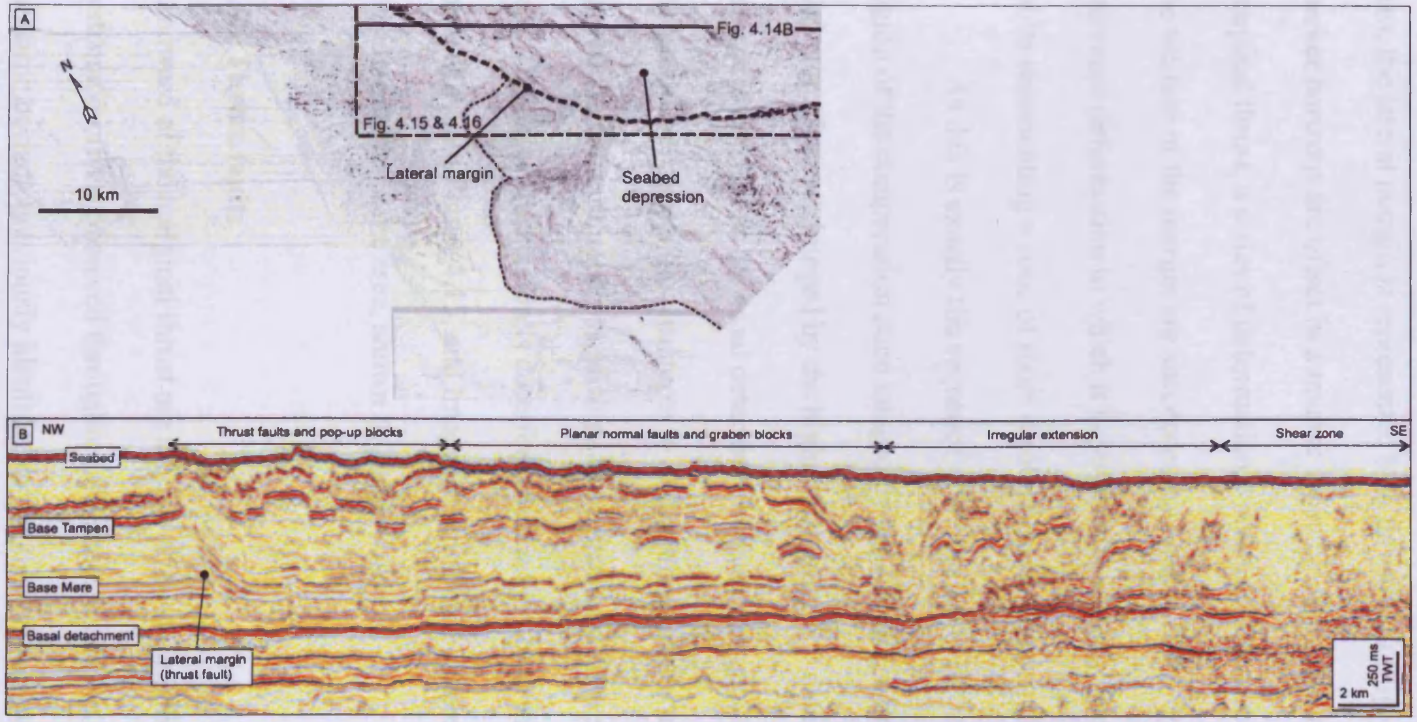

Figure 4.14. A: Annotated seabed dip-map from a the 3D survey PL251, which images a section of the southern lateral margin of the compression zone some 40 km up-dip of the distal margin. Note the trend of the lateral margin (indicated by bold dashed line), and presence of further seabed features including two lobe-like depositional features immediately to the south, closely-spaced SSE-NNW trending lineations in the NW quadrant of the survey area, and rough character of the seabed basinward of the compression margin. Location of the PL251 3D survey shown in Fig. 4.2. B: 3D seismic dip-profile through the compression zone lateral margin. Note the undeformed succession basinward of the lateral margin, which features the Tampen and Møre Slides and a continuation of the basal detachment horizon. The lateral margin is represented by a thrust fault and is succeeded in the proximal direction by a series of further thrust faults, planar normal faults and finally listric normal faults, representing a mixture of contractional and extensional deformation showing an increasing degree of deformation in the proximal direction. Note the presence of the shear zone in the SE extreme of the section. Location shown in A.

A 3D seismic dip-line, shown in Figure 4.14B, reveals that in seismic section, the margin corresponds to a clear change from undeformed strata downslope, to disrupted seismic facies units upslope. At its most distal extent within the 3D survey area, the lateral margin is represented by a thrust fault (Fig. 4.14B), across which marker horizons are offset in a reverse sense by up to 140 m. Landward of the marginal thrust, a series of deformational styles are observed, whereby thrust faults in the vicinity of the margin are succeeded by normal faults, followed by a zone of increased deformation in which it is possible to identify several large listric normal faults representing a zone of more disorganised extension (Fig. 4.14B).

As this is exactly the sequence of deformation recorded from the central region of the compression zone imaged by the 2D data, a brief exploration of the analogous features imaged by the higher resolution 3D data follows. 3D mapping of key horizons such as the basal detachment and stratigraphic marker horizons allows the internal details of the structures to be examined across a continuous area as opposed to intermittent cross sections as is the case with areas covered only by 2D data. The following section is described with reference to time structure and attribute maps shown in Figure 4.15, and images taken from a coherency volume generated for the compression zone area, shown in Figure 4.16.

4.6.1 Thrust faults

Landward of the marginal thrust are a series of faults which are identified from systematic offsets observed throughout the succession (Fig. 4.17A), all detaching into the same horizon previously identified as the basal detachment associated with the broader compression zone. In the vicinity of the marginal thrust, a series of seven thrust faults are observed, occurring in pairs of opposite verging dip which

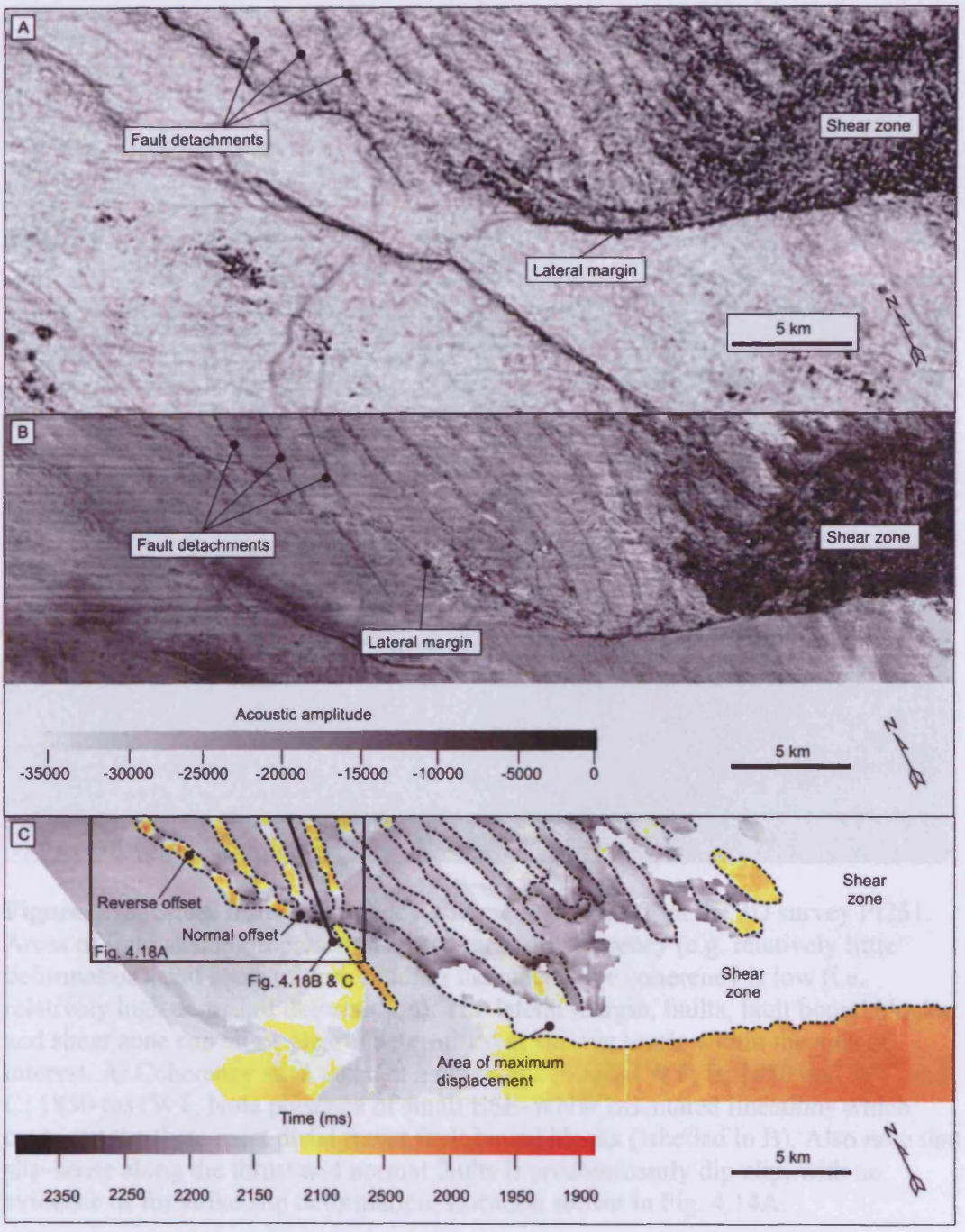

Figure 4.15. A: Dip-map of the basal detachment horizon INS2. Note NW-SE trending lineations which mark detachment points of the fault pairs (labelled). Also note the sharply defined lateral margin of the compression zone and dark-shaded area which represents highly disaggregated material within the shear zone (both labelled). B: Acoustic amplitude map of the basal detachment horizon. Note lateral margin, fault detachments and shear zone which can all be delimited from the amplitude signature (all labelled). C: Time structure map of the Base Møre Slide horizon, showing planform characteristics of the lateral margin, thrust faults, normal faults and fault-bound blocks. Tracking of the marker horizon is difficult in the proximal direction as the intensity of the deformation increases. Mapping of horizons within the shear zone was not possible. Location shown in Fig. 4.14A.

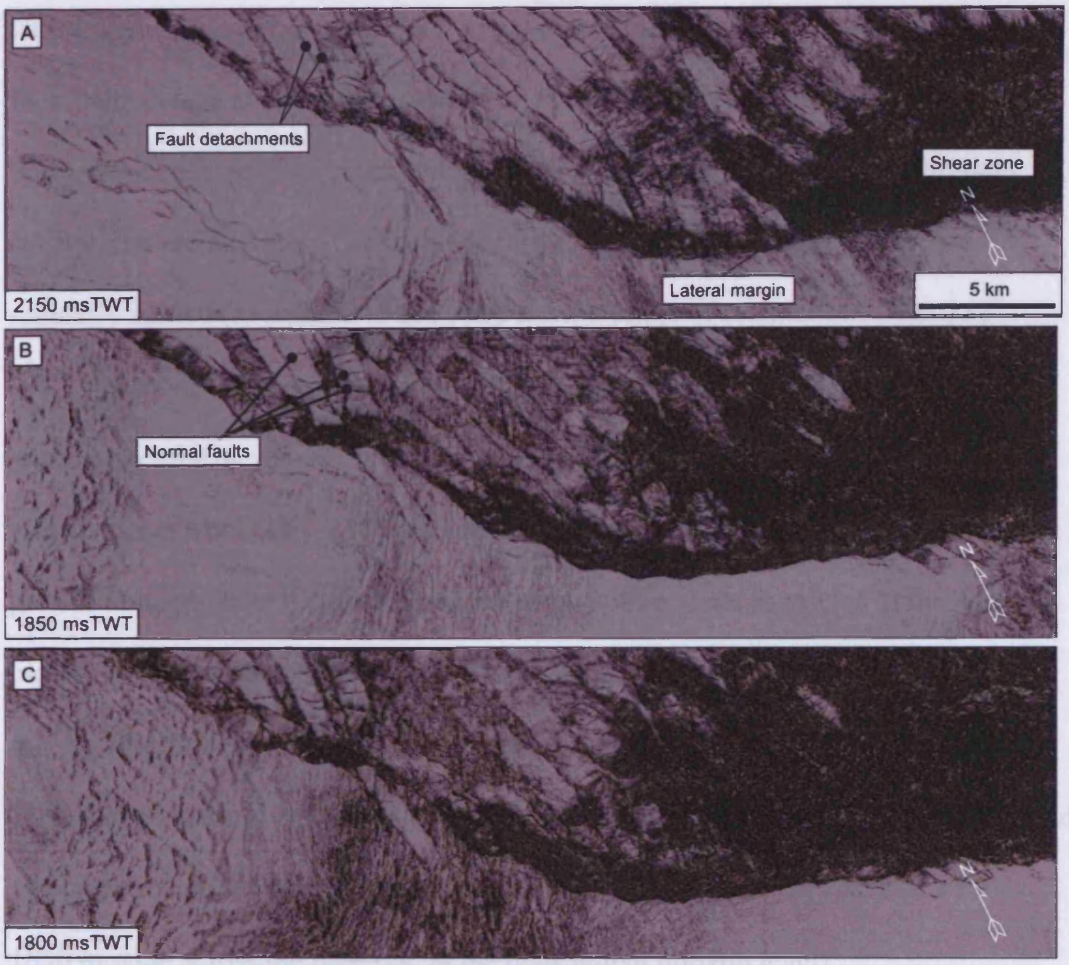

Figure 4.16. Slices from a coherency volume generated from the 3D survey Pl251. Areas of light shading represent a high degree of coherency (e.g. relatively little deformation), and areas of dark shading indicate where coherency is low (i.e. relatively high degree of deformation). The lateral margin, faults, fault bound blocks and shear zone can all be clearly determined at various levels within the area of interest. A: Coherency slice taken at a depth of 2150 msTWT; B: 1850 msTWT, and C: 1850 msTWT. Note presence of small ESE-WNW orientated lineations which cross-cut the three most distal thrust fault bound blocks (labelled in B). Also note that slip-sense along the thrust and normal faults is predominantly dip-slip, with no evidence of for strike slip deformation. Location shown in Fig. 4.14A.

varies from 30° to 60° (Fig. 4.17A). In cross section perpendicular to fault strike, the fault pairs detach at a common point (Fig. 4.17A), and define laterally continuous upwardly-displaced fault blocks which taper downwards towards the detachment surface and are interpreted as 'pop-up' blocks. The fault pair detachments are regularly spaced (average 1.43 km), and show a range of orientations from 158° – 178°. Proximal faults were observed to be slightly steeper (by 12° on average) and have greater throw values (by 4 m on average) than the distal bounding faults. Fault heights range from 690 – 1139 m, with distal faults on average more than 200 m greater in height than their proximal partners. Within some examples of the pop-up blocks, reflections exhibit convex-upward geometries interpreted as evidence of folding (Fig. 4.17A). The presence of intervening 'horst blocks' is interpreted from zones between the pop-up blocks which show much less evidence of deformation and displacement (labelled in Fig. 4.17B). The horst blocks are in the range of 1550 – 1650 m wide across the base (i.e. at the detachment horizon level).

Closer examination of the Base Møre horizon time structure map (Fig. 4.15C) and coherency data taken from the zone of thrust fault pairs (Fig. 4.16) reveals a subtle series of narrow, linear features trending ESE-WNW, which cross cut the zone of thrust faults and pop-up blocks. A representative seismic profile taken parallel to the strike of the thrust faults shows the planview features to correspond to a series of normal faults which detach into the same horizon as the thrust faults and affect the entire succession up to and including the seabed (Fig. 4.18). Eleven such faults are observed to cross cut the zone of thrust fault pairs, bisecting both footwall and hanging wall of the three pairs of thrust faults which follow the frontal thrust (Fig. 4.18A). The cross-cutting faults can be traced for a lateral distance of up to 6.5 km and trend between 118° and 125°. They are spaced an average of 0.53 km apart, dip at

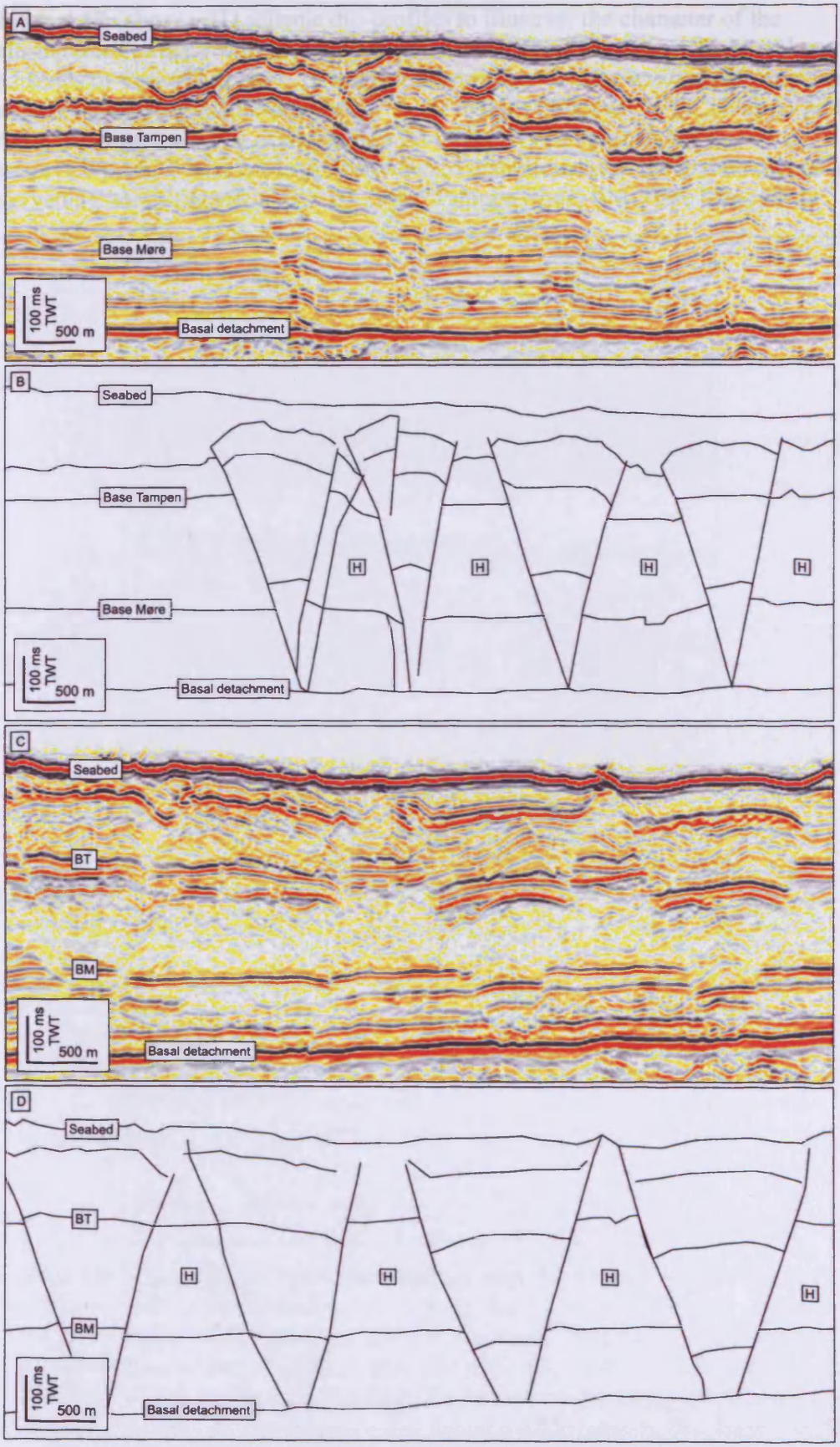
A
Seabed
Base Tampen
Base Møre
100 ms TWT
500 m
Basal detachment
B
Seabed
Base Tampen
H
H
H
H
Base Møre
100 ms TWT
500 m
Basal detachment
C
Seabed
BT
BM
100 ms TWT
500 m
Basal detachment
D
Seabed
BT
H
H
H
H
BM
100 ms TWT
500 m
Basal detachment

Figure 4.17 (above). 3D seismic dip-profiles to illustrate the character of the deformational structures in detail. A: Uninterpreted profile showing the lateral margin and series of thrust fault pairs. B. Interpreted profile. Note the upward displacement of the fault bound blocks and intervening 'horst' blocks (labelled 'H'). C: Uninterpreted profile showing the series of planar normal fault pairs and graben blocks. D: Interpreted profile. Note increasing downward displacement of the graben blocks and intervening horsts (labelled 'H'). BT: Base Tampen Slide, BM: Base Møre Slide.

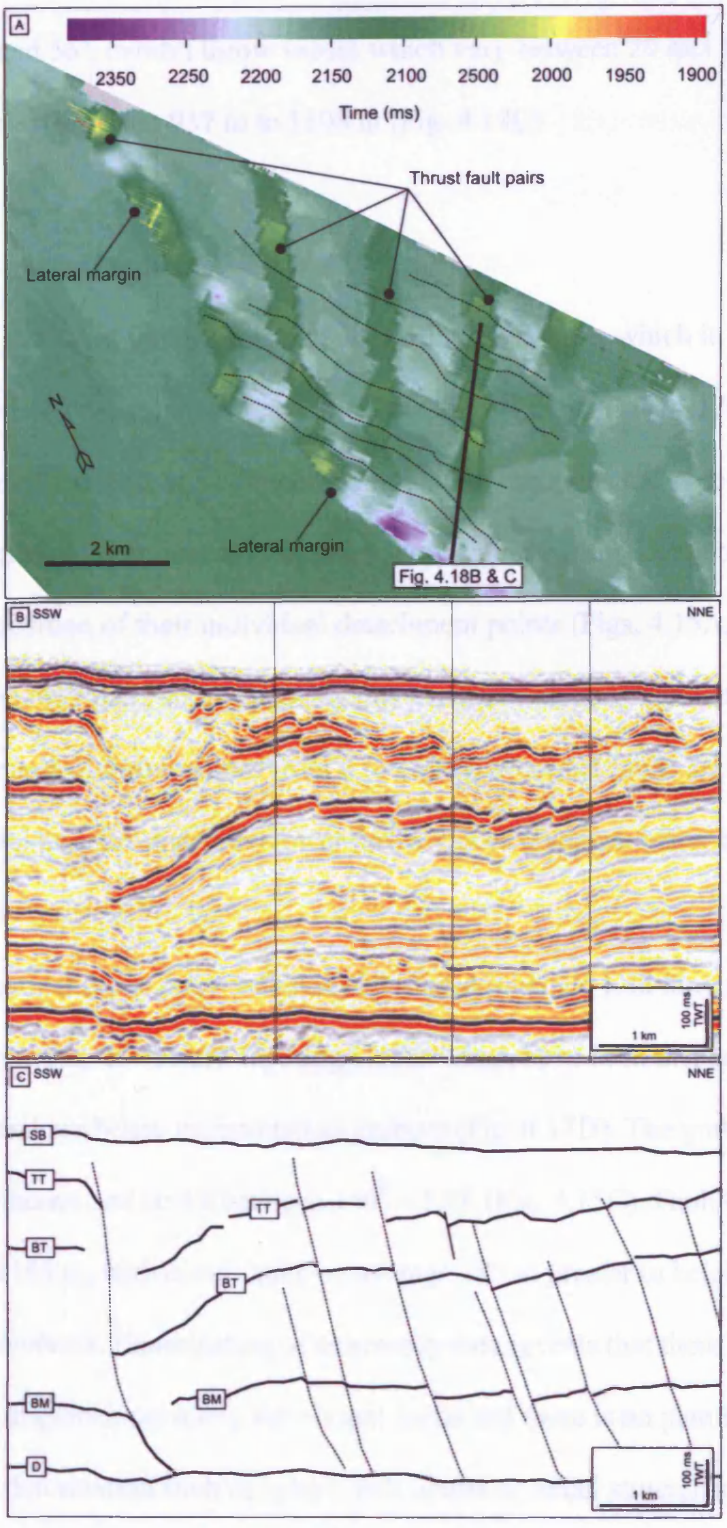

Figure 4.18. A: Base Møre Slide time structure map showing planform character of ESE-WNW trending planar normal faults (indicated by solid black lines) which cross-cut the thrust faults pairs. Location shown in Fig. 4.15C. B: Uninterpreted 3D seismic traverse through the zone of cross-cutting planar normal faults. C: Interpreted profile. Note undeformed succession basinward of the lateral margin and position basal detachment horizon. SB: Seabed; TT: Top Tampen Slide horizon; BT: Base Tampen Slide horizon; BM: Base Møre Slide horizon; D: Detachment horizon. Location shown in Fig. 4.15C.

between 45° and 56°, exhibit throw values which vary between 20 and 100 m, and fault heights varying from 937 m to 1108 m (Fig. 4.18C).

4.6.2 Planar normal faults

Landward of the thrust faults a series of six further fault pairs, which in this case exhibit normal offsets, are interpreted as planar normal faults (Fig. 4.17C & D). The fault pairs initially detach at a common point on cross sections taken perpendicular to strike, but increasingly proximal fault pairs show an increasing degree of separation between the position of their individual detachment points (Figs. 4.15A, 4.15B, 4.17C & 4.17D). The fault pairs show opposing dip sense and range in inclination from 26° to 63° and a range of throw values from 0 to 140 m. Proximal faults are less-steep than their distal partners and show lower throw values (average differences of 3° and 9 m, respectively).

The normal faults pairs are regularly spaced (average 1.48 km), and define laterally continuous, downward-tapering blocks which have been displaced downwards, and are hence interpreted as grabens (Fig. 4.17D). The grabens are laterally continuous and strike between 160° – 170° (Fig. 4.15C). Fault heights vary from 512 to 1183 m, with distal faults on average 185 m greater in height than their proximal equivalents. Examination of coherency data reveals that there is no element of strike-slip displacement along the normal faults and there is no planform evidence of strike-slip deformation such as splays, pull-aparts or reidel structures (Price and Cosgrove 1990; Fig. 4.16). The degree of general deformation exhibited by the sediments increases landwards, reflected in the grabens by increasing displacements and the distance between the detachments of the individual faults within each pair (Fig. 4.9). The sheared zone (Fig. 4.3) encroaches upon the normal faults and the

grabens increasingly in the landward direction (Fig. 4.15A, 4.15B & 4.16). The intervening 'horsts', which show no evidence of internal deformation or shear deformation at the detachment horizon become increasingly narrow upslope, with basal widths of between 1450 and 1500 m (Fig. 4.17D).

4.6.3 Zone of increased deformation

Landward of the most proximal planar normal fault pair, the sediments within the compression zone become noticeably more deformed (Fig. 4.14B). Combining the configuration of sufficiently coherent and continuous reflections, systematic zones of disruption throughout the succession, seabed character and time structure and attribute maps, it is possible to interpret further 'horsts', and normal faults (Fig. 4.14B). The faults in this region exhibit both planar and listric geometries in dip-section and occur individually (as opposed to in pairs). Remaining horst blocks appear narrower than more distal examples, and exhibit internal deformation (Fig. 4.14B). Seven irregularly spaced listric normal faults have been identified from the 3D data, with dips ranging from 30° to 39°, and have throw values ranging from 80 to 280 m. Two horst blocks are interpreted, and along with faults strike between 150° – 158° (Fig. 4.15C). It is possible that further faults and horsts are present in this area, but are difficult to identify due to the increasing disaggregation of the sediments which they affect.

Deformation and remoulding of the sediments becomes increasingly intense upslope, and in the most proximal (SW) end of the profile shown in Figure 4.14B, the material above the detachment surface is almost completely structureless and is interpreted as a continuation of the shear zone identified updip of the southern margin of the compression zone using the 2D and bathymetry data (this chapter; section 4.5.4). The extent of the shear zone within the area covered by the 3D survey PL251

can be clearly delineated from the coherency data, where it is represented by dark-shaded, textured areas representative of the highly disaggregated nature of the material (labelled on Fig. 4.16). Less disrupted material appears lighter and smoother (labelled in Fig. 4.16A). Further details on the origin and application of coherency data can be found in (chapter 1, section 1.4).

4.7 Summary of interpretations

4.7.1 Identification of a frontally confined submarine mass wasting deposit

It has been shown that the area of the Storegga Slide complex historically referred to as the 'compression zone' can be linked updip to a number of other geological features across a basal detachment horizon. Deformed sediments up to 640 m thick lie above the basal horizon which can be correlated continuously updip over a distance of some 135 km to the headwall area of the Storegga Slide where it is associated with the headwall historically referred to as 'headwall R'. In the present study the compression zone is therefore interpreted as a confined distal region of a large submarine MWD, and therefore constitutes a frontally confined element of the pre-dominantly frontally emergent Storegga Slide. This interpretation has been made on the basis of: 1) the extreme thickness of the distal region, which is considered a major controlling factor in the eventual development of frontally confined event as opposed to a frontally emergent example (Frey Martinez et al. 2006); 2) the configuration of the distal region which is organised into a series of regularly spaced, large scale compressional faults and folds; and 3) the relatively limited translation (i.e. 4%) inferred by the degree of shortening calculated from the distal region, and close proximity of

remnant, untranslated slide bodies (Frey Martinez et al. 2005, 2006). For simplicity, this confined MWD is hereinafter referred to as the 'Confined Storegga Slide' (CSS).

Identification of primary constraining features including the headwall, distal margin and lateral margins, all linked across a continuous basal detachment horizon has allowed the full extent of the CSS to be constrained, and it is outlined as such in Figure 4.19. The total section length of the CSS is 135 km, with a thickness which varies between 40 m in the vicinity of the headwall scarp and 640 m in the vicinity of the distal margin. The total area defined in the present study is 3510 km^2, which corresponds to a volume of approximately 1,227 km^3, reflective of the great thickness of the sediments in the distal region. To provide some context, the total area affected by the Storegga Slide (including areas of erosion and deposition), and total volume of material removed have been estimated as 95,000 km^2 and 2500 – 3500 km^3 respectively (Bryn et al. 2005a). Slide bodies T1 and T2 are interpreted as 'remnant' slide blocks (i.e. unfailed and untranslated) on the basis of their lack of internal deformation and clear rooting into the underlying strata (Frey Martinez et al. 2005; chapter three, section 3.5.3c). Slide block R is interpreted as an intact block of failed material which has been translated within the CSS, based on the degree of observable disaggregation and lack of rooting (Fig. 4.11).

4.7.2 Distribution of deformation and kinematic indicators

A clear succession of deformational styles is observed from the distal and updip regions of the CSS, with thrusts in the distal region being succeeded by normal faults and grabens, then further, more disorganised extension in the form of degraded horsts, planar normal faults and listric normal faults with increasing proximity (Figs. 4.4,

4.11 & 4.12). The distribution of these deformational styles is summarised on Figure 4.19.

Along the southern margin of the Storegga Slide, up-dip of the distal region, a shear zone has developed within which material is highly deformed and disaggregated to the point of being structureless in seismic section (Fig. 4.14B). The broad extent of the shear zone can be confidently mapped north of the southern lateral margin based on the 2D seismic profiles, but to the east can only be inferred from the character of the seabed using the bathymetry data (Fig. 4.3). The outline of the shear zone as it has been interpreted in the present study is shown in Figure 4.19.

In the area covered by the 3D survey PL251 (Fig. 4.2), a series of normal faults which cross cut the thrust faults associated with the compression zone were identified (Fig. 4.18). The crosscutting nature of the faults suggest that they post-date the formation of thrust faults and therefore represent a second phase of deformation which resulted in extension to the NE (Fig. 4.19).

The gross general transport direction of the CSS can be constrained given the presence of primary kinematic indicators which are the headwall, distal margin and lateral margins (chapter two). Kinematic indicators are summarised in Figure 4.19, with primary kinematic indicators represented by bold arrows which point in the general transport direction suggested by their orientation. The combination of the primary elements suggests a general transport direction to the NW. In the distal region of the CSS, the transport direction can be further evaluated using the orientation of the distal margin and thrust faults, with the transport direction assumed to be perpendicular to the observed orientations (Farrell 1984; Ramsey and Lisle 2000; chapter two, section 3.5.3). In this case, the thrust faults in close proximity to the distal margin also suggest a transport direction to the NW (Fig. 4.19). Updip of the

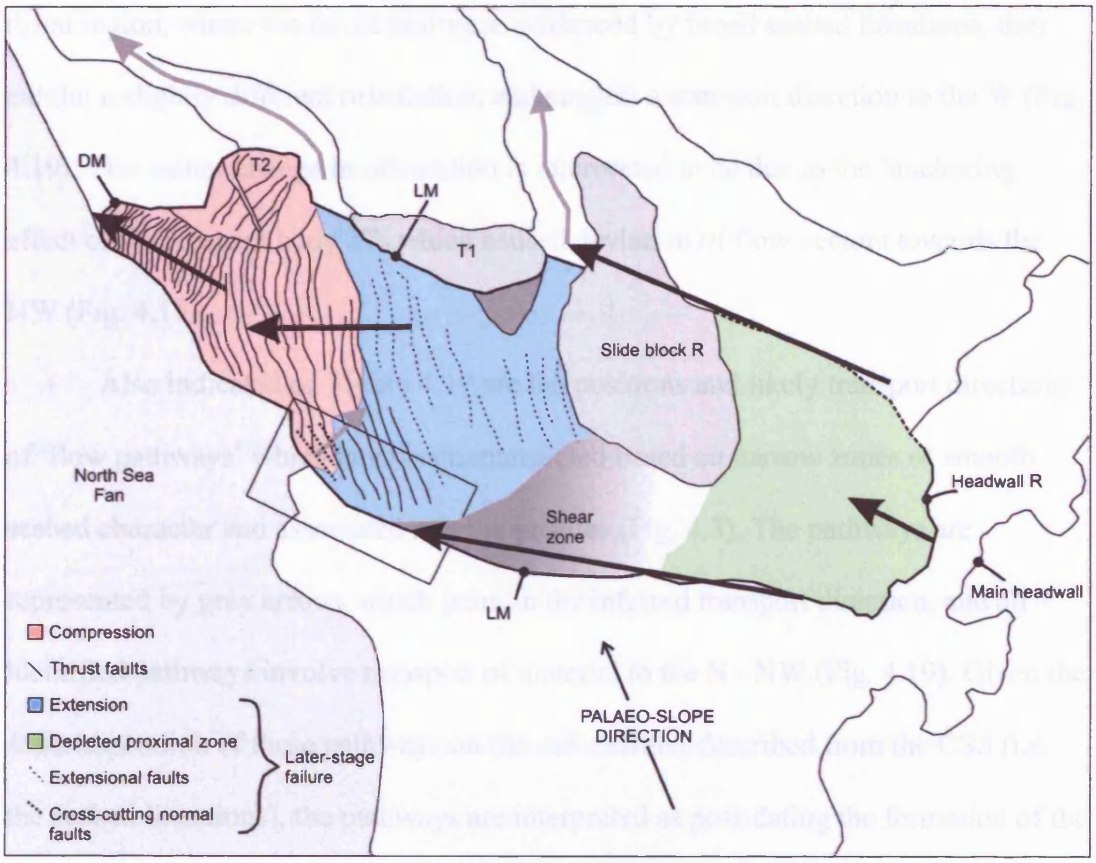

Figure 4.19. Map to show the full extent of the Confined Storegga Slide, as constrained by the positions of the distal margin, lateral margins and headwall R. These features can be used to infer the main direction of transport of the event, which is indicated by bold arrows. The directional information imparted by features representative of the inferred later-stage deformation, i.e. sediment flow pathways and cross-cutting extensional faults, is indicated by grey arrows. DM: distal margin; LM: lateral margin.

distal region, where the thrust faults are evidenced by broad seabed lineations, they exhibit a slightly different orientation, and suggest a transport direction to the W (Fig. 4.19). This minor change in orientation is interpreted to be due to the 'anchoring' effect of the remnant body T2, which caused deviation of flow vectors towards the NW (Fig. 4.19).

Also indicated on Figure 4.19 are the positions and likely transport directions of 'flow pathways' which have been interpreted based on narrow zones of smooth seabed character and associated seismic profiles (Fig. 4.3). The pathways are represented by grey arrows which point in the inferred transport direction, and all identified pathways involve transport of material to the N - NW (Fig. 4.19). Given the superimposition of these pathways on the deformation described from the CSS (i.e. the seabed lineations), the pathways are interpreted as post-dating the formation of the broad NNW-SSE thrust faults which the seabed lineations represent, and therefore represent a later stage of slope failure as part of the Storegga Slide development. The pathways may have formed as part of the same later stage of deformation interpreted from the presence of the cross-cutting normal faults which affect the thrust faults associated with the distal region of the CSS, imaged by 3D survey PL251 (Fig. 4.19). The direction of material transport suggested by both the cross-cutting faults and the sediment flow pathways (i.e. to the N - NE) is broadly complimentary (Fig. 4.19).

4.7.3 Magnitude of translation

The amount of translation undergone by sediments within a frontally confined mass wasting unit can be constrained by the degree of shortening exhibited by the compressional deformation of sediments within the distal region (Frey Martinez et al. 2006). In the CSS, it has been shown how numerous thrust faults deform the

succession into a series of popped-up blocks and intervening horsts. Based on line-length balancing and bed-length measurement using the best positioned 2D profiles, the total amount of shortening has been calculated as c. 5 km, or 4% of the total undeformed length (this chapter, section 4.5). Other features can further be used to indicate the general degree of translation, including the presence of remnant slide blocks T1 and T2 which have not fully failed and undergone translation. The presence of such 'rooted' blocks was interpreted by Frey Martinez et al. (2005) to rule out extensive translation of sediments within a MWD.

4.7.4 Strain history

The remarkable succession of deformational styles recorded from the CSS associated with the compression zone is interpreted to be the result of two different phases of deformation: 1) compression as a result of the downslope translation of sediments within and updip of the compression zone, resulting in regularly spaced, well-preserved thrust pair-bound pop-up blocks and intervening undeformed horsts, and 2) the later development of extensional deformation as a result of removal of material originally involved in the formation of the compression zone during a subsequent phase of slope failure as part of the multi-phase Storegga Slide event.

Evidence for this is manifested as irregular extension observed throughout the sediments updip of the distal region of the CSS, sediment flow pathways indicating the removal of material to the north, and cross-cutting extensional faults along the southern lateral margin which indicate extension to the NE (Fig. 4.19). The effect of the later stages of slope failure and removal of material has resulted in increasing deformation in the landward direction manifested in the increasing 'degradation' of grabens and intervening horsts updip of the distal region (Figs. 4.9 & 4.10).

Increasingly deformed grabens are succeeded upslope by a zone of increased sediment disaggregation and more disorganised extension, in the form of irregularly spaced planar and listric normal faults (Fig. 4.10). Direct evidence of later removal of material following development of the CSS is interpreted from the presence of sediment 'pathways' which cross cut the mid- and proximal regions (Fig. 4.3 & 4.19). The series of planar normal faults which were identified from the 3D data to affect the zone of thrust faults (Fig. 4.18), clearly cross cut the faults and associated fault blocks, evidencing a later phase of extension following the formation of the compressional deformation. The orientation of the cross cutting normal faults (NW - SE) and dip direction (NE), suggest an extensional regime orientated NE - SW with slip of material to the NE.

4.8 Discussion

4.8.1 Previous interpretations

The compression zone has been interpreted as the distal zone of a frontally confined submarine MWD, the Confined Storegga Slide, located in the mid-slope region of the predominantly frontally emergent Storegga Slide. Previous works on the compression zone are few in number, and begin with the efforts of Haflidason et al. (2004) and Bryn et al. (2005a) who identified and briefly considered the large-scale contractional deformation of the compression zone as part of a broad-scale characterisation study of the Storegga Slide complex seabed, aimed at determining the sequence of failure phases during the Storegga Slide.

Gafeira et al. (2007) provided the first detailed insight into the slope failure process of the southern flank of the Storegga Slide and applied the results of a

morphological analysis of seabed elements based on the 3D survey PL251 to the broader-scale sequence of sliding in the area. The marginal area of the compression zone was briefly considered and the sequence of thrust and normal fault pairs was attributed speculatively to initial compression followed by extension and related extensional reactivation of some thrusts (Gafeira et al. 2007). The most recent and detailed study of the compression zone was conducted by Færseth and Sætersmoen (2008), who like the present study, interpreted an 'intact slump' on the basis that the failed mass has moved along an upwards-concave rupture surface and showed a wide range of internal deformation.

The major difference in the interpretation of Færseth and Sætersmoen (2008) and the present study is that the former concluded that the compression zone as it is observed today was formed by a single phase of slope failure with concurrent development of contractional and extensional domains. This was attributed to frontal buttressing against the distal margin, and changes in the velocity of dislocation and translation relating to the geometry of the basal detachment surface, respectively (Færseth and Sætersmoen, 2008). Post-failure modification by subsequent slide phases was not considered. The outline of the slump interpreted by Færseth and Sætersmoen, (2008) narrows upslope to suggest that the headwall occupies a laterally restricted zone downslope of the southern region of headwall 'R' and does not include the slide bodies T2 or slide block R.

Færseth and Sætersmoen (2008) calculated that 14% shortening has occurred in the distal region of the compression zone by lateral compaction, based on a thickness comparison between the thrusted region versus the 'original thickness of sediments in the westernmost part of the proximal segment'. In addition, ptygmatic folding interpreted to affect some 30 km of the up-dip region was concluded to

contribute a further shortening of 14 km, resulting in a total shortening of 30 – 35 km according to Færseth and Sætersmoen (2008). Evidence for compressional deformation up-dip of the compression zone was not identified in the present study, and as a result the latter has arrived at comparatively lower values of shortening (e.g. lower-end result of 5 km).

4.8.2 Frontally confined model

Considering the observations and interpretation made in previous sections, we can now present a model for the formation of the CSS, which also constitutes a revised interpretation for the compression zone, in the form of a scaled, schematic dip section from headscarp to distal margin (Fig. 4.20).

In frontally confined submarine mass wasting deposits, it is expected that the net accumulation observed from the distal region in the form of compressional deformation balances with depletion in the upslope realm of the failure which has occurred due to mobilisation and translation of the failed mass downslope (*sensu* Varnes 1978; Frey Martinez et al. 2006). Evidence for the later-stage modification of the compression zone by subsequent phases of the Storegga Slide has been presented in the present study in the form of two separate stages of deformation. This interpretation can be further illustrated by Figure 4.20, where in the proximal region, overlying the basal shear surface is a relatively thin veil of structureless mass wasting deposits that is overly depleted in comparison to the distal region.

It is possible to reconstruct the likely sequence of events and volumetric changes by considering a number of time stages, summarised by Figure 4.21:

Step 1 (Fig. 4.21A): Pre-failure conditions. The pre-failure slope template can be reconstructed based on the thickness, dip and configuration of intact sediments

from landward of Storegga Slide main headwall, and basinward of the distal margin (Fig. 4.6).

Step 2 (Fig. 4.21B): Development of the CSS. Compressional strain as a result of the downslope displacement of the failed sediments would have been concentrated in the distal region. The well-preserved compressional deformation found within the distal zone yields shortening values of approximately 5 km, or 4%, which translates directly into the actual distance over which the failed sediments were displaced (*sensu* Varnes 1978; Frey Martinez et al. 2006). It is expected that sediments in the proximal region of mass wasting deposits experience extension approximating to the amount of shortening observed from the distal region (i.e. 4%; Fig. 4.21B). Slide block R, a large partially deformed slide block, is interpreted as having been translated as a large, intact element (Fig. 4.21B) and it reasonable to assume that it has been translated over a distance of c. 5 km consistent with that calculated for the CSS as a whole.

Step 3 (Fig. 4.21C): Post-event modification. Restoration of the likely slope profile and distribution of deformation illustrated in the previous stage (Fig. 4.21B) allow a comparison to that observed from the present day (Fig. 4.21C). A large volume of sediments have been eroded and removed by later phases of failure, most likely from the southern area of the Storegga Slide main headwall (Fig. 4.19). This is evidenced by intense and irregular extension in the up-dip region of the CSS, and sediment flow pathways superimposed upon it.

4.8.3 Relative timing

Establishing the exact timing of the thrust propagation within the compression zone relative to the Storegga Slide 'phases' is confused by the provenance attributed to the compression zone in the previous Storegga Slide studies. The first attempt to evaluate

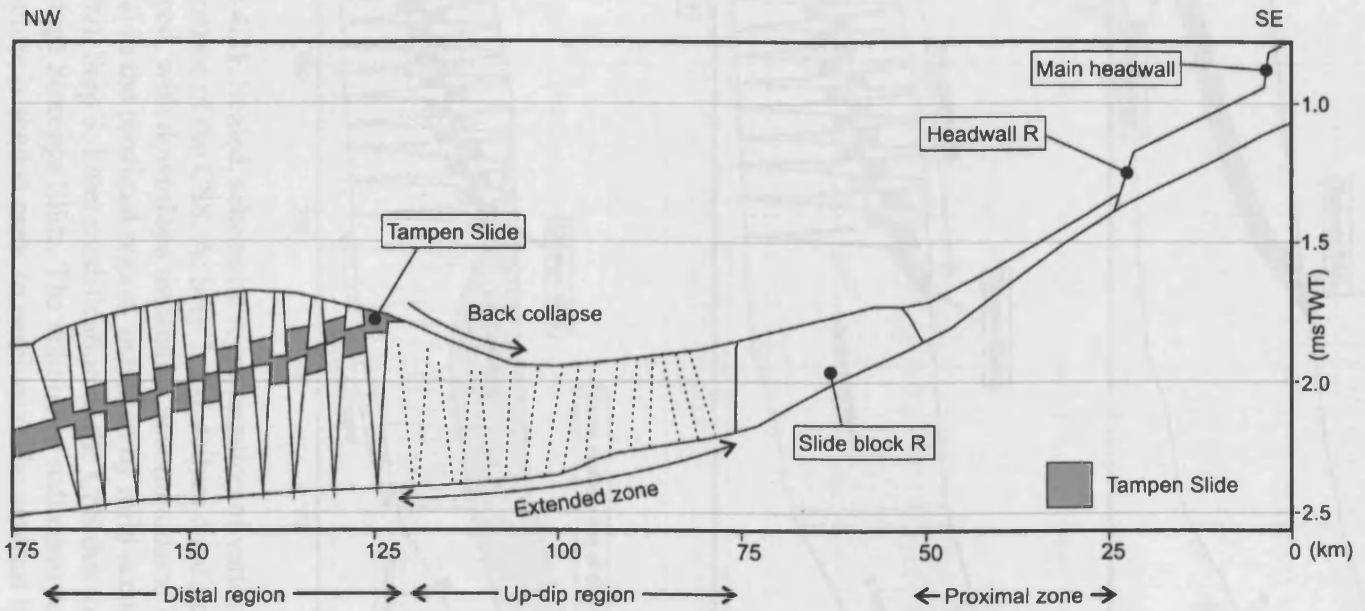

Figure 4.20. Scaled, schematic dip-section through the CSS. Note that the proximal and up-dip regions are heavily depleted in relation to the distal region. This contradicts classical models for slope failure which predict that accumulation in the distal region is balanced by depletion in the proximal region (sensu Varnes, 1978). Location shown in Fig. 4.2.

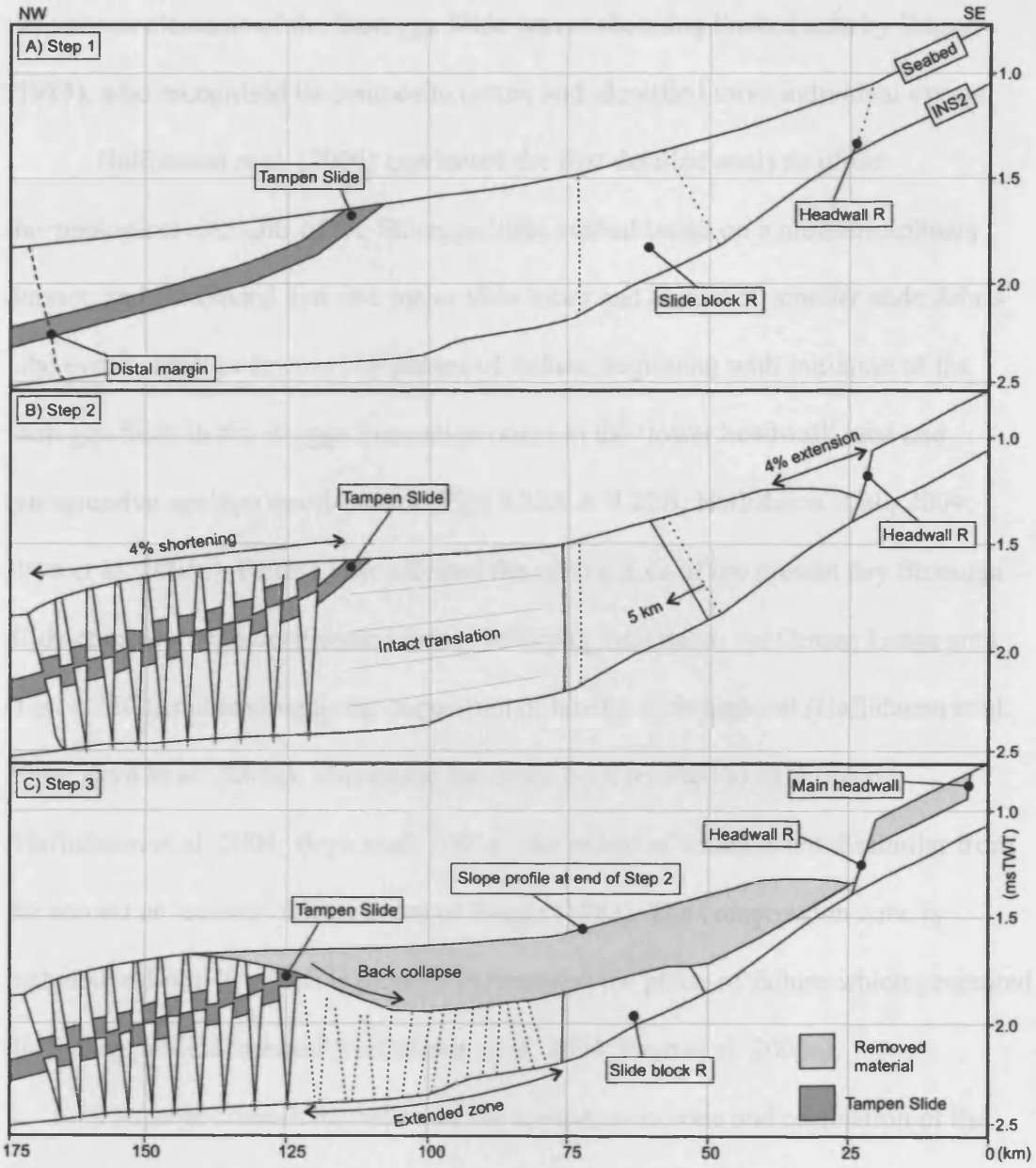

Figure 4.21. Scaled, schematic representation of various time-stages to illustrate development of the CSS. A: Step 1: Pre-failure conditions. B: Step 2: CSS has developed, with downslope translation accommodated in the form of mild depletion (i.e. 4%) in the proximal region, balanced by mild accumulation in the distal region (also 4%). Step 3: Later modification of the CSS due to slope failure as part of the multi-stage Storegga Slide. The volume of sediments removed by the inferred later-stage failure is shaded grey, to emphasize the contrast between the slope profile expected after development of the CSS, and the actual slope profile observed today. The volume of removed sediments is shaded grey. Location shown in Fig. 4.2.

the various elements of the Storegga Slide was made using limited data by Bugge (1983), who recognised its composite nature and identified three individual events.

Halfidason et al. (2004) conducted the first detailed analysis of the morphological elements of the Storegga Slide seabed based on a multidisciplinary dataset, and concluded that five major slide lobes and almost 60 smaller slide debris lobe events attest to several key phases of failure, beginning with initiation of the Storegga Slide in the Brygge Formation oozes in the 'lower headwall' area and retrogressive upslope development (Figs 4.22A & 4.22B; Haflidason et al., 2004; Bryn et al. 2005a). Failure later affected the central area of the present day Storegga Slide complex, with deep-seated failure affecting material in the Ormen Lange area (Fig. 4.22C), and leading to the deposition of blocky slide material (Haflidason et al. 2004; Bryn et al. 2005a). This phase has since been referred to as 'Lobe II' (Haflidason et al. 2004; Bryn et al. 2005a), the extent of which is not dissimilar from the second or 'central' failure event of Bugge (1983). The compression zone is included in Lobe II, which is thought to represent the phase of failure which generated the Storegga Slide tsunami (Haflidason et al. 2004; Bryn et al. 2005a).

The large-scale deformation of the compression zone and correlation of the basal detachment horizon with a deep-seated failure plane in the headwall area were taken to be indicative of the 'enormous momentum and energy released during this phase of the Storegga Slide' by Haflidason et al. (2004), who assigned various parameters to Lobe II including an area of 20,278 km^2, maximum volume of 780 km^3 and a run out distance of 410 km (Haflidason et al. 2004). The outline of Lobe II from a summary figure presented by Halfidason et al. (2004) clearly indicates its continuous downslope extent throughout the mid-slope region of the Storegga Slide

Figure 4.22. Series of maps to show the interpreted development and sequence of the Storegga Slide phases. A: Outline of the Storegga Slide Complex and main slide elements, including the lower headwall, main headwall, headwall R and slide block R (after Bryn et al., 2005a); B: Initial phase of sliding occurred in the lower headwall region and retrogressed upslope; C: Sliding then affected the central Ormen Lange area with deep detaching, blocky slide deposits, and westward movement of Slide block R, initiating compression in the compression zone. This phase of sliding is linked to the Storegga Slide tsunami; D: Sliding retrogressed further to eventually affect the northern main headwall region; E: The final phase of sliding affected the southern sections of the main headwall and headwall R.

(Fig. 4.22C). It is clear then, that along with the sediments involved in the CSS, Lobe II is further comprised by a frontally emergent element which would justify its further description as 'erosive', and as the 'strongest single candidate to create the Storegga tsunami' (Haflidason et al. 2004). These attributes clearly do not relate to the confined, relatively 'in place' deformation of the CSS. However, Haflidason et al. (2004) did conclude that 'Lobe II' was later affected by 'failed and disintegrated sediments' during a subsequent phase of failure. In the later summary of the failure sequence by Bryn et al. (2005a), 'deep erosion' in the Ormen Lange area is charged with the development of further retrogressive failure sourced from an area of the main headwall in the south (Fig. 4.22E).

According to Bryn et al. (2005a), the collapse of further sediments from the central main headwall area resulted in the stage of failure attributed to Lobe II, and also initiated westward movement of slide block R which is deemed responsible for the compression observed from the distal region of the CSS. Doubt was shed on the established chronology by Gafeira et al. (2007), who identified that the lateral margin of the compression zone cross-cuts, and therefore post-dates minor compressional features to the south of the compression zone, previously interpreted as contemporaneous or later (Haflidason et al. 2004). The results of the present study are in general agreement with the sequence of slide phases in the southern area of the Storegga Slide, as laid out in Figure 4.22. The present study suggests that formation of the CSS (equivalent to 'Lobe II' of Haflidason et al. 2004, and the inferred west-wards movement of 'Slide Block R' of Bryn et al. 2005a) occurred prior to further failure from the southern main headwall. However, the findings of the present study suggest that a large volume of material was involved in the latter (Fig. 4.21C), in

contrast to the previously interpreted minor volumes (Haflidason et al. 2004; Bryn et al. 2005a).

4.8.4 Timescale and tsunamigenic potential of the Confined Storegga Slide

A significant question which is often left open from the study of submarine MWDs is the actual time duration of the event, and the speed at which the failed sediments move downslope. An intuitive way of back-calculating the velocity of downslope translation is to look at studies based on the modelling of tsunamis' generated by the specific MWD in question, since the structure and height of water waves generated by submarine slope movements are strongly dependant on the time-displacement history of the latter (Harbitz 1992). Previous studies which have modelled the tsunami apparently generated by the Storegga Slide have suggested velocities in the range of 10 – 35 m/s (Harbitz 1992; De Blasio et al. 2003; Bondevik et al. 2005; Bryn et al. 2005a). These estimates are based on a pseudo-simultaneous event however, considering the effect of several phases of retrogressive failure inline with the reconstructed 'phases' of the Storegga Slide.

Færseth and Sætersmoen (2008) agreed with Schwarz (1982), who concluded that submarine MWDs are likely to translate downslope at speeds of 5 m/s or less. Færseth and Sætersmoen (2008) further postulated that the cumulative total duration of translation and development of the associated deformation is likely to have been 1 hour, and invoke two-stage model of progression involving a period of initial acceleration at the leading edge, followed by a more gradual slowing down. Given the absence of detailed real-time measurements from suitable analogues, high-resolution seismic stratigraphic or core-based dating, it difficult to ascertain whether or not such a short time scale for the formation of such large-scale and extensive deformation is

accurate. Based on the deep-seated failure surface, limited downslope translation and 'anchoring' effect of remnant slide bodies, the present study favours a model which involves slow and gradual acceleration followed by gradual deceleration. We speculate that given the extremely limited downslope translation of the failed mass involved in the Confined Storegga Slide, it was not possible for significant velocities (i.e. in the order of 35 m/s) to be obtained, and agree with Færseth and Sætersmoen (2008) that a figure of 5 m/s or less is more appropriate.

The main factors affecting the tsumigenic potential of a submarine mass wasting deposit are the volume and/ or thickness of the failed mass, and the initial acceleration (Haugen et al. 2005). Given the emphasis placed throughout this study on the notable thickness and volume of material involved in the Confined Storegga Slide, and indeed confined MWDs in general, such events could be considered to have high tsuamigenic potential. Conversely, the confined model suggest that with high thickness/ volume of failed material comes limited translation, as with the case of the Confined Storegga Slide and the interpretation of limited velocity and low initial acceleration. It is thought unlikely therefore that very large confined MWDs can ever overcome the inertial constraints to displace at speeds needed for significant tsunami generation.

4.9 Conclusions

- Using a combination of 2D and 3D seismic reflection data and bathymetry data, the area of the Storegga Slide historically referred to as the 'compression zone', has been shown to represent the downslope region of a discrete submarine MWD, informally named the 'Confined Storegga Slide'.

- Based on the deep-seated failure surface, steep frontal ramp, close association with 'pinned' blocks of remnant pre-failure stratigraphy, and limited downslope translation, the Confined Storegga Slide has been interpreted as a 'frontally confined' submarine MWD, first identified by Frey Martinez et al. 2006.
- The Confined Storegga Slide has a section length of c. 135 km and varies in thickness from c. 40 m in the headwall region to 640 m in the vicinity of the downslope margin. A total area of 3,510 km^2 is affected, corresponding to a sediment volume of approximately 1,227 km^3.
- Fault displacement analysis of over 30 pairs of thrust faults evident over 30 km of the seabed, based on 2D seismic lines, has shown that a total shortening of c. 5 km has occurred in the downslope region, which equates to the distance of downslope translation of the failed sediments.
- Analysis of up-dip 2D seismic data and 3D seismic has revealed the presence of later-stage extensional deformation and translation of sediments in a direction orthogonal to the Confined Storegga Slide, interpreted as the result of later stage failure as part of the multi-phase Holocene Storegga Slide.
- Comparison of scaled, schematic models of the likely pre-failure slope configuration and the present day conditions shows that a significant volume of material has been removed following the development of the Confined Storegga Slide.

CHAPTER FIVE

5.0 Summary and Discussion

5.1 Introduction

This project has used industrially acquired 2D and 3D seismic reflection data, with supplementary bathymetry data to conduct a detailed analysis of the architecture and structural elements of submarine mass wasting deposits from the Norwegian continental margin, with additional examples from the Levant margin. The integration of 3D seismic interpretation with a combination of other data types has allowed for thorough coverage of different examples of both recently formed, exposed mass wasting deposits, and older, buried examples. Following sections of this chapter will firstly aim to summarise the key scientific results of each core research chapter, and then assess the significance of the project results for various aspects of submarine mass wasting deposits and related topics. The previous chapters have been structured in three semi-independent units as a result of focussed investigation into the various questions that this research has attempted to address. The main aim of this chapter is to draw together the scientific results presented in the preceding chapters and revisit the objectives of this project in order to evaluate the contribution of the research presented. This chapter will then conclude with a discussion of the implications of this work for the economic and engineering geology of the areas affected by submarine mass wasting processes, and consider avenues of potential further work.

5.2 Summary of results

5.2.1 Results from the development of a subsurface evacuation model for a submarine slope failure (chapter two).

Chapter two presented a focussed study of a discrete submarine MWD, buried beneath c. 200 m of overburden, which developed on the northern margin of the later Storegga Slide. The MWD in question, informally named the 'South Vøring Slide' (SVS), was initially identified during regional mapping using the 2D and 3D seismic datasets, and identified as being non-typical based on aspects of its geometry and morphology.

The principal objective of **chapter two** was to conduct further geometrical and quantitative analysis on the SVS in order to explain its deviation from other examples of MWD's found within the study area, and present a model for its development. An integrated 3D seismic approach was used to characterise the SVS and show that it could not be explained by a classical retrogressive model, often invoked to account for the development of mass wasting in fine-grained deposits from continental margins. The research presented in **chapter two** showed that the defining characteristic of the SVS is the high relative volume loss evidenced by a thinning of some 40%, seen with only modest extension in the downslope direction of only 4.5%.

In order to explain the volume loss and development of the SVS, a model involving the mobilisation of an approximately 40 m thick interval at the lower part of the SVS, and its removal from beneath a thin overburden which subsequently underwent extensional fragmentation was invoked. This implicated the liquefaction of a substantially thick fine-grained unit in the development of a submarine MWD for the first time. **Chapter two** highlighted a novel mechanism for the development of a

MWD, and given its locality in a setting of prolific slope instability, it raises the possibility that liquefaction could have played a role in the development of further mass wasting events in the area. Furthermore, the findings of **chapter two** showed the power of 3D seismic data as a tool for the investigation of submarine MWDs, and very much supports the notion that 3D seismic data can be used to gain an improved understanding of the processes involved.

5.2.2 Results from a study of the kinematic indicators from submarine mass wasting deposits (chapter three).

Chapter three provided the first comprehensive compilation of all of the kinematic indicators which may be found from submarine MWDs. The aim of **chapter three** was to identify all of the various types of deformation structures and features associated with MWDs, and present them using a suitable classification scheme and illustrated, worked examples taken from the 3D dataset available for this project. A further aim was to develop recognition criteria for each feature using seismic data, and a workflow for their analysis in terms of kinematic information, so that the end results might find broad applicability for seismic interpreters working on MWDs in various settings and locations.

A classification scheme based on context within the MWD body was devised and used to catalogue the various kinematic indicators identified during initial reconnaissance mapping. The best examples resulting from this process were then chosen to illustrate each kinematic indicator type and presented in **chapter three** along with the results of further analysis conducted in order to deduce information pertaining to the direction and magnitude of transport, mode of emplacement, dominant mass wasting process or rheology.

The results of **chapter three** further highlighted the use of 3D seismic data in the investigation of submarine MWDs, specifically as they provide large areal coverage which allows swift and confident evaluation of the direction of translation, and in many cases also allow the degree of translation of the displaced slide material to be constrained. Imaging of the basal shear surface, analysis of internal architectures and determination of transport direction are areas which have been shown to be of particular benefit.

5.2.3 Results from the identification of a frontally confined submarine slope failure in the Storegga Slide (chapter four).

Chapter four presented the results of a study which focuses on a large, contractionally-deformed marginal region of the Holocene-age Storegga Slide historically referred to as the 'compression zone'. Following the recent identification of two end-member types of MWD toe zones, 'frontally confined' and 'frontally emergent', it was noted during reconnaissance mapping of the study area that the deformation style observed from the compression zone shares many common characteristics with the distal zones of submarine MWDs which are 'frontally confined'. In order to test the frontally confined model, **chapter four** uses a composite dataset including 3D seismic, 2D seismic and bathymetry data to conduct a multi-scale interpretation of the compression zone and surrounding area.

Focussed interpretation within the traditionally delineated 'compression zone' was first of all carried out to characterise the deformation before the regional 2D seismic and bathymetry data were used to conduct a broad-scale correlation, with focus on the upslope (landward) direction. Several key features associated with MWD's, including a distal margin, lateral margins, varying zones of deformation and

a headscarp were identified and genetically linked across a laterally extensive basal detachment horizon, enabling a revised interpretation of the compression zone as a frontally confined submarine MWD, informally named the 'Confined Storegga Slide' (CSS), from within the predominantly frontally emergent Storegga Slide. Identification of primary constraining features has allowed an accurate estimation of the area, volume and degree of translation of the CSS. Focussed interpretation of the 3D seismic data led to the identification of multi-stages of deformation, and construction of a scaled model to illustrate the formation of the CSS and a later stage of deformation and volumetric change.

5.3 Implications of research

Based on the summary of results from the core research chapters, three topics will be discussed further to develop themes which have arisen throughout the course of this project: development of the basal shear surface; the role of liquefaction in the development of submarine mass wasting events; and 3D seismic data and submarine mass wasting deposits: Quo Vardis?

5.3.1 The role of liquefaction in submarine mass wasting events

An interesting theme raised in this project (chapter two) is the role of liquefaction in the development of submarine slope failures. It appears that there are two ways in which the liquefaction of sediments is associated with slope failures: 1) the small scale liquefaction of relatively thin units (> 10 m) associated with the basal failure surface; and 2) liquefaction of relatively thick units (10's of metres) which comprise a large portion of the failed mass. In the case of the former, features which form due to liquefaction including clastic dykes, sand volcanoes, loads structures and dewatering

structures, have been reported from outcrop examples of submarine MWDs (e.g. Farrell 1984; Strachan 2002a & b). Such features, generally considered to represent 'in place' deformation (Collinson 1994; Maltman 1994) are attributed to the liquefaction of sandy units which closely underlie the basal failure surface due to the imposition of unidirectional shear and/ or rapid loading during the emplacement of the MWD (Strachan 2002b).

On a larger scale, the results of chapter two show that liquefaction can play a more significant role in the development of slope failures. Where substantially thick or laterally continuous layers undergo liquefaction, they can constitute either a large proportion of the failed mass, or form an extensive basal lubrication layer. As discussed in chapter two, section 2.6, a type of onshore slope failure which occurs due to liquefaction is that of quick clay slides. These large-scale, destructive slope failures involve the liquefaction of substantially thick units of clay which flow rapidly and involve heavy depletion of the source areas (Bjerrum 1955; Rosenqvist 1966; Carson 1977). The liquefied clay commonly constitutes the entire failed and translated mass, with only minor incorporation of the underlying substrate or overlying units (Rosenqvist 1966; Carson 1977).

The liquefaction of subaqueous sedimentary units was implicated by Wilson et al. (2004), who cited the liquefaction of a laterally extensive fine-sand contourite layer as being critical in the development of the 12 km long Afen Slide from the Faeroe-Shetland Channel. Whilst it has traditionally been thought that clay-rich sediments are not prone to liquefaction due to the high cohesion and platy nature of the minerals, there has been growing acknowledgement of its occurrence and the many factors involved following its recent implication in a number of onshore slope failures (Gratchev et al. 2006). The widespread occurrence of quick clay deposits and

slope failures in glaciated onshore regions is testament to this. The liquefaction of clay-rich sediments in the submarine realm has been hinted at previously. Kerr (1962) and Edgers & Karlskrud (1983) noted that subaqueous slope failures have several characteristics in common with onshore quick clay slides, including the high mobility and long run out of fine-grained subaqueous units and ability to translate across extremely shallow slopes. The role of liquefaction in the Storegga Slide, along with the unexplained collapse of a borehole at a depth of 600 – 800 m below the seafloor, was discussed by Bugge (1981).

The present study has presented geometric and volumetric evidence for the large-scale liquefaction of a fine-grained unit in a subaqueous setting (the South Vøring Slide (SVS); chapter two). The near complete removal of the liquefied interval has resulted in a heavily depleted and deformed slope failure unit remarkably reminiscent of the sites of onshore quick clay landslides. There are several key characteristics which set the SVS firmly apart from classical examples of submarine slope failures which involve the translation or transfer of material downslope over a basal shear surface. Such classical models involve large extensional offsets at the headscarp and high values of extension in the upslope region, which are balanced by a contractionally strained zone at the downslope margin. Thus, depletion in the upslope region is balanced volumetrically by accumulation in the downslope region, with minimal volume loss (c. 10%) due to porosity changes, dewatering and compaction, etc). This 'end-member' style of slope failure due to shear failure can be illustrated by the Israel Slump Complex (ISC) from the Levant margin, described by Frey Martinez et al. (2006).

The SVS represents a type of slope failure which differs markedly; the base of the SVS is defined by a horizon which lacks evidence of shear failure, and which,

aside from a thin residuum of the mobilised material, is directly overlain by the fractured and extended overburden which forms the top surface. As such, the base of the SVS can be likened to a 'weld', whereby mobile material has been removed between two interfaces which are now juxtaposed (Jackson et al. 1994). As opposed to minimal volume loss and maximal translation observed from classical models of submarine slope failures, volume loss in the case of the SVS is maximal, with an estimated 50% of the undeformed, pre-failure slope template removed during its development (chapter two). Despite the high volume loss which suggests a high degree of material transfer, the actual values of extension which would attest to this transfer are minimal. The SVS can therefore be placed at the opposite end of the spectrum of slope failure styles from classical shear failure types.

Interestingly, an example of a slope failure which can be placed between the two end member types, is that described by Davies and Clarke (2006) from the NE Atlantic margin. This particular slope failure, attributed to overpressure generation from the underlying silica diagenetic front, resulted in mobilisation of a basal unit and translation of the overlying coherent unit (Davies and Clark 2006). Although shear failure due to overpressure build up is the primary failure mechanism, liquefaction occurred locally where a sediment fluid mixture was expelled onto the contemporary seabed via faults in the rigid overburden, leading to minor volume loss and moderate downslope translation of the collective mass (Davies and Clark 2006).

The identification of a submarine slope failure due to the liquefaction of a substantially thick fine-grained unit leads to consideration of where else such slope failures may occur. An obvious consideration is that further slope failure units due to this mechanism may have occurred in the study area, but may have yet gone undetected due to a lack of 3D seismic data, or have been modified by later sliding.

Other glaciated continental margins elsewhere, such as that of Canada or Antarctica, which may have also developed fine-grained units could also be at risk. Likely triggering mechanisms for the liquefaction of fine-grained units are discussed in chapter two, section 2.6. Although in the case of the SVS, an undermining triggering mechanism was deemed to be the most likely scenario for the onset of liquefaction, earthquakes are a plausible and widely-cited triggering mechanism (e.g. seismicity due to isostatic rebound is thought to have been a major trigger in the Storegga area; Evans et al. 2002). This is because cyclic loading due to the oscillatory transmission of seismic waves induces elevated pore fluid pressures which often fail to be completely dissipated before the next pore fluid response (Maltman 1994), particularly in the case of fine-grained units.

There are several key questions raised by the study presented in chapter two, and much further work is required to fully define the likelihood of further slope failures developing due to the liquefaction of thick fine-grained units. Certainly more studies using 3D seismic data must be performed as a way of identifying possible further examples. In order to fully define the failure conditions necessary to result in the development of such slope failures, incorporation of borehole studies would be required to examine the lithologies and geotechnical conditions in detail.

5.3.2 Development of the basal failure surface

One of the major powers of 3D seismic data highlighted by the present study is its use as a tool to image and study the basal shear surface of submarine MWDs over large areas. Previously this has not been possible using other remotely sensed geophysical techniques or the study of field outcrops.

A key question which remains open pertains to the initiation and evolution of the basal failure surface. Prior consideration has been based on the study of onshore

analogies, numerical models and outcrop examples of submarine slope failures (Farrell 1984; Fleming and Johnson 1989; Martel 2004; Petley et al. 2005). This surface is often described as a shear fracture, which develops progressively during the slope failure event, with failure dependant on its prior formation (Bjerrum 1967). The knowledge of the basal shear surface has been furthered in this study in two ways: 1) it provides a 3D map of basal shear surface and documents and accounts for the typical geological structures found in and associated with it. 2) It highlights the importance of other seismically mappable geological interfaces that occupy a similar position to the basal shear surfaces but that do not form as a shear fracture (see chapter two, section 2.6). Here, any specific evidence relating to the propagation and development of this surface is considered further.

Farrell (1984) attempted to relate the deformation observed from ancient outcrop examples of submarine MWDs to the development of the basal failure surface by likening the upslope extension – downslope compression model for classical slope failures (*sensu* Varnes 1978; Frey Martinez et al. 2005, 2006) to the theoretical cross section of a dislocation loop. In this model, the fault tip line spreads out radially from a point of initial failure, within which material has slipped and outside of which material is unslipped, and it is assumed that slip on the fault is maximal at the initial failure point and nil at the tip line (Williams and Chapman 1983). Extensional strain in the MWD would therefore develop where the dislocation propagates in the opposite direction to the slip direction, and contractional strain would be evident where the dislocation propagates in the same direction as the slip direction (Farrell 1984). It follows therefore, that the extensional slip zone will be upslope of the initial failure point, and contractional strain will develop downslope of the initial failure (Farrell 1984). It was further suggested that cessation of the slope failure event occurs due to

the failed mass regaining cohesion with the underlying failure surface, with the failed mass halting at its distal edge first, followed by propagation of a compressional strain wave towards the proximal region (Farrell 1984). In the present study, although it has been possible to examine complete slope failure units (e.g. in chapters two and four), no evidence has been found to support the theory of Farrell (1984). This is because unlike conventional extensional or compressional faults the low angle of the basal shear surface and highly disrupted internal architecture of MWDs means that detailed 3D displacement plots for the basal shear surface cannot be made. A limitation of the 3D seismic, is therefore that even though useful for determining position, morphology and depth of the basal shear surface, it is less useful in determining the point of initial failure.

Martel (2004) carried out a study based on a 3D elastic model for the development of a basal shear surface of an onshore slope failure, in which the basal surface was considered to be a shear fracture. The study found that such a model was able to account for the observed distribution of deformation commonly associated with onshore slope failures, and that the failure surface did not initiate simultaneously beneath the entire failure area, with deformation preceding large displacements (Martel 2004). Displacements at the ground surface were found to evolve in line with the propagation of the slip surface at depth, and stress concentrations were found to be higher around the perimeter of the slip surface than near the ground surface, leading to the conclusion that cracks at the upslope head and side flanks of the failure would open at depth and propagate upwards (Martel 2004). This agrees with the interpretation of Fleming and Johnson (1989), who considered failure surfaces to nucleate at depth and propagate up based on observations of the progressive development of en echelon fractures which appeared along the side flanks of an

onshore slope failure (chapter three, section 3.6.1). Martel (2004) concluded that the representation of this process at the surface would initiate at the upslope head and propagate downslope in an 'unzipping' fashion, and citied the presence of arcuate zones of en echelon fractures to be indicative of a 'substantially progressed' slope failure with significant development and propagation of a slip surface at depth.

The results of chapter three, section 3.6.1, were found to support the findings of Fleming and Johnson (1989), relating to development of the lateral margins of onshore slope failures, and so the results therefore support the idea that submarine slope failures also develop by upward propagation of deep-seated failure planes. Further support for this idea comes from the Levant margin, where two 'early-stage' slope failures, first described by Frey Martinez et al. (2005) can be used to apply the findings of Martel (2004), which are based on numerical modelling of onshore slope failures, to submarine examples. Figure 5.1A shows a seabed dip-attribute map of the area affected by the early-stage slope failures, labelled 'protoslumps' by Frey Martinez et al. (2005). The protoslumps are defined by lineations which are parallel and perpendicular to the slope direction, delimiting downslope-elongate chute-like features (Fig. 5.1A; Frey Martinez et al. 2005). On the surface, the slope-perpendicular lineations define the upslope margins of the slope failures, and are the most well-developed, conspicuous feature (Fig. 5.1A). The slope-perpendicular lineations define the lateral margins and are less-well developed than the upslope margins (Fig. 5.1A).

In a representative seismic dip-section through one of the protoslumps, it can be seen that no internal chaotic facies is observed, although there is evidence of deformation in the form of small-scale disruption which is concentrated along a horizon approximately 100 m below the seabed (Fig. 5.1B). At the upslope margin of

the protoslump, offsets corresponding to a seabed depression are interpreted as a crown-crack (Frey Martinez et al. 2005). This feature detaches into the deformed horizon which is interpreted to represent the early stage development of a failure surface for this protoslump (Fig. 5.1B). There does not appear to be any substantial development of a distal margin or contractionally strained region downslope, and no indication of the loss, gain, or transfer of material (Fig. 5.1B). Frey Martinez et al. (2005) took this to be representative of a lack of translation and further proof of immature development.

Based on its more pronounced seabed expression, the laterally continuous crown-crack seen on the seabed dip-map (Fig. 5.1A) appears to be better developed that the lateral margins of the protoslumps, which are more subtle in appearance. This supports the model of Martel (2004), which predicts that at the surface, fracturing initiates at the upslope margin, and is followed by the development of fractures along the lateral margins. Martel (2004) further predicts that development of such features can only occur once the failure surface itself is substantially developed, and there is evidence for this in the Levant margin protoslump, in the presence of the deformed basal horizon into which the crown-crack detaches. The observable development of a basal shear surface and upslope margin, with less well developed lateral margins and no translation or transfer of the material conforms precisely to the predictions of Martel (2004) and supports the notion that the basal failure surface must first develop before full failure can occur (Bjerrum 1967; Martel 2004; Petley et al. 2005).

5.3.3 3D seismic data and submarine mass wasting deposits: Quo Vadis?

As highlighted in chapter three, section 3.6, there is much scope for further investigation of submarine MWDs, and indeed, deep water processes as a whole

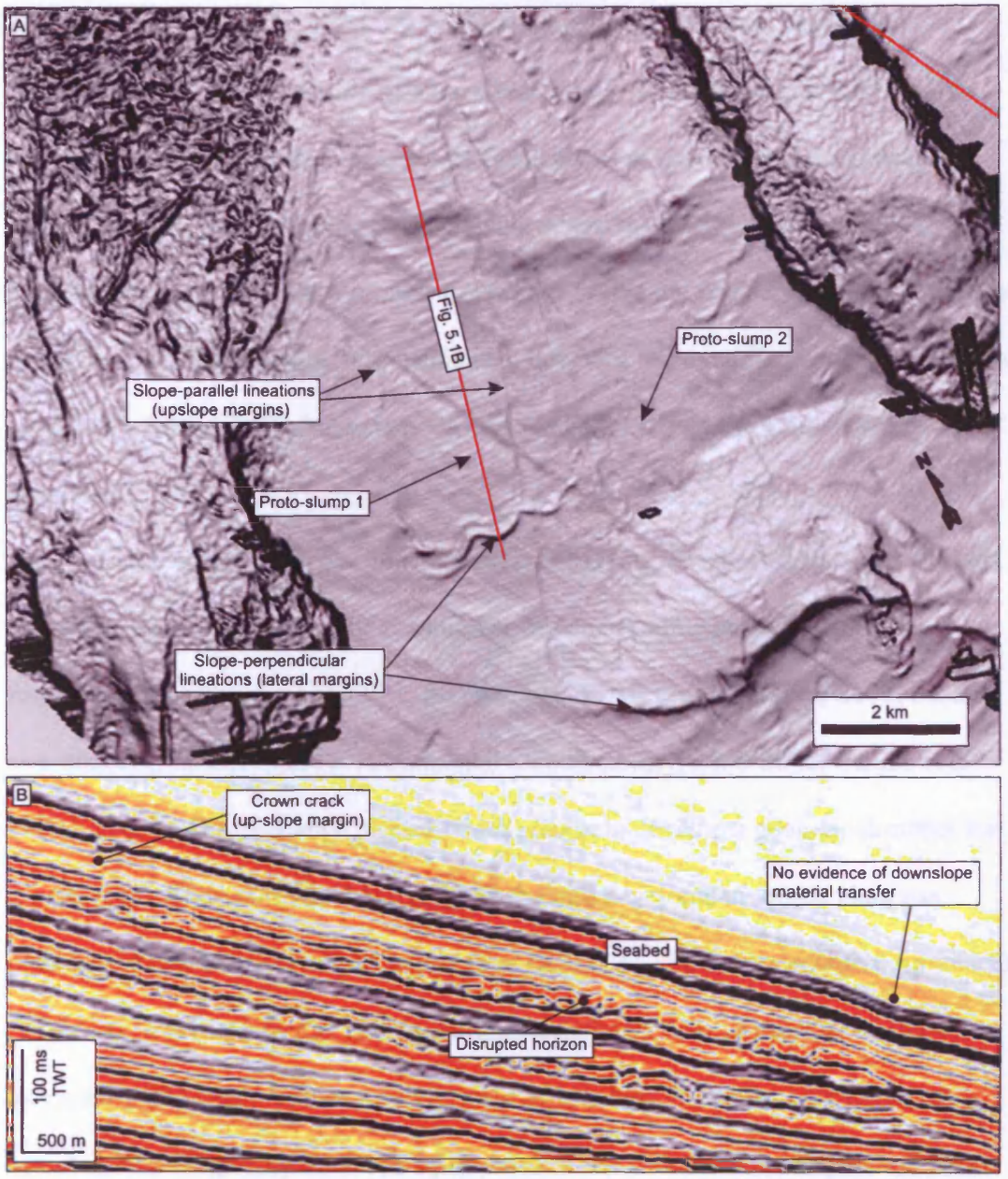

Figure 5.1. Protoslumps from the Levant margin seabed (after Frey Martinez et al. 2005). A: Seabed dip-map showing clear evidence for the development of upslope and lateral margins, represented by well developed slope-perpendicular lineations and less-well developed slope-parallel lineations respectively. B: 3D seismic dip-section through one of the protoslumps, showing a crown-crack which affects the seabed as well as the shallow subsurface succession, detaching into a horizon at c. 100 m below the seabed. The horizon features small scale disruption which is interpreted as early development of a basal detachment surface and limited slip of material. The fact that a toe region has not developed (e.g. contractional deformation or accumulation of material) in the downslope position is taken as evidence for the immature stage of slope failure development. Location shown in (A).

(Posamentier and Kolla 2003), using 3D seismic data techniques. Such potential lies in the three dimensional nature of data, which allows a combined morphological, volumetric and quantitative approach to the analysis of depositional units and large areal coverage, with further geological data yielded by analysis of various attributes (chapter three, Section 3.6). In order to evaluate where the future may lie for the study of submarine MWDs using 3D seismic data however, we must first consider the major motivating factors behind the study of such phenomena, and the main outstanding questions.

Large advances in our understanding of MWDs have been made over the past twenty years or so, due largely to a number of wide-ranging projects which have focussed on marine slope stability, for example, STRATAGEM (2000-2003; Stoker and Shannon 2005), COSTA (Continental Slope Stability, 2000-2002; Canals et al. 2004), and the Ormen Lange project which sought to develop a geological model for the Storegga Slide motivated primarily by the safe development of the giant gas discovery beneath the headwall region (See Bryn et al. 2005a for executive summary). Advances in our knowledge and the various techniques that we may use to study submarine slope failures as a result of these efforts have led to the emergence of remotely sensed geophysical techniques, such as 3D seismic data analysis and multi-beam surveys as major avenues of research (e.g. Urgeles et al.1997; Frey Martinez et al. 2005). The amount of data acquired by the industry in the ongoing search for oil and gas is becoming increasingly available to academia, which along with adoption of data manipulation techniques, has facilitated research to a broader end, i.e. application to more than just the search for natural resources. Broadly speaking, there are two major interlinking areas of ongoing concern and activity: hazard analysis, and the development of natural resources.

5.3.3a Hazard analysis

Submarine slope failures are of interest and concern in a social sense because of the hazard that they pose, mainly to coastal populations and offshore installations. One of the greatest risk factors is the potential for large slope failures to generate tsunamis (Lee et al. 1991). Seafloor stability must also be considered when developing coastal regions and considering reliable corridors for communication installations (Locat and Lee 2002). The study of slope failures in the submarine environment is challenging compared to onshore examples, due to the inaccessibility, the differing nature of the slope sediments, and other factors not associated with subaerial slopes such as the effect of wave-action, and high level of saturation. Although we have the ability to identify areas which are generally at risk of future submarine slope failure, we are unable to accurately predict where or when a future event might occur, particularly when the triggering mechanism is unpredictable (as with the commonly implicated occurrence of earthquakes). Monitoring programmes employed in high-risk areas onshore are not applicable to the submarine realm (Locat and Lee 2002) and so alternative methods must be sought to help estimate the potential losses and risk to human life and infrastructure due to submarine slope failures, that in turn can be used to construct mitigation strategies.

The main avenues of research currently being pursued in order to further our forecasting abilities are the continued study of pre-existing examples of slope failure (back analysis approach); testing and characterisation of as yet un-failed slopes, and numerical modelling. As far as the characterisation of existing examples of submarine slope failures is concerned, 3D seismic data clearly has a large and important role to play, for reasons which have been touched upon at various stages throughout this project. In the first instance, seafloor mapping using 3D seismic surveys can be used

to identify recent slope failures on previously unexplored submarine slopes, in a similar way to multi-beam data which image the seafloor, due to the large areal coverage combined with high resolving power (Cartwright and Huuse 2005). In areas of historic instability, the availability of 3D seismic data presents the opportunity to examine many other examples of MWD's buried in the subsurface succession (e.g. chapter two). Whilst the study of existing submarine slope failures essentially involves the study of such events at their final stage (Locat and Lee 2002), this approach is nonetheless revealing and effective in that final geometries of the depositional units can be used to interpret the dynamic evolution and failure processes involved (see chapter one, section 1.1). As is the basic premise of this project, further characterisation studies will continue to grow the catalogue of observed features, parameters and architectures to ultimately define the full spectrum of slope failure types and in doing so, fully define the range of processes and failure mechanisms involved. 3D seismic data is particularly useful in this sense due to the quantitative and volumetric analysis afforded.

Stability analysis of submarine slopes

A major technique in analysis of submarine slopes stability is the measurement of various geotechnical parameters. However, there are inherent problems with the collection of such parameters, particularly regarding the accurate measurement of in situ parameters such as pore pressure (Strout and Tjelta 2005). The incorporation of geotechnical information is no doubt essential, but equally as important is the insight into the subsurface provided by 3D seismic data. In areas of historic instability, 3D seismic data play a valuable role in the full definition of the geological model for slope failure in a particular region. Important factors in the predisposition of a slope to

failure include the geometry and distribution of sedimentary packages and potential glide planes, possible sources of overpressure generation and triggering mechanisms.

An excellent example of this is the analysis of the Storegga Slide, for which 3D seismic data was used to help characterise the geometry and distribution of ubiquitous contourites deposits, implicated in the sliding due to their tendency to cause slope oversteepening and host laterally continuous 'weak layers' (Bryn et al. 2005b). In addition, 3D seismic data were further used to map gas hydrates throughout the region and provide input parameters for modelling of the evolution of the stability zone through time (Bünz et al. 2005). Large areas affected by polygonal faulting have been identified and studies using 3D seismic data, and implicated in fluid flow and overpressure generation in the northern-Storegga Slide area (Berndt et al. 2004).

The imaging and detailed analysis of silica diagenetic fronts, which have been associated with overpressure generation and resultant slope failure (Volpi et al. 2003; Davis and Clark 2006 see chapter two, section 2.6) has also been facilitated by 3D seismic data. This same technique can be applied to areas considered at risk of failure, through identification of the various pre-conditioning or triggering factors discussed above. Combination with geotechnical or sedimentological data would facilitate the broad scale prediction of unstable sedimentary packages, weak layers and presence or focus of overpressure generation.

Furthermore using a seabed mapping approach, 3D seismic data can identify possible areas of future failure, as features diagnostic of incipient failure such as crown cracks and partially formed lateral margins can be clearly identified from seabed horizon maps. Frey Martinez et al. (2005) used 3D seismic data from the Levant Margin, Mediterranean Sea, to identify two elongate chute-like features

defined by slope-parallel and perpendicular lineations interpreted as lateral margins and crown cracks. Advanced deformation or displacement of the sediments was absent, and the features where labelled 'protoslumps', interpreted to be the product of failed or immature slope failures (Frey Martinez et al. 2005).

Numerical modelling

Numerical modelling is considered to be of great importance in the ongoing study of submarine slope failure given the difficulty involved in direct observation (Locat and Lee 2002), and provides a further way of understanding existing slope failures and predicting their future occurrence. Modelling based on existing submarine MWDs allows reconstruction of conditions prevalent at the time of failure, the results of which can be further input into the testing of various scenarios applicable to areas which have been identified as at risk of potential future failure. 3D seismic data once again has an important role to play in the provision of dimensional constraints for geomechanical models which serve as a static framework for the various parameters. Numerical modelling is similarly an important tool for the study and prediction of related hazards including tsunami generation. Key variables which effect the scale of slope failure-generated tsunamis which can be derived directly from 3D seismic data include the volume, length and thickness of the causative slope failure.

5.3.3b Production of natural resources

Submarine slope failures are relevant to the ever-expanding search for oil and gas reserves for two main reasons: engineering implications posed by the necessity of drilling through MWDs and the safety and stability of offshore installations (seabed and shallow hazards); and the development of reservoirs in submarine MWDs.

Inherently unstable continental margins are being increasingly explored for hydrocarbon reserves and the difficulties of safety developing and producing from such fields, which are situated beneath submarine slopes which may be unstable, or have historically been unstable, can be complex. The obvious concern is the stability of the present day seafloor onto which offshore installations must be affixed, and prior to this it must be ensured that there is little or no risk of slope failure in the vicinity of any installations, or indeed upslope of them, should they be impacted by failure originating from a more proximal position. Further consideration must be given to the impact of drilling operations on the stability of the slope. The discovery of Ormen Lange beneath the steep headwall region of the Storegga Slide is a prime example of just this scenario, and has been made famous by the huge effort in data acquisition and analysis that has been undertaken to understand, asses and mitigate the risk and potential of future slope instability (the reader is referred to the special publication on the Ormen Lange project, issues 1-2 of Marine and Petroleum Geology, volume 22; 2005).

Submarine MWDs at or near the seabed can pose as significant shallow drilling hazards to exploration and development well drilling operations. Units or lithologies which possess excessively low strength, as can be the case with homogenised, rapidly deposited MWDs are hazardous because of the unpredictable nature of the strength, rock and fluid properties within such units. Such unpredictability leaves drilling operations exposed to hazards such as loss of drilling fluids and borehole collapse, with the additional economic implication of increased drilling times (Frey Martinez et al. 2005). Accurately mapping and predicting the occurrence of such units within the shallow succession is therefore imperative to the safety of drilling operations. Frey Martinez et al. (2005) used 3D seismic data from

offshore Israel to identify many MWDs throughout the subsurface succession, illustrating how 3D seismic data has an important ongoing role to play in the diagnosis and mitigation against shallow drilling hazards.

An altogether different concern is the development of reservoirs which occur in submarine MWDs, which form an increasing part of the exploration and production portfolio of oil companies, particularly in deep water passive margins, rifts and collisional belts (Welbon et al. 2007). Examples include the Statfjord Field and Halten Terrace area, offshore Norway (Hesthammer and Fossen 1999; Welbon et al. 2007). As with all reservoir types, the major challenge for successful exploitation is the accurate prediction of geometrical and petrophysical characteristics. Specific challenges in the case of MWDs relate to the scale and complexity of such reservoirs, and constraining the impact of factors such as the range distribution and effect of deformation, thickness variation, geometry and impact of lithological mixing. While a combination of predictive tools can be used, including seismic data, well data and outcrop studies, 3D seismic data is recognised as being of prime importance as a result of the geomorphological understanding and empirical observations they provide (Welbon et al. 2007).

5.4 Project limitations and recommendations for further work

The combination of more than one type of data, and the varying scales of investigation have allowed a thorough investigation of the mass wasting deposits in the study areas. While many new observations and some advances in our understanding have been made by this project, certain limitations have been imposed, by limited data availability, data quality, data gaps and the limited amount of other data types aside from seismic and bathymetry. The remainder of this section now

provides a discussion of the project limitations together with a number of suggestions as to how further work may be of use in overcoming them.

This project has focussed on the use of 3D seismic data to better constrain the structures and evolutional mechanisms of large-scale submarine mass wasting deposits. Only in recent years has 3D seismic data been used to study submarine MWDs, and the power of this data type in the use of submarine MWD investigations has been demonstrated by the results of this project. Despite the large volume of 3D seismic data available for this project, some of the MWDs imaged are very large, and so detailed interpretation has been possible only for relatively small subareas in some cases. Whilst analysis of these samples have proven to be successful, the inclusion of more 3D seismic data would allow for a more complete and informed comparison of MWDs from the study areas. As the use of 3D seismic data in the study of MWDs is still relatively new, new observations and information relating to their architecture and evolution is of high value to our understanding.

The most significant limitation imposed on this project has been the lack of well data to establish sedimentary character and absolute ages of the various MWDs in the study area. In chapter two, the age of the South Vøring Slide was loosely constrained by identifying overlying sedimentary packages and assigning their age using published data. The timing of the Confined Storegga Slide investigated in chapter four is referenced to relative time in relation to the other slide phases alongside it. Exactly how long it took for the Confined Storegga Slide to develop is unknown and the timing of large-scale submarine slope failure remains an open question. The establishment of absolute ages and timescales for the development of submarine MWDs such as those described in this project may help further the

understanding of why they occurred and when and where they may occur in the future.

Outside the scope of this study there are major aspects of submarine MWDs which are poorly understood, for example the high flow mobility of long run-out examples, transformation of slides and slumps into debris flows and/ or turbidites, and the development of the basal shear surface. Aspects such as these have been commented on or discussed where possible throughout this project, although for greater insight, the integration of other data types, particularly geotechnical data would be required. A further major source of high-quality data on submarine MWDs comes from ancient examples studied at field-outcrops. The many excellent and vigorous studies based on such examples has provided a wealth of information and in particular allows the small scale detail, which cannot be obtained from seismic data, to be examined. As such, the study of submarine MWDs can surely benefit from the integration of both outcrop data with seismic data, as the two provide opposing levels of stratigraphic fidelity.

CHAPTER SIX

6.0 Conclusions

The investigations undertaken during the course of this research have provided a wealth of information relating to diverse aspects of submarine mass wasting deposits, primarily from the Norwegian continental margin, with other examples from the Levant margin of the east Mediterranean Sea. Observations and resultant conclusions have led to insights into the dynamic evolution and emplacement of large submarine mass wasting deposits and the range of deformational features associated with them. Although this study has focussed primarily on submarine mass wasting deposits from one geographical region, it is expected that the results will find broad applicability to other examples of submarine mass wasting deposits in other setting and locations worldwide. The following sections list a number of statements with the aim of summarizing the conclusions of this project.

6.1 General conclusions

- The interpretation and analysis of seismic reflection data is a powerful tool in the investigation of submarine mass wasting deposits.
- Geometric and volumetric analysis of 3D seismic data can be used to determine the likely mechanisms responsible for the development and emplacement of submarine mass wasting deposits.
- 3D seismic data can be used to identify and analyse the full spectrum of kinematic indicators which occur in association with submarine mass wasting deposits.
- The 3D nature of such data allows the imaging and analysis of the basal failure surfaces of submarine mass wasting deposits, which is not possible by any other means, and which yields much pertinent information relating to the dynamic emplacement of such events.

6.2 A subsurface evacuation model for the development of a non-typical submarine mass wasting deposit from the Norwegian continental margin

- 3D and 2D seismic reflection data from the Norwegian continental margin have allowed the identification and mapping of a discrete submarine mass wasting deposit, informally named the 'South Vøring Slide' (SVS), from the Norwegian continental margin.
- Detailed mapping of the 3D data has allowed the characterisation and analysis of the deformation associated with SVS. Line-length balancing performed on representative dip-sections from the 3D data was used to determine that failed material which remains in the SVS area has undergone a very limited amount of downslope translation.
- Detailed mapping using a combination of 3D and 2D data has allowed for an estimation of the volume of material removed during the development of the SVS, which was concluded to be too high to be explained by the straightforward transfer of material downslope over a basal failure surface as with typical examples of submarine mass wasting deposits in the area.
- Based on the 3D architecture of the SVS, geometrical and volumetric analysis and comparisons with an analogous onshore slope failure mechanism, it was determined that the SVS is likely to have developed due to the mobilisation of a substantially thick, fine grained unit which was evacuated from beneath a thin overburden, which subsequently underwent extensional fragmentation.
- The proposed model for the development of the SVS highlights the potential role of the liquefaction of fine grained units in submarine slope failures.

6.3 Kinematic indicators from submarine mass wasting deposits

- An integrated 3D seismic interpretation approach of time-structure mapping, attribute extraction and 3D-visualisation has revealed a wide range of deformation features associated with mass wasting deposits, which record kinematic information pertaining to the direction and magnitude of transport, mode of emplacement, dominant process and rheology of the mass wasting event.

- Compilation and cataloguing of the many examples of kinematic indicators identified from the study areas has allowed for the first comprehensive overview of kinematic indicators from submarine mass wasting deposits.
- Kinematic indicator types have been defined, assigned seismic recognition criteria, illustrated using best examples from the study areas, and the kinematic information they impart has been discussed and presented alongside a worked example to demonstrate their use in the analysis of mass wasting events.
- Kinematic indicators can be used in the swift and confident analysis of the direction of translation and in many cases also allows the degree of translation of displaced material to be constrained.
- The ability to image large features associated with basal failure surfaces, such as ramp and flat geometries, allows for new insights into their development and propagation, and the development of the mass wasting event as a whole.

6.4 A 'frontally confined' submarine mass wasting deposit recognised from the Holocene Storegga Slide

- Using a combination of 2D and 3D seismic reflection data and bathymetry data, the area of the Holocene Storegga Slide historically referred to as the 'compression zone' has been interpreted as the downslope region of a discrete submarine mass wasting deposit based on up-dip correlation with other diagnostic features, including translated and rooted slide blocks, lateral margins and a headwall scarp, across an extensive basal detachment surface.
- The mass wasting deposit has been interpreted as an example of a 'frontally confined' submarine mass wasting deposit of Frey Martinez et al. 2006, based on the deep-seated nature of the detachment surface; frontal buttressing of the failed sediments against a steep frontal ramp at the downslope margin; the close association with rooted blocks of pre-failure stratigraphy; and limited downslope translation. The newly defined mass wasting deposit has been informally named the 'Confined Storegga Slide' (CSS).
- The distal region of is characterised by well preserved contractional deformation in the form of over 30 pairs of oppositely-dipping thrust faults, detaching above a deep-seated basal failure horizon which occurs some 640 m

below the seabed. A total shortening (i.e. downslope translation) of 4.24 km has been measured based on fault-displacement analysis and line-length balancing of thrust faults imaged on 2D seismic lines.

- The total area affected by the CSS is 3,510 km^2, which corresponds to a volume of approximately 1,227 km^3.
- Up-dip of the distal region, a large area of the CSS is characterised by extensional deformation which is interpreted to have developed during a later stage of deformation based on cross-cutting fault relationships and the superimposition of sediment transport pathways identified from the bathymetry data, which are orientated orthogonal to the transport direction of the CSS.
- Comparison of the likely pre-failure slope configuration with that of the likely post-CSS and present day conditions shows that a significant volume of material has been removed at some point following the development of the CSS.

6.5 Implications for economic and engineering geology

- Seabed or near-surface submarine mass wasting deposits constitute a significant hazard for seafloor engineering and hydrocarbon drilling operations due to their excessively low strength.
- The observations and subsequent results of this project have shown that 3D seismic data is an excellent tool for the identification and constraint of the extent of submarine mass wasting deposits, which can be used to optimise the planning of specific site surveys.
- Reconstruction of the development and movement directions of submarine mass wasting events, as described by this project, is a useful tool in determining the present day hazard posed by slope instability for future seabed engineering and drilling operations.
- Historical submarine slope failure has implications for the organisation of basin sediments and must therefore be taken into account when undertaking biostratigraphic or sequence stratigraphic analysis of the study areas.

7.0 References

A

Abbot, P.L. 1996. *Natural Disasters*. Dubeque, IA: Wm. C. Brown Publishing Co.

Anderson, E.M. 1936. The dynamics of the formation of cone-sheets, ring-dykes, caldron-subsidences. *Proceedings of the Royal Society of Edinburgh* 56, pp. 128-157.

B

Ben-Avraham , Z. 1989. The structure and tectonic setting of the Levant continental margin-eastern Mediterranean. *Tectonophysics* 8, pp. 351-362.

Berg, K., Solheim, A. and Bryn, P. 2005. The Pleistocene to recent geological development of the Ormen Lange area. *Marine and Petroleum Geology* 22, pp. 45-56.

Berndt, C., Bünz, S., Clayton, T., Mienert, J. and Saunders, M. 2004. Seismic character of bottom simulating reflectors: examples from the mid-Norwegian margin. *Marine and Petroleum Geology* 21, pp. 723–733.

Bjerrum L. 1967. Progressive failure in slopes of overconsolidated plastic clay and clay shales: *Journal of the Soil Mechanics and Foundations Division of the American Society of Civil Engineers* 93, pp. 1-49.

Berg, K., Solheim, A., and Bryn, P. 2005. The Pleistocene to recent geological development of the Ormen Lange area. *Marine and Petroleum Geology* 22, pp. 45-56.

Bertoni, C. and Cartwright, J.A. 2006. Major erosion at the end of the Messinian Salinity Crisis: evidence from the Levant Basin, Eastern Mediterranean. *Basin Research* 19, pp. 1-18.

Bondevik, S., Løvholt, F., Harbitz, C., Mangerud, J., Dawson, A. And Svendsen, J.I. 2005. The Storegga Slide tsunami – comparing field observations with numerical simulations. *Marine and Petroleum Geology* 22, pp. 195-208.

Bøe, R., Hovland, M., Instanes, A., Rise, L. and Vasshus, S. 2000. Submarine slide scars and mass movements in Karmsundetand Skudenedfjorden, southwestern Norway: morphology and evolution. *Marine Geology* 167, pp. 147-165.

Bradley, D. and Hanson, L. 1998. Palaeoslope analysis of slump folds in the Devonian Flysch of Maine. *Journal of Geology* 106, pp. 305-318.

Brekke, H. 2000. The tectonic evolution of the Norwegian Sea and continental margin with emphasis on the Vøring and Møre basins. In: Nøttveddt, A. et al. eds. *Dynamics of the Norwegian margin.* Geological Society, London, Special Publication. Vol.167. pp 327–378.

Brown, A.R. 1999. *AAPG Memoir; 42, SEG Investigations in Geophysics; 9: Interpretation of Three-Dimensional Seismic Data. Fifth Edition.* Tulsa, OK: AAPG/SEG.

Brown, A. R. 2003. *AAPG Memoir; 42, SEG Investigations in Geophysics; 9: Interpretation of Three-Dimensional Seismic Data. Sixth Edition.* Tulsa, OK: AAPG/SEG

Brown, E.H., Holbrook, W.S., Hornbach, M.J., and Nealon, J. 2006. Slide structure and role of gas hydrate at the northern boundary of the Storegga Slide, offshore Norway. *Marine Geology* 229, pp. 179-186.

Bryn, P., Berg, K., Forsberg, C.F., Solheim, A. and Kvalstad, T.J. 2005a. Explaining the Storegga Slide. *Marine and Petroleum Geology* 22, pp. 11-19.

Bryn, P., Berg, K., Stoker, M.S., Haflidason, H. and Solheim, A. 2005b. Contourites and their relevance for mass wasting along the Mid-Norwegian Margin. *Marine and Petroleum Geology* 22, pp. 85-96.

Buchbinder, B. and Zilberman, E. 1997. Sequence stratigraphy of Miocene-Pliocene carbonate-siliciclastic shelf deposits in the eastern Mediterranean margin (Israel): effects of eustacy and tectonics. *Sedimentary Geology* 112, pp. 7-32.

Bukovics, C. and Ziegler, P.A. 1985. Tectonic development of the Mid-Norway continental margin. *Marine and Petroleum Geology* 2, pp. 2-22.

Bugge, T. 1981. Submarine slides on the Norwegian continental margin, with special emphasis on the Storegga area. *Institutt for kontinentalsokkelundersøkelser* 110, pp. 1-152.

Bull, S., Cartwright, J. and Huuse, M. 2009. A review of kinematic indicators from mass-transport complexes using 3D seismic data. *Marine and Petroleum Geology* 26, pp. 1132-1157.

Bünz, S., Mienert, J., Vanneste, M. and Andreassen, K. 2005. Fluid flow impact on slope failure from 3D seismic data: A case study in the Storegga Slide. *Basin Research* 17, pp. 109-122.

C

Canals, M., Lastras, G., Urgeles, R., Casamor, J.L., Mienert, J., Cattaneo, A., De Batist, M., Haflidason, H., Imbo, Y., Laberg, J.S., Locat, J., Long, D., Longva, O., Masson, D.G., Sultan, N., Trincardi, F. and Bryn, P. 2004. The slope failure dynamics and impacts from seafloor and shallow sub-seafloor geophysical data: Case studies from the COSTA project. *Marine Geology* 213, pp. 9-72.

Carson, M.A. 1977. On the retrogression of landslides in sensitive muddy sediments. *Canadian Geotechnical Journal* 14, pp. 582-602.

Cartwright, J. and Huuse, M. 2005. 3D seismic technology: the geological 'Hubble'. *Basin Research* 17, pp.1-20.

Cartwright, J. 2007. The impact of 3D seismic data on the understanding of compaction, fluid flow and diagenesis in sedimentary basins. *Journal of the Geological Society of London* 164, pp. 881-893.

Collinson, J. 1994. Sedimentary deformational structures. In: Maltman, A. ed. *The Geological Deformation of Sediments.* London: Chapman & Hall, pp. 127-165.

Cosgrove, J.W. 2007. The use of shear zones and related structures as kinematic indicators: a review. In: Ries, A.C., Butler, R.W.H., and Graham, R.H. Eds. *Deformation of the continental crust: the legacy of Mike Coward.* Geological Society, London, Special Publication. Vol. 272, pp. 59-74.

D

Dalley, R.M., Gevers, E.C.A., Stampfli, G.M., Davies, D.J., Gastaldi, C.N., Ruijtenberg, P.A. and Vermeer, G.J.O. 1989. Dip and azimuth displays for 3D seismic interpretation. *First Break* 7, pp. 86-95.

Davies, R. and Clark, I. 2006. Submarine slope failure primed and triggered by silica and its diagenesis. *Basin Research* 18, pp. 339-350.

De Blasio, F.V., Issler, D., Elverhøi, A., Harbitz, C.B., Ilstad, T., Bryn, P., Lien, R., and Løvholt, F. 2003. Dynamics, velocity and run-out of the giant Storegga Slide. In: Locat, J. and Mienert, J. Eds. *Submarine Mass Movements and their Consequences*, pp. 223-230. The Netherlands: Kluwer Academic Press.

E

Edgers, L. and Karlsrud, K. 1983. Soil flows generated by submarine slides – case studies and consequences. In: *Behaviour of Off-Shore Structures, Proceedings of the International Conference* Elsevier, pp. 425-437.

Elliot, C.G. and Williams, P.F. 1988. Sediment slump structures: a review of diagnostic criteria and application to an example from Newfoundland. *Journal of Structural Geology* 10, pp. 171-182.

Embley R.W. and Jacobi, R. 1977. Distribution and morphology of large submarine sediment slides and slumps on the Atlantic continental margins. *Marine Geotechnology* 2, pp. 205-208.

Enachescu, M.E. 1993. Amplitude interpretation of 3-D reflection data. *The Leading Edge* 12, pp. 678-685.

Escher, A. and Watterson, J. 1974. Stretching fabrics folds and crustal shortening. *Tectonophysics* 22, pp. 223-231.

Eva, S.J. and Maltman, A.J. 1994. Slump-folds and palaeoslope orientations in Upper Silurian rocks, North Wales. *Geological Magazine* 131, pp. 685-691.

Evans, D., Harrison, Z., Shannon, P.M., Laberg, J.S., Nielsen, T., Ayers, S., Holmes, R., Hoult, R.J., Lindberg, B., Haflidason, H., Long, D., Kuijpers, A., Anderson, E.S. and Bryn, P. 2005. Palaeoslides and other mass failures of Pliocene to Pleistocene age along the Atlantic continental margin of NW Europe. *Marine and Petroleum Geology* 22, pp. 1131-1148.

Evans, D., King, E.L., Kenyon, N.H., Brett, C. and Wallis, D. 1996. Evidence for long-term instability in the Storegga Slide region off western Norway. *Marine Geology* 130, pp. 281-292.

Evans, D., McGiveron, S., Harrison, Z., Bryn, P. and Berg, K. 2002. Along-slope variation in the late Neogene evolution of the mid-Norwegian margin in response to uplift and tectonism. In: Doré, A.G., Cartwright, J.A., Stoker, S., Turner, J.P., White, N. Eds. *Exhumation of the North Atlantic Margin: Timing, Mechanisms and Implications for Petroleum Exploration.* Geological Society, London, Special Publication. Vol. 196. pp.139-151.

Eyal, Y. 1996. Stress field fluctuations along the Dead Sea rift since the middle Miocene. *Tectonics* 15, pp. 157-170.

F

Farrell, S.G. 1984. A dislocation model applied to slump structures, Ainsa Basin, South Central Pyrenees. *Journal of Structural Geology* 6, pp. 727-736.

Farrell, S.G. and Eaton S. 1987. Slump strain in the tertiary of Cyprus and the Spanish Pyrenees. Definition of palaeoslopes and models of soft sediment deformation. In: Jones, M.E., Preston, R.M.F. Eds. *Deformation of Sediments and Sedimentary Rocks.* Geological Society, London, Special Publication. Vol. 29. pp. 181-196.

Farrell, S.G. and Eaton, S. 1988. Foliations developed during slump deformation of Miocene marine sediments, Cyprus. *Journal of Structural Geology* 10, pp. 567-576.

Fleming, R.W. and Johnson, A.M. 1989. Structures associated with strike-slip faults that bound landslide elements. *Engineering Geology* 27, pp. 39-114.

Frey Martinez, J., Cartwright, J. and Hall, B. 2005. 3D seismic interpretation of slump complexes: examples from the continental margin of Israel. *Basin Research* 17, pp. 83-108.

Frey Martinez, J., Cartwright, J. and James, D. 2006. Frontally confined versus frontally emergent submarine landslides: a 3D seismic characterisation. *Marine and Petroleum Geology* 23, pp. 585-604.

Forsberg, C.F. and Locat, J. 2005. Mineralogical and microstructural development of the sediments on the Mid-Norwegian margin. *Marine and Petroleum Geology* 22, pp. 109-122.

Færseth, R.B. and Sætersmoen, B.H. 2008. Geometry of a major slump structure in the Storegga slide region offshore western Norway. *Norwegian Journal of Geology* 88, pp. 1-11.

G

Gafeira, J., Bulat, J. and Evans, D. 2007. The southern flank of the Storegga Slide: imaging and geomorphological analyses using 3D seismic. In: Lykousis V., Sakellariou, D., Locat, J. Eds. *Submarine Mass Movements and Their Consequences.* Dordrecht, The Netherlands: Springer, pp. 57-66.

Garfunkel, Z. 1998. Constraints on the origin and history of the Eastern Mediterranean basin. *Tectonophysics* 298, pp. 5-35.

Garfunkel, Z. and Derin, B. 1984. Permian-Early Mesozoic tectonism and continental margin formation of Israel and its implications for the history of the eastern Mediterranean. In: Dixon, J.E. and Robertson, A.H.F. Eds. *The Geological Evolution of the Eastern Mediterranean.* Boston. MA: Blackwell Scientific Publications, pp. 187-201.

Gawthorpe, R.L. and Clemmey, H. 1985. Geometry of submarine slides in the Bowland Basin (Dinantian) and their relation to debris flows. *Journal of the Geological Society of London* 142, pp. 555-565.

Gee, M.J.R., Gawthorpe, R.L. and Friedmann, J.S. 2005. Giant striations at the base of a submarine landslide. *Marine Geology* 214, pp. 287-294.

Gee. M.J.R., Gawthorpe, R.L., and Friedmann, S.J. 2006. Triggering and evolution of a giant landslide, offshore Angola revealed by 3D seismic stratigraphy and geomorphology. *Journal of Sedimentary Research* 76, pp. 9-19.

Gee, M.J.R., Uy, H.S., Warren, J., Morley, C.K. and Lambiase J.J. 2008. The Brunei slide: A giant submarine landslide on the North West Borneo Margin revealed by seismic data. *Marine Geology* 246, pp. 9-23.

Geertsema, M. Cruden, D.M. and Schwab, J.W. 2006. A large rapid landslide in sensitive glaciomarine sediments at Mink Creek, northwestern British Columbia, Canada. *Engineering Geology* 83, pp. 36-63.

Gratchev, I.B., Sassa, K., Osipov, V.I. and Sokolov, V.N. 2006. The liquefaction of clayey soils under cyclic loading. *Engineering Geology* 86, pp. 70-84.

H

Haflidason, H., Sejrup, H.P., Nygård, A., Mienert, J., Bryn, P., Lien, R., Forsberg, C.F. Berg, K., Masson, D. 2004. The Storegga Slide: architecture, geometry and slide development. *Marine Geology* 213, pp. 201-234.

Hampton, M.A., Lee, H.J. and Locat, J. 1996. Submarine landslides. *Reviews of Geophysics* 34, pp. 33-59.

Harbitz, C.B. 1992. Model simulations of tsunamis generated by the Storegga Slides. *Marine Geology* 105, pp.1-21.

Hart, B.S. 1999. Definition of subsurface stratigraphy, structure and rock properties from 3-D seismic data. *Earth Science Reviews* 47, pp. 189-218.

Haugen, K.B., Løvholt, F. And Harbitz, C.B. 2005. Fundamental mechanisms for tsumani generation by submarine mass flows in idealised geometries. *Marine and Petroleum Geology* 22, pp. 209-217.

Heezen, B.C. and Ewing, M. 1952. Turbidity currents and submarine slumps, and the 1929 Grand Banks earthquake. *American Journal of Science* 250, pp. 849-873.

Hesthammer, J. and Fossen, H. 1999. Evolution and geometries of gravitational collapse structures with examples from the Statfjord Field, northern North Sea. *Marine and Petroleum Geology* 16, pp. 259 – 281.

Hjelstuen, B.O., Eldholm, O. and Faleide, J.I. 2007. Recurrent Pliestocene mega-failures on the SW Barents Sea margin. *Earth and Planetary Science Letters* 258, pp. 605-618.

Hjelstuen, B.O., Sejrup, H.P., Haflidason, H., Nygård, A., Berstad, I.M. and Knorr, G. 2004. Late Quaternary seismic stratigraphy and geological development of the south Vøring margin, Norwegian Sea. *Quaternary Science Reviews* 23, pp. 1847-1865.

Hjelstuen, B.O., Sejrup, H.P., Haflidason, H., Nygård, A., Ceramicola, S. and Bryn, P. 2005. Late Cenozoic glacial history and evolution of the Streogga Slide area and adjacent slide flank regions, Norwegian continental margin. *Marine and Petroleum Geology* 22, pp. 57-69.

Hjelstuen, B.O., Eldholm, O. and Faleide, J.I. 2007. Recurrent Pleistocene mega-failures on the SW Barents Sea margin. *Earth and Planetary Science Letters* 258, pp. 605-618.

Homza, T. 2004. A structural interpretation of the Fish Creek Slide (Lower Cretaceous), northern Alaska. *AAPG Bulletin* 88, pp. 256-278.

Huvenne, V.A.I., Croker-Peter, F. and Henriet J.P. 2002. A refreshing 3D view of an ancient sediment collapse and slope failure. *Terra Nova* 14, pp. 33-40.

I

Imbo, Y., De Batist, M., Canals, M., Prieto, M.J. and Baraza, J. 2003. The Gebra Slide: a submarine slide on the Trinity Peninsula Margin, Antarctica. *Marine Geology 193*, pp. 235-252.

J

Jackson, M.P.A., Vendeville, B.C. and Shultz-Ela, D.D. 1994. Structural dynamics of salt systems. *Annual Review of Earth and Planetary Sciences* 22, pp. 93 – 117.

K

Kerr, P.F. 1962. Possible quick-clay motion in turbidity currents. *Science* 137, pp. 420-421.

King, E.L., Sejrup, H.P., Haflidason, H., Elverhøi, A. and Aarseth, I. 1996. Quaternary seismic stratigraphy of the North Sea Fan: glacially-fed gravity flow aprons hemipelagic sediments, and large submarine slides. *Marine Geology* 130, pp. 293-315.

Kvalstad, T.J., Andresen, L., Forsberg, C.F., Berg, K., Bryn, P. and Wangen, M. 2005. The Storegga slide: evaluation of triggering sources and slide mechanics. *Marine and Petroleum Geology* 22, pp. 245-256.

L

Laberg, J.S. and Vorren, T.O. 2000. The Trænadjupet Slide, offshore Norway-morphology, evacuation and triggering mechanisms. *Marine Geology* 171, pp. 95-114.

Laberg, J.S., Vorren, T.O., Dowdeswell J.A., Kenyon, N.H. and Taylor, J. 2000. The Andøya Slide and the Andøya Canyon, north-eastern Norwegian-Greenland Sea. *Marine Geology* 162, pp. 259-275.

Lastras, G., Canals, M., Amblas, D., Ivanov, M., Dennielou, B., Droz, L., Akhmetzhanov, A., TTR-14 Leg 3 Shipboard Scientific Party. 2006. Eivissa slides, western Mediterranean Sea: morphology and process. *Geo-Marine Letters* 26, pp. 225-233.

Lastras, G., Canals, M., Hughes-Clarke, J.E., Moreno, A., De Batist, M., Masson, D.G. and Cochonat, P. 2002. Seafloor imagery from the BIG'95 debris flow, western Mediterranean. *Geology* 30, pp. 871-874.

Lastras, G., Canals, M., Urgeles, R., De Batist, M., Calafat, A.M. and Casamor, J.L. 2004. Characterisation of the recent BIG'95 debris flow on the Ebro margin, Western Mediterranean Sea, after a variety of seismic reflection data. *Marine Geology* 213, pp. 235-255.

Lastras, G., De Blasio, F.V., Canals, M. and Eleverhøi, A. 2005. Conceptual and numerical modeling of the BIG'95 Debris flow, western Mediterranean Sea. *Journal of Sedimentary Research* 75, pp. 784-797.

Lee, H.J., Schwab, W.C. and Booth, J.S. 1991. Submarine landslides: An introduction. In: *Submarine Landslides: Selected Studies in the U.S. Exclusive Economic Zone*. Ed. by W.C. Schwab, H.J. Lee and D.C. Twichell. US Geological Survey Bulletin Vol 2002, pp. 1-13.

Lewis, K.B. 1971. Slumping on a continental slope inclined at 1-4°. *Sedimentology* 16, pp. 97-110.

Locat, J. and Lee, H.J. 2002 Submarine landslides: Advances and challenges. *Canadian Geotechnical Journal* 39, pp. 193-212.

Lucente, C.C. and Pini, G.A. 2003. Anatomy and emplacement mechanism of a large submarine slide within a Miocene foredeep in the northern Apennines, Italy: a field perspective. *American Journal of Science* 303, pp. 565-602.

M

Maltman, A.J. 1994. Introduction and overview. In: Maltman, A. Ed. *The Geological Deformation of Sediments.* London: Chapman and Hall, pp. 127-165.

Maltman, A.J. and Bolton, A. 2003. How sediments become mobilized. In: Van Rensbergen, P., Hills, R.R., Maltman, A. J. and Morley, C. K. Eds. *Subsurface sediment mobilization.* Geological Society, London, Special Publication. Vol. 216. pp 9-21.

Martel, S.J. 2004. Mechanics of landslide initiation as a shear fracture phenomenon. *Marine Geology* 203, pp. 319-339.

Martinsen, O.J. 1989. Styles of soft-sediment deformation on a Namurian (Carboniferous) delta slope, western Irish Namurian Basin, Ireland In: Whatley, M.K.G. and Pickering, K.T. Eds. *Deltas: Sites and Traps for Fossil Fuels*. Geological Society, London, Special Publication. Vol. 210. pp. 167-177.

Martinsen, O.J. and Bakken, B. 1990. Extensional and compressional zones in slumps and slides in the Namurian of County Clare, Ireland. Journal *of the Geological Society of London* 147, pp. 153-164.

Martinsen, O.J. 1994. Mass movements. In: Maltman, A. Ed. *The Geological Deformation of Sediments*. London: Chapman and Hall, pp. 127-165.

Masson, D.G., Harbitz, C.B., Wynn, R.B., Pedersen, G. and Løvholt, F. 2006. Submarine landslides: Processes, triggers and hazard prediction. *Philosophical Transactions of the Royal Society* 364, pp. 2009-2039.

Masson, D.G., Hugget., Q.J. and Brunsden, D. 1993. The surface texture of the Saharan Debris Flow deposit and some speculation on submarine debris flow processes. *Sedimentology* 40, pp. 583-598.

Mollard, J.D. and Hughes, G.T. 1973. Earthflows in the Grondines and Trois Riviéres area, Québec: Discussion. *Canadian Journal of Earth Sciences* 10, pp. 324–328.

Moore, D.G., Curray, J.R. and Emmel, F.J. 1976. Large submarine slide (olistostrome) associated with Sunda Arc subduction zone, northeast Indian Ocean. *Marine Geology* 21, pp. 211-226.

Moscardelli, L., Wood, L. and Mann, P. 2006. Mass-transport complexes and associated processes in the offshore area of Trinidad and Venezuela. *AAPG Bulletin* 90, pp. 1059-1088.

Mulder, T. and Cochonant, H.P. 1996. Classification of offshore mass movements. *Journal of Sedimentary Research* 66, pp. 43-57.

N

Nemec, W. 1990. Aspects of sediment movement on steep delta slopes. *Special publication of the International Association of Sedimentologists* 10, pp. 20-73.

Nissen, S.E., Haskell, N.L., Steiner, C.T. and Coterill, K.L. 1999. Debris flow outrunner blocks, glide tracks, and pressure ridges identified on the Nigerian continental slope using 3-D seismic coherency. *The Leading Edge* 18, pp. 595-599.

Nygård, A., Sejrup, H.P., Haflidason, H. and Bryn, P. 2005. The glacial North Sea Fan, southern Norwegian Margin: architecture and evolution from the upper continental slope to the deep-sea basin. *Marine and Petroleum Geology* 22, pp. 71-84.

O

Odenstad, S. 1951. The landslide at Sköttorp on the Lidan River. *Proceedings of the Royal Swedish Geotechnical Institute* 4, pp. 1–38.

O'Leary, D.W. 1986. The Munson-Nygren slide: a major lower-slope slide off the Georges Bank. *Marine Geology* 72, pp. 101-114.

O'Leary, D.W. 1991. Structure and morphology of submarine slab slides: clues to origin and behaviour. *Marine Geotechnology* 10, pp. 53-69.

O'Leary, D.W. 1993. Submarine mass movement, a formative process of passive continental margins: the Munson-Nygren landslide complex and the southeast New England landslide complex. In: Schwab, W.C., Lee, H.J., Twichell, D.C. Eds. *Submarine Landslides: Selected Studies in the U.S Exclusive Economic Zone*. U.S Geological Survey Bulletin 2002, pp. 23-39.

P

Petley, D.N., Higuchi, T., Petley, D.J., Bulmer, M.H. and Carey J. 2005. Development of progressive landslide failure in cohesive materials. *Geology* 33, pp. 201-204.

Posamentier, H.W. and Kolla, V. 2003. Seismic geomorphology and stratigraphy of depositional elements in deep-water settings. *Journal of Sedimentary Research* 73, pp. 367-388.

Posamentier, H.W., Davies, R.J., Cartwright, J.A. and Wood, L. 2007. Seismic geomorphology – an overview. In: Davies, R.J., Posamentier, H.W., Wood, L.J.,

Cartwright, J.A. Eds. *Seismic Geomorphology*. Geological Society, London, Special Publication. Vol. 277. pp. 1-14.

Pratson, L.F. 2001. A perspective on what is known and what is not known about seafloor instability in the context of continental margin evolution. *Marine and Petroleum Geology* 18, pp. 499-501.

Price, N.J. and Cosgrove, J.W. 1990. *Analysis of geological structures*. Cambridge: Cambridge University Press.

Prior, D.B., Bornhold, B.D. and Johns, M.W. 1984. Depositional characteristics of a submarine debris flow. *Journal of Geology* 92, pp. 707-727.

R

Ramsay, J.C. and Lisle, R.J. 2000. *The Techniques of Modern Structural Geology*. London: Academic Press.

Rosenqvist, I.Th. 1966. Norwegian research into the properties of quick clay – a review. *Engineering Geology* 1, pp. 445-450.

Rupke N. A. 1967. Large-scale slumping in a flysch basin, southwestern Pyrenees, in: *Journal of the Geological Society of London* 132, pp. 121–130.

S

Schnellmann, M., Anselmetti, F.S., Giardini D. and McKenzie, J.A. 2005. Mass movement-induced fold-and-thrust belt structures in unconsolidated sediments in Lake Lucerne (Switzerland). *Sedimentology* 52, pp. 271-289.

Schwartz, H-U. 1982. Subaqueous slope failures. *Contributions to Sedimentology* 11, pp. 116.

Stoker, M.S. and Shannon, P.M. 2005. Neogene evolution of the NW European Atlantic margin: results from the STRATAGEM project. *Marine and Petroleum Geology* 22, pp. 965-968.

Sheriff, R.E. and Geldart, L.P. 1983. *Exploration seismology, volume 2: Data-processing and Interpretation*. Cambridge: Cambridge University Press.

Simm, R. and White, R. 2002. Phase, polarity and the interpreter's wavelet. *First Break* 20, pp. 277-281.

Solheim, A., Berg, K., Forsberg, C.F. and Bryn, P. 2005. The Storegga Slide: repetitive large scale sliding with similar cause and development. *Marine and Petroleum Geology* 22, pp. 97-107.

Strachan, L.J. 2002(a). From geometry to genesis: a comparative field study of slump deposits and their modes of formation. *Unpublished PhD Thesis*, Cardiff University

Strachan, L.J. 2002(b). Slump-initiated and controlled syndepositional sandstone remobilisation: an example from the Namurian of County Clare, Ireland. *Sedimentology* 49, pp. 25-41.

Strachan L.J. 2006. Slump folds as estimators of palaeoslope: a case study from the Fisherstreet Slump of County Clare, Ireland. *Basin Research* 18, pp. 451-470.

Strout, J.M. and Tjelta, T.I. 2005. In situ pore pressures: What is their significane and how can they be reliably measured? *Marine and Petroleum Geology* 22, pp. 275-285.

T

Tibor, G. and Ben-Avraham, Z. 1992. Late Tertiary seismic facies and structures of the Levant passive margin off central Israel. *Marine Geology* 105, pp. 253-273.

Tréhu, A.M., Bohrmann, G., Rack, F.R., Torres, M.E. et al. 2003. *Proceedings of the Ocean Drilling Program*, Initial Reports, 204.

Trincardi, F. and Normark, W.R. 1989. Pleistocene Suvero slide, Paola basin, southern Italy. *Marine and Petroleum Geology* 6, pp. 324-335.

Trincardi, F. and Argnani, A. 1990. Gela Submarine slide: a major basin-wide event in the Plio-Quaternary foredeep of Sicily. *Geo-marine Letters* 10, pp. 13-21.

Twiss, R.J. and Moores, E.M. 1992. *Structural geology*. New York: W.H. Freeman and Company.

U

Urgeles, R., Canals, M., Baraza, J., Alonso, B. and Masson, D. 1997. The most recent megaslides on the Canary islands: The El Golfo debris avalanche and the Canary debris flow, West Hierro Island. Journal of Geophysical Research 102, pp. 20,305–20,323.

Urgeles, R., Leynaud, D., Lastras, G., Canals, M. and Mienert, J. 2006. Back-analysis and failure mechanisms of a large submarine slide on the Ebro slope, NW Mediterranean. *Marine Geology* 226, pp. 185-206.

V

Vanneste, M., Mienert, J. and Bünz, S. 2006. The Hinlopen Slide: A giant, submarine slope failure on the northern Svalbard margin, Arctic Ocean. *Earth and Planetary Science Letters* 245, pp. 373-388.

Varnes, D.J. 1978. Slope movement types and processes. In: Schuster R.L., Krizek, R.J. Eds. *Landslides, Analysis and Control*. National Academy of Sciences, Washington, Special Report 176, pp. 11-33.

Volpi, V., Camerlenghi, A., Hillenbrand, C.-D., Rebesca, M. and Ivaldi, R. 2003. Effects of biogenic silica on sediment compaction and slope stability on the Pacific margin of the Antarctic Peninsula. *Basin Research* 15, pp. 339-363.

W

Webb, B.C. and Cooper, A.H. 1988. Slump folds and gravity slide structures in a Lower Palaeozoic marginal basin sequence (the Skiddaw Group), NW England. *Journal of Structural Geology* 10, pp. 463-472.

Welbon, A.I.F., Brockbank, P.J., Brunsden, D. and Olsen, T.S. 2007. Characterising and producing from reservoirs in landslides: challenges and opportunities. In: Jolley, S.J., Barr, D., Walsh, J.J. and Knipe, R.J Eds. *Structurally Complex Reservoirs.* Geological Society, London, Special Publication Vol. 292. pp 49-74.

Williams, G. and Chapman, T. 1983. Strains developed in the hanging walls of thrusts due to their slip-propagation rate: a dislocation model. *Journal of Structural Geology* 5, pp. 563-571.

Wilson, C.K., Long, D. and Bulat, J. 2004. The morphology, setting and process of the Afen Slide. *Marine Geology* 213, pp. 149-167.

Winkelmann, D., Geissler, W., Schneider, J. and Stein, R. 2008. Dynamics and timing of the Hinlopen/Yermak Megaslide north of Spitsbergen, Arctic Ocean. *Marine Geology* 250, pp. 34-50.

Woodcock, N.H., 1979. Sizes of submarine landslides and their significance. *Journal of Structural Geology* 1, pp. 137-142.